

Fatigue analysis of wind turbine blade materials using a continuum damage mechanics framework

Bhangale, J.A.

DOI

[10.4233/uuid:7ea21785-c7ec-49db-85c4-d2e2f6ce6e9b](https://doi.org/10.4233/uuid:7ea21785-c7ec-49db-85c4-d2e2f6ce6e9b)

Publication date

2021

Document Version

Final published version

Citation (APA)

Bhangale, J. A. (2021). *Fatigue analysis of wind turbine blade materials using a continuum damage mechanics framework*. [Dissertation (TU Delft), Delft University of Technology].
<https://doi.org/10.4233/uuid:7ea21785-c7ec-49db-85c4-d2e2f6ce6e9b>

Important note

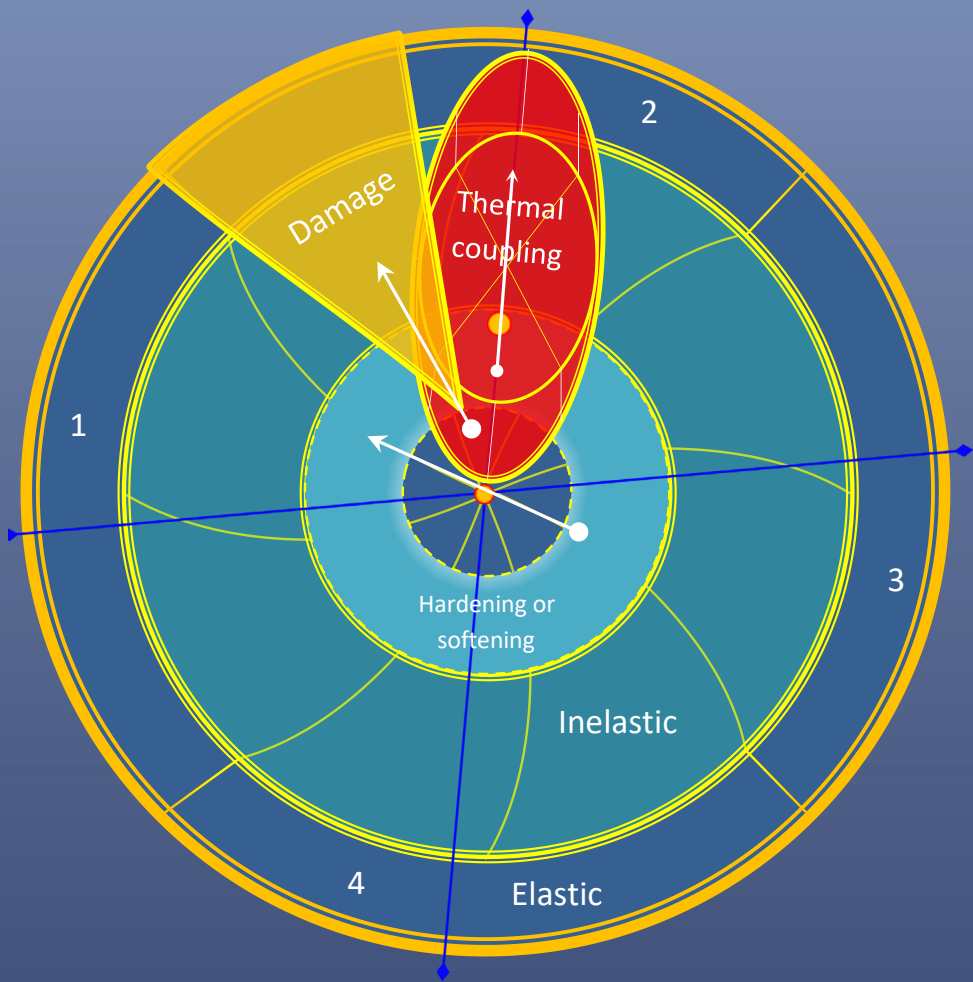
To cite this publication, please use the final published version (if applicable).
Please check the document version above.

Copyright

Other than for strictly personal use, it is not permitted to download, forward or distribute the text or part of it, without the consent of the author(s) and/or copyright holder(s), unless the work is under an open content license such as Creative Commons.

Takedown policy

Please contact us and provide details if you believe this document breaches copyrights.
We will remove access to the work immediately and investigate your claim.



Fatigue analysis of wind turbine blade materials using a continuum damage mechanics framework

Jaykarna Bhangale

**FATIGUE ANALYSIS OF WIND
TURBINE BLADE MATERIALS USING A
CONTINUUM DAMAGE MECHANICS
FRAMEWORK**

Fatigue analysis of wind turbine blade materials using a continuum damage mechanics framework

Dissertation

for the purpose of obtaining the degree of doctor
at Delft University of Technology
by the authority of the Rector Magnificus Prof.dr.ir. T.H.J.J. van der Hagen
chair of the Board for Doctorates
to be defended publicly on
Wednesday, 2 June 2021 at 15:00 o'clock

By

Jaykarna Ashok BHANGALE

Master of Engineering in Polymer Engineering,
University of Pune, India
born in Bhalod Yawal, India

This dissertation has been approved by the promotor
Dr.ir. R.C. Alderliesten and Prof.dr.ir. R. Benedictus

Composition of the doctoral committee:

Rector Magnificus,	chairperson
Prof.dr.ir. R.C. Alderliesten,	Delft University of Technology, Promotor
Prof.dr.ir. R. Benedictus,	Delft University of Technology, Promotor

Independent members:

Prof.dr. R. Talreja	Texas A&M University, USA
Prof.dr. P. Brøndsted	Brøndsted Materials Consult, Denmark
Prof.dr.ir. W. Van Paepegem	Ghent University, Belgium
Prof.dr.ir. B. Rosic	University of Twente, the Netherlands
Prof.dr.ir. L.J. Sluijs	Delft University of Technology
Prof. dr. ir. S. van der Zwaag	Delft University of Technology, reserve member

The work presented in this thesis is part of an Industrial PhD project carried out in collaboration between Suzlon Energy Ltd., Netherlands and Department of Aerospace Structures and Materials, Technical University of Delft, Netherlands.



Keywords: Wind turbine blade, material fatigue analysis, continuum damage mechanics, thermodynamics, cyclic deformation

Printed by: ProefschriftMaken(<https://www.proefschriftmaken.nl/en>)

Front: Hypothetical representation of fatigue phenomenon

Copyright © 2021 by J.A. Bhangale

ISBN 978-94-6423-259-2

An electronic version of this dissertation is available at

<http://repository.tudelft.nl/>

“Observation was more important than theory in the study of physics” PW Bridgman, 1927.

“ज्याच शरीर चांगल त्याची बुद्धी चांगली; ज्याची बुद्धी चांगली त्याच मन चांगल; ज्याच मन चांगल त्याच सर्वच चांगल”

“The better the body, the better the intellect; The better the intellect, the better the mind; The better the mind, the better is everything” AR Bhangale.

Table of Contents

TABLE OF CONTENTS	VII
SUMMARY	XI
NOMENCLATURE	XIII
ABBREVIATIONS	XV
1 INTRODUCTION	1
1.1 Prerequisites to fatigue analysis	4
1.2 Fatigue analysis framework	8
1.2.1 Traditional phenomenological framework.....	9
1.2.2 Reviews and surveys of the traditional framework	11
1.2.3 The framework from the thermodynamic theory of irreversible processes with internal variables.....	14
1.2.4 Continuum Damage Mechanics framework.....	20
1.2.5 Cyclic inelasticity theory.....	25
1.3 Scope and methodology	30
2 THEORY OF FATIGUE PHENOMENON	33
2.1 Deformation mechanism	34
2.1.1 Elastic deformation	35
2.1.2 Inelastic deformation	35
2.2 Damage mechanism	40
2.2.1 Development.....	42
2.2.2 Measurement of damage.....	44
2.2.2.1 Strain energy	44
2.2.2.2 Stiffness (Global)	44
2.3 Thermal contribution	45

2.4	Coupling between different mechanism.....	46
2.4.1	Deformation coupling	46
2.4.2	Damage coupling.....	47
2.4.3	Thermal coupling.....	48
3	MATHEMATICAL FORMULATION FOR THEORY	49
3.1	Generic formulation	50
3.1.1	Fundamental laws	50
3.1.2	Declaration of state variables	54
3.1.3	Choice of thermodynamic potential and state law	56
3.1.4	Choice of dissipation potential and evolution law	59
3.1.5	Coupling between different mechanisms	62
3.1.6	The expression for thermodynamic and dissipation potential	63
3.2	Elasticity coupled with damage	64
3.3	Inelasticity coupled with damage	65
3.3.1	Elastic domain	65
3.3.2	Flow rule.....	66
3.4	Fatigue damage.....	68
4	VALIDATION OF THEORY AND MATHEMATICAL FORMULATION	75
4.1	Experimental details	76
4.1.1	Materials	76
4.1.2	Process	78
4.1.3	Test specification	80
4.2	Validation of theory	83
4.2.1	Static.....	83
4.2.2	Fatigue.....	86
4.2.2.1	Damage analysis	86
4.2.2.2	Observations on recorded data from strain sensors.....	89
4.2.2.3	Cyclic inelasticity	95
4.3	Validation of mathematical formulation	102
4.3.1	Hysteresis curve analysis.....	102
4.3.2	Damage measurement.....	106

4.3.3	Softening behaviour	118
4.3.4	Parameter dependency.....	119
4.3.4.1	Parameters dependency on stress ratio.....	119
4.3.4.2	Parameters for non-linear damage evolution law.....	123
4.3.4.3	Parameters for constant life diagram.....	128
4.3.5	Non-linear damage evolution	129
4.3.6	Construction of constant life diagram.....	132
5	CONCLUSION	141
5.1	A retrospective view on the CDM framework	142
5.2	Specific conclusions.....	143
5.3	Contribution to wind turbine blade application	144
5.4	Reflective summary.....	145
6	FUTURE OUTLOOK.....	147
	REFERENCES.....	151
A	APPENDIX.....	191
A.1	Traditional literature reviews and surveys	192
A.2	Test results.....	194
A.2.1	Biax OKD.....	194
A.2.2	Triax OKA.....	195
A.2.3	Triax OOA	196
A.2.4	UDG OKA	198
A.2.5	UDGH 3KD	200
A.2.6	UDGH OOD.....	201
A.2.7	UDGH OOA	202
A.2.8	Ply drop	204
A.3	Test result analysis	205
A.3.1	Failure images for all configurations.....	205
A.3.2	Hysteresis curves from various strain sensors	206
A.3.3	Hysteresis curves for R-1 stress ratio	207
A.3.4	Hysteresis curves for R0.1 stress ratio	208

A.3.5	Hysteresis curves for R10 stress ratio	209
A.3.6	Elastic strain development for all material configurations	210
A.3.7	Inelastic strain development for all material configurations	211
A.3.8	Elastic strain energy development for all material configurations	212
A.3.9	Inelastic strain energy development for all material configurations	213
A.3.10	The probability distribution function of inelastic strain energy for all material configurations	214
A.3.11	Stiffness degradation for all material configurations	215
A.3.12	The probability distribution function of hysteresis stiffness for all material configurations	216
A.3.13	Averaging scheme to identify damage evolution trend.....	217

ACKNOWLEDGEMENTS..... 219

CURRICULUM VITAE..... 221

LIST OF PUBLICATIONS..... 223

Summary

The work done for this thesis is related to fatigue analysis of various material types used in the wind turbine blades. For the analysis, a framework from the thermodynamics of irreversible processes with internal variables and Continuum Damage Mechanics (CDM) is used. Thermodynamic principles provide a generic framework that is valid for the entire fatigue phenomenon. CDM framework is then applied to characterize a specific mechanism under consideration. As the fatigue phenomenon consists of many mechanisms and their interactions, the scope of work is limited to setting the generic framework and to characterize only a few and their interactions to demonstrate the framework potential.

The thesis consists of four main sections: introduction, theory, mathematical formulation, and validation.

Before starting the framework construction, a decent idea about vastness in fatigue analysis methodologies adopted by the research community is required. Hence chapter 1 is prepared to give readers, not in detail, but a helicopter view of the field. This overview allows drafting the achievable scope and methodology for this research work keeping in mind the ultimate goal of analysing full-scale wind turbine blade sustaining fatigue throughout its operational life.

Chapter 2 gives a generic theory consisting of the systematic categorization and detailing of fatigue phenomenon into contributing mechanisms and their interaction with each other. The theory forms the basis for the amount of detail to be considered in the mathematical formulation.

In chapter 3 first, a basic generic framework is provided so that the assumptions made and their implication are well understood. An only better understanding of assumptions helps to formulate a generic framework that can accommodate complicated situations of the blade materials along with the different scales. In section 3.4, the mathematical formulation for specific mechanisms like fatigue damage is derived using the generic framework. Due to the scope of the work, the inelasticity coupling with fatigue damage is not introduced using cyclic inelasticity theory but by using the phenomenological relationship between inelastic strain and damage. To derive fatigue damage evolution Lemaitre's generic damage potential was applied to various material types used in the blade.

Chapter 4 consist of the validation of the CDM framework for practical situations. Various types of materials are used in wind turbine blade design, and hence a careful selection of eight material configurations was made for successful validation. During validation, the complete experimental set up plays a vital role in the accuracy of recorded information, and its relevance to validation. Hence a dedicated section of experimental details is given in section 4.1. It includes the specification of the set up followed. During the experiment, various sensors monitor coupon behaviour. In section 4.2.2 results from these sensors are discussed, along with their usability range. Next step is to validate the theory and mathematical formulation for the selected material configurations. It starts with the validation of different mechanisms, their contribution, and interdependence using hysteresis curve analysis in section 4.2.2. It also gives the most suitable parameter for a description of damage based on sharp features and distinction in stress levels. Section 4.3 provides non-linear damage accumulation and fatigue life estimation for all materials, along with the parameters estimation procedure. Next, in this section, the model validity is assessed by comparing traditional methodology and currently proposed CDM framework to experimental results. The comparison is made based on both error matrices and the accuracy in the prediction of SN curve parameters. Best practices learned during the execution of the test and analysis of results are given in the respective sections.

Chapter 5 gives a retrospective view on CDM methodology, and the subsection provides specific conclusions about the direct application of work to the wind turbine blade materials. The chapter concludes with a hypothetical pictorial representation of the fatigue phenomenon that gives visual guidance for understanding the existence of various mechanisms with their contributions and interactions. The last section gives a future outlook for CDM methodology to meet the ultimate goal of fatigue analysis on the full-scale wind turbine blade.

Nomenclature

Basic symbol

Symbol	Unit	Description
T	°C	Temperature
m	kg	Mass
V	mm ³	Volume
t	sec	time
x	mm	Distance
ρ	kg/m ³	Mass density
e	J/kg	Energy per unit mass
Ω	-	Surface
N	-	Number of cycles
U	J	Total internal energy
$u = \frac{U}{m}$	J/kg	Specific internal energy
S	J/K	Entropy
s	J/kg.K	Specific entropy
\vec{q}	W/m ²	Heat flux
$\overrightarrow{\text{grad}}T = \frac{\partial T}{\partial x_i}$	°C	Temperature gradient
w^e	N.mm/mm ³	Elastic work done or strain energy
w_i^e	N.mm/mm ³	Elastic work done or strain energy at i th cycle
W^p	N.mm/mm ³	Inelastic work done or strain energy
w_i^p	N.mm/mm ³	Inelastic work done or strain energy i th cycle
ψ	J/kg	Helmholtz free energy
φ	J/kg	Dissipation potential
σ_{ij}	MPa	Cauchy stress tensor
ε_{ij}	mm/mm	Total strain tensor
ε_{ij}^e	mm/mm	Elastic strain tensor
ε_{ij}^p	mm/mm	Inelastic strain tensor

ε_{ij}^{ve}	mm/mm	Viscoelastic strain tensor
ε_{ij}^{vp}	mm/mm	Viscoplastic strain tensor
σ_y	MPa	Yield strength
σ_u	MPa	Ultimate strength (Tensile or compressive)
Y	N.mm/mm ³	Strain energy density release rate
D	-	Damage variable
α_j	mm/mm	Strain related to Kinematic hardening
X_j	MPa	Stress related to Kinematic hardening
r	mm/mm	Strain related to isotropic hardening
R	MPa	Stress related to Isotropic hardening
Z	N.mm/mm ³	Ageing energy
a	-	Phase change/ageing variable
E_{ijkl}	N/mm ²	Stiffness tensor in Viot form as E_{ij}
C_{ijkl}	mm ² /N	Compliance tensor in Voigt form as C_{ij}
$\sigma_{eq} = \left(\frac{3}{2}\sigma_{ij}^D\sigma_{ij}^D\right)^{1/2}$	MPa	von Mises equivalent stress
$\varepsilon_{eq} = \left(\frac{2}{3}\varepsilon_{ij}^D\varepsilon_{ij}^D\right)^{1/2}$	mm/mm	von Mises equivalent strain
$\sigma_{ij}^D = \sigma_{ij} - \frac{1}{3}\sigma_{kk}\delta_{ij}$	MPa	Stress deviator
$\varepsilon_{ij}^D = \varepsilon_{ij} - \frac{1}{3}\varepsilon_{kk}\delta_{ij}$	mm/mm	Strain deviator
$\sigma_H = \frac{1}{3}\sigma_{kk}$	MPa	Hydrostatic stress
$\varepsilon_H = \frac{1}{3}\varepsilon_{kk}$	mm/mm	Hydrostatic strain
p	mm/mm	Effective plastic strain
dp	mm/mm	Incremental change in effective plastic strain
λ	-	Plasticity multiplier
$R_v = \frac{\sigma_H}{\sigma_{eq}}$	-	Triaxiality ratio
σ_{max}	MPa	Maximum stress
σ_{min}	MPa	Minimum stress
σ_m	MPa	Mean stress
σ_a	MPa	Amplitude stress
ε_{max}	$\mu\varepsilon$	Maximum strain

ε_{min}	$\mu\varepsilon$	Minimum strain
ε_m	$\mu\varepsilon$	Mean strain
ε_a	$\mu\varepsilon$	Amplitude strain

Operational symbol

(\cdot)	Scalar product $u \cdot v = u_i v_i$
δ_{ij}	Kronecker's Delta
\dot{x}	Rate of change of quantity x w.r.t time
\tilde{x}	Damage state entity of x
$(:)$	Double contraction $A:B = A_{ij}B_{ij}$
Δx	Range of x

Abbreviations

CDM	Continuum damage mechanics
CLD	Constant life diagram
MMWK	Multiaxial multilayer warp knitted
NCF	Non-crimp fabric
ECR glass	Electrical, Corrosion Resistance glass fibre as per ASTM D578
H/R glass	High performance/Reinforcement glass fibre
Biax	Biaxial NCF 833g/m ² /ECR glass fiber in $\pm 45^\circ$
Triax	Triaxial NCF 1185g/m ² /ECR glass fibre in $0\pm 45^\circ$
UDG	Unidirectional NCF 1265g/m ² /ECR glass fibre in 0°
UDGH	Unidirectional NCF 1265g/m ² /H/R glass fibre in 0°
UDC	Unidirectional pultruded plate/100% carbon fibre at 0°
DGEBA	diglycidyl ether of bisphenol A

ECH	Epichlorohydrin
POPDA	Poly(oxypropylene) diamine
IPDA	Isophoronediamine
DETA	Diethylenetriamine
UVCB	unknown or variable composition, complex reaction products
CG	Clip-on extensometer
SG	Strain gauge
CL	Constant life

1

Introduction

The first chapter¹ gives the scope and methodology followed for the research work done for this thesis. A necessary first step to decide the scope and methodology is to understand the requirements from the application and the work done in the past in similar areas. Hence first, a brief overview of the wind turbine blade is given, followed by a description of various frameworks used in fatigue analysis of materials. The description includes systematic categorization of the methodology developed over the years in the respective framework and their distinct features.

¹ Parts of this chapter have been published in [1]

Over the last century due to the exponential growth of human footprints on planet earth, there is a continuous push for developing new technologies in every sector. The energy sector and particularly the area of wind energy is a field that sees demand for pushing the limits of known technologies and the exploration of new ones. This demand is driven by the need for integrated socio-economic and ecological policies. That means the source of energy to be more reliable, cheaper, and greener than fossil fuel-based source. **Figure 1** shows exponential growth in the wind energy installation over the last thirty years with a forecast for the next decade. Such growth fuels the need for integrated policy to meet the future demand for low cost and high volume.

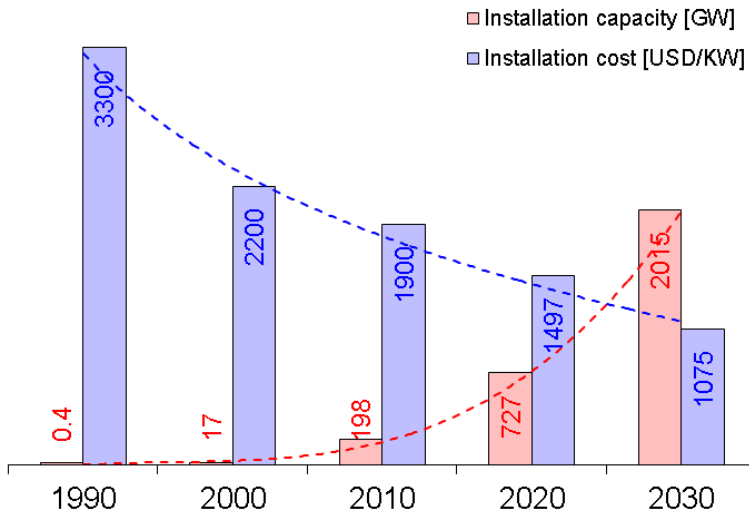


Figure 1 Energy outlook (<https://www.iea.org/>, <https://gwec.net/>)

One of the critical requirements to make new technologies feasible is to validate the theories underlying these new technologies. The theories related to material technologies are of no exception to this requirement mainly due to new material types that are added continuously in the market to meet the demand of the growing wind sector, see **Figure 2**. In this work, theories related to material deformation under fatigue loading are of prime focus.

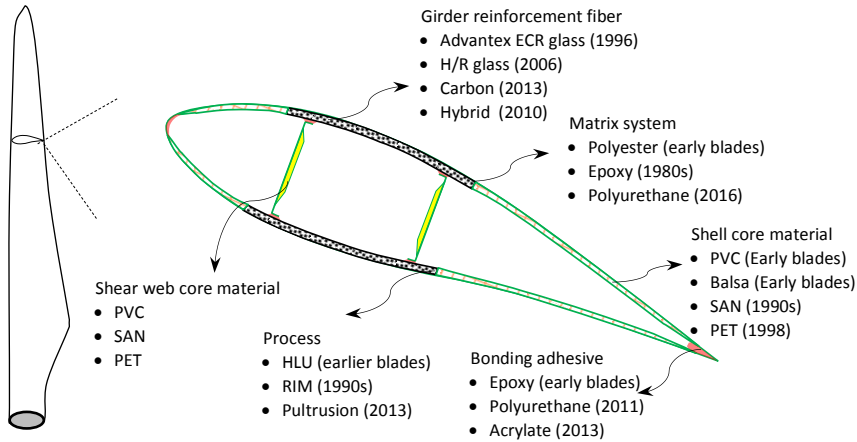


Figure 2 Introduction of new materials in wind turbine blade construction

In the material technology area, over the last century, a transition can be observed in how the understanding of the fatigue phenomenon is developed. Initially, the development of fundamental theories outpaced the experimental observations. More recently, facilitated by the development in sophisticated testing capabilities, the experimental observations outpaced the development of theories. Hence today, material deformation theories are developed, and experimental results are generated in different fatigue research communities that are not in synchronization. In many cases, oversimplified theories, that are developed on prior art, are fitted to new experimental datasets without awareness of other (often more) theoretical work.

For example, in the case of composite materials of a wind turbine blade, the fatigue phenomenon consists of many mechanisms and their interactions depending on or associated with, the intrinsic structure the material has at its respective length scales. Hence for composite materials, only a unified approach can characterize the fatigue phenomenon fully. In these cases, the use of oversimplified theories is accepted even for describing the most complex fatigue behaviour [1, 2]. Such acceptance leads to the generation of a massive amount of experimental data only to fulfil the standard requirements. In many cases, this data is not in synchronization with the underlying governing theories, ultimately creating a gap between experiments and theory.

An overview with a systematic categorization of different fatigue analysis frameworks can increase the awareness of the presence of different frameworks. Based on such knowledge, a most appropriate analysis framework can be identified which not only

represent the specific experimental dataset but also addresses the gap between the governing theory and experiments.

For the construction of a framework based on the unified approach requires several prerequisites and specific steps to be followed. Hence, these prerequisites are discussed in the next section, followed by the systematic categorization of different analysis frameworks. The systematic categorization provides the necessary background knowledge to define the steps required to construct a framework to characterize the respective mechanisms fully.

1.1 Prerequisites to fatigue analysis

Any framework used in fatigue analysis is built upon a specific research objective and corresponding methodology. Hence, before adopting a fatigue analysis framework, sufficient attention must be given to its prerequisites, which in sequence, can be written as

- Prior knowledge of loading conditions and corresponding damage mechanisms on the structure and its sub-components during operation.
- Selection of length scale at which fatigue analysis needs to be performed.
- Selection of the analysis methodology.

These prerequisites are discussed in the below paragraphs.

In wind turbines, the loads experienced by blades are instantaneous loads, and periodic loads, and both consist of deterministic as well as of stochastic nature loadings. The periodic loads are responsible for fatigue, and their loading patterns include coupled flapwise and edgewise bending. These loading patterns occur due to a combination of gravity, inertia, aerodynamic and operational loads. Here, inertia loading is caused by centrifugal and gyroscopic effects, which are acting on the blade during rotation [3, 4]. The aerodynamic loads are inherently unsteady due to variations in intensity and direction of wind speed over time and height caused by atmospheric turbulence [5, 6]. Figure 3 gives the schematic distribution of aerodynamic loading at an extreme event. The operational loads originate mainly from actions of the control system like braking, yawing, and blade-pitch control [7].

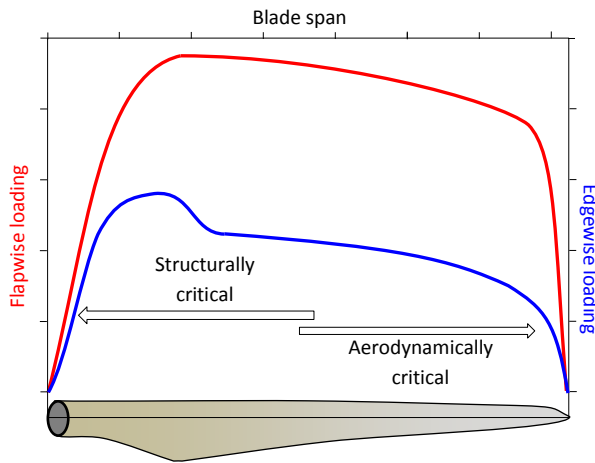


Figure 3 Schematic distribution of aerodynamic loading (extreme case) and structural zones of blade

The estimation of these loads on the wind turbine blade, which experiences different environmental conditions during its 20 years of nominal operation life, is generally done through computational fluid dynamics (CFD) analyses. IEC 61400 norms describe the load cases that a wind turbine is experiencing during its design lifetime. Each of these load cases is simulated in time using CFD analyses. The output of this CFD analysis is in the form of a load time history, which is further processed structurally into stresses or strains [8]. By applying cycle counting methods, (e.g. rainflow countings) number of load cycles count for all stress or strain ranges is computed. Figure 4 gives a schematic of this fatigue modelling methodology in wind turbine blades. If the stresses exceed a limit, then depending on the geometrical shape and space, they introduce damage in respective blade constituents. Brøndsted and Nijssen [6] provided an overview of a few of such failure mechanisms. In the absence of prior knowledge of the critical loading conditions and associated damage locations, the analysis efforts are directionless and could lead to a waste of time.



Figure 4 Methodology of fatigue modelling for the wind turbine blade

A wind turbine blade is a large-scale structure and made up of various forms of composite materials (monolithic, sandwich and joints). The blade cross-section is tailor-made using these materials to meet the structural requirements. As these materials are present in various forms at any cross-section, they show strong interaction with the surrounding materials and blade geometry. The industry follows building block approach for efficient design of the blade and its constituents against various loadings. This approach consists of a combination of experimental and analytical or numerical methods at different scales to understand the deformation and failure behaviour in details. **Figure 5** gives the general categorization of various scales in the building-block approach.

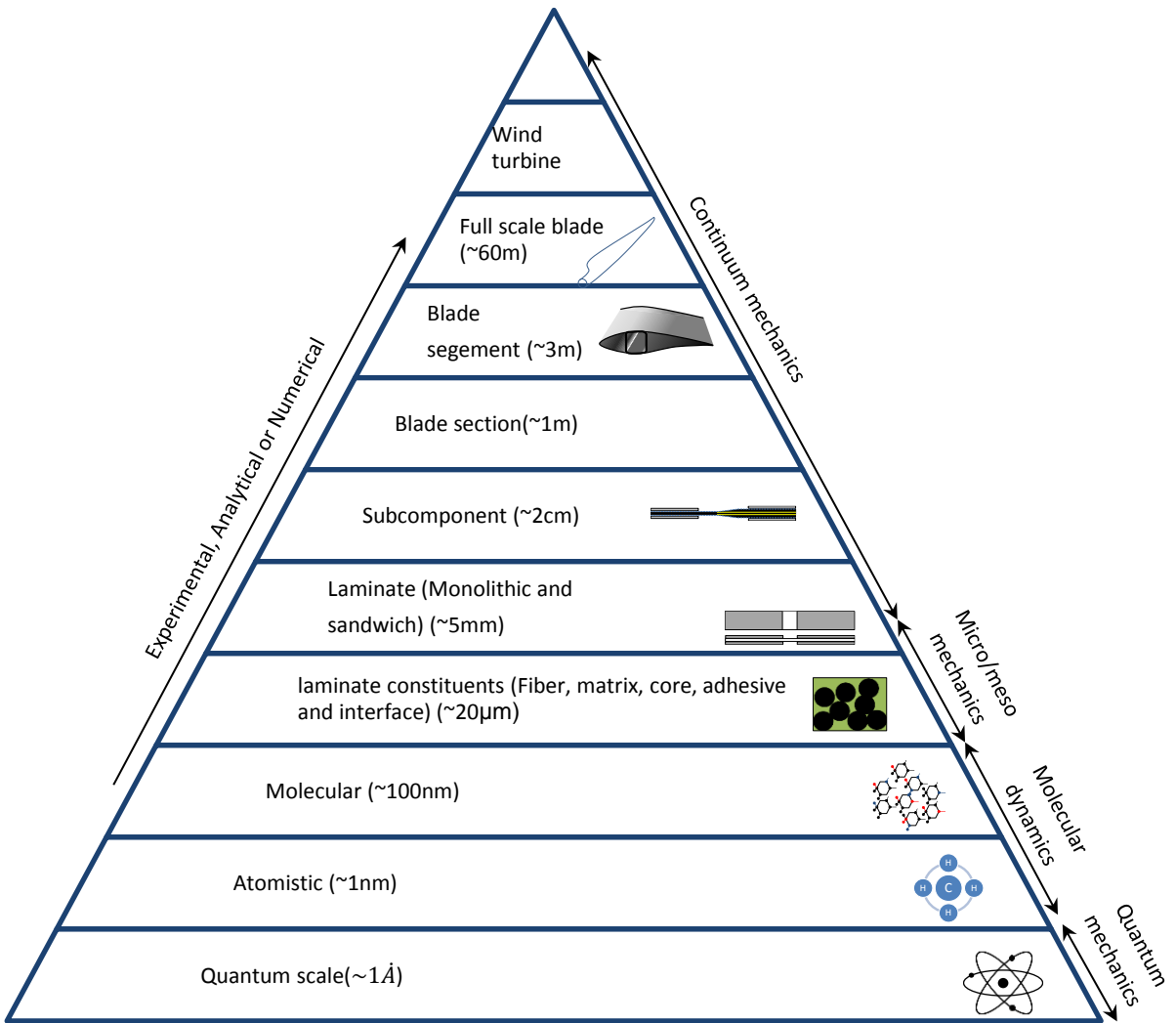


Figure 5 Building block approach

As in composite materials, various properties like stiffness and strength show length scales dependency [9], the scale at which the fatigue analysis is performed is an important aspect. In some cases, the product scale determines the choice of scale for analysis, whereas in other cases detailed understandings of specific mechanisms determine this choice. In the past, there were many attempts made [10, 11, 12, 13, 14, 15, 16, 17]² to link different scales or to link different theories so that information from different scales can be extracted or used in its exact sense without transforming them to any generalization. This field is generally referred to as multiscale modelling and is computationally very expensive. Take for example the characterization of individual damage mechanisms at micro-scale requires analysis framework based on micromechanics theory that nowadays is available for many materials and specifically for composites [18, 19, 20, 21, 22, 23, 24]². In the case of characterization of macro-scale damage using micro-scale properties requires the computation of damage at the micro-scale as well as its homogenized representation at the macro-scale without losing critical features from micro-scale. Carrying these critical features from micro to macro scale requires model grid size to be very small. Solving model equations over all these small grids for the whole blade is computationally very expensive. Section 1.3 gives the choice of scales selected for this work and associated reasoning.

The methodology followed in fatigue analysis can be categorized as physical or empirical (phenomenological). The physical methodology consists of three main steps viz. observation, governing theory, and validation, as shown in Figure 6a. The first step in a physics-based methodology is observing the phenomenon in detail. The second step consists of developing fundamental constitutive theories and their mathematical formulations which can describe the phenomenon completely and support the detailed observations. The validation of each theory and its mathematical formulation for its genericness is the last and crucial step in this physics-based methodology. Here, the experimental set up is designed to observe the desired mechanisms in detail.

² Only most relevant references are cited here to make a point.

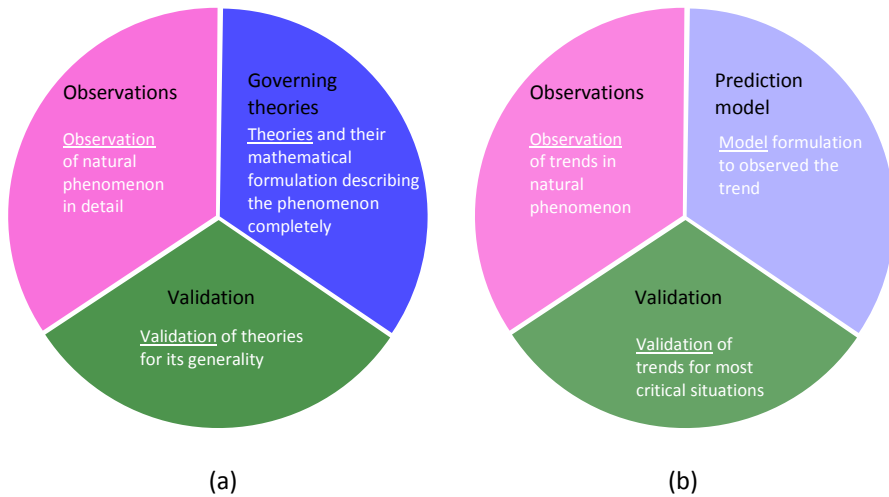


Figure 6 Analysis methodology (a) Physical (b) Empirical

The empirical methodology, as shown in **Figure 6b**, also consists of three steps, observations, development of prediction model and validation. The observation step consists of the identification of the trends in the given phenomenon or mechanism which are critical or relevant to the specific application. In this methodology, many times, efforts are not made to link the trends back to the constitutive theories. The prediction model representing the trends in observations replaces the theoretical part. During validation, the experimental setup is designed to address the most critical or relevant situation in the actual product.

Sometimes the phenomenon and associated mechanisms are too broad to consider in a single scope of physics-based methodology. This lack of scope creates a gap in mathematical formulation continuity, and this gap can be filled by following another methodology. When a different methodology is used to address this gap, then the overall methodology can be referred to as a mixed methodology. Section **1.3** gives the methodology followed for this thesis work and associated details.

1.2 Fatigue analysis framework

More than 150 years have passed since humanity encountered fatigue phenomenon in engineering applications. An ocean of information on fatigue analysis got generated over these years using different analysis frameworks. Due to this abundant information, it is challenging to prepare a single overview or systematic breakdown of all mechanisms, their physical understanding, and their mathematical modelling.

Here an attempt is made to prepare an overview of all the relevant contributions done in the area of fatigue analysis. This overview is the main scope of this section. The best way to get acquainted with different analysis framework is by systematic categorization of the methodology and learning from surveys and critical reviews in respective categories. In this paper, the fatigue analysis frameworks are categorized by their methodology.

1.2.1 Traditional phenomenological framework

Traditionally fatigue data is analysed within a very simplified framework. The simplicity in the application of this traditional framework favoured its widespread use in engineering application to date. [Figure 7](#) gives a schematic representation of different stages within this framework.

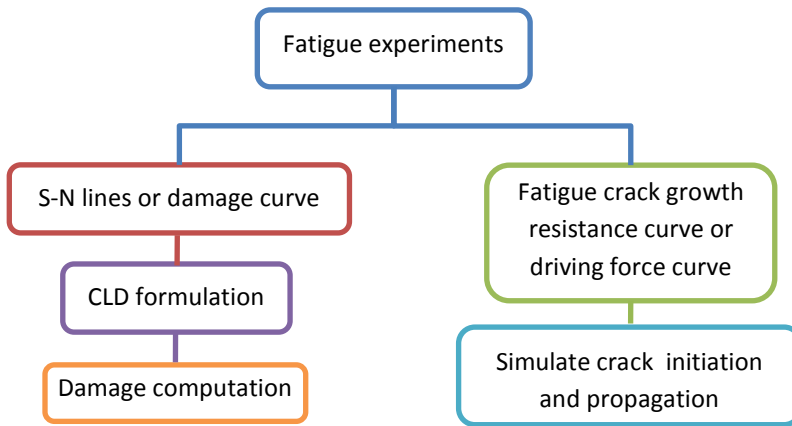


Figure 7 Traditional phenomenological framework of fatigue data analysis

The first stage comprises the execution of fatigue experiments at various stress or strain levels and for various stress or strain ratios. After that, the experimental results are analyzed in different ways, depending on the damage type.

In case a single crack forms the dominant damage mechanism degrading the structure, its initiation and propagation over time are monitored and studied. The study of crack propagation using methods of solid mechanics is known as fracture mechanics. Griffith [25] did the pioneering work in this field, and later over the 20th century, this field gave one of the analysis tools inseparable from product design. The curve of fatigue crack growth rate against either stress intensity factors or strain energy release rates is known as the fatigue crack growth resistance curve. A power-law form represents the central linear region in this fatigue resistance curve famously known as Paris–Erdogan law [26]. Resistance curves become the input to the

simulation of crack propagation in a finite element environment. Few modelling techniques have developed over the past three decades but among them, Virtual Crack Closure Technique (VCCT), Cohesive Zone Modeling (CZM), extended finite element method (XFEM), and phase-field modelling is the most widely used. This framework is not reviewed further as it is not in the scope of current work.

When final failure or gross damage is considered, for any stress or strain ratio number of cycles to failure is assumed to follow a power-law relationship with the input constraints. This power-law relationship is also known as the Basquin law [27] or Coffin-Manson law [28, 29]. This law is represented graphically as a stress/strain-life (SN) curve, also known as the Wohler curve [30] which is linear under a log-log or semi-log scale. The SN curve is a very simplified way of data representation, but in reality, many materials show a non-linear SN curve [31, 32]. To identify any nonlinearity, one of the practices followed in the industry is to perform fatigue tests that give failure lives scattered over at least four orders of magnitude in life. In the case of nonlinearity in the data, the SN curve formulation needs to be adapted accordingly. In some materials, the initial non-linear region of the SN curve is ranging from a few 100cycles to a few 100 thousand cycles [33, 206 p439].

The next step in this framework is to construct a constant life diagram (CLD), also known as Haigh diagram [34], which represents lines for constant life in mean and alternating stress/strain space. The CLD construction increases the life prediction capability to non-tested stress ratios. The formulation of constant lifelines and their estimated model parameters are input (material allowable) to structural analysis. The first formulation was proposed by John Goodman [35], followed by Gerber [36] and Soderberg [37]. Further over a century many formulations like Morrow [38], Harris with co-workers [39 p.633], Piecewise linear [40], Kassapoglou [41], Kawai [42] and Boerstra [43] were proposed. All these formulations can be represented by Marin's generic expression [44] as given below.

$$\left(\frac{\sigma_a}{\sigma_e}\right)^n + \left(f \frac{\sigma_m}{\sigma_u}\right)^m = 1 \quad \text{Equation 1}$$

Where σ_e denotes an equivalent fully reversed stress amplitude that leads to the same fatigue life under the combination of σ_a and σ_m at a specified stress ratio. n , m , and f are model parameters in the respective formulations.

This mathematical form equates the sum of ratios of stresses to unity. To satisfy this unity condition at $\sigma_a = 0$, σ_m attend the value of σ_u for any number of cycles till infinity. Physically there is no explanation possible for such a situation where a single point is representing failure life for any number of cycles. Due to practical difficulties in the execution of tests at high mean and low alternating loading the practice of

merging constant lifelines to single point continued. Another reason for the acceptance of the traditional framework is because of very few applications in reality that demand validation at low amplitude loadings.

The analysis in the traditional framework is based on survival probability only; in other words, failed or not failed hence does not give insight into how much damage structure has sustained over particular life or vice versa. Many attempts were made in the past to get more understanding from the traditional framework by using either a strength or stiffness reduction rule as input [45, 46]. Ramakrishnan and Jayaraman [47] proposed a stiffness degradation rule considering micro-scale properties for the case of uni-directional ceramic matrix composites. This rule also addresses the interfacial strength impact on stiffness degradation. In the last two decades application of strength and stiffness reduction rules and formulation of new ones for different materials continued to date [48, 49, 50, 51, 52, 53, 54, 55]².

The last step in the traditional framework is the calculation of damage accumulation. Various empirical rules for damage accumulation were proposed and reviewed in the past. Out of these, one popular and the extensively applied rule is linear damage rules [183, 184]. This rule assumes linear dependency of damage on fatigue life. In the case of composite materials, the damage does not show linear dependency on life as is discussed in detail in section 2.2. The simplicity of these rules in terms of computing damage makes their application very attractive even to a complicated situation like wind turbine blades.

1.2.2 Reviews and surveys of the traditional framework

Different ways of categorization have been followed in many textbooks, explicitly or implicitly explaining the categorization [56, 57, 58, 59, 60, 61, 62, 63, 64, 65, 66, 67]. In the current thesis, the categorization proposed is based on the 'what and how questions', as illustrated in Figure 8.

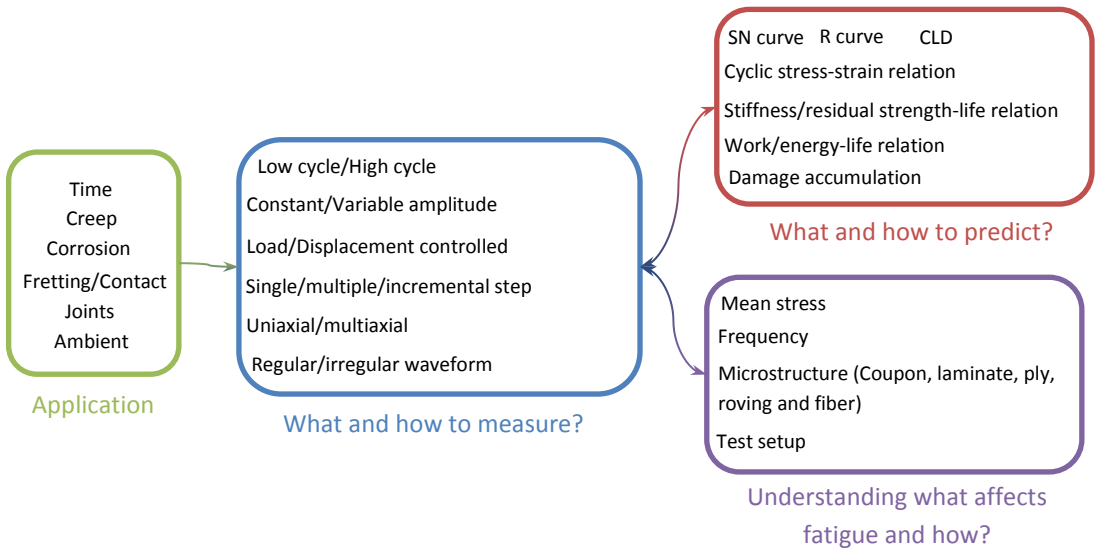


Figure 8 Categorization of fatigue analysis field through ‘what and how question’

Analysis of measured fatigue data is performed for two reasons, to improve understanding and prediction. Here, answering what and how question in the areas of measurement, prediction and understanding provides the list of various methodologies followed in the respective area **Figure 8**. For example, in the area of measurement, answering the question ‘what and how to measure’ provides different types of fatigue test methodologies followed for various materials and loading situations. In the area of prediction, answering question ‘what and how to predict’ provides the list of different methodologies followed to predict the fatigue behaviour in the untested region. Similarly, in the area of understanding, answering question ‘what affects fatigue and how’ gives the list of various parameters influencing the fatigue behaviour. By selectively searching the literature reviews or surveys for individual methodology or parameter influence a list of research done can be generated in the respective category.

Table 1 gives a timestamp overview of surveys and reviews presented for these three ‘what and how’ categories in chronological order.

What and how to measure?

1962	Coffin L. F. [68]
1973	Dew-Hughes D., Way J. [74]
1992	Geary W. [86]
1993	Bartsch et al [87]
1999	Bogdanovich A., Sierakowski R. [94]
2003	Kuang K., Cantwell W. [101]
2007	Della C., Shu D. [106]
2013	Wang et al. [114]
2016	Vacchieri E. [122]

What and how to predict?

1963	Kaechele L. [69]
1970	O'Neill M. J. [71]
1972	Schijve J. [73]
1974	Krempf E. [75]
1976	Socie D., Marrow J. [76]
1978	Hashin Z., Rotem A. [77]
1981	Garud Y. [79]
1991	Sendeckyj G. [84]
1994	Andersons J. [88]
1996	Lee S., You B. [91]
2001	Yokobori T. [96]
2001	Degrieck J, Van Papaegem W [97]
2003	Harris B. [102]
2003	Philippidis T., Passipoularidis V. [103]
2004	Krueger R. [105]
2008	Post et al. [108]
2009	Passipoularidis V., Brøndsted P. [109]
2009	Garnich M. Akula V. [110]
2013	Pascoe et al. [113]
2014	Bak et al. [116]
2015	Khan et al. [118]
2015	Sevenois R., Paepegem W. [120]
2016	Santecchia et al. [121]
2018	Antolovich et al. [126]
2018	Tabiei A., Zhang W. [127]
2018	Maierhofer et al. [128]
2019	Rajkumar et al. [130]
2020	Jimenez-Martinez M. [131]

What affects fatigue and how?

1965	Manson S.S. [70]
1972	Plumbridge W. [72]
1979	Reifsnider K., Stinchomb W. [78]
1987	Reifsnider K. [80]
1989	Konur O., Matthews F. [81]
1991	Bulloch J. [82]
1991	Liu H. W. [83]
1992	Kumar R. [85]
1994	Vasudeven et al. [89]
1995	Read P.C.J.L., Sheno R. [90]
1996	Schutz W. [92]
1999	Lawson et al. [93]
2000	Birman V., Byrd L. [95]
2001	Lemaitre J. [98]
2002	Mao-hong Yu [99]
2002	Qatu M. [100]
2003	Tay T. [104]
2007	Icardi et al. [107]
2012	Wicaksono S., Chai G. [111]
2013	Alderliesten R. [112]
2014	Abdullah et al. [115]
2015	Kaminski et al. [117]
2015	Mortazavian S. Fatemi A. [119]
2016	Zerbst et al. [123]
2016	Chowdhury P., Sehitoglu H [124]
2016	Adedipe et al. [125]
2019	Alam et al. [129]
2020	Vassilopoulos A. [132]

Table 1 Timestamp overview of reviews presented in the area of fatigue

Appendix A.1 gives the related topics of all reviews listed in the above table to limit the space here. From this overview, one can see that every area within the fatigue analysis field is going through either constant evolution in existing methodologies or identification of new methodologies to get more understanding of underlying mechanisms.

1.2.3 The framework from the thermodynamic theory of irreversible processes with internal variables

In search of more understanding, many studies adopt a physics-based methodology. The basis for this adoption is in the similarity of qualitative mechanical behaviour of most of the materials. Due to this similarity, it is possible to generalize the behaviour at the macro-scale with the help of macro-scale (bulk) mechanisms (elastic behaviour, yielding, inelastic strain, anisotropy induced by strain, cyclic inelasticity, and damage development) that are similar for these materials. One such possibility is provided by the well-established continuum damage mechanics (CDM) framework. This framework requires input from the thermodynamic theory of continuum and from general concepts of thermodynamics of irreversible processes with internal variables. The generalization of material behaviour is made by approximating the irreversible process by a sequence of constrained states that are near equilibrium, and that can be characterized locally by a finite set of internal variables. Figure 9 shows the link of this framework to the thermodynamic theory of continuum as given by Perzyna [133].

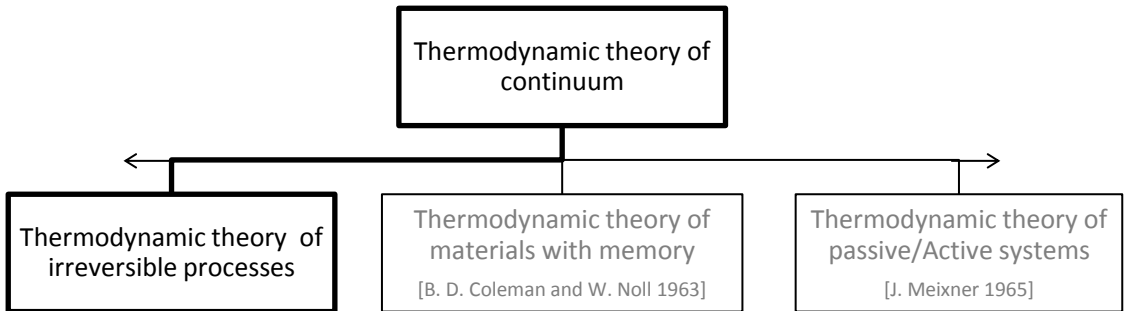


Figure 9 Link of the thermodynamic theory of irreversible processes (Arrow indicate a link with other theories like rational and extended thermodynamics)

The explicit use of the thermodynamic framework in studies on the deformation of solids started in the mid-20th century. Earlier to that, a few great scientists used the concepts in their work with or without mentioning it explicitly, like Lord Rayleigh for viscous flows, Lord Kelvin for the thermoelectric effect, Rudolf Clausius for restating thermodynamics laws, Pierre Duhem for the thermodynamic potential, Onsager's

reciprocal relations, Percy Bridgman for making thermodynamics principles operational to various situations. Later in the 1960-70s, the researchers listed in [Table 2](#) matured the concept of irreversible thermodynamics related to different deformation mechanisms.

In [Table 2](#), only a few contributions from researchers related to the field of mechanics of continuous media are listed. In all cases, they continued work throughout their career in other areas of science, as illustrated in [Figure 10](#). As the concepts of irreversible thermodynamics based on internal state variables got matured over the latter half of the 20th century, its potential as a basis for understanding complex deformation and damage behaviour of various materials got well recognized. A schematic flow chart of steps followed while setting up the basic framework of these thermodynamic concepts is shown in [Figure 11](#).

The framework starts with fundamental laws that are central principles of thermodynamics. These laws are general, pervasive and apply to both micro and macro scales of the material as a whole or every element within it.

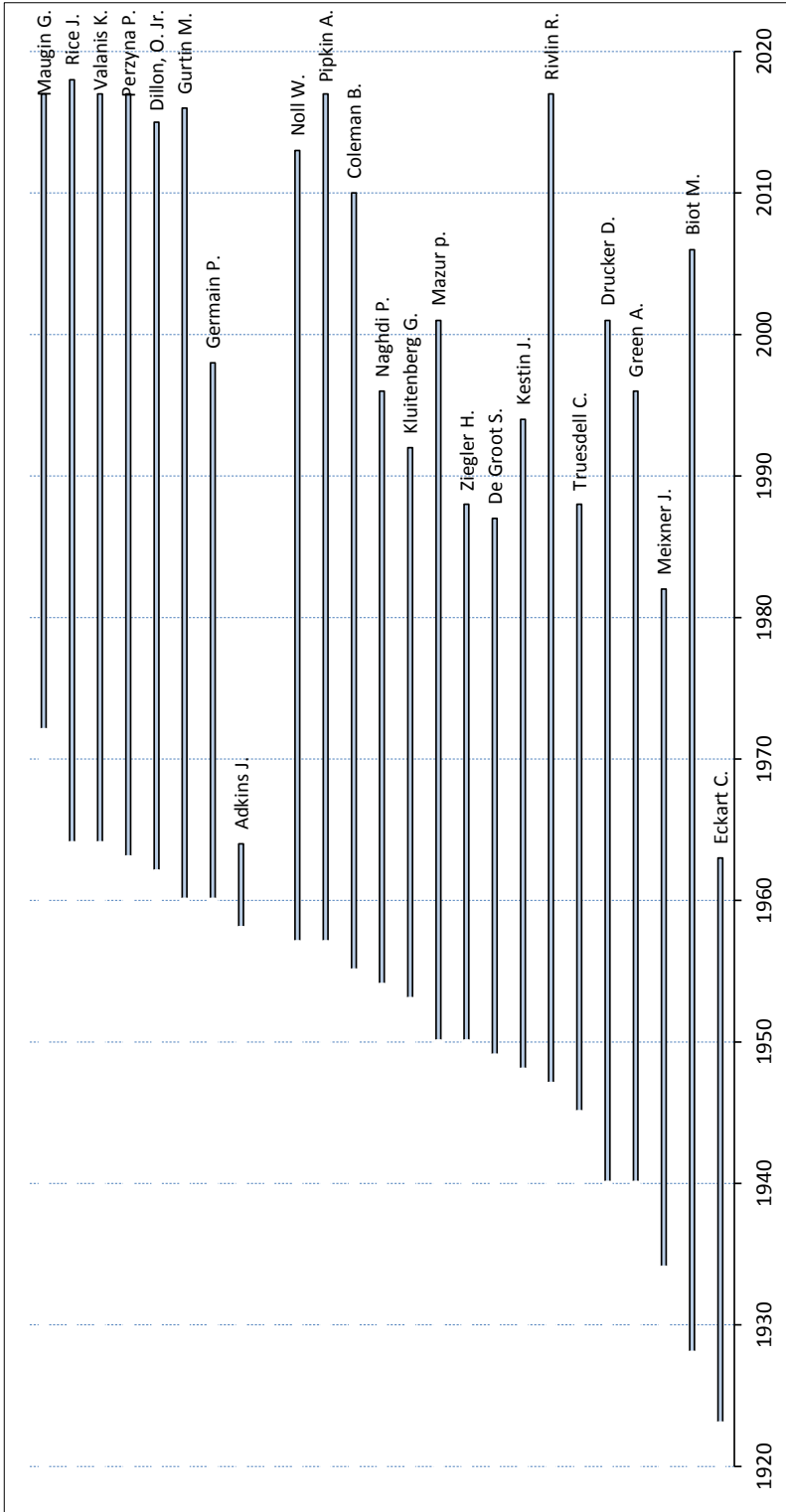


Figure 10 Contributions from various researchers over time in the field of irreversible thermodynamics

Eckart C. [134]	Finite inelastic deformation concept and classical theory of inelasticity
Biot M. [136]	Theory of isothermal linear viscoelastic and Non-linear thermoelastic systems
Meixner J. [135]	Theory of Isothermal linear elastic, dissipative, Passive and viscoelastic systems
Green A. [137]	Non-linear mechanics with memory and elastic-plastic continuum
Drucker D. [146]	General plasticity theory and the postulate of stability
Truesdell C. [141]	Rational thermodynamics, Non-linear field theories of mechanics
Rivlin R. [150]	Isotropic finite elasticity, Constitutive equations in continuum physics, Anisotropic finite elasticity, Internal variable theories and fracture
Kestin J. [153]	A general theory for continuum mechanics
De Groot S. [381]	A general theory of the thermodynamics of irreversible processes, Non-equilibrium Thermodynamics
Ziegler H. [138]	Dissipation potential, a non-linear extension to viscoelasticity
Mazur p. [381]	Non-equilibrium Thermodynamics
Kluitenberg G. [143]	Thermodynamics of irreversible processes
Naghdi P. [149]	General theory in non-linear and linear elasticity, plasticity, Viscoelasticity and thermodynamics
Coleman B. [144]	Thermodynamic theory of materials with memory, ideas and methods of a theory of constitutive structure
Pipkin A. [148]	A theoretical foundation for the structure and representation of material response functions
Noll W. [140]	Principle of material objectivity, General theory and its mathematical construction for continua, Foundations of Linear Viscoelasticity, non-linear field theories of mechanics
Vakulenko A. [139]	Continuum theory of a medium with cracks
Adkins J. [142]	Theory of non-linear diffusion, Symmetry relationships
Germain P. [155]	A general theory for continuum mechanics
Gurtin M. [147]	Non-linear continuum mechanics and thermodynamics
Dillon, O. Jr. [154]	Coupling between thermal, elasticity and plasticity, Strain gradient plasticity
Perzyna P. [145]	Thermodynamics of dissipative materials, A general theory of thermomechanics
Valanis K. [151]	Viscoelastic potential and its thermodynamic foundations
Rice J. [152]	Elastic-plastic fracture mechanics, Application of internal variable theory to plasticity
Maugin G. [156]	A general theory for continuum mechanics

Table 2 Evolution in the concept of irreversible thermodynamics related to mechanics of continuous media

When the material is deformed, its microstructure changes in either a reversible or irreversible manner. Each change can be characterized as a material's specific property and described by certain parameters known as state variables because they only depend on the initial and final states of a material. State variables are further divided into observable variables (which can be observed and directly measured) and internal variables (which are not directly observed but derived from observable variables). Maugin [157] gave a critical review on the use of internal variables of state in rational thermodynamics.

The energy involved in any change in state can be linked to its (state) potential. Hence when a state potential is written as a function of the state variable, then it defines the condition of the state. This functional relationship is known as state law. When a change in the state consists of dissipation of input energy in any form, then the process is known as the dissipative process. The description of such a process requires the evolution of such dissipation. Similar to the state potential when the dissipation potential is written as a function of associated variables, then it gives the evolution of dissipation. This relationship is known as evolution or complementary law.

The last part of the framework is to identify the coupling between different mechanisms. When two or more different mechanisms simultaneously represent the material's behaviour under loading, then they are considered coupled. In such a coupling, variable(s) associated with one mechanism is modified by the change of the value or the evolution rate of the variable(s) associated with the other mechanism. These couplings can be of direct, indirect, or secondary nature [403]. In the direct coupling, the absolute value of one variable influence the other variable. In the case of indirect coupling, the absolute value of one variable influence the rate of another one. Whereas in the secondary coupling, a third variable value is influenced by the second one where the first and second variable shows either direct or indirect coupling.

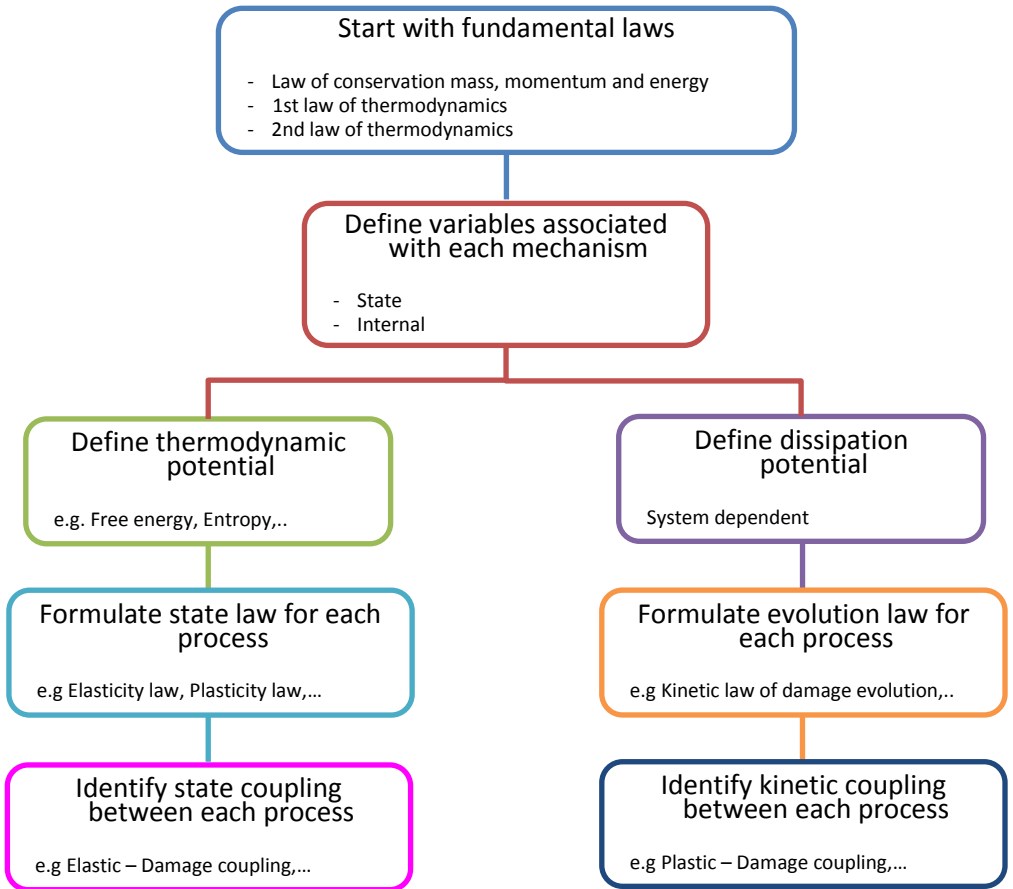


Figure 11 A schematic flow chart of steps followed while setting up the framework for irreversible thermodynamics with internal variables

1.2.4 Continuum Damage Mechanics framework

The framework of irreversible thermodynamics plays a fundamental role in constructing Continuum Damage Mechanics (CDM) models for various damage mechanisms. Damage during deformation in the physical sense means breakage of atomic/molecular bonds or generation of some defects in an atomic/molecular structure that results in discontinuities in a material at the micro or macro scale. These discontinuities result in strain dissipation. Depending on the nature of discontinuities, they either are represented by single or multiple damage variables and their associated variable strain energy release rate. Here, damage potential as a function of the strain energy release rate gives the evolution of the damage variable, and this functional relationship is called damage evolution law. The discontinuities in the material can be at the micro or macro scale, and hence the definition of damage variables also can be given at respective scales. If the damage variable is defined using continuum scale material properties (as described in 2.2.2), then the damage state can be treated as a continuum. This concept is schematically illustrated in Figure 12 using reference [263 p.351].

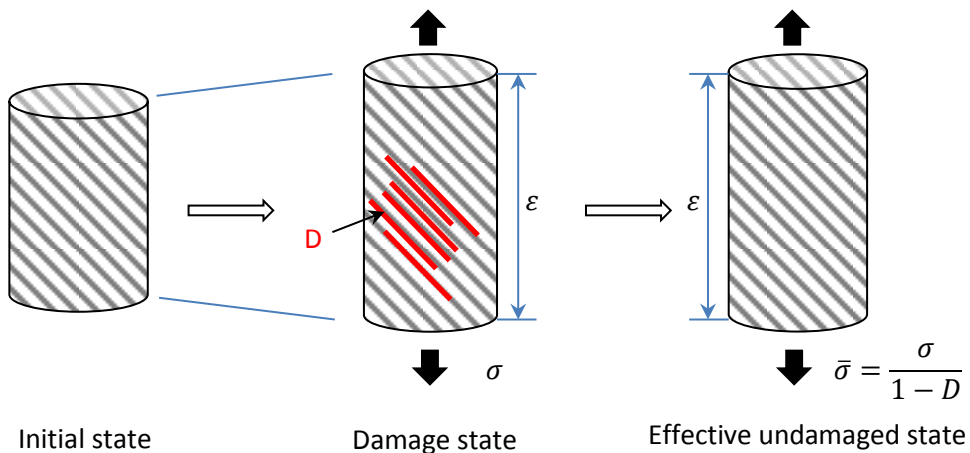


Figure 12 Treating damage as a continuum

Until the end of the 20th century, the CDM framework was applied and matured for various types of damages. Table 3 gives a time stamp overview of the contributions during this time to develop the framework by multiple researchers. This table gives only the first contribution from these researchers; in many cases, they continued their work over the following decades.

Introduction

1958	Kachanov L. [158]	Introduction of scalar damage variable
1968	Rabotnov Y. [159]	Concept of effective stress
1971	Lemaitre J. [160]	Concept of strain equivalence and general CDM theory
1972	Hayhurst D. [161]	Creep damage theory based on the internal state variable
1974	Leckie F. [162]	Creep damage theory based on the internal state variable
1975	Sidoroff F. [163]	Formulation of three-dimensional plasticity theory in a unified framework
1976	Dafallas Y., Popov E. [164]	Multidimensional stress space cyclic plasticity model based on the plastic internal variable
1977	Chaboche J. [165]	Description of cyclic viscoplasticity and damage behaviour using internal state variable
1978	Savalle S. [166]	Cyclic damage model based on the internal variable
1980	Murakami S., Ohno N. [168]	2 nd order tensor representation of creep damage variable along with anisotropic damage law
	Cordebois J., Sidoroff F. [169]	Three-dimensional damage and induced elastic anisotropy for elastic-plastic material
1981	Fonseka G., Krajcinovic D. [170]	A general theory of continuum damage mechanics for brittle materials
1982	Mazars J. [171]	Damage evolution for concrete structure and elasticity coupled damage theory
1983	Ladevèze P. [172]	Use of three independent scalar damage variables to describe the damage in composites
1985	Ortiz M. [173]	Rate independent damage model describing anisotropic elastic degradation of concrete
1987	Simo J., Ju J. W. [174]	Elasto-plastic damage model constructed in both stress and strain space
	Chow C., Wang J. [175]	Anisotropic damage evolution for ductile fracture of aluminium alloy
	Lesne P., Savalle S. [177]	Differential damage rule under fatigue and creep loading
	Chrzanowski M., Hult J. [167]	Time-dependent rupture model for linearly viscous ideal fibre bundles
1989	Benallal A. [178]	No hardening-damage coupling
	Chrysochoos A. [176]	Description of the dissipative phenomenon during the elastoplastic deformation process
1990	Taleja R. [179]	Characterization of damage as a second-order tensor field, the kinetic equation for stiffness –damage relationship and intralaminar cracking
1993	Voyiadjis G., Kattan P. [180]	Micromechanics based damage evolution in composite materials
1994	Saanouni et al. [181]	The hypothesis of Total Energy Equivalence

Table 3 Evolution CDM framework

The CDM framework is applied successfully to various materials including metal, rubber, concrete, soil, rock and composite [246]. Such a successful application was possible mainly due to a few concepts that define the effective variables for the continuum state. These concepts include-

- *Decomposition of the strain tensor*: It is assumed that for small deformations the total strain tensor is given by the addition of the elastic and plastic components.

$$\varepsilon_{ij} = \varepsilon_{ij}^e + \varepsilon_{ij}^p \quad \text{Equation 2}$$

- *Effective stress concept*: The effective stress is the stress acting on the unit surface diminished by the surface of defects. For the one-dimensional case, Rabotnov [159] introduced the effective stress concept as-

$$\tilde{\sigma} = \frac{\sigma}{1-D} \quad \text{Equation 3}$$

- *Principle of strain equivalence* [160] which states that “any constitutive equation of damaged material is derived in the same way as for the virgin material if the effective stress replaces the stress”.

The hypothesis of Total Energy Equivalence [181] The mechanical behaviour of damaged material in the current damaged configuration is derived from the state- and the dissipation-potential functions of the equivalent material in the fictitious undamaged configuration of by replacing the state variables in them by the corresponding effective state variables.

Similar to the area of fatigue phenomenon, the area of CDM is having an extensive scope and is interlinked to other mechanisms like elasticity, inelasticity, ageing, and thermal effects. Hence to get acquainted with this area, a systematic categorization of the scope of CDM application is needed. This categorization can be done based on damage type like brittle, ductile, creep, fatigue, and their coupling with other mechanisms[182], as shown in Figure 13.

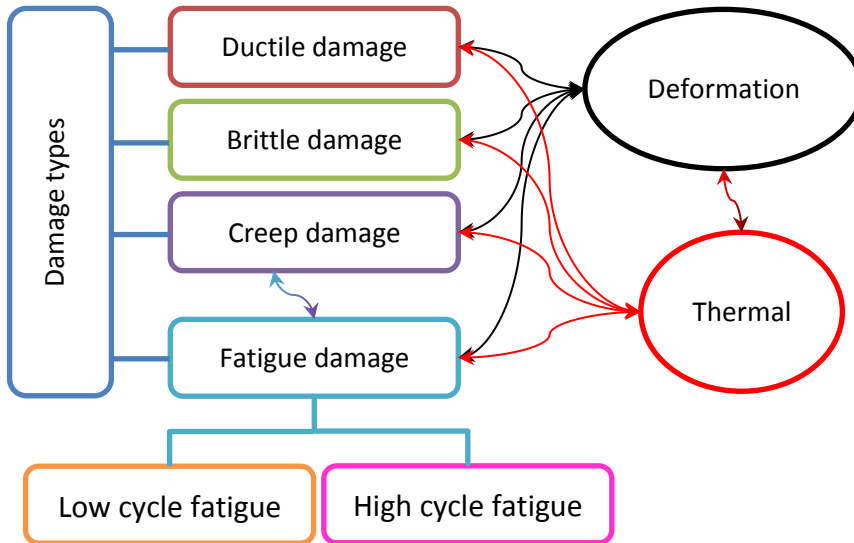


Figure 13 Categorization and coupling of the CDM framework

As the current thesis has its focus on fatigue damage, [Table 4](#) list only fatigue damage related evolution laws derived using the CDM framework over time in chronological order. For comparison purposes, the empirical linear damage accumulation law stated by Miner in 1945 is listed as the first law. Despite its low accuracy to capture non-linear damage accumulation, Miner's linear rule is used even today in most of the complex damage calculations. The main reason is its simplicity and ease in implementing various design environments.

1945	Miner M [183]	Linear damage accumulation law
1958	Kachanov L. [185]	Creep damage evolution in power-law form
1974	Chaboche J. [186]	First differential form of non-linear damage accumulation law (NLCD)
1979	Lemaitre J., Plumtree A. [187]	Coupled creep-fatigue non-linear damage evolution law
1982	Cordeois J. Sidoroff F. [191]	Anisotropic damage evolution law
1983	Ladevèze P [172]	Anisotropic damage evolution law + Difference in tension and compression behaviour
1984	Lemaitre J. [188]	Potential of dissipation based coupled and uncoupled elasticity-damage evolution law
1987	[189]	Damage evolution law for low and high cycle fatigue separately
1995	[190]	Damage evolution law for very low cycle fatigue
1999	[405]	Two scale damage evolution law based on micromechanics
1990	Tiejun W., Zhiwen L. [192]	Lemaitre model (1984) + some initial and final damage
1991	Jessen S., Plumtree A. [193]	Chaboche model applied to pultruded glass/polyester rods
1991	Chow C. et al. [194]	Anisotropic damage evolution law + elasticity and plasticity coupled with damage
1991	Arnold S., Kruch S. [195]	Extension of Chaboche model for initially isotropic and anisotropic material
1993	Paas et al. [196]	Damage potential in the power-law form relating to equivalent strain and damage
1996	Cheng et al. [197]	Modification of dissipation potential given by Lemaitre (1984) to include loss of ductility
1998	Voyiadjis G., Echle R. [198]	Damage evolution law defined at micromechanics level for metal matrix composite
2000	Peerling et al. [199]	Modified Pass et al. methodology
2001	Abdel Wahab et al. [200]	Lemaitre model applied to fatigue of adhesively bonded joints
2010	Khonsari et al. [201]	Damage evolution law based on entropy production
2019	Pandey et al. [202]	Modified Abdel Wahab model by using damage evolution law in exponential form

Table 4 Timestamp overview of damage evolution law derived for fatigue loading

With the help of the CDM framework, damage evolution and its coupling with deformation (as shown in [Figure 13](#)) can be described. Under fatigue loading, the material deforms in various ways; hence a unified framework is required to describe all these deformation mechanisms. The theory of elasticity addresses the elastic deformation, while the cyclic inelasticity theory addresses the inelastic deformation under fatigue loading. The next section gives a brief introduction to this cyclic inelasticity theory.

1.2.5 Cyclic inelasticity theory

Inelastic deformation in the physical sense means irreversible changes in microstructure that do not lead to the generation of discontinuity during the deformation process. Under non zero mean stress cyclic loading, materials show more changes in microstructure than monotonic loading because of the presence of two loading situations. The cyclic amplitude load is superimposed on to constant minimum stress (except the tension-compression loading). As a result of an additional change in microstructure, the material shows either hardening/softening or no change in response to applied loading in the subsequent cycle. The elastic domain defines the threshold state of material between elastic and inelastic deformations and is represented as a surface in the space of stresses, illustrated in [Figure 14 \[203\]](#).

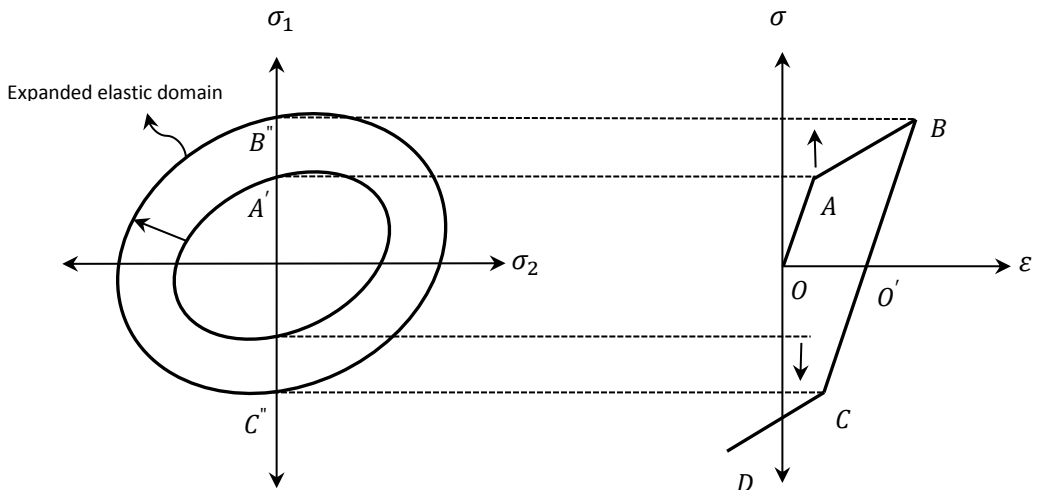


Figure 14 Schematic of isotropic hardening during reverse loading showing (Left) expansion of the elastic domain in 2D space of principal stresses and (Right) the resulting stress-strain curve

When this elastic domain expands or contracts uniformly in all directions as a result of prior loading, then the material is said to be isotropically hardened or softened. [Figure 14](#) gives a schematic of this behaviour after Dunne and Petrinic [203 P.28]. In this figure, the elastic domain considered has a constant value in both tension and compression loading. When the material is reloaded from point O' in tension, it starts inelastic deformation at a stress level of point B instead of point A whereas, in the previous loading, it started at point A. When the material is loaded from point O' in compression, it shows inelastic deformation at a stress level of point C. The stress

level at both points B and C are higher than stress levels of previous loading point A. This expansion is called isotropic hardening.

When the elastic domain is translated to new space of stresses without change of shape or size as a result of prior loading, then this type of hardening/softening is referred to as kinematic hardening/softening. Figure 15 gives a schematic of this behaviour after Dunne and Petrinic [203 P.28]. When the material is reloaded from point O' in tension, it starts inelastic deformation at a stress level of point B. As a result of an increase in the elastic domain at the tension side, the elastic domain at the compression side decreases since the elastic domain is not changing its shape or size. When the material is loaded from point O' in compression, it shows inelastic deformation at a stress level of point C that is lower than previous loading point A. This lowering of stress level in compression due to gain in previous tension loading is called Bauschinger's effect. Section 2.1.2 gives the physical sense of this effect for composite materials.

When the elastic domain is translated to new space of stresses with a change of shape or size due to previous loadings, then this type of hardening/softening is referred to as mixed hardening/softening.

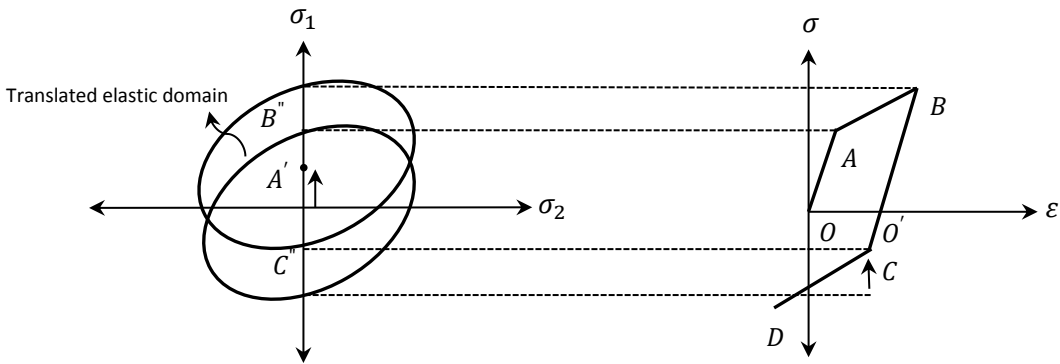


Figure 15 Schematic of kinematic hardening during reverse loading showing (Left) translation of elastic domain in 2D space of principal stresses and (Right) the resulting stress-strain curve

The inelastic strain consists of two parts: plastic and viscous component. The plastic strain evolution is associated with certain limited stress intensity, and the mathematical formulation is based on the rate-independent formalism [204, 205]. This theory is known as cyclic plasticity theory. If the viscous component is present in the

deformation, then the mathematical formulation needs to be adapted for rate-dependent base, and this theory is known as cyclic viscoplasticity theory [205, 206]. In both theories, the mathematical formulation consists of the following steps [203, 207] -

- a) First define the elastic domain, that gives a boundary to the linear elastic region.
- b) Formulation of flow rule that describes the relationship between stresses and strains development post elastic region.
- c) Application of consistency condition to get the direction of stresses.
- d) Formulation of hardening/softening rule to define change of loading surface during flow.
- e) Determination of inelastic modulus, and
- f) Calculation of stresses and inelastic strains.

In almost all materials, Hook's law characterizes the elastic response and the Ramberg-Osgood law [422] characterizes the plastic response. Hence generalization in the elastic domain and flow rules expressions are possible for most of the materials and derived using thermodynamic potentials. Section 3.3 gives the derivation of the elastic domain and flow rule in detail. Unlike the elastic response, the post elastic region (hardening/softening) behaviour for multimillion cycles is different for every material. Hence, the generalization of the hardening rule is not possible. So far, an earlier proposed hardening rule from literature is modified to address the changes and differences from new materials. Due to this, over time, one can see an evolution in hardening/softening rule formulation, as shown in Table 5. To the author's knowledge, there exists no hardening/softening rule for high cycle fatigue situations, and the field of cyclic inelasticity is still an active field of research.

1923	Masing G. [208]	Approximation for cyclically stabilized material behaviour
1956	Prager W. [209]	Linear kinematic hardening rule (LKH)
1959	Ziegler H. [210]	Modification of Prager rule
1966	Armstrong P., Frederick C. [211]	A first non-linear model with recall or dynamic recovery' term (NLKH)
1967	Mroz Z. [212]	Multilinear model, based on the two-surface model
1975	Dafalias Y., Popov E. [213]	Improvement of Mroz model
1979	Chaboche J. et al. [214]	decomposed NLKH + isotropic hardening linked to strain history via internal variable
1991	Chaboche J. [215]	Chaboche model (1979) + recovery term with power function or with a threshold
1985	Tanaka et al. [216]	Effect of strain path shapes and histories under non-proportional multiaxial loading
1986	Burlet H., Cailletaud G. [217]	NLKH + variable temperature
1987	Benallal A. Marquis D. [218]	NLKH + Isotropic hardening variable including non-proportionality
1989	Bower A. [219]	NLKH + second kinematic variable for decreasing ratchetting rate
1992	Guionnet C. [220]	NLKH + dynamic recovery term
1993	Ohno N. Wang J. [221]	Chaboche model (1979) + critical activation state for recovery term
1995	McDowell D. [222]	Ohno-Wang model + critical activation state to non-coaxiality
1996	Calloch S., Marquis D. [223]	Benallal-Marquis methodology + Tanaka
	Jiang Y., Sehitoglu H. [224]	Ohno-Wang model + critical activation state to non-coaxiality
1998	Voyiadjis et al. [225]	Chaboche (1991) + direction of the stress rate
2000	Abdel-Karim M., Ohno N. [226]	Blend of NLKH + Ohno-Wang model
2002	Yoshida F., Uemori T. [227]	Isotropic hardening + kinematic hardening describing Bauschinger effect
2002	Bari S., Hassan T. [228]	Chaboche model [1991-94] + Burlet-Cailletaud model
2003	Doring et al. [229]	Isotropic + kinematic hardening for multiaxial non-proportional cyclic loading
2002	Kang et al. [230]	Ohno-Wang model with memory function + isotropic hardening
2003	[231]	Ohno-Wang model + change in the elastic domain due to the evolution of plastic strain
2005	[232]	Ohno- Abdel-Karim model + Temperature dependent parameter
2006	[233]	Kang et al [2005] + isotropic hardening
2009	[234]	Kang et al [2006] + damage-coupling
2005	Chen et al [235]	superpose the Ohno-Wang model upon the Burlet-Cailletaud model
2006	Halama et al. [236]	Ohno- Abdel-Karim model + non-proportional term in ratcheting parameters.
2009	[237]	Ohno- Abdel-Karim model + Calloch and Marquis model
2019	[238]	Chaboche model + Jiang-Sehitoglu memory surface
2013	Varvani-Farahani et al [239]	Improved Bower model by involving new ratcheting rate coefficients

Table 5 Timestamp evolution in hardening rules in cyclic inelasticity

Over the last 40 years, many researchers combined the framework from CDM with the cyclic inelasticity theory to build a comprehensive mathematical formulation for various materials and loading conditions. [Table 6](#) gives a list of reviews capturing all the work done in the area of CDM and cyclic inelasticity.

1981	Konig J., Maier G. [240]	Review of recent developments in the shakedown analysis of elastoplastic structures
1986	Chaboche J. [241]	Review of time-independent constitutive theories for cyclic plasticity
1987	Murakami S. [242]	Classification and bibliography of material damage on the microscale, Damage variable nature
	Chaboche J. [243]	Damage definitions and measures, damage growth equations and anisotropy effects and use of CDM for local approaches of fracture
1999	Skrzypek J., Ganczarski A. [244]	Classification and bibliography of material damage on the microscale
2003	Pandeya et al. [245]	Review of deformation based temperature rise
	Skrzypek A. [395]	Trends review in damage mechanics
	Betten J. [395]	Classification and bibliography of material damage on the microscale
2006	Desmorat R. [246]	Application of CDM framework to concrete, elastomers, rocks, and other materials
2007	Ambroziak A., Klosowski P. [247]	Trend review in isotropic damage evolution
2008	Chaboche J. [248]	Review of some plasticity and viscoplasticity constitutive theories
	Kang G. [249]	Ratchetting: Recent progress in phenomenon observation, constitutive modelling and application
2010	Horstemeyer et al. [250]	Historical review of internal state variable theory for inelasticity
	Amiri M., Khonsari M. [251]	Review on thermodynamics of friction and wear
2015	Ohno N. [252]	Review of material models of cyclic plasticity with extended isotropic hardening
2017	Hashiguchi K. [253]	Critical reviews and assessments of cyclic plasticity models
2018	Farahani et al. [254]	Review on ratcheting in pressurized pipes and equipment
2019	Paul S. [255]	Review of experimental aspects in ratcheting fatigue

Table 6 Timestamp overview of reviews done in the area of CDM and cyclic inelasticity

So far, in this section, various frameworks that have been adopted in the field of fatigue analysis are discussed. Based on this discussion, the scope and methodology for this thesis can now be formulated, bearing in mind that the goal of achieving a detailed understanding of material behaviour and life prediction at any damage state under fatigue loading for wind turbine blade materials.

1.3 Scope and methodology

As discussed in section 1.2.2, the traditional framework for fatigue analysis is going through a continuous evolution to expand understanding of material behaviour. However, for the traditional framework achieving a detailed understanding of material behaviour is still a target to achieve due to following shortfalls-

- The fatigue life prediction includes only the final damage state and not the intermittent damage states.
- The fatigue life prediction lacks both qualitative and quantitative description of associated different mechanisms and their coupling.
- The mathematical formulation is not consistent for different scales and requires test programs and test results analysis at every scale. This process is costly and time-consuming.

As new materials are explored continuously for new technologies in wind turbine blade manufacturing, it is vital to understand these materials behaviour in a detailed manner. Here, the use of another framework can be explored to achieve better understanding. In the previous section, we have seen that the thermodynamic theory and CDM framework have been applied successfully to many material types and variety of applications, but not yet applied to the wind turbine blade materials. For this thesis work, the scope is defined to identify the potential of thermodynamic theory and CDM framework to understand the fatigue behaviour of wind turbine blade materials. Application of another framework requires that it can address the shortfalls of the existing framework. We can rise a research question against each of the shortfalls from the traditional framework, and around each question, a specific objective can be defined as follows.

- Estimate fatigue life not only at final damage state but also any intermittent damage state.
- Provide both qualitative and quantitative description of different mechanisms involved in fatigue phenomenon.
- Formulate consistent mathematical formulation valid for multiple scales.

The CDM framework potential can be judged based on answers provided against these questions. For the construction of a mathematical framework, specific scales in the building block approach and their associated theory needs to be selected. The blade laminate and subcomponent scale are selected as the area of focus for this

thesis work. In these two scales, many material configurations are possible that can be incorporated in blade design. These material configurations are constructed using monolithic and sandwich laminate to meet the end requirements. [Figure 16](#) gives the general features of these laminates. After checking the potential of CDM frameworks to address these research questions for the selected scale, this framework can be further developed and expanded to the complex situations in the blade section and finally to the full-scale blade. The scope of this thesis work is limited to the application of thermodynamic theory and CDM framework to the selected scales only.

As a first step, various configurations from monolithic laminate types are selected as almost all load-carrying elements in the blade are made from them. This scale provides the basis for future work of applying the framework to the next scales within the building block. From the subcomponent scale, a ply drop configuration is selected because, in ply drops, the damage mode predominantly consists of single crack development at the interface of ply drop. Whereas in other configurations multiple damage mode exists in the individual constituents of the configuration. [Section 4.1.1](#) gives further details of selected material configurations.

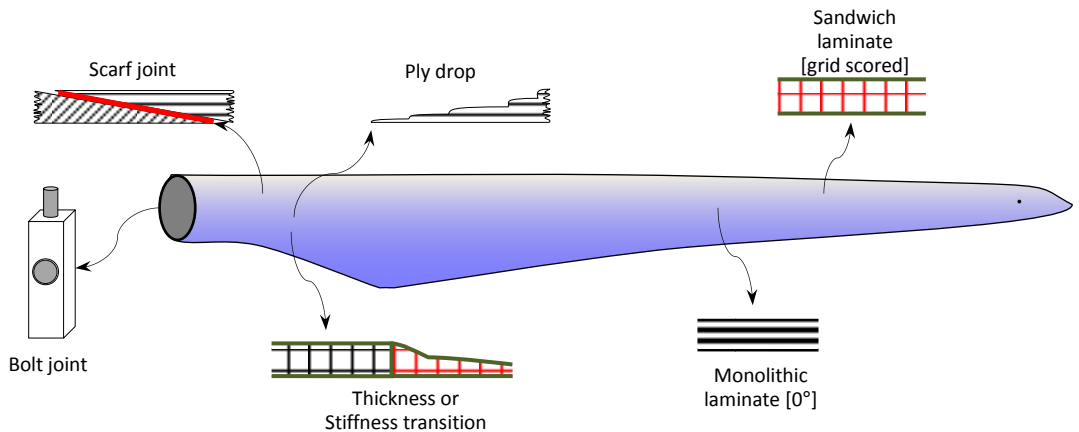


Figure 16 Laminate and subcomponent scales of blade materials

The theory developed for both these scales is a continuum based. The micromechanics based formulation is not considered in this study because even though this formulation is available for all mechanisms involved in the fatigue phenomenon, its application to laminate and higher scales (macro) is not yet convincingly demonstrated [[256, 10](#)].

A mixed methodology is followed to construct the mathematical formulation. At first, a physics-based methodology is followed to demonstrate that the governing theories for different mechanisms are indeed providing the most representative explanation of materials behaviour (section 2). Next, in section 3.1, a generic mathematical formulation that applies to overall fatigue phenomenon is given. The formulation starts with fundamental laws and leads to the derivation of constitutive laws for mechanisms under consideration. The elasticity, fatigue damage and their coupling are introduced in the framework using the consistent mathematical formulation, whereas the plasticity and its coupling with fatigue damage included empirically. The thermal and viscous contributions and its effects on other mechanisms are ignored, assuming their contributions to be very small.

2

Theory of fatigue phenomenon

The previous chapter summarizes the past work done in the area of fatigue analysis. In this chapter,³ the focus is on describing a governing theory related to the fatigue response of wind turbine blade materials. It starts with a systematic categorization of the different mechanisms playing a role in fatigue phenomenon and providing their detailed description. This theory forms the basis for the amount of detail to be considered in the mathematical formulation.

³ Parts of this chapter have been published in [2]

Fatigue phenomenon is associated with underlying deformation and damage mechanisms. Figure 17 gives a schematic view of all the mechanisms involved and their subcategorization, and their detailed description is given in the next subsections.

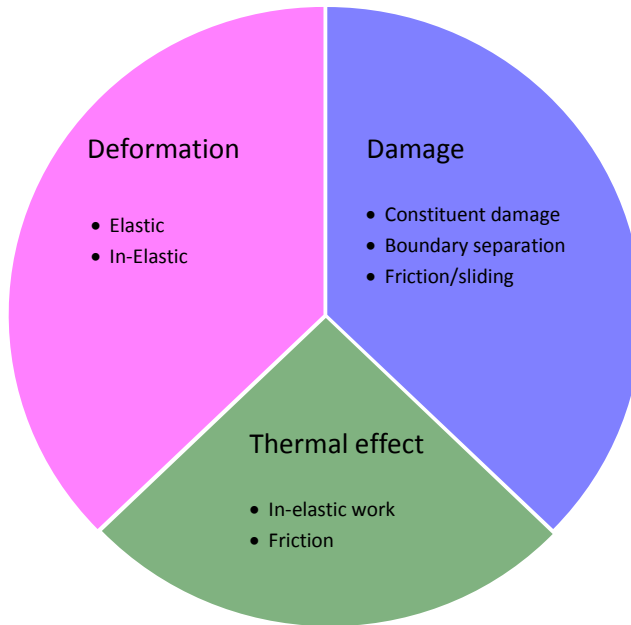


Figure 17 Fatigue phenomenon and associated mechanisms

2.1 Deformation mechanism

The theory of deformation mechanism in various materials and the governing laws associated with them were well established over the last century. The timestamp overviews provided in Table 1 to Table 6 outlines those citations and their successful application to respective materials. This general theory of deformation mechanism is rewritten here in the context of composite materials.

During deformation under external loadings, either instantaneously or cyclically, material changes its state from a lower energy level to higher energy level, and this energy gets stored in its atomic or molecular structure. It is this energy that tries to bring the material back to its original state once the external loadings diminish. The return path of material from a higher state to its original state consists of two portions.

- Elastic deformation

- Inelastic deformation

This categorization helps in defining thermodynamic potential in a most representative way and is discussed further in the mathematical formulation chapter, i.e. chapter 3.

2.1.1 Elastic deformation

The recoverable part of a change in internal energy is responsible for elastic deformation and is considered a fully reversible mechanism. This energy result only in atomic bonds stretching, rotation, and vibration, which are reversible in nature. It also means all the strain endured during this loading is recoverable, refer to [Figure 18](#). This mechanism is present in both homogeneous materials like pure metals and also heterogeneous material like composites. As a result of a reversible change of state of the material, even though material experiences rise in temperature due to change in internal energy, there is no heat dissipated or loss during the elastic phase for any number of cycles. Of course, this is an ideal situation, but the description of this state is the first step towards comprehensive mathematical formulation.

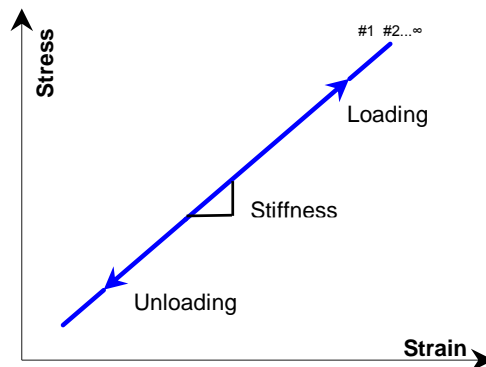


Figure 18 Elastic deformation

2.1.2 Inelastic deformation

The deformation caused by the microstructural changes that do not lead to discontinuity or macro-scale void generation in the phase but results in a permanent change in microstructure compared to its original state is called as inelastic deformation. The non-recoverable part of a change in internal energy is responsible for inelastic deformation. A specific branch in mechanics of deformation evolved to study this mechanism under cyclic loading and is known as cyclic inelasticity.

Here the inelastic part represents both loading intensity-dependent (plastic) and independent mechanism (viscous). Due to this broad definition, the inelastic

deformation manifests itself in different ways in stress-strain space, see [Figure 19](#). The inelastic response is associated with the dissipative effects of microstructural material degradation, stored energy variations, and thermal coupling [[257](#), [258](#), [259](#), [260](#)].

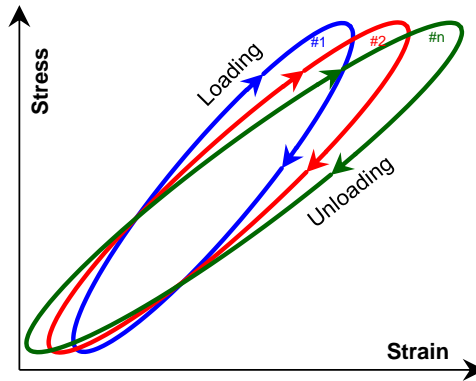


Figure 19 In-elastic deformation resulting in the formation of hysteresis and its translation

One persistent manifestation of inelastic deformation is the formation of a hysteresis in stress-strain space. The hysteresis curve represents a non-recoverable part credited over the loading-unloading stage in a given time. Understanding the cause of this hysteresis provides necessary input during the mathematical formulation of fatigue.

During the fatigue test (except the tension-compression), two loading situations exist, the superposition of a cyclic amplitude load on to constant minimum stress. Due to the presence of a constant load, the non-recovered part does not get reverse fully. This small amount of non-reversible part from the earlier cycle makes the loading application path in the next cycle differ from the previous one, and as a result, the hysteresis curve translates to a new space [[262](#)]. In cyclic inelasticity, this translation is known as a hardening or softening mechanism.

Physically in composite materials, the hardening or softening arises as a result of microstructural changes in the soft phase (matrix system or the interface of fibre and matrix). These changes are caused by entropic resistance to align the molecular network or to undergo significant collective molecular movement towards loading direction by matrix or interface and shows load as well as volume content dependency [[261](#)]. Higher load dependency obviously introduces higher elastic and inelastic deformation. The volume content of the soft phase determines the amount of inelastic deformation getting generated over the cycle. For low volume content, the inelastic deformation is more significant as the fibre contributes only to elastic deformation [[437 Ch 5](#)].

Depending on the control mode of loading, and on the material type, the translation of the hysteresis curves can be different. This difference is schematically illustrated by Lemaitre and Chaboche [263 P.111] and shown in Figure 20.

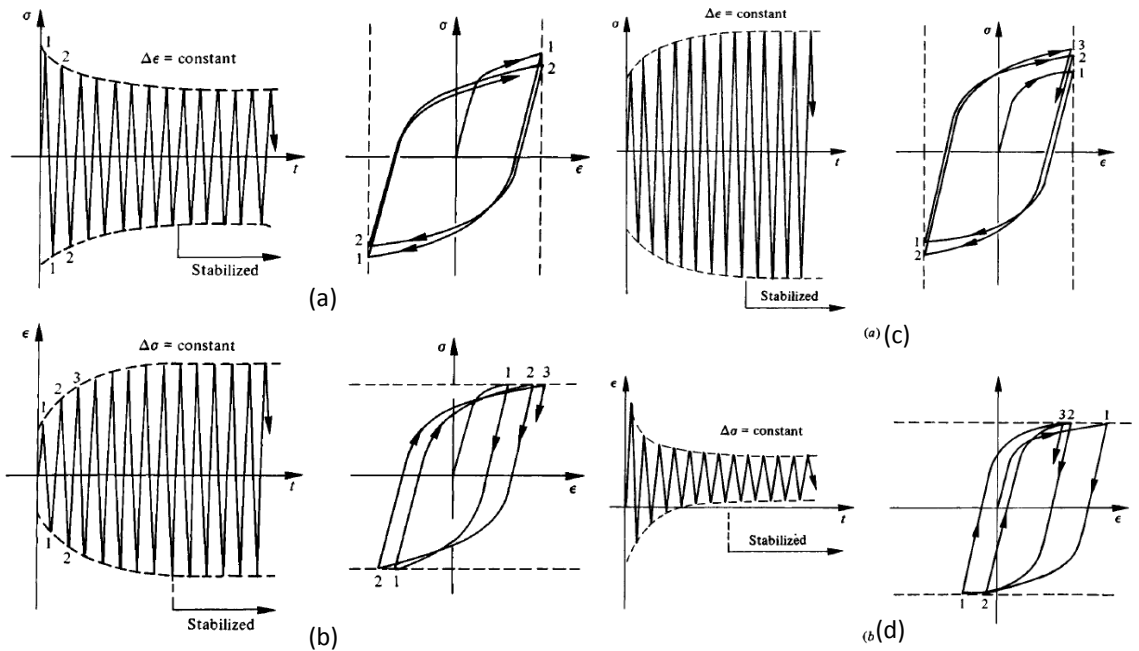


Figure 20 Cyclic softening (left) and hardening (right); (a, c) strain-controlled and (b, d) stress-controlled [263]

In general, thermoset composite materials show cyclic softening behaviour [264].

The rate of translation of hysteresis curves in subsequent cycles does not always remain constant, and it depends on applied constraints [56]. Two different types of translation of hysteresis curves reported in the literature. In one case, the strain progresses with a reduced rate and finally stops after stabilization, leading asymptotically to elastic or plastic shakedown [265]. As a result, the hysteresis loop can be traced over and over again in subsequent cycles. While in another case, the strain progresses with constant rate and referred to as strain ratcheting. Due to persistent strain addition, ratcheting is the most critical situation in engineering applications. The schematic representation of shakedown and ratcheting is given by Lemaitre and Chaboche [263 P.113] and shown in Figure 21.

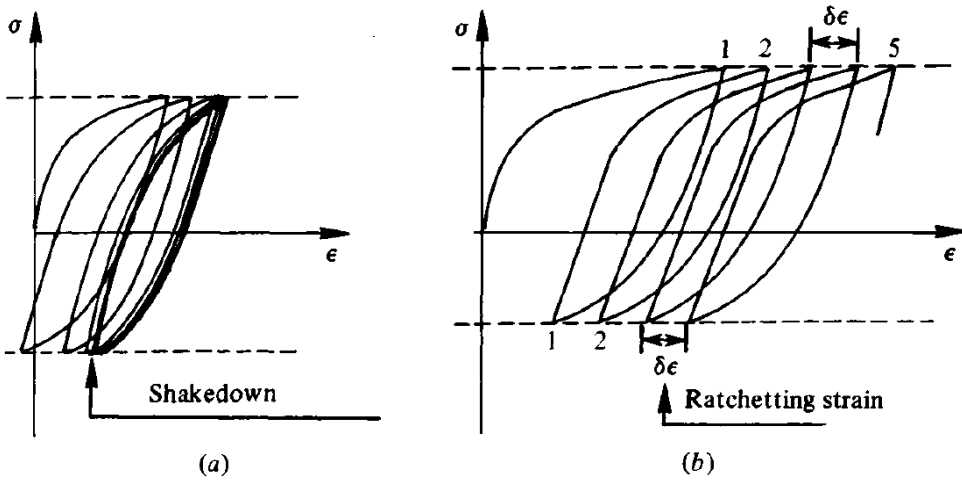


Figure 21 Mechanism of (a) shakedown (b) strain ratchetting under stress-controlled fatigue test[263]

Consider now two cases of fatigue loading viz. load controlled and displacement controlled condition applied to materials. Figure 22 schematically shows the strain ratchetting characteristic of materials under load controlled condition. Here the translation of the hysteresis loop in strain space is given for various stress ratios showing different translation behaviour of hysteresis curves. Similarly, Figure 23 illustrates the stress relaxation characteristic of materials under displacement controlled condition, here the translation of the hysteresis loop in stress space is given for various strain ratios showing different translation behaviour of hysteresis curves. Identifying the dependency of this softening characteristic on various parameters is a crucial aspect in the understanding of fatigue behaviour of given material.

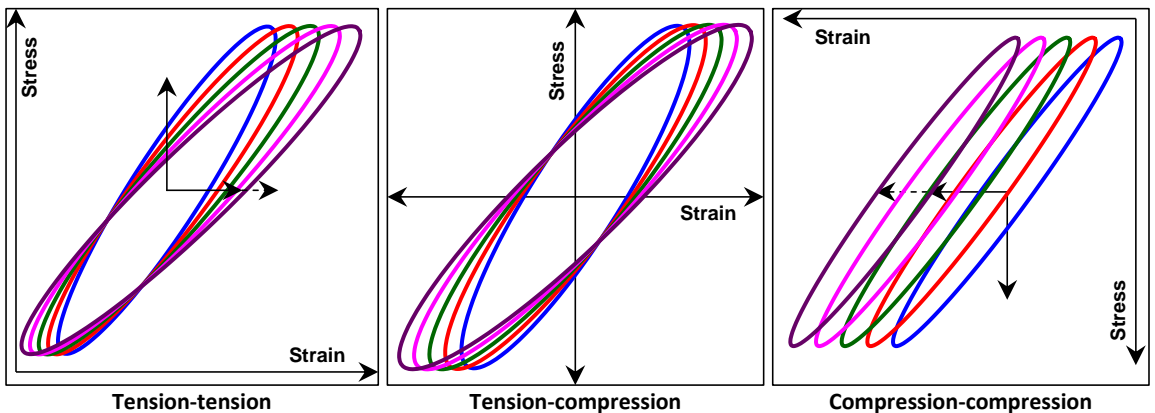


Figure 22 Translation of hysteresis under load controlled test

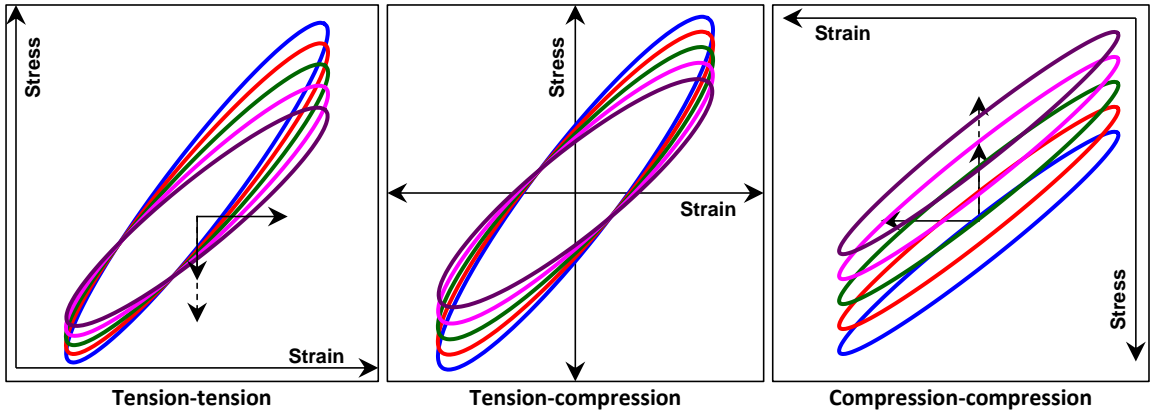


Figure 23 Translation of hysteresis under displacement controlled test

During fatigue tests, when both tension and compression loads are present, the development of inelastic strain during the compression loading is influenced by tension loading and vice versa. Composite materials consist of two or more constituents with different mechanical properties. As a result when the material undergoes the same pre-strain in one direction, and if this strain is sufficiently high, inelastic deformation occurs in the constrained phase or component with lower elastic limit, while the other one behaves elastically. For example, during the tension loading path, the material undergoes microstructural changes resulting in inelastic strain development in the softer phase. On un-loading, when the applied load is zero, one phase or component is in tensile stress, and the other one is in compressive residual stress.

On reloading in the same direction, to the same stress level, both behave elastically; but on reloading in the opposite direction, the residual stress in the softer phase helps the applied stress to cause premature inelastic strain development. Thus the behaviour is asymmetrical, and the material is softer for the reverse loading than it was in an original state. Due to this, the material appears softer in compression due to tension loading. This direction-dependent, asymmetrical softening behaviour is known as Bauschinger's effect [211, 266]. Figure 15 gives the schematic illustration of this effect.

2.2 Damage mechanism

At any stage during the application of cyclic external loading, a weak section within the material (if any) leads to a discontinuity or void generation in respective material phases or interfaces. The microstructure is no longer able to sustain the change in the state due to atomistic or molecular or micro-scale bond failure. In the case of composite materials, it may be the failure of the matrix atomistic bonds or matrix chain entanglement breakage or interface delamination. This discontinuity is referred to as damage.

An extensive amount of literature is available on different damage mechanisms observed in composite [267, 268, 269, 270, 271, 272]. The overall damage development is highly complex, due to the presence of different damage mechanisms with strong unilateral features and their interactions. Hence, characterization of damage at microscale requires the development of mathematical formulation with anisotropic and unilateral damage evolution. Whereas at macro scale by ignoring the detailed microstructure, the discontinuity introduced into the displacement field can also be ignored, and the mathematical formulation can be constructed using continuum theory [275].

The various damage mechanisms observed during fatigue testing of composite materials can be categorized as follow-

- Constituent damage
 - Microcracking
 - Chemical degradation
 - Crazeing
 - Fibre breakage
- Boundary separation
 - Fiber-matrix interface debonding
 - Inter-tow or inter-ply delamination
 - Interface cracking
- Friction/sliding at debonded or delaminated interface

Figure 24. illustrate a few of these damage mechanisms.

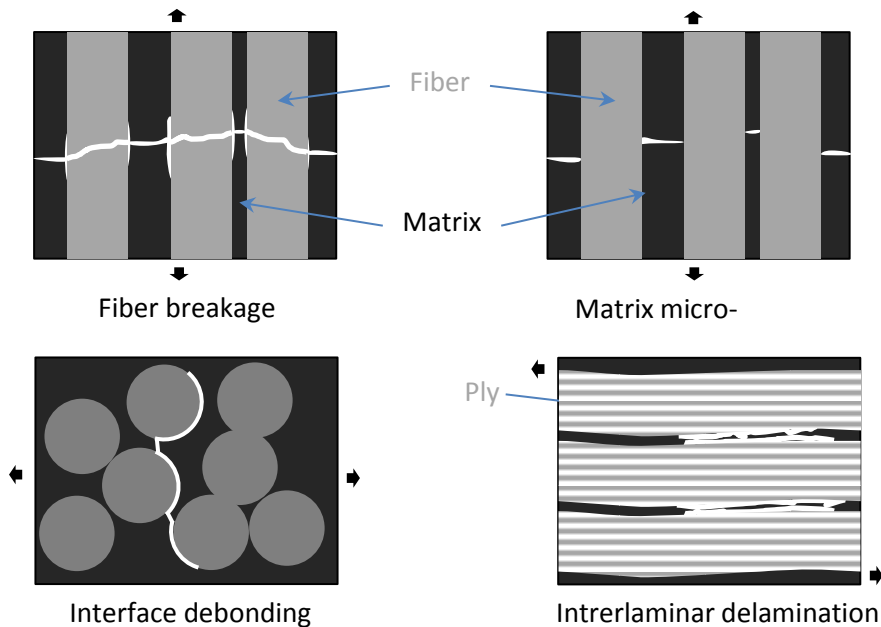


Figure 24 Schematics of various damage mechanisms

One key feature of damage development under fatigue loading is its stochastic nature. During fatigue testing for any two coupons from the same material configuration and under the same test conditions, the damage development is not similar. In composite materials, the stochastic nature of the damage is associated with many factors; some of them are listed below. The characterizing influence of each factor has received considerable attention in the literature, and most relevant references are cited here along with the factors given.

- Sources for variation in constituents properties
 - Fiber-matrix interface [276, 277, 278, 280]
 - Constituent molecular composition variation [281, 282, 283, 284, 285, 286]
- Sources for Micro and/or meso scale inhomogeneous structure
 - Ply architecture [287, 288, 289, 291, 292, 293, 294, 295, 296, 297, 298, 299]
 - Fiber volume fraction variation [290, 292, 319, 321]
- Sources for geometric (macro-scale) inhomogeneous structure
 - Ply drop [300, 301, 302, 303, 305, 306, 307, 308]
 - Thickness taper [304, 309, 310, 311, 312]
- Variability in coupon manufacturing conditions
 - Process settings like time, temperatures and pressure [315, 316, 317, 318, 320]
- Variability in test conditions
 - Loading frequency and pattern (sine, triangular or square wave) [313, 314]
 - Control mode (load and displacement)

Due to these factors, for composite materials, generating correct damage mode in the specific areas for all loading situations is still a target to achieve [355, 356, 357, 358, 359, 360, 361, 362, 363, 364].

2.2.1 Development

Even though the contribution of each damage mechanism to final failure is highly dependent on the specific composite and its lay-up, it is possible to identify certain general features. Many researchers reported generic features of damage evolution for a variety of composite materials under different loading conditions [268, 271, 272, 273, 274, 322, 323, 324, 325, 326]². Generically the damage evolution is categorised in the following successive three stages:

1. **Initiation stage:** In the case of tensile in-plane load transfer, this stage consists of the formation of random micro-cracks in the matrix and at the off-axis fibre/matrix interface. Under compressive loading, the cracks generated under tensile load either close or for sufficiently large debond angles result in the propagation of the already debonded crack. Due to this, under fatigue loading, material stiffness rapidly drops over a small percentage (<15%) of life compared to total life. In the case of interlaminar load transfer situations, like ply drop or interlaminar shear, this stage may not exist. The deterioration of the interface at the interlaminar load transfer boundary shows a damage initiation threshold with deformation [327]. Hence no macro-scale damage may be observed until that critical deformation.
2. **Progression stage:** During this stage under tensile loads, the micro-cracks saturate over the loaded area. This area further experiences friction due to sliding and heat generated thereof. Different micro-cracking mechanisms can occur: micro-cracks can develop parallel or orthogonal to the fibres or even orthogonal to the loading direction. Under compression loads, a secondary effect due to the inelastic deformation of the matrix starts to appear. Due to the inelastic deformation of the matrix, it is no longer supporting nearby fibres and leads to the micro buckling of fibres. As most of the weak spots are exhausted during the initiation stage, the property drop at this stage is more gradual, and the length of this stage can extend up to 70% of the total life. For the interlaminar load transfer situation, the interlaminar boundary starts showing deterioration once critical deformation is reached (a delayed initiation). Once the damage generates at the interface, it propagates very rapidly through the already deteriorated region, making the length of this stage small and very close to the fracture stage.

3. **Fracture stage:** During this stage, under tension loads, the saturation of micro-cracks leads to interlaminar delamination in the interior of a laminate. The growth of interlaminar delamination is driven by strong interlaminar stresses in the region where these intra-laminar micro-cracks cross. If the loads are sufficiently high, then it results in fibre breakage, and fracture of coupon occurs. Under compression loads, global buckling is observed in fibres or even in gauge length due to the loss of main load-carrying elements. During this stage, material properties drop very steeply over a short period (<15% of total life).

Reifsnider [268] presented the first generic graphical form for damage development. Figure 25 gives a similar representation.

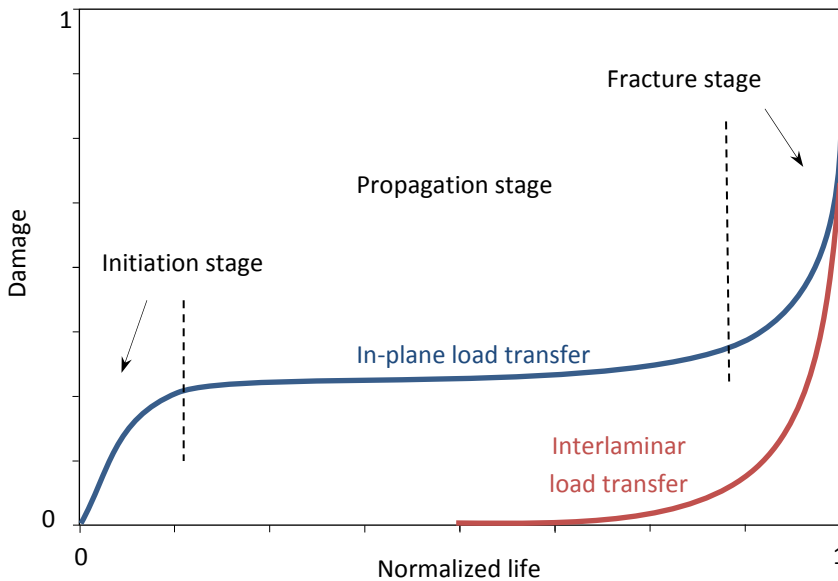


Figure 25 Generic damage development stages

In the literature on homogeneous materials, two distinct types of fatigue damage growth are reported due to their peculiar nature: Low cycle fatigue damage driven by inelastic deformation and high cycle fatigue damage governed by elastic deformation. In composite materials, such difference exists only when the fibre-matrix interface formed is having similar or higher performance than the matrix leading to the formation of cohesive type damage development. In general, the interface formed is weaker than the matrix, hence damage is an adhesive failure at the interface and occurs before the loads reach the elastic limit of the matrix (soft phase) [276, 277, 278,

280]. As a result, composite materials show damage driven by both elastic and inelastic deformation.

2.2.2 Measurement of damage

As damage is not a material property, its measurement is done in indirect ways and depends on the end-use of the analysis. The measurement of the damage is done through various parameters which show damage dependency. Lemaitre et al. [328] gave a comprehensive summary of these parameters. This section gives the details of a few other parameters and their range of usability.

2.2.2.1 Strain energy

Since the early 20th-century, development in strain energy trend is used to understand the response of materials to applied loading. In metal fatigue, various studies have been performed to understand the effect of mean stress, low and high cycle fatigue and ambient temperature [329, 330, 331, 332, 333, 334, 335, 336, 337, 338, 339, 340, 341, 342, 343, 344, 345]². These studies concluded that in metals, the inelastic strain development is the cause of fatigue damage and that the strain energy shows a power-law type relationship with final life.

Strain energy is also proposed as a damage measure [346, 347, 348, 349, 350, 351, 352, 353, 354] for many other materials. The area encapsulated in the hysteresis curve is referred to as inelastic strain energy. As illustrated in Figure 22 and Figure 23, the hysteresis curve shows translations in stress-strain space for some stress/strain ratios. This translation is also part of the total dissipation potential that materials exhibit along with the formation of the hysteresis curve. Hence using inelastic strain energy, only the hysteresis curve, as a representation of dissipation potential is not sufficient. The selection of inelastic strain energy as a damage measurement applies to situations where the hysteresis curve does not translate in stress-strain space and only changes its shape (size and orientation). Section 4.3 gives a few more peculiar observations regarding this strain energy.

2.2.2.2 Stiffness (Global)

Stiffness⁴ is the most commonly used parameter for damage representation. The exactness of damage representation using stiffness depends on the strain sensor type, and the location of the damage over coupon length. If the area of damage accumulation and strain measurement is the same, then the stiffness represents damage accurately. Vassilopoulos [65] gave a brief review of strain sensors and their

⁴ The term 'Stiffness' used in this thesis refers to extensive property of a material configuration.

usable ranges in fatigue testing of composites. Stiffness calculated based on strain sensors that measure an average strain over the entire specimen length (global stiffness) seems like representing damage more accurately. Section 4.2.2.2 presents and discusses the results from strain sensors used in this work. The expression for the damage parameter 'D' using stiffness is as follows.

$$D = 1 - \frac{\tilde{E}}{E} \quad \text{Equation 4}$$

Where

\tilde{E} is the stiffness of damage state

E is the stiffness of non-damage state

2.3 Thermal contribution

Materials change their state (e.g. glassy to rubbery) and hence deformation behaviour under certain thermal conditions. These conditions can be applied externally, for example, testing at elevated temperature, or they can be generated internally as in case of fatigue testing. Due to applied loading, the material's internal energy increases, leading to a rise in temperature. During unloading, as material response lags, this rise in temperature does not get reverse completely and accumulate as heat within material. For composite materials, the polymer matrix is most sensitive to thermal effects, as its transition from glassy to rubbery state occurs at a much lower temperature than most of the fibres. The fibres, except natural fibres, are formed at extremely high temperatures and hence shows the transition in state at a much higher temperature.

In the case of wind turbine blades, the matrix is made of a thermoset polymer material (epoxy/polyester/polyurethane), which shows a transition from glassy state to rubbery state at temperatures a few tens of degrees higher than the maximum operating temperature of wind turbine blades. During operations, due to low rotation speed, the wind turbine blade experiences fatigue loads at well below 1Hz frequency. When the frequency and load levels during material testing are higher than operational conditions, then thermal contribution needs specific considerations in the analysis.

Many researchers studied the thermal contribution due to cyclic loading [365, 366, 367, 368, 369, 370, 371] along with the mathematical formulation and experimental quantification. In the case of damage generated in the gripping area of the composite

specimens, the heat source could very well be the result of a gripping effect [360]. This gripping effect is a result of clamp pressure and tab design. The tabs are applied on the specimen so that loads can be introduced in the gauge area without damaging its surface. However, at the tab end, the clamping pressure and load introduction create a stress concentration and many times, the damage gets initiated at this point. Hence careful consideration or avoidance of gripping effect is required.

The thermal contribution is not considered in this study, as its contribution is assumed to be very small. During all fatigue tests, an air blower was placed near the coupon surface to keep the temperature within $\pm 10^{\circ}\text{C}$ range to that of the test start temperature.

2.4 Coupling between different mechanism

Section 1.2.4 mentions the coupling between different mechanisms observed due to change in microstructure. As these mechanisms coexist with each other, their interaction needs to be considered in the theory, to develop the appropriate mathematical formulation. These couplings broadly can be categorized as follows.

2.4.1 Deformation coupling

No material shows ideal (elastic or inelastic) behaviour throughout different states of deformation. Hence, different deformation mechanisms either in coexistence or independently represent a different state of the material. The elastic-plastic coupling refers to changes in the elastic property (e.g. stiffness) due to the development of plastic deformation in a previous cycle [372, 373]. During plastic deformation, the material undergoes microstructural changes; it will either harden or soften as a result of the change in elastic response in the next loading cycle.

Similarly, the viscous coupling refers to the viscoelastic effect due to time-dependent elastic strain development and viscoplastic effect due to time-dependent plastic strains [374]. Figure 26 shows a schematic of elastic-inelastic coupling behaviour. As the material softens in cycle #1, the size of the hysteresis curve for cycle #n has increased and affected the tangent stiffness in cycle #n. The major axis of the ellipse represent overall resistance to elastic deformation (as defined in section 4.3) and is not affected

when calculated between the minimum and maximum value (chord stiffness⁵). Hence the calculation method for stiffness needs to be selected based on intended use [375].

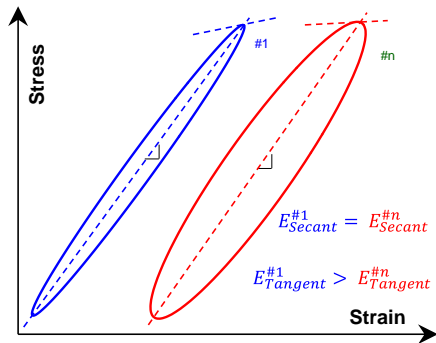


Figure 26 Elastic-inelastic deformation coupling

2.4.2 Damage coupling

Due to the occurrence of damage material loses effective resistance area, and this leads to change in elastic as well as inelastic behaviour. Figure 27 shows a schematic of this behaviour. Due to the damage incurred in between cycle #1 and #n, the slope of the hysteresis curve for cycle #n is less than cycle #1. Depending on the stress levels, either elastic or inelastic deformation is influenced by the damage. For example, in case of high cycle fatigue, as the stress levels are sufficiently low to consider them within the elastic region, the elastic-damage coupling plays a dominant role in determining the final life. In case of low cycle fatigue, i.e. when stress levels are sufficiently high to introduce inelastic deformation, the inelastic-damage coupling plays a dominant role in determining the final life.

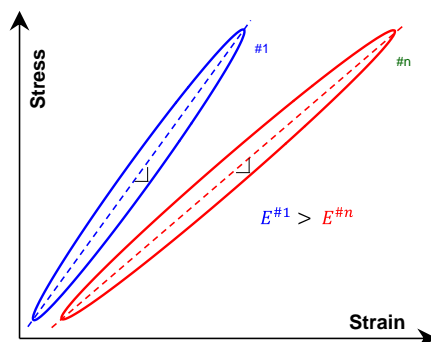


Figure 27 Elastic-damage coupling

⁵ As per ASTM E 111

2.4.3 Thermal coupling

When during cyclic loading the temperature in material approaches the state transition temperature, it shows a change in both elastic and inelastic response. Here to derive thermomechanical constitutive equations existence of thermo-elastic potential is assumed. The displacement and temperature fields are then obtained by adding this potential into the energy equation [144, 376, 377, 378, 379].

3

Mathematical Formulation for theory

The systematic categorization of theory from the previous chapter is used to define the mathematical formulation in this chapter⁶. It starts with constructing a generic framework using thermodynamic principles that apply to overall fatigue phenomenon. Later this generic framework is applied to specific mechanisms to ultimately derive a non-linear damage evolution law and an expression for the fatigue life at any damage state.

⁶ Parts of this chapter have been published in [2]

Constructing a mathematical formulation to characterize various mechanisms, such as those described in chapter 2, either individually or combined, constitutes a crucial aspect in predicting material behaviour. Without such a formulation, the prediction is limited to the scope of experimental observations only. Hence, the more generic the formulation is, the broader is its applicability to practical situations. As stated in section 1.2.3, the theory from the thermodynamics of irreversible processes with internal variables does fit this purpose of genericity. The mathematical formulations associated with this theory and applicable to various phenomena consist of two parts; generic formulation and application of this generic formulation to specific mechanism under investigation. The generic formulation, which is developed quite completely and already given in many textbooks [381 - 402], is rewritten here in the context of fatigue phenomenon. The mathematical formulation for various mechanisms and their coupling are derived by applying the CDM framework in subsequent sections 3.2 to 3.4.

3.1 Generic formulation

The construction of a generic mathematical framework applicable to the overall fatigue phenomenon starts by applying fundamental laws to the change of state of a material observed during the fatigue process.

3.1.1 Fundamental laws

According to the principle of conservation of energy, the total energy contented within an arbitrary material volume V can only change if energy flows into or out of the volume considered through its boundary Ω . In its global form, this principle can be formulated as [381]

$$\frac{d}{dt} \int^V \rho e dV = \int^V \frac{\partial \rho e}{\partial t} dV = - \int^{\Omega} J_e d\Omega \quad \text{Equation 5}$$

and in a local form as

$$\frac{\partial \rho e}{\partial t} = -div J_e \quad \text{Equation 6}$$

Where

ρ is the mass density

e = energy per unit mass

J_e = energy flux per unit surface and unit time

= $\rho e v + P \cdot v + \sum_k \psi_k J_k + J_q$ = Convective term + mechanical work + potential energy flux + heat flow

For the application of the First Law of thermodynamics, processes need not be carried out under specified conditions, such as isothermally or adiabatically. In other words, thermodynamic reversibility is not a necessary condition during application of first law. Therefore this law can be applied to both reversible mechanisms like elastic deformation and irreversible mechanisms like inelastic deformation and written as below.

$$\Delta E = W + Q \quad \text{Equation 7}$$

Where

ΔE is the change in the total energy of the material [Joules]

Q is the heat effect associated with the deformation (positive if absorbed, negative if dissipated).

W is the work (positive if done on the body)

The energy term ΔE consists of a change in kinetic energy K , potential energy ψ , and the internal energy U [385].

$$\Delta E = \Delta K + \Delta\psi + \Delta U$$

In the case of fatigue loading, the mechanical work W is the expended energy and consists of work of deforming the body, work against friction and work that increases the kinetic and potential energy of the body. Friction work is difficult to know from the in-plane fatigue test and does not contribute to the internal energy. Frictional work may reduce internal energy because it raises the temperature of the material during working. For deformation processes, the kinetic and potential parts can be ignored from both energy and work terms. Hence,

$$\Delta U = W + Q \quad \text{Equation 8}$$

Where

U is the total internal energy

the heat effect Q consists of two components, heat generated within the volume V by external agencies and the heat received by conduction through the boundary Ω .

In its global form, the first law of thermodynamics can then be formulated as [263]

$$\frac{d}{dt} \int^V \rho u \, dV = \int^V \sigma_{ij} : \dot{\epsilon}_{ij} \, dV + \int^V r \, dV - \int^V \text{div} \, \vec{q} \, dV \quad \text{Equation 9}$$

and in a local form as

$$\rho \frac{du}{dt} = \sigma_{ij} : \dot{\epsilon}_{ij} - \text{div} \, \vec{q} \quad \text{Equation 10}$$

or

$$\text{div}\vec{q} = \sigma_{ij} : \dot{\epsilon}_{ij} - \rho \frac{du}{dt}$$

Where

u is specific internal energy equals total internal energy divided by mass.

σ_{ij} is Cauchy symmetric stress tensor

$\dot{\epsilon}_{ij}$ is symmetric deformation tensor of second order

r is the volumetric density of the internal heat production by external agencies (e.g. inductive heating)

\vec{q} is the heat flux vector

As per the second law of thermodynamics for every volume element of any material and surroundings that may be experiencing a change in state, at every instant in time, entropy production is positive. This entropy production can be due to entropy transferred across the boundaries during the change and entropy production inside the material [385].

$$\Delta S_{system} = \Delta S_e + \Delta S_i \quad \text{Equation 11}$$

Where

S is the total entropy of material

S_e is entropy supplied to the material by its surroundings

S_i is entropy produced inside the material

This equation is known as the entropy balance equation. The entropy is expressed in specific entropy form as [381]

$$S = \int^V \rho s dV$$

$$\frac{dS_i}{dt} = \rho \int^V \dot{\gamma} dV$$

Where

s is specific entropy of material per unit mass

$\dot{\gamma}$ is the entropy production rate per unit volume per unit time

In the case of a fatigue test, only heat is exchanged with surrounding, and volume or physical matter remains constant. Hence fatigue test can be referred to as a close system. For any close system, the rate of entropy production is always greater than or equal to the rate of heating divided by the temperature.

$$dS \geq \frac{dS_e}{dt} = \frac{Q}{T}$$

From Equation 9, the entropy balance equation in its global form can be written as [263]

$$\int^V \rho \frac{ds}{dt} dV = \int^V \frac{r}{T} dV - \int^V \text{div} \frac{\vec{q}}{T} dV + \int^V \rho \dot{\gamma} dV$$

and in a local form as

$$\rho \frac{ds}{dt} = \dot{\gamma} + \frac{r}{T} - \text{div} \frac{\vec{q}}{T} \quad \text{Equation 12}$$

As the fatigue testing for wind turbine blade materials is carried out at room temperature, the internal heat production by external agencies is absent, i.e. $r=0$. Hence, from [Equation 12](#) we can write

$$\int^V \rho \frac{ds}{dt} dV \geq - \int^V \text{div} \frac{\vec{q}}{T} dV \quad \text{Equation 13}$$

[Equation 13](#) is known as a global form of Clausius–Duhem inequality and is a necessary condition for maintaining thermodynamic consistency for constitutive relation at any given situation. In its local form, this inequality is expressed as

$$\rho \frac{ds}{dt} \geq -\text{div} \frac{\vec{q}}{T} \quad \text{Equation 14}$$

Using quotient rule for division by a scalar, the divergence term is expanded as

$$\text{div} \frac{\vec{q}}{T} = \frac{\text{div} \vec{q}}{T} - \frac{\vec{q} \cdot \overrightarrow{\text{grad}} T}{T^2} \quad \text{Equation 15}$$

Substituting [Equation 15](#) into [Equation 13](#)

$$\rho \frac{ds}{dt} + \frac{\text{div} \vec{q}}{T} - \frac{\vec{q} \cdot \overrightarrow{\text{grad}} T}{T^2} \geq 0 \quad \text{Equation 16}$$

From [Equation 9](#)

$$\rho \frac{ds}{dt} + \frac{1}{T} \left(\sigma_{ij} : \dot{\varepsilon}_{ij} - \rho \frac{du}{dt} \right) - \frac{\vec{q} \cdot \overrightarrow{\text{grad}} T}{T^2} \geq 0 \quad \text{Equation 17}$$

Multiplying both sides by T

$$\rho \left(T \frac{ds}{dt} - \frac{du}{dt} \right) + \sigma_{ij} : \dot{\varepsilon}_{ij} - \frac{\vec{q} \cdot \overrightarrow{\text{grad}} T}{T} \geq 0 \quad \text{Equation 18}$$

The first term of [Equation 18](#) consist of the entropy and internal energy quantity that cannot be measured directly during any change of state of a material. Hence the first term needs to be replaced by a measurable quantity that has a functional relationship with entropy and internal energy.

The change of state of the material also involves a change in a few material properties. These properties often referred to as thermodynamic state variables. As the state variables represent the current state of the material, the different mechanisms involved during any change of state can be described using these variables. Hence before identifying the measurable quantity, first, these variables need to be declared so that the different mechanisms can be explicitly addressed in the mathematical formulation.

3.1.2 Declaration of state variables

State variables are observable variables and internal variables. The observable variables that can be monitored or recorded during the change of state of the material are-

- Pressure P
- Temperature T
- Volume V
- Mass m
- position coordinates x
- Heat capacity C_p
- Elastic strain ε_{ij}^e

For a given state, each of these variables known as fluxes has resultant conjugate associates known as thermodynamic forces. These thermodynamic forces are always intensive quantities (means properties of the material that does not depend on the amount of material, e.g. stress) and cause fluxes of the corresponding extensive variables (means properties of the material that depend on the amount of material, e.g. displacement). For a material transiting from state A to state B, the pair of the state variables and their conjugate associates can be represented, as shown in [Figure 28](#).

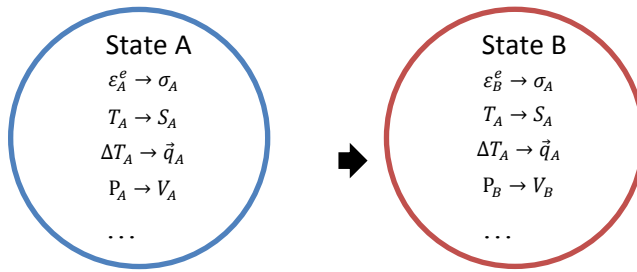


Figure 28 Observable variables and their conjugate associates in respective state of material during the change of state

At constant volume, to address the reversible deformation process, only two variables are required, i.e. temperature and elastic strain.

The observable state variables can address reversibility in the system, but for any mechanism that depends on history, there is a need to introduce a variable that represents history. Internal variables can address this by their values at each instant in the local state in combination with evolution law. For example, during the deformation under fatigue loading, dissipation of energy causes the irreversibility, and the most evident manifestation is the formation of a hysteresis curve. Here separate state variables like plastic strain and viscous strain need to be assigned to describe the hysteresis. The rate of change of these state variables describes the development of hysteresis formation over time. Similarly, for the description of mechanisms like damage and degradation due to ageing, when considered in the mathematical formulation, requires assignment of the respective state variables.

The internal variables used to describe the deformation behaviour are-

- Inelastic strain ε_{ij}^I
- Plastic strain ε_{ij}^p
- Viscoelastic strain ε^{ve}
- Viscoplastic strain ε^{vp}
- Isotropic strain hardening variable r
- Kinematic strain hardening variable α_j
- Damage D
- Ageing a
- Friction

For a material undergoing irreversible deformation from state A to state B, the internal variables and their conjugate associates can be represented with [Figure 29](#).

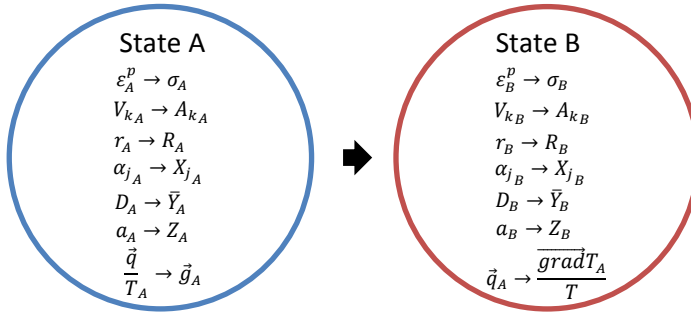


Figure 29 Internal variables and their conjugate associates in respective state of material during the process

The variables to describe the measurable quantity that has a functional relationship with entropy and internal energy are herewith declared. Now the measurable quantity is selected in the next section using the thermodynamic potential of the material.

3.1.3 Choice of thermodynamic potential and state law

The energy involved in any changes in the state of a material can be identified as its (state) potential. The state law (equation of state/constitutive equation) can be derived using this thermodynamic potential. A state law established in terms of independent variables describes the state of the system. For example, in case of elastic deformation, the equation of state is determined by the coefficient of thermal expansion, Young's modulus and Poisson's ratio (Hook's law), and are assumed to be independent of stress and temperature [380].

Here, the Helmholtz free energy is chosen as a thermodynamic potential as proposed by Lemaitre and Chaboche [263], that also has a functional relationship with entropy and internal energy. Introducing Helmholtz free energy⁷ as

$$\psi = u - Ts \tag{Equation 19}$$

Differentiating to time gives

$$\frac{d\psi}{dt} = \frac{du}{dt} - T \frac{ds}{dt} - s \frac{dT}{dt} \tag{Equation 20}$$

or

⁷ Here Helmholtz free energy measures the useful work obtainable from a closed thermodynamic system at a constant temperature and volume that is more representative to fatigue test situation than Gibbs free energy as it is a measure of a maximum of reversible work that may be performed by a thermodynamic system at a constant temperature and pressure without increasing total volume or allowing heat to pass to or from external bodies.

$$T \frac{ds}{dt} - \frac{du}{dt} = - \left(\frac{d\psi}{dt} + s \frac{dT}{dt} \right)$$

With Equation 2 while substituting Equation 20 into the first term of Equation 18, one can write

$$\sigma_{ij} : \dot{\varepsilon}_{ij}^e + \sigma_{ij} : \dot{\varepsilon}_{ij}^I - \rho \left(\frac{d\psi}{dt} + s \frac{dT}{dt} \right) - \frac{\vec{q} \cdot \overrightarrow{\text{grad}} T}{T} \geq 0 \quad \text{Equation 21}$$

Equation 21 represents an inequality in the form of thermodynamic potential.

Different mechanisms coexist during the change of state. Hence writing the thermodynamic potential as the sum of contributions from all involved mechanisms (as shown in Figure 17) one gets

$$\psi = \psi_{elastic} + \psi_{inelastic} + \psi_{damage} + \psi_{therm} \quad \text{Equation 22}$$

Where, $\psi_{inelastic} = \psi_{plastic} + \psi_{viscoelastic} + \psi_{viscoplastic}$

Where, $\psi_{plastic} = \psi_{hardening} + \psi_{aging} + \psi_{friction}$

Where, $\psi_{hardening} = \psi_{iso} + \psi_{kin} + \psi_{stored}$

In the general functional form, the individual potentials are described by many researchers [403, 404, 405, 406, 407, 408, 409] as

$$\begin{aligned} \psi_{elastic} &= f(\varepsilon_{ij}^e, T, D) \\ \psi_{stored} &= f(\alpha_i, r, T, D) \\ \psi_{therm} &= f(\varepsilon_{ij}^e, T, D) \\ \psi_{aging} &= f(a, T) \\ \psi_{damage} &= f(T, D) \\ \psi_{iso} &= f(r, T, D) \\ \psi_{kin} &= f(\alpha_j, T, D) \\ \psi_{viscoelastic} &= f(\varepsilon_{ij}^{ve}, T, D) \\ \psi_{viscoplastic} &= f(\varepsilon_{ij}^p, \varepsilon_{ij}^{vp}, \alpha_j, r, T, D) \\ \psi_{friction} &= f(\varepsilon^\pi, T, D) \end{aligned} \quad \text{Equation 23}$$

For the case of fatigue loading, one can ignore the store-, the viscous-, the ageing- and the friction part, reducing the potential to

$$\psi = \psi(\varepsilon_{ij}^e, T, r, \alpha_j, D) \quad \text{Equation 24}$$

Chain rule gives the rate of change of specific free energy associated with the change of state of the material as follows-

$$\dot{\psi} = \frac{\partial \psi}{\partial \varepsilon_{ij}^e} : \dot{\varepsilon}_{ij}^e + \frac{\partial \psi}{\partial T} \dot{T} + \frac{\partial \psi}{\partial r} \dot{r} + \frac{\partial \psi}{\partial \alpha_j} \dot{\alpha}_j + \frac{\partial \psi}{\partial D} \dot{D} \quad \text{Equation 25}$$

Each term in the above equation describes the extent of change in the material due to the respective mechanism during fatigue loading.

Incorporating Equation 25 into Equation 21 gives inequality in the form as [263]

$$\left(\sigma_{ij} - \rho \frac{\partial \psi}{\partial \varepsilon_{ij}^e} \right) : \dot{\varepsilon}_{ij}^e + \sigma_{ij} : \dot{\varepsilon}_{ij}^l - \rho \left(s + \frac{\partial \psi}{\partial T} \right) \dot{T} - \rho \frac{\partial \psi}{\partial r} \dot{r} - \rho \frac{\partial \psi}{\partial \alpha_j} \dot{\alpha}_j - \rho \frac{\partial \psi}{\partial D} \dot{D} - \frac{\vec{q} \cdot \overrightarrow{\text{grad}} T}{T} \geq 0 \quad \text{Equation 26}$$

This relation should be satisfied with the fatigue process described by Equation 24.

For elastic deformation in a uniform temperature field, the internal state remains unchanged hence $\dot{\varepsilon}_{ij}^l = 0, \dot{r} = 0, \dot{\alpha}_j = 0, \dot{D} = 0, \overrightarrow{\text{grad}} T = 0$ and $\dot{T} = 0$. This reduces Equation 26 to

$$\left(\sigma_{ij} - \rho \frac{\partial \psi}{\partial \varepsilon_{ij}^e} \right) : \dot{\varepsilon}_{ij}^e - \rho \left(s + \frac{\partial \psi}{\partial T} \right) \dot{T} \geq 0 \quad \text{Equation 27}$$

This inequality should be satisfied with any choice of $\dot{\varepsilon}_{ij}^e$ and \dot{T} Hence

$$\sigma_{ij} = \rho \frac{\partial \psi^e}{\partial \varepsilon_{ij}^e} \quad \text{Equation 28}$$

Equation 28 is known as elasticity laws and give relations between observable state variables and their conjugate associates.

Analogously state law for isotropic hardening, kinematic hardening and damage can be defined. For example, in the case of isotropic hardening, the increase in the radius of yield surface is given by

$$R = \rho \left(\frac{\partial \psi}{\partial r} \right) \quad \text{Equation 29}$$

The back stress in case of kinematic hardening can be characterized as

$$X_j = \rho \left(\frac{\partial \psi}{\partial \alpha_j} \right) \quad \text{Equation 30}$$

And the damage governing variable, strain energy density release rate, is given by

$$\bar{Y} = -\rho \left(\frac{\partial \psi}{\partial D} \right) \quad \text{Equation 31}$$

Generically the state law for thermodynamic forces associated with other variables can be defined as [263]

$$A_i = \rho \left(\frac{\partial \psi}{\partial V_i} \right) \quad \text{Equation 32}$$

Where $V_i = \{\varepsilon_{ij}^e, r, \alpha_j, D, a, \vec{q}\}$ is the flux vectors and $A_i = \rho\{\sigma_{ij}, R, X, \bar{Y}, Z, \overrightarrow{\text{grad}T}/T\}$ is their thermodynamic conjugate force vector.

3.1.4 Choice of dissipation potential and evolution law

Equation 32 provides information related to the local state of material by giving relations between state variables and associated variables. However, to describe the dissipation process, the evolution of internal variables with time is needed. This relation is known as evolution law or complimentary law.

For dissipation to occur, substituting Equation 27, Equation 28 in Equation 26, one can write

$$\Phi = \sigma_{ij} \dot{\varepsilon}_{ij}^I - R\dot{r} - X_j \dot{\alpha}_j - Y\dot{D} - \frac{\vec{q} \cdot \overrightarrow{\text{grad}T}}{T} \geq 0 \quad \text{Equation 33}$$

where the first four terms represent mechanical dissipation (inelastic dissipation and dissipation associated with the evolution of the internal variable), and the last term is thermal dissipation (conduction of heat). Here Φ represents dissipation per unit volume and equals to the sum of the products of the force variable and respective flux variables. This dissipation is related to entropy generation via $\Phi = T\dot{\gamma}$. For this dissipation to occur, it is assumed that there exists a dissipation potential φ [263] as

$$\varphi = \varphi_{inelastic} + \varphi_{damage} + \varphi_{therm} \quad \text{Equation 34}$$

Assuming normality hypothesis is valid, the complementary laws can be derived in the same way as Equation 32. The normality hypothesis state that the direction of increment in the inelastic strain is normal to the tangent to the yield surface at the load point or in the physical sense, the local microstructural rearrangements (e.g. plastic strain) proceeds at a rate governed by its associated thermodynamic forces (e.g. stress)[410].

$$A_i = \dot{\lambda} \frac{\partial \varphi}{\partial \dot{V}_i} \quad \text{Equation 35}$$

Where $\dot{\lambda}$ is known as plasticity multiplier whose value is identified by the Prager's [414] consistency condition and represents the irreversible strain developed either at micro-scale or mesoscale. The complementary laws given by Equation 35 is in the form of thermodynamic forces as a function of evolving flux variables. In case of fatigue loading, generally, the thermodynamic forces A_k governing the respective mechanism are known and associated flux variables \dot{V}_k are varying quantities. Due to this, above equation is difficult to work. Here the complementary laws can be expressed in the form of the evolution of flux variables as functions of governing thermodynamic force variables using the principle of duality and Legendre-Fenchel transformation [411, 412]. Therefore writing the dissipation potential in its dual form, which is a function of flux variables as

$$\varphi^* = \varphi_{inelastic}^* + \varphi_{damage}^* + \varphi_{therm}^* \quad \text{Equation 36}$$

Where, $\varphi_{inelastic}^* = \varphi_{plastic}^* + \varphi_{viscoelastic}^* + \varphi_{viscoplastic}^*$

Where, $\varphi_{plastic}^* = \varphi_{hardening}^* + \varphi_{aging}^* + \varphi_{friction}^*$

Where, $\varphi_{hardening}^* = \varphi_{iso}^* + \varphi_{kin}^* + \varphi_{store}^*$

In the general functional form, the individual potential is described as follow-

$$\varphi_{plastic}^* = f(\sigma_{ij}; D, T)$$

$$\varphi_{aging}^* = f(Z; T, r, a)$$

$$\varphi_{therm}^* = f(\bar{g}; T, D)$$

$$\varphi_{iso}^* = f(R; D, T)$$

$$\varphi_{kin}^* = f(X; D, T)$$

$$\varphi_{store}^* = f(R, X; D, T)$$

$$\varphi_{damage}^* = f(Y; D, T)$$

$$\begin{aligned}\varphi_{viscoelastic}^* &= f(\sigma_{ij}; T, D) \\ \varphi_{viscoplastic}^* &= f(\sigma_{ij}, R, X; T, D) \\ \varphi_{friction}^* &= f(\sigma^\pi; T, D)\end{aligned}$$

Similar to [Equation 28](#), the evolution law can be derived for different mechanisms. For example, the rate of change of inelastic strain as a function of governing stress is given by

$$\dot{\varepsilon}_{ij}^I = \dot{\lambda} \frac{\partial \varphi^*}{\partial \sigma_{ij}} \quad \text{Equation 37}$$

In the case of kinematic hardening, the evolution of strain hardening variable is given as

$$\dot{\alpha}_j = -\dot{\lambda} \frac{\partial \varphi^*}{\partial X_j} \quad \text{Equation 38}$$

In the case of isotropic hardening, the rate of change of radius of yield surface is given by

$$\dot{r} = -\dot{\lambda} \frac{\partial \varphi^*}{\partial R} \quad \text{Equation 39}$$

The rate of change of damage development as a function of governing strain energy density release rate is given as

$$\dot{D} = -\dot{\lambda} \frac{\partial \varphi^*}{\partial \bar{Y}} = \dot{\lambda} \frac{\partial \varphi^*}{\partial Y} \quad \text{Equation 40}$$

Let the flux vectors J and their thermodynamic conjugate force vector X be

$$\dot{V}_i = \rho \{ \dot{\varepsilon}_{ij}^I, \dot{r}, \dot{\alpha}_j, \dot{D}, \vec{q}/T \} \quad \text{Equation 41}$$

$$A_i = \rho \{ \sigma_{ij}, -R, -X, -\bar{Y}, -\vec{g} \} \quad \text{Equation 42}$$

Then generically the evolution law can be written as

$$\dot{V}_i = \dot{\lambda} \frac{\partial \varphi^*}{\partial A_i} \quad \text{Equation 43}$$

Here the generalized flux \dot{V}_i represents the rate of change of the internal variables, while the generalized force A_i stands for their cause.

3.1.5 Coupling between different mechanisms

The coupling between different mechanisms exists due to the change in microstructure. As these mechanisms coexist with each other, their interaction needs to be considered in theory, to develop a consistent mathematical formulation. A state coupling exists between two mechanisms i and j if a change in the state variable V_i induces a change in the associated variables A_j [413]. Hence,

$$\frac{\partial A_j}{\partial V_i} \neq 0 \text{ OR } \frac{\partial^2 \psi}{\partial V_j \partial V_i} \neq 0$$

If there is no coupling between i and j , then the potential can be split into parts. Qualitative microscopic considerations can determine these couplings or uncouplings [416]. For example, the damage is coupled with elasticity so that-

$$\frac{\partial^2 \psi}{\partial \varepsilon_{ij}^e \partial D} \neq 0$$

Here as damage D increases the effective resistance area and hence elastic strain decreases [refer section 2.4.2]. A kinetic coupling between two mechanisms i and j exists if variation in state variables V_i leads to modification of the rate of flux variables \dot{J}_j [413]. Hence,

$$\frac{\partial \dot{J}_j}{\partial V_i} \neq 0 \text{ OR } \frac{\partial^2 \phi}{\partial X_j \partial V_i} \neq 0$$

For example, the coupling of damage on the mechanism of plasticity as damage develops it lower the yield stress and increases the plastic strain rate.

3.1.6 The expression for thermodynamic and dissipation potential

In the generic framework so far, only functional forms are used for both potentials. Characterization of any mechanism using the state law and evolution law requires the analytical expression for respective parts of thermodynamic potential [Equation 23](#) and dissipation potential [Equation 36](#). From literature, one can see that the generalized expression can describe few mechanisms—for example, Hook’s law for elasticity and Ramberg-Osgood law for plasticity. Following references [[384](#), [417](#), [403](#), [406](#)], the expression for different mechanisms described in [chapter 2](#), is given as

$$\begin{aligned} \rho\psi = & \frac{1}{2} E_{ijkl} \varepsilon_{ij}^e \varepsilon_{kl}^e (1 - D) + R_\infty \left[r + \frac{1}{b} \exp(br) \right] + \frac{X_\infty}{3} \sum_i C_i \alpha_j \alpha_j \\ & + a(cr - L) + L - b\alpha T \text{tr}(\varepsilon^e) - \rho \frac{\bar{C}}{2T_0} T^2 + .. \end{aligned} \quad \text{Equation 44}$$

The [blue](#) part represents damage coupled elastic potential, the parts with different shades of [aqua](#) colour represent inelastic (isotropic hardening, kinematic hardening and ageing) potential and the [red](#) part is thermal (linear thermo-elasticity and thermal expansion) contribution in the total potential of the material. From inelastic potential viscous part is ignored.

An analytical expression for the dissipation potential φ is-

$$\begin{aligned} \varphi^* = & (\tilde{\sigma}_{ij}^D - X_j^D)_{eq} - R - \sigma_y + \left[c - \beta \exp\left(-\gamma \frac{r}{1 - D}\right) \right] \\ & + \frac{3}{4X_\infty} X_j^D X_j^D + [a_\infty - a]Z + \varphi_D^* + \frac{1k}{2T} \vec{g} \cdot \vec{g} + .. \end{aligned} \quad \text{Equation 45}$$

Here the [orange](#) part is the damage potential, for which [section 3.4](#) gives its mathematical form specific to the fatigue damage. The above expressions for of potentials consider the contribution from only a few mechanisms because not all mechanisms play a role in the fatigue phenomenon. Some of these contributions are defined with the help of internal variables. These internal variables are a function of other state variables, and hence it is necessary to define their relationship. The analytical form for this relationship is not yet established for all internal variables and is still subject of active research. One example is the relationship between back stress

and plastic strain, for which [Table 5](#) gives the timestamp overview of the evolution in this relationship.

The state of the material (including various couplings) at any given time during the fatigue process can be characterized with the help of [Equation 44](#), and [Equation 45](#). To characterize the damage state, first, it's coupling with elastic and inelastic deformation needs to be characterised. Hence in the next subsections [3.2](#) and [3.3](#), the derivation of the governing thermodynamic force variables related to the corresponding mechanisms are given.

3.2 Elasticity coupled with damage

The blue part in [Equation 44](#), and [Equation 45](#) represent the elastic potential affected by the damage. To characterize this coupling means finding the relationship between the governing variable of damage mechanism (strain energy density release rate \bar{Y}) and the elastic deformation (elastic strain). Here the procedure given by Lemaitre et al. [[417, 415](#)] is followed to derive this relationship. Considering only elastic deformation is affecting the damage we can write from [Equation 28](#) and [Equation 44](#)

$$\sigma_{ij} = \rho \frac{\partial \psi^e}{\partial \varepsilon_{ij}^e} = E_{ijkl} \varepsilon_{kl}^e (1 - D) \quad \text{Equation 46}$$

From [Equation 37](#) and [Equation 44](#)

$$\bar{Y} = -\rho \left(\frac{\partial \psi}{\partial D} \right) = -\frac{1}{2} E_{ijkl} \varepsilon_{ij}^e \varepsilon_{kl}^e$$

From [Equation 46](#)

$$\bar{Y} = -\frac{1}{2(1-D)} \sigma_{ij} \varepsilon_{ij}^e \quad \text{Equation 47}$$

The above equation characterizes the damage coupling with elastic deformation. For the sake of future scope and completeness, [Equation 47](#) can also be written in the form of equivalent stress to simplify the characterization in case of the multiaxial stress state. For this, writing the stress and strain in their component form as

$$\sigma_{ij} = \sigma_{ij}^D + \sigma_H \delta_{ij}$$

$$\varepsilon_{ij}^e = \varepsilon_{ij}^{eD} + \varepsilon_H^e \delta_{ij}$$

And further writing the deviatoric and hydrostatic component using the law of linear isotropic elasticity as

$$\varepsilon_{ij}^{eD} = \frac{1 + \nu}{E} \frac{\sigma_{ij}^D}{1 - D}$$

And

$$\varepsilon_H^e = \frac{1 - 2\nu}{E} \frac{\sigma_H}{1 - D}$$

Substituting these in [Equation 47](#) and rearranging

$$Y = -\bar{Y} = \frac{\sigma_{eq}^2}{2E(1 - D)^2} R_v \quad \text{Equation 48}$$

Where σ_{eq} is Von Mises equivalent stress $\sigma_{eq} = \left[\frac{3}{2} (\sigma_{ij} - \sigma_H \delta_{ij})(\sigma_{ij} - \sigma_H \delta_{ij}) \right]^{1/2}$ and R_v is triaxiality function that indicates brittleness of the material.

Equation 48 characterizes the damage coupling with elastic deformation in a multiaxial stress state.

3.3 Inelasticity coupled with damage

Inelastic deformation consists of a plastic and viscous component. The viscous component is ignored in the formulation presented here, assuming its contribution to be very small. For plastic deformation, the application of the general framework is not as straightforward as elasticity due to the use of state variables as state functions to address irreversibility. For example, the back stress responsible for kinematic hardening is a function of plastic strain, and its computation requires solving state function formulations and their evolution law simultaneously.

Computation of damage evolution coupled with plasticity requires the derivation of plasticity multiplier in [Equation 40](#). This section gives the derivation for plasticity multiplier using the definition of elastic domain and flow rule as per [[417](#), [418](#)].

3.3.1 Elastic domain

An elastic domain, considering both isotropic and kinematic hardening, is defined by function f that depends on stress tensor components as

$$f = (\tilde{\sigma}^D - X^D)_{eq} - \sigma_y - R \leq 0 \quad \text{Equation 49}$$

where the superscript D refers to the deviatoric component of stress. The hydrostatic component of stress is ignored assuming no damage gets generated due to them. Also, they are responsible for volume change, which deviates from the closed system assumption made for the fatigue process. For damage coupling, using effective stress concept, we can write

$$(\tilde{\sigma}^D - X^D)_{eq} = \left[\frac{3}{2} \left(\frac{\sigma_{ij}^D}{1-D} - X_j^D \right) : \left(\frac{\sigma_{ij}^D}{1-D} - X_j^D \right) \right]^{1/2} \quad \text{Equation 50}$$

After combining Equation 49 and Equation 50, one can write-

$$f = \left[\frac{3}{2} \left(\frac{\sigma_{ij}^D}{1-D} - X_j^D \right) : \left(\frac{\sigma_{ij}^D}{1-D} - X_j^D \right) \right]^{1/2} - \sigma_y - R \quad \text{Equation 51}$$

The characterization of isotropic R and kinematic X hardening variables are not in the scope of this thesis work.

3.3.2 Flow rule

The flow rule can be written in terms of plastic potential F using Equation 43 as

$$\dot{\varepsilon}_{ij}^p = \dot{\lambda} \frac{\partial F}{\partial \sigma_{ij}} \quad \text{Equation 52}$$

where, the plastic potential F can be defined from Equation 45 as

$$F = f + \frac{3}{4X_\infty} X_j^D X_j^D + \left[c - \beta \exp \left(-\gamma \frac{r}{1-D} \right) \right] \quad \text{Equation 53}$$

in which the second and third terms represent kinematic and isotropic dynamic recovery effects respectively. Solving Equation 52 will give the rate of change of plastic strain development as

$$\begin{aligned} \dot{\varepsilon}_{ij}^p &= \dot{\lambda} \frac{\partial F}{\partial \sigma_{ij}} = \frac{\partial (\sigma^D - X^D)_{eq}}{\partial \sigma_{ij}} \dot{\lambda} \\ &= \frac{\partial}{\partial \sigma_{ij}} \left[\frac{3}{2} \left(\frac{\sigma_{ij}^D}{1-D} - X_j^D \right) \left(\frac{\sigma_{ij}^D}{1-D} - X_j^D \right) \right]^{1/2} \dot{\lambda} \end{aligned}$$

Using chain rule

$$= \frac{1}{2} \frac{\frac{3}{2} \cdot 2 \left(\left(\frac{\sigma_{ij}^D}{1-D} - X_j^D \right) \left(\frac{1}{1-D} - \frac{\partial X_j^D}{\partial \sigma_{ij}} \right) \right)}{\left(\frac{\sigma^D}{1-D} - X^D \right)_{eq}} \dot{\lambda}$$

$$\dot{\varepsilon}_{ij}^p = \frac{3}{2} \frac{\sigma_{ij}^D - X_j^D}{(\sigma^D - X^D)_{eq}} \frac{\dot{\lambda}}{1-D}$$

Equation 54

Or

$$\dot{\varepsilon}_{ij}^p = \sqrt{\frac{3}{2}} \frac{\dot{\lambda}}{1-D} \cdot n$$

where n is the unit outward normal to the elastic domain[241] and defined as

$$n = \frac{\partial f / \partial \sigma}{(\partial f / \partial \sigma : \partial f / \partial \sigma)^{1/2}} = \sqrt{\frac{3}{2}} \frac{\sigma_{ij}^D - X_j^D}{(\sigma^D - X^D)_{eq}}$$

To derive the plasticity multiplier $\dot{\lambda}$ in Equation 37 one can start with the accumulated plastic strain rate \dot{p} which is equivalent to absolute value of the derivative of the principal value of the plastic strain rate $|\dot{\varepsilon}^p|$ while considering deviatoric part only-

$$\begin{aligned} \dot{p} &= \left(\frac{2}{3} \dot{\varepsilon}_{ij}^p : \dot{\varepsilon}_{ij}^p \right)^{1/2} \\ &= \left[\frac{2}{3} \left(\frac{3}{2} \frac{\sigma_{ij}^D - X_j^D}{(\sigma^D - X^D)_{eq}} \frac{\dot{\lambda}}{1-D} : \frac{3}{2} \frac{\sigma_{ij}^D - X_j^D}{(\sigma^D - X^D)_{eq}} \frac{\dot{\lambda}}{1-D} \right) \right]^{1/2} \\ &= \frac{\dot{\lambda}}{\left(\frac{\sigma_{ij}^D}{1-D} - X_j^D \right)_{eq} (1-D)} \cdot \left[\frac{3}{2} \left(\frac{\sigma_{ij}^D}{1-D} - X_j^D \right) \left(\frac{\sigma_{ij}^D}{1-D} - X_j^D \right) \right]^{1/2} \end{aligned}$$

From Equation 50 and rearranging the terms

$$\dot{p} = \frac{\dot{\lambda}}{(1-D)}$$

Equation 55

or

$$\dot{\lambda} = \dot{p}(1-D)$$

Equation 55 defines the unknown parameter, plasticity multiplier, in Equation 40.

3.4 Fatigue damage

This section gives the derivation of damage evolution law specific to fatigue phenomenon using [Equation 40](#). The generic framework in the previous section uses time as a reference variable, which means that the increment of damage is given as a function of the increment of time, and strain or stress. In the case of fatigue, usually, the concept of the applied loading cycle is used to evaluate the evolution of damage and to measure the fatigue lifetime. Hence two types of damage evolution can be formed: as a function of time and as a function of cycles [\[419\]](#). The equations then depend on the load through globally defined quantities over a cycle, such as amplitude, maximum value, and mean value. Hence in the functional form, we can write-

$$\frac{dD}{dt} = f(\sigma_{ij}, T, D) \quad \text{Equation 56}$$

$$\frac{dD}{dN} = f(\Delta\sigma, H_z, T, D) \quad \text{Equation 57}$$

where H_z is frequency. Assuming H_z and T are constant and known for the experimental setup followed in the validation stage one can write

$$\frac{dD}{dN} = f(\Delta\sigma, D) \quad \text{Equation 58}$$

For different experimental setup, the influence of H_z and T on the values of the coefficients of the damage evolution law needs appropriate consideration.

Starting from the damage evolution law given by [Equation 40](#)

$$\dot{D} = -\lambda \frac{\partial \varphi_D^*}{\partial \bar{Y}} = \lambda \frac{\partial \varphi_D^*}{\partial Y} \quad \text{Equation 59}$$

Lemaitre [\[420\]](#) proposed a generalized representation for the damage potential in the form of power function of strain energy density release rate Y as-

$$\varphi_{D(Y:D)}^* = \frac{X}{(\chi + 1)(1 - D)} \left(\frac{Y}{\bar{X}} \right)^{\chi+1} \quad \text{Equation 60}$$

Lemaitre defined parameter X as energy strength of damage and χ damage exponent; both are functions of the temperature. Reference [417 p-110] gives the procedure to determine both values.

From Equation 59, for damage rate governed by plasticity (through accumulated plastic strain p) one can write

$$\begin{aligned}\dot{D} &= \frac{\partial \varphi_D^*}{\partial Y} \dot{p}(1-D) \\ \dot{D} &= \left(\frac{Y}{X}\right)^\chi \dot{P}\end{aligned}\tag{Equation 61}$$

In the above equation parameters Y and \dot{P} requires a specific definition related to fatigue damage. In case of fatigue testing of composite material, a thin rectangular shape coupon is loaded in-plane direction. This situation resembles the one-dimensional case. Hence Equation 48 becomes -

$$Y = \frac{1}{2E} \left(\frac{\sigma}{1-D}\right)^2$$

For fully reverse loading assuming $\sigma = \sigma_{max} = \frac{\Delta\sigma}{2}$ is the stress when damage occurs, the above equation becomes-

$$Y = \frac{1}{8E} \left(\frac{\Delta\sigma}{1-D}\right)^2\tag{Equation 62}$$

For the one-dimensional case, we can also write $\dot{P} = |\dot{\varepsilon}^p|$, hence with Equation 61, one gets

$$\dot{D} = \left(\frac{\Delta\sigma^2}{8EX(1-D)^2}\right)^\chi |\dot{\varepsilon}^p|\tag{Equation 63}$$

In the case of plasticity coupled with damage, the plastic strain rate, given by Equation 54, needs to be updated consistently. The numerical methods used to obtain the solution are not in the scope of the current work hence computation of plastic strain rate is performed using an empirical methodology. In practice, most of the materials

show the existence of a cyclic law [186, 416, 421] approximated by a power function similar to Ramberg-Osgood law [422].

$$\Delta\varepsilon^p = \left[\frac{\Delta\sigma}{k(1-D)} \right]^m \quad \text{Equation 64}$$

where k and m are material dependent parameters, with m is a positive exponent.

Section 4.3 gives proof of cyclic law validity to the materials used in this work. Taking the derivative of $\Delta\varepsilon^p$ to time gives the plastic strain rate as follows-

$$\dot{\varepsilon}^p = m \frac{\Delta\sigma^{m-1} \dot{\Delta\sigma}}{k^m(1-D)^m} \quad \text{Equation 65}$$

as

$$\frac{d\Delta\sigma^m}{dt} = \frac{d\Delta\sigma^m}{d\Delta\sigma} \frac{d\Delta\sigma}{dt}$$

Equation 65 gives the evolution of the plastic strain rate for any stress level. In addition to this plastic strain development, materials either show shakedown or ratchetting in strain development with respect to the number of cycles, as shown in Figure 21. This characteristic needs to be included in the framework to calculate total plastic strain development. Li et al. [423] and Huang et al. [424] added this additional development of inelastic strain as a softening parameter in the strain rate expression. They proposed softening behaviour as a function of stress level and the number of cycles. Because Equation 65 already includes the stress level dependency, here only the dependency on the number of cycles is added as

$$\dot{\varepsilon}^p = m \frac{\Delta\sigma^{m-1} \dot{\Delta\sigma}}{k^m(1-D)^m N^\alpha} \quad \text{Equation 66}$$

The parameter α is similar to that used by Marco and Starkey [427] and Chaboche [186]. For the materials used in this study, the dependency of the softening parameter on the stress level and the number of cycles is shown in section 4.3.3.

Hence Equation 63 becomes

$$\dot{D} = \left(\frac{\Delta\sigma^2}{8EX(1-D)^2} \right)^x m \frac{\Delta\sigma^{m-1} \dot{\Delta\sigma}}{k^m(1-D)^m N^\alpha} = \frac{\Delta\sigma^{M-1} \dot{\Delta\sigma}}{K(1-D)^M N^\alpha} \quad \text{Equation 67}$$

where $K = \frac{(3EX)^\chi k^m}{m}$ and $M = m + 2\chi$ are material and temperature-dependent functions.

Integration of [Equation 67](#) with time gives damage per cycle, assuming a change in damage is negligibly small over a single cycle.

$$\begin{aligned} \frac{dD}{dN} &= \int_{\text{cycle}} \dot{D} dt = 2 \frac{1}{K(1-D)^M N^\alpha} \int_0^{\Delta\sigma} \Delta\sigma^{M-1} d\Delta\sigma \\ &= \frac{2\Delta\sigma^M}{KM(1-D)^M N^\alpha} \end{aligned} \quad \text{Equation 68}$$

Integrating [Equation 68](#) over the whole fatigue process, i.e. from $D=0$ to $D=1$ and $N=0$ to $N=N_F$ results in the fatigue life equation as follows-

$$\begin{aligned} \int_{D=0}^1 \frac{dD}{dN} dN &= \frac{2\Delta\sigma^M}{KM} \int_0^{N_F} \frac{dN}{N^\alpha} \\ \int_{D=0}^1 (1-D)^M dD &= \frac{2\Delta\sigma^M}{KM} \int_0^{N_F} \frac{dN}{N^\alpha} \\ N_F &= \left[\frac{KM(1-\alpha)}{2(M+1)\Delta\sigma^M} \right]^{\frac{1}{1-\alpha}} \end{aligned} \quad \text{Equation 69}$$

[Equation 69](#) is the expression for constant life curves, and [Figure 30](#) gives a schematic representation of these curves in mean and amplitude stress space, also known as Constant Life Diagram (CLD).

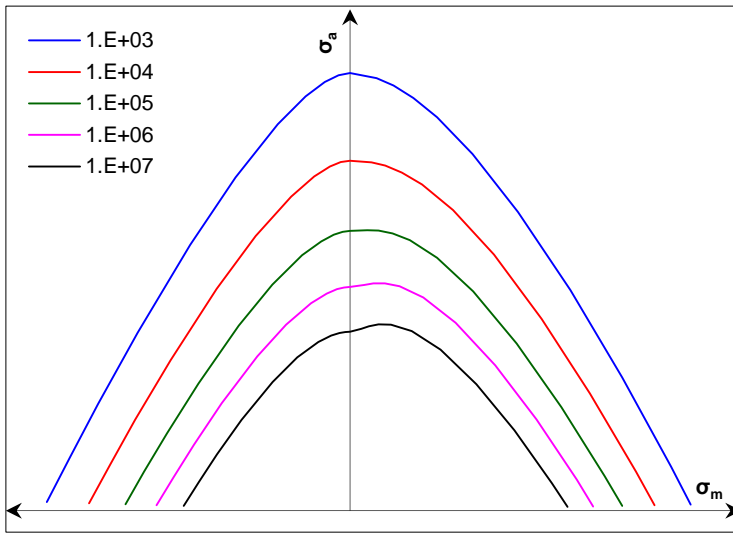


Figure 30 Constant Life Diagram (CLD)

One peculiar feature of Equation 69 is that the constant lifelines do not meet at one point on the abscissa. In the past very few times, similar representation was reported [109, 425, 426]. This way of representation is different from traditional representation [34 to 43] where all constant lifelines merge at an ultimate static value. In the mathematical formulation of traditional representation, the constant lifelines are represented by equating sum of the ratio of stresses to unity. This means the static value is used as one single point to represent any life when mean stresses reach to ultimate strength value. On the abscissa, as the mean stress value reduces than ultimate strength, the effect of time or creep is there in reality hence constant lifelines intersecting abscissa at the various point seems more realistic than merging at a single point.

In the case of constant amplitude loading, integrating Equation 68 for constant $\Delta\sigma$ and between $D= 0$ to D and $N= 0$ to N gives intermediate fatigue life at any damage state as

$$\int_{D=0}^D \frac{dD}{dN} dN = \frac{2\Delta\sigma^M}{KM} \int_0^N \frac{dN}{N^\alpha}$$

$$N = \left[\frac{KM(1-\alpha)}{2(M+1)2\Delta\sigma^M} [1 - (1-D)^{M+1}] \right]^{\frac{1}{1-\alpha}} \quad \text{Equation 70}$$

In the case of multi-step or variable amplitude loading, the integration scheme needs to be adopted for the respective load block [186].

Hence combining Equation 69 and Equation 70 one can write for the damage at life N

$$\frac{N}{N_F} = [1 - (1 - D)^{M+1}]^{\frac{1}{1-\alpha}}$$

$$D = 1 - \left[1 - \left(\frac{N}{N_F} \right)^{1-\alpha} \right]^{\frac{1}{M+1}} \tag{Equation 71}$$

Equation 71 is an expression for non-linear damage evolution to life, which is schematically illustrated in Figure 31.

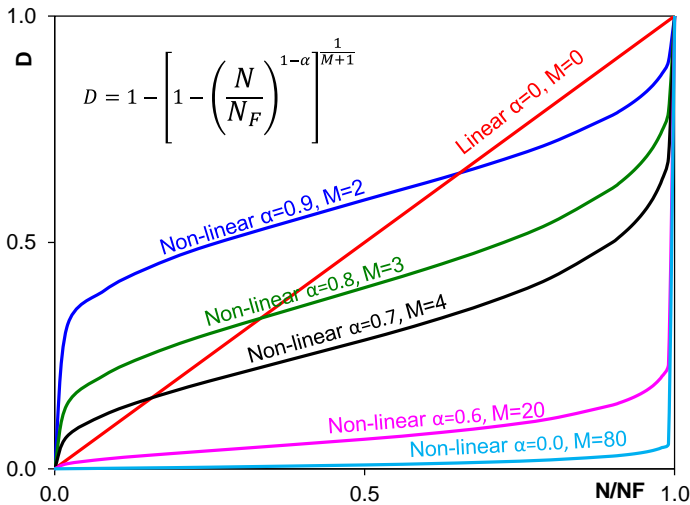


Figure 31 Damage evolution to life

The non-linear development of damage resembles closely with the generic damage development stages reported in the literature [268] and shown in Figure 25. This resemblance makes the mathematical formulation consistent with the presented theory, and section 4.3.5 gives consistency with experimental observations. Equation 71 also shows resemblance with many forms proposed in the literature (Table 4) that makes this form more generic and applicable to a wide variety of materials. The non-linear damage accumulation law (Equation 71) and constant life curve expression (Equation 69) enables the complete characterization of the fatigue damage coupled with elastic and plastic deformation.

4

Validation of theory and mathematical formulation

Previous chapters give a detailed description of the governing theory and its associated mathematical formulation for describing the fatigue phenomenon. This chapter⁸ provides the required validation of both theory and mathematical formulation for the assessment of the framework's applicability in fatigue analysis of wind turbine blade materials.

⁸ *Parts of this chapter have been published in [3]*

The application of any framework to a real-time product requires validation of a theory and its mathematical formulation for a range of operating conditions. The selection of the number of conditions during the validation stage is based on critical operating conditions and regulatory guidelines. The first part of this chapter provides the details of the experimental methodology followed. In the next subsections, the results from experiments are discussed. Based on the correlation with these experiments, the validity of the theory and mathematical formulation is provided.

4.1 Experimental details

The validation of a reliable theory depends on the proper design of the experimental setup. The intention behind the experimental setup used in this thesis work is to minimize the gap between theory and application. Below, the subsections give the details of the experimental setup followed.

4.1.1 Materials

The material configuration at the laminate scale consists of reinforcement of multiaxial multilayer wrap knitted (MMWK) fabric, also known as a non-crimp fabric (NCF) and matrix of epoxy/amine. The fabric architecture in these laminates consists of uniaxial, biaxial, and triaxial roving placement and are made up of E-CR or H/R type glass fibres, see [Figure 32](#). The E-CR glass fibre is **E**lectrical - **C**orrosion **R**esistance; alumino-lime silicate; moderate strength and modulus glass fibre, whereas, the H/R glass fibre is **H**igh performance/**R**einforcement; calcium aluminosilicates; high strength and modulus glass fibre. Except for the recent use of pultruded carbon profiles in the girder region of blade, most of the reinforcements are in NCF form.

The constituents of these fabrics are-

- Structural rovings for structural load carrying purpose
- Stabilizing yarns or stitch yarns to aid manufacturing

A thick roving bundle of $>1200\text{tex}^9$ is used generally for a structural roving, but if the fabric areal weight is lower than $\sim 1000\text{g/m}^2$, then even smaller ranges up to 600 tex roving are used at the expense of extra cost.

⁹ Tex = weight in grams of 1000m of roving

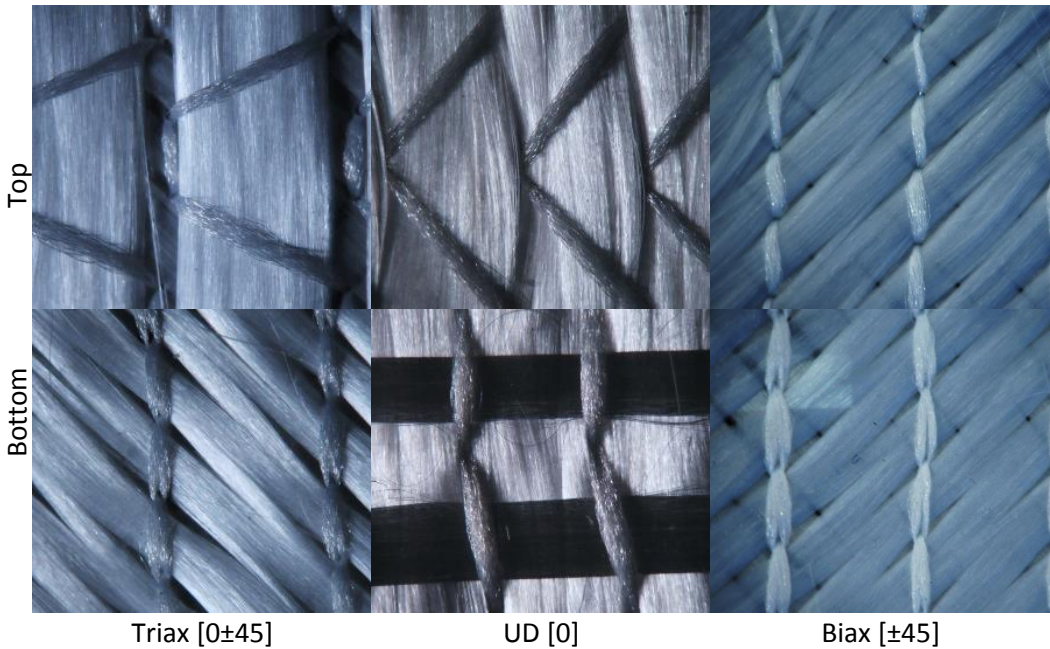


Figure 32 Wind turbine blade reinforcement types

The stabilizing yarns are made generally from <300 tex roving with cheaper E-glass fibres, and to meet the purpose of manufacturing aid, they are often placed off-axis to main structural roving. This placement creates a second-order impact on the final properties. While carrying any in-plane loads, the damage initiates first in or at these off-axis fibres before creating any damage into the main structural roving. The stabilizing and stitch yarn introduces micro (within the roving bundle) and meso (within ply) scale heterogeneity and makes the material response very complex to understand, to model, and to predict at each scale. The stitching yarn content and method (chain/tricot) not only introduces micro waviness in roving bundles but also influences the resin content locally and in the final laminate through the extra space they create.

The epoxy/amine matrix system consists of a blend of multicomponent and multifunctional monomers. Table 7 gives the details of the two matrix systems used in all experiments presented in this chapter.

Supplier	Resin	Hardener
Olin	Airstone 780E [DGEBA/ECH]	785H [POPDA/IPDA/DETA]
ABCL	Epotec YD535LV [DGEBA/ECH]	TH7257 [POPDA/IPDA/UVCB]

Table 7 Details of the two matrix systems used in all experiments presented in this chapter

The ply drop configuration from the subcomponent scale consists of pultruded carbon plate with rectangular geometry with 100% fibres oriented in the length direction of the plate. For bonding purpose, peel-ply is applied carefully on the surface during the manufacturing stage of the pultruded profile. Removal of peel-ply gives an optimal surface for bonding the pultruded profiles.

A total of eight material configurations were selected. To ease reading and identification, short-forms are used. For example, in “Triax OOA”, “Triax” indicates the Fabric structure, “O” the fibre manufacturer, the second “O” the fabric manufacturer, and “A” the matrix manufacturer. **Table 8** gives the list of letters used for other material configurations.

Short-form	Fibre		Fabric		Matrix
	Manufacturer	Type	Manufacturer	Type	Manufacturer
Triax OKA	Owens Corning	Advantex SE1500 (E-CR glass fibre)	Kush Synthetics Ltd.	Triax	ABCL ¹⁰
Triax OOA	Owens Corning	WS2000 (E-CR glass fibre)	Owens Corning	Triax	ABCL
UDG OKA	Owens Corning	Advantex SE1500 (E-CR glass fibre)	Kush Synthetics Ltd.	UDG	ABCL
UDGH 3KD	3B	HipertexW2020 (H/R glass fibre)	Kush Synthetics Ltd.	UDGH	Dow ¹¹
UDGH OOD	Owens Corning	WS3000 (H/R glass fibre)	Owens Corning	UDGH	Dow
UDGH OOA	Owens Corning	WS3000 (H/R glass fibre)	Owens Corning	UDGH	ABCL
Ply drop	Zoltek	Panex-35 (50K carbon fibre)	Zoltek	Pultruded plate	Dow
Biax OKD	Owens Corning	Advantex SE1500 (E-CR glass fibre)	Kush Synthetics Ltd.	Biax	Dow

Table 8 Material configurations short forms

4.1.2 Process

To manufacture all the laminates, the vacuum Assisted Resin Infusion Moulding (VARIM) process was adopted. **Figure 33** schematically illustrates the process setup.

¹⁰ Aditya Birla Chemical Ltd.

¹¹ In 2015 Olin Corporation announced merger of Dow Chemical Company's Epoxy businesses.

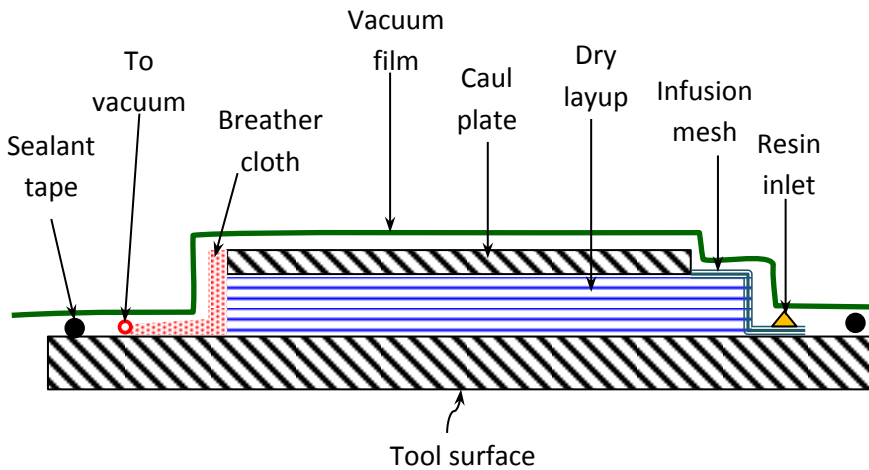


Figure 33 Schematic of VARTM process

All the monolithic laminates were made with the help of a caul plate to achieve a flat surface, without the use of a peel-ply. A peel-ply would lead to extra resin accumulation at the surface, which does not contribute to the load transfer but increases the cross-sectional area. The latter would invalidate assumption in the stress calculation. The ply drop laminates were prepared in one shot infusion by using inserts in the laminate build-up, which later were removed to get the step of dropped ply.

The Infusion was carried out at $30\pm 5^{\circ}\text{C}$ temperature under full vacuum using a degassed resin system. Once all the dry reinforcements were fully impregnated, gradual reduction in vacuum up to 50% was applied to achieve uniform compaction during the consolidation stage and hence to achieve uniform fibre volume fraction across the length of infusion.

A two-step cure process was adopted to reduce the generation of internal stress. The first pre-cure step cure was performed at 65°C for 3:30hrs and the second post-cure step was at 80°C for 7:00hrs. Before the application of the second step cure in a separate hot air oven, the laminate was demolded and trimmed for sharp edges.

After post-cure, tabs made of a printed circuit board (PCB) applied carefully using adhesive glue on top of the laminate. One of the lessons learned during the course of this work is, achieving a thin and uniform bond line thickness is crucial for proper introduction of compression load in the gauge area and to reduces unwanted damage initiation in the gripping area. Such bond line thickness can be achieved by using

infusion tab bonding with the help of the same or a tougher matrix system than of the base laminate.

Afterwards, coupons of required shape were extracted from the cured laminates using a water-cooled diamond cutter saw. In all processes, care was taken to keep fibre alignment in the required direction. The glass transition temperature and the fibre volume content was measured on post cured laminate for quality assurance purpose.

4.1.3 Test specification

For fatigue testing of composite materials, there exists no single Standardized methodology where necessary test requirements and conditions are specified considering all test scenarios. Hence in this work, general guidelines from ISO13003 [428] and ASTM D3479 [429] standard were followed, but the test method was adapted to execute compression loaded fatigue tests. [Table 9](#) gives the details of the overall methodology followed.

Requirement	Details
Control mode	Load controlled (for seven material configurations) Strain controlled (Only for biax laminate)
Amplitude type	Constant amplitude test
Stress ratio (R)	Minimum 3 (tension-tension, compression-compression and tension-compression)
Load levels	Minimum 4 (scattered over >4 decades)
Number of coupons	Minimum 3 coupons per level
Coupon geometry	As per Figure 35
Clamp pressure	60-80bar
Frequency	1Hz – load level aimed for <1000 cycles 2Hz – load level aimed for < 10,000 cycles 3Hz – load level aimed for < 100,000 cycles 5Hz – load level aimed for < 1,000,000 cycles
Strain measurement	Actuator displacement Strain gauges Clip-on extensometer

Table 9 Fatigue test methodology details

In the case of the Biax material, deviation from the above-specified methodology was adopted to find out the minimum number of stress ratios required for accurate prediction. Here, four stress levels were tested only for fully reverse loading, while for the other stress ratios, only one stress level was tested. All the monolithic laminates were tested in the length direction of the fabric, which is also the stitching direction. The ply drop configuration was tested in the length direction of the pultruded plate, which is the direction of the fibres. In all coupon configurations, symmetry across the mid-plane was maintained during lay-up.

The coupon geometries from the OPTIMAT database[186, 430] were selected for monolithic laminates. Figure 34 gives the details of the geometries used. In case of ply drop configuration, the ply drop had a chamfer of 1:20 over its thickness, covered with two layers of biax fabric, to reduce the stress concentration at the tip of the dropped ply. Under the compression loading, to avoid the failure by buckling, coupons with sandwich-type construction were made, see Figure 35 (bottom). For sandwich ten layers of biax fabric was used, which is equivalent to 13.2% of the overall coupon stiffness and the stress in carbon ply calculated by correcting the load for this stiffness contribution. Figure 35 gives a schematic of the ply drop configuration.

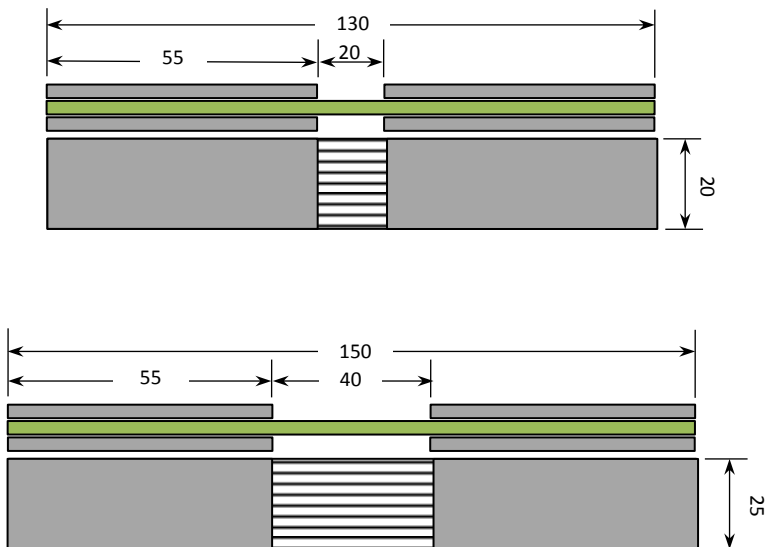


Figure 34 Monolithic laminate configurations; (top) Unidirectional, (bottom) Multidirectional

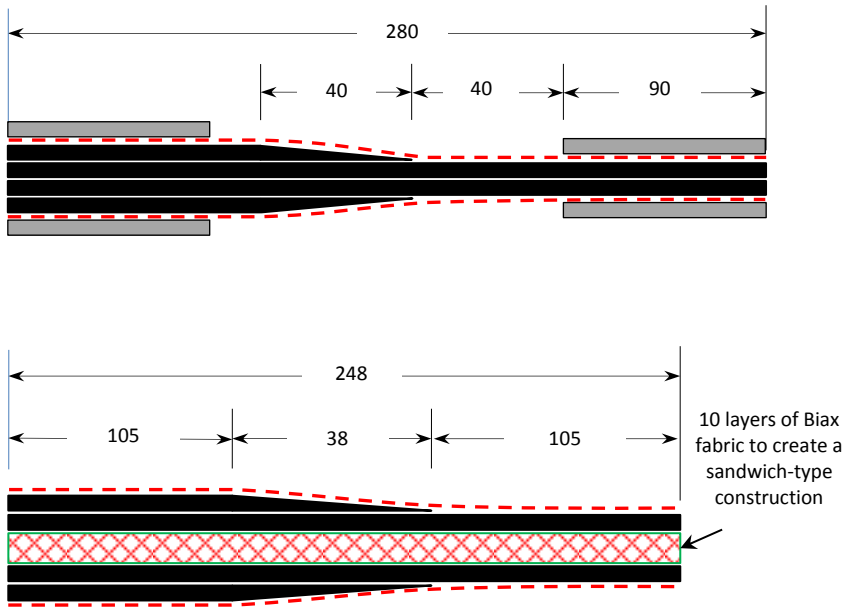


Figure 35 Ply drop configurations; (top) R0.1, (bottom) R=-1 and R=10

During the execution of all the tests, raw data were acquired from all three strain sensors given in Table 9 and load sensors over the entire testing time. Also, hysteresis curve tracking was performed throughout the test at few randomly selected cycles per coupon to limit extensive data handling and post-processing. One of the lessons learned in this work is to record hysteresis curves for any change in the material state. For example, during the damage initiation state in the ply drop test, record hysteresis curves over that period of time. The damage initiation state can be tracked by following the increase in displacement or reduction in stiffness of coupon.

The test was executed by a third party lab (WMC¹² and Risø¹³) under the coordination of the author for various internal projects in Suzlon Energy Ltd. Before executing the test at the third-party lab, pilot-scale testing was performed. The Pilot-scale tests consist of a certain minimum amount of tests done on the same coupons. This pilot step helped to define critical requirements of the test method and also to get consistent and accredited data set.

The experimental records collected during the test execution for all the material configurations are given in Appendix A.2 for reference purpose.

¹² Knowledge Centre WMC (Wind turbine, Materials and Constructions), Kluisgat 5, 1771MV, Wieringerwerf, The Netherlands.

¹³ Risø DTU National Laboratory for Sustainable Energy, Frederiksborgvej 399, 4000 Roskilde, Denmark.

4.2 Validation of theory

This section provides details of damage and deformation mechanisms occurring in various material configurations. In each subsection, results from selected material configurations are presented to highlight deviations or agreements with theory, while the rest data is given in Appendix A.3 to proof representativeness.

Before starting the fatigue results analysis to understand damage and deformation mechanisms, the prerequisite is to understand the static behaviour, as its understanding provides a strong basis for understanding fatigue behaviour.

4.2.1 Static

Figure 36 gives an average static response for all eight configurations. The stress-strain curves show deformation behaviour from pure elastic (in the case of UD laminate) to highly non-linear (inelastic) nature (in case of Biax laminate).

Specifically, in the case of the biax OKD material configuration, a non-linear response is consistent in both tension and compression loading. Under compression loading, the laminate is stronger than the tension side. This higher strength is due to the existence of different damage mechanisms under tension and compression loading. Under tension loading, the damage develops as follows. First, short micro-cracks at the interface of fibre-matrix grow in fibre direction followed by transverse cracking at the interface with the stabilizer yarn fibre. Both these micro-cracks saturate over the gauge length in due course of deformation along with rotation (scissoring effect) of ± 45 rovings towards the loading direction. In the end, fibre pull-out occurs with separation of the specimen due to excessive de-bonding. However, under compression loading the damage mode varies depending on gauge length; for more extended gauge (45° fibres not running between clamp to clamp) buckling forms the predominant failure mode whereas a through-the-thickness-shear or brooming type failure was noticed for shorter gauge length.

In the case of UD laminates, regardless of any fibre types used, the tension loaded response is highly linear until fracture. In contrast, compression shows a small non-linearity near the fracture stage. This non-linearity is due to buckling of 0° fibres provoked either by in-elastic deformation of matrix or by damage. Under tension load, coupon failure occurs when a minimum amount of fibres have failed. The damage process is not local but distributed in small clusters of fibre breakage, and its nature is stochastic [431, 432]. Also, a small number of micro-cracks develop in the gauge area at

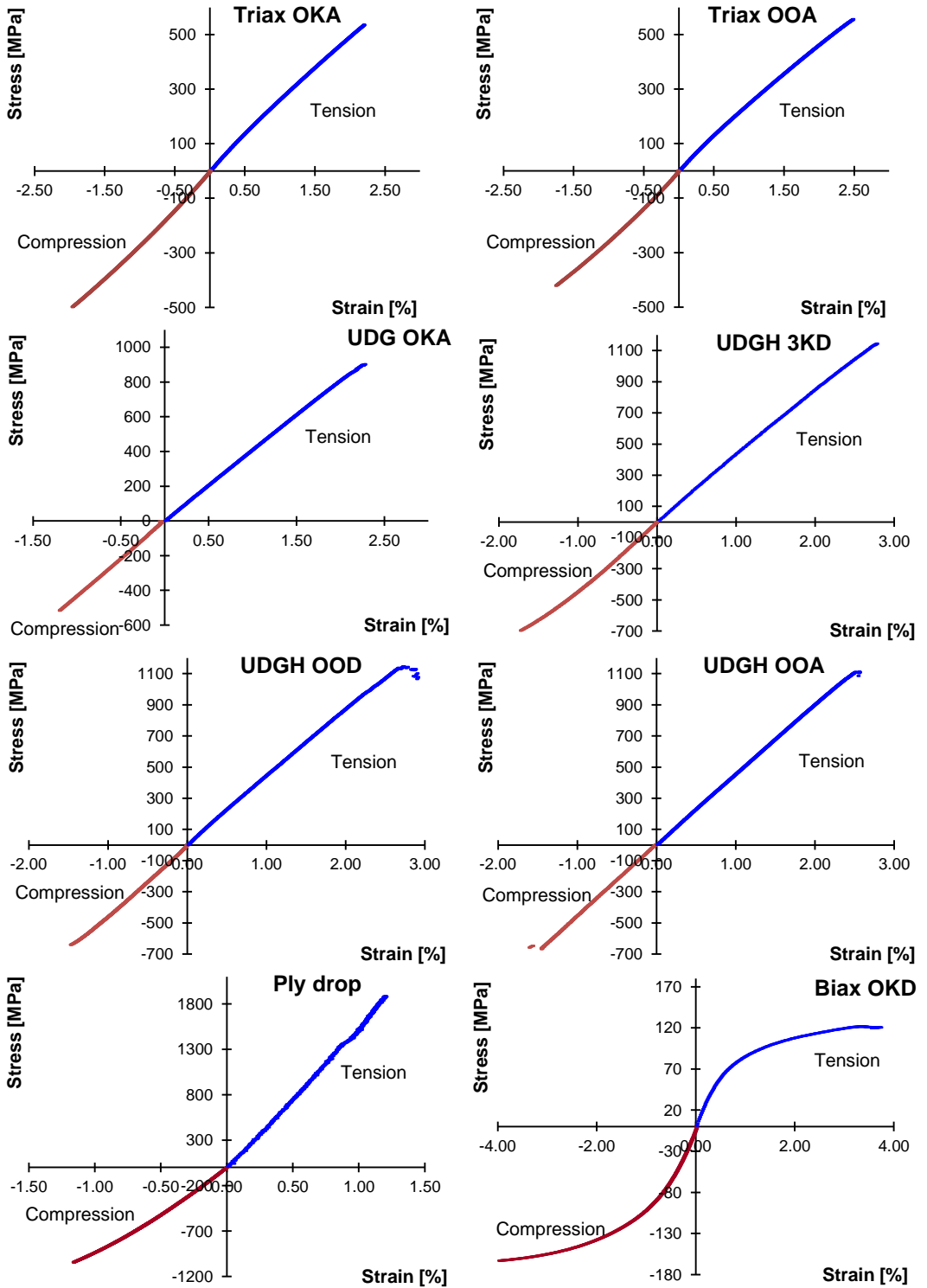


Figure 36 Static stress-strain curves (average) for all material configurations

the stabilizing yarn interface. These micro-cracks contribute to the initiation of the longitudinal splitting of main structural rovings leading to the final coupon failure.

In the case of Triax laminates, both the tension and compression responses are slightly non-linear. Under tension loading, the $\pm 45^\circ$ plies show gradual micro-cracks development before the laminate fractures at the 0° plies. The reason for not having a fracture in ± 45 ply is due to its higher fracture strain than the 0° ply.

In the case of ply drops, the tension loaded response is linear with delamination as the type of damage developing between terminated ply and adjacent continuous ply. The damage is catastrophic, and no initiation or propagation stage exist until the last moment of fracture. The compression response is slightly non-linear, and the damage mode was the through-thickness-shear failure of continuous carbon plies in a catastrophic nature. This catastrophic nature also caused delamination to occurs almost simultaneously between dropped ply and adjacent continuous ply.

4.2.2 Fatigue

This section presents the analysis of the fatigue test results. Here the understanding of quasi-static deformation and damage mechanisms, discussed in the previous section, guides the reasoning developed during the fatigue analysis. First, the damage developed during the fatigue loading is discussed, and then the analysis of deformation behaviour and associated details are discussed.

4.2.2.1 Damage analysis

In most configurations, the damage mechanism in fatigue is quite similar to that of quasi-static loading. Only for a few configurations, the final failure of a single coupon per stress ratio is discussed, to highlight peculiarities observed in the damage development rather than documenting all cases.

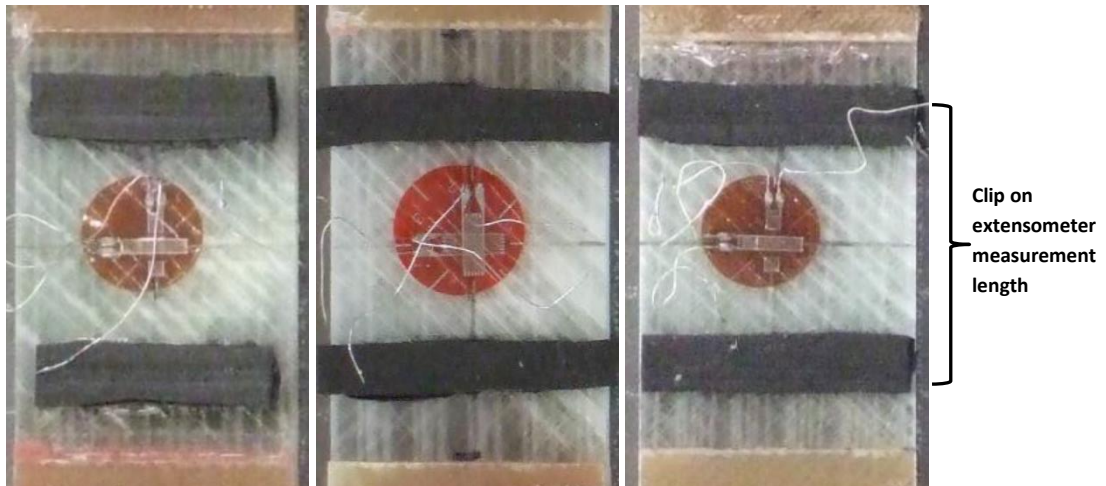
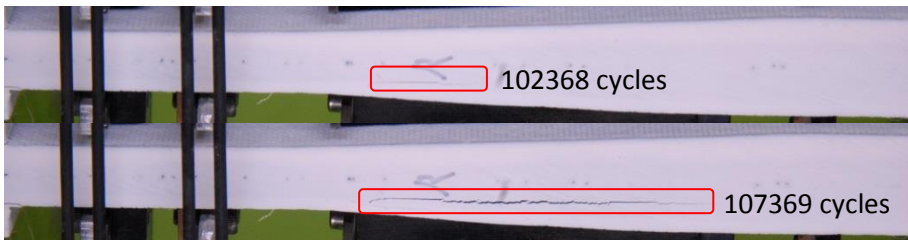


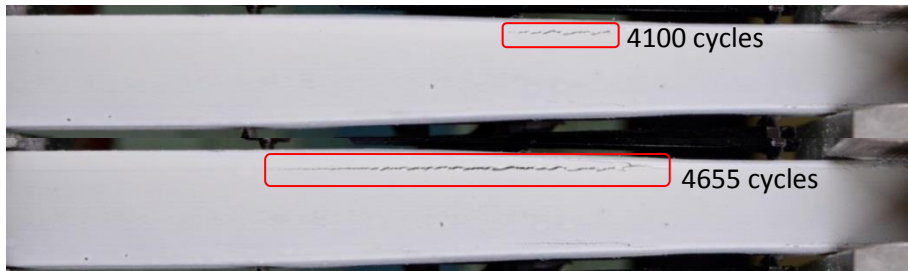
Figure 37 Damage images for Biax OKD material configuration at the time of test stop; (left) $R=10$, (middle) $R=-1$, and (right) $R=0.1$

For strain-controlled biax under tension dominated loading condition, the damage mechanism is very much similar to that of the quasi-static load condition, whereas under compression dominated loading the damage starts at the cross-over point of stitch yarn, 45° roving, 90° and 0° stabilizing yarn. Under both types of loadings, damage saturates and propagate along 45° roving resulting in further loss of stiffness. The test stopped at a 30% reduction in stiffness; hence information about the fracture stage is not available. In all cases, the damage was developed within the gauge area and in-between the clip-on extensometer measurement length, see Figure 37.

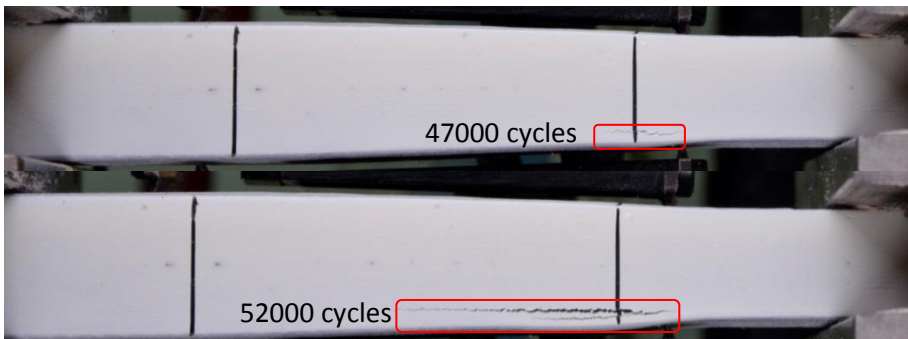
In the case of ply drop, the observed damage mechanism is similar under quasi-static tension and tension dominated fatigue loading. Damage in compression dominated fatigue is different from that of quasi-static loading. In all cases, the delamination type damage occurs between dropped ply and continuous ply, and it initiated and propagated rapidly only towards the end of life over very few cycles, see the photos in [Figure 38](#). Until that point, no sign of damage was observed at the macro-scale (visually). This behaviour justifies the use of the term ‘delayed initiation’ in the theory of damage, as discussed in section [2.2.1](#).



(a)



(b)



(c)

Figure 38 Damage images for ply drop material configuration; (a) $R=0.1$, (b) $R=-1$, and (c) $R=10$; showing damage initiation and propagation towards the end of life over very few cycles

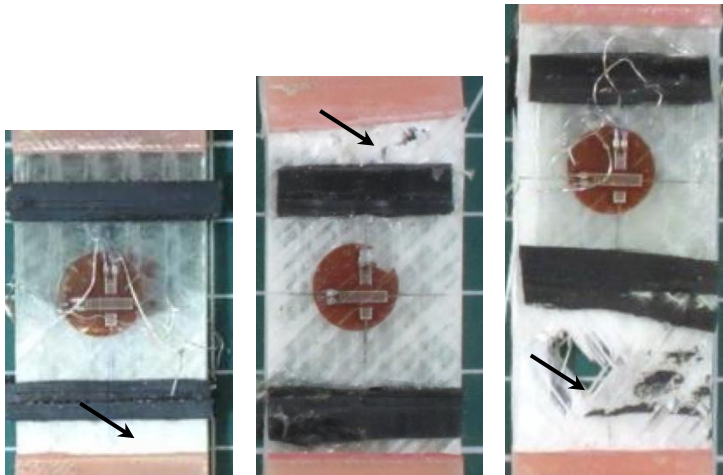


Figure 39 Final failure images for Triax OKA material configuration; (left) $R=10$, (middle) $R=-1$, and (right) $R=0.1$; indicating final failure occurred either at the tab start region or within the clamping region

In all the Triax and UD configurations, it was observed that the gauge area sustain only a partial portion of the damage. In many coupons, the final failure occurred either at the tab start region or within the clamping region, as indicated by the arrows in Figure 39. In these configurations, the initiation and propagation of micro-cracks in off-axis fibre roving is a standard damage type for tension dominated fatigue.

Under compression dominated fatigue, after some time from the test start, an off-axis movement in the grips is observed, and the intensity of movement depends on the load level. In the early stage of the test, the introduction of the compression loads in the gauge area happens without the observation of such off-axis movement. However, due to damage and in-elastic deformation of the matrix, the material is losing its rigidity. This loss of rigidity provokes buckling in the coupon and results in off-axis movement. The exact nature of the damage was not visible at the macro scale, and that was also not investigated in this work. However, using 3D computed tomography Fraise & Brøndsted [363] suggested that the shear crack formation in resin-rich areas could be the damage mode under compression fatigue.

The damage development outside the gauge area suggests that the behaviour observed or recorded is coupon behaviour and not material's. Hence, careful consideration before using any such data in the product design stage is advisable.

4.2.2.2 *Observations on recorded data from strain sensors*

In the previous section 4.2.2.1, the goal was to understand the damage mechanism under various fatigue load conditions. A similar understanding is required for the deformation mechanism. However, first, the applicability of the recorded data to represent the mechanism under investigation needs assessment. Depending on the area of measurement of strain sensors, the data obtained represents either partly or entirely the mechanism under investigation. The response from various strain sensors is given only for few cases out of eight material configurations tested, to discuss the peculiar aspect of deformation measurement (indicated by arrows in the respective figures). The cause of this peculiar behaviour is discussed in the next subsection 4.2.2.3.

In the case of the Triax OKA material configuration, the actuator displacement and clip-on extensometer show consistent trends, see Figure 40, whereas in the case of the UDGH OOA material configuration both these sensors readings deviate in trends, see Figure 41. The hysteresis curves for Triax shows consistent clockwise rotation with more rotation at the tensile side than compression for both these sensors. In comparison, the hysteresis curves for UDGH from actuator displacement show clockwise rotation with more rotation at the compression side while curves from clip-on extensometer show translation in strain space. For both Triax and UDGH, strain gauge detachment from the coupon surface occurred at about 1000 cycles.

In the case of Biax strain-controlled fatigue testing, the movement of the actuator is controlled using clip-on extensometer readings. Hence clip-on extensometer reading is the most suitable measure for damage and deformation. Figure 42 gives the difference in trend for actuator displacement and the clip-on extensometer. The actuator displacement readings show additional strain softening at the tensile side, and the hysteresis curves translate towards lower stress and strain values. Whereas for the clip-on extensometer clockwise rotation at the compression side is more than the tensile side. Here, the strain gauge got detached from the coupon surface after 600 cycles.

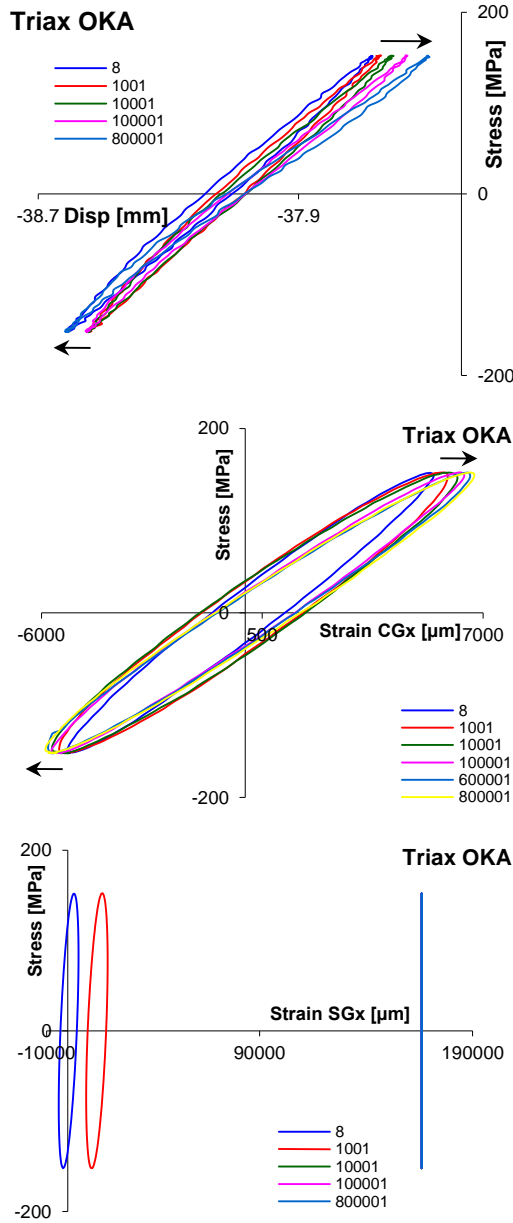


Figure 40 Hysteresis curves from various strain sensors for Triax OKA; Load controlled; $\sigma_m=0\text{MPa}$, $\sigma_a=152\text{MPa}$; (top) Actuator displacement, (middle) Clip-on extensometer, and (bottom) Strain gauge; (legend shows cycle number)

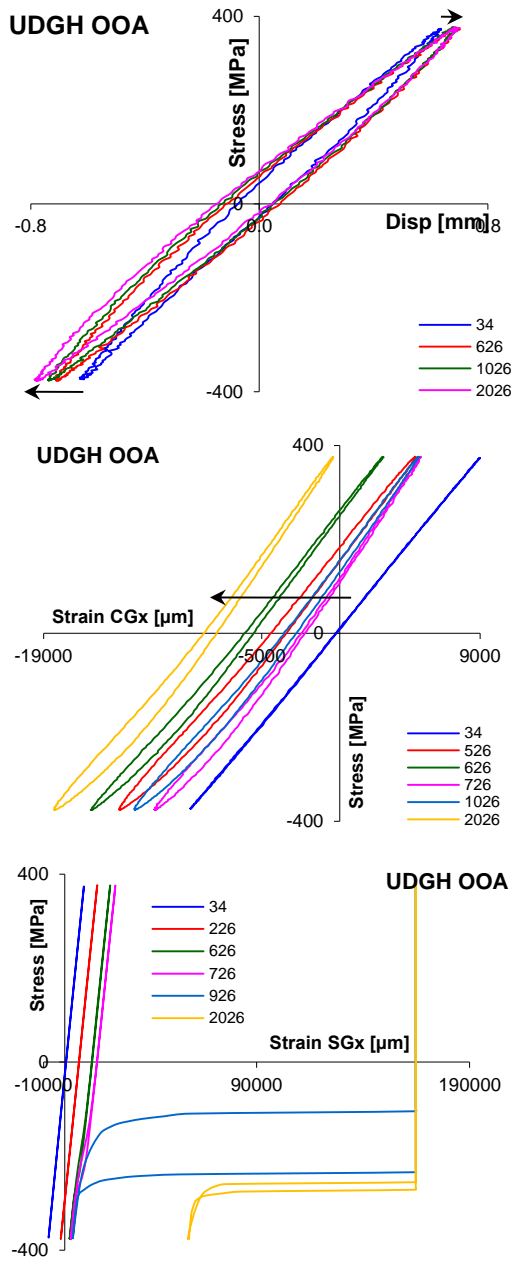


Figure 41 Hysteresis curves from various strain sensors for UDGH OOA; Load controlled; $\sigma_m=0\text{MPa}$, $\sigma_a=376\text{MPa}$; (top) Actuator displacement, (middle) Clip-on extensometer, and (bottom) Strain gauge; (legend shows cycle number)

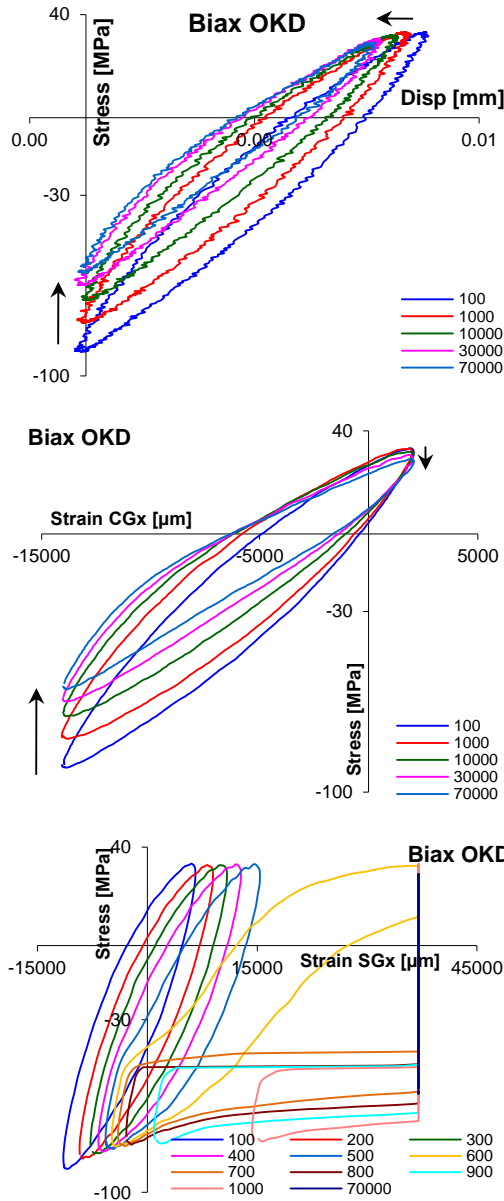


Figure 42 Hysteresis curves from various strain sensors for Biax OKD; Strain controlled; $\epsilon_m = -6000\mu\text{m}$, $\epsilon_a = 8000\mu\text{m}$; (top) Actuator displacement, (middle) Clip-on extensometer, and (bottom) Strain gauge; (legend shows cycle number)

In the case of ply drops, the clip-on extensometer shows a distinct change in shape and orientation of hysteresis curves compared to actuator displacement, see [Figure 43](#). As the delamination develops in-between clip-on extensometer measurement length,

the incident was captured more clearly than actuator displacement. Strain gauge sensors were not used in ply drop configuration testing.

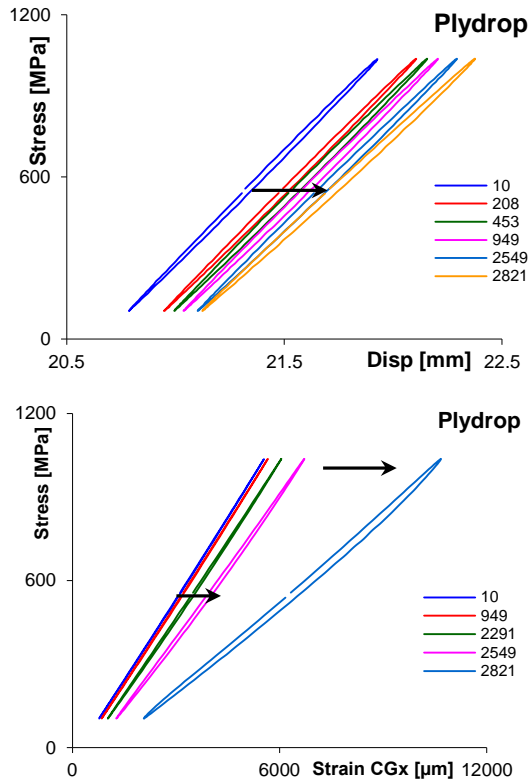


Figure 43 Hysteresis curves from various strain sensors for Ply Drop; Load controlled; $\sigma_m=567\text{MPa}$, $\sigma_a=464\text{MPa}$; (left) Actuator displacement, and (right) Clip-on extensometer; (legend shows cycle number)

In general, as the strain gauges are applied on the coupon's gauge length and are covering only a small percentage of the total deformed area, they tend to give very local information about strain development. This type of information is helpful in cases where a strain field discontinuity is present; for example, the region of terminated ply in the ply drop material configuration. One peculiar observation is that the strain gauges delaminate quite early in the fatigue test, due to damage at the surface and low bond strength. As the strain gauges delaminate from a surface partially or entirely, their data is of very limited use in the analysis. Nevertheless, due to their accurate local coverage, the initial values recorded can be used to describe absolute coupon behaviour at the start of the fatigue test.

Whereas the clip-on extensometer covers a relatively larger area than strain gauges, they capture more general information about strain development. However, they

suffer one drawback of mechanical slip. The slip amount depends on the surface quality of the coupon and its change during the test. As the damage location is captured only partially by clip gauge area, the data from clip gauge also has limited use in the analysis. Similar to strain gauges, recorded extensometer data also needs to be scrutinized for any abnormality in trend to find the usability of recorded data. In some cases, the clip-on extensometer showed a deviation from the elliptical shape of the hysteresis curves at the compression side compared to tension, see [Figure 41 \(Middle\)](#) and [Figure 42 \(Middle\)](#). Section 4.2.2.3 provides a discussion on the cause for this response due to its relevance in that section.

In the case of actuator displacement readings, the measuring scope includes not only the entire coupon length but also includes grips and any jig/fixture assembly used in the load string path. Due to this, the strain data calculated from actuator displacement is too inaccurate to represent absolute coupon behaviour. However, for comparative analysis, this data seems most accurate as it captures the entire coupon area and also the entire damaged area. This comparative use, the error gets cancelled out. Hence the data from actuator displacement can be used in further analysis. Therefore except biax OKD and ply drop configuration for remaining configurations, actuator displacement is used in further analysis.

4.2.2.3 *Cyclic inelasticity*

Previous sections give details of the damage mechanism and usability of various strain sensors. Now in this section attention is given for understanding deformation behaviour and their coupling with damage. The cause for the peculiarities from strain sensors, described in the previous section, are also discussed here. This section gives only the peculiar aspect of hysteresis curves relevant to describe inelastic behaviour under cyclic loadings. Appendix A.3.3 to A.3.5 give the hysteresis curves for a typical coupon per stress ratio for all material configurations to demonstrate the unique behaviour.

The elliptical shape in the hysteresis curve is very consistent for all material configurations from high stiffness ply drop configuration to that of soft biaxial configuration. The distinguishing features of these hysteresis curves under different stress ratios and materials were studied extensively in the past [433, 434, 436, 437]². These features are-

- I. Size
- II. Shape
- III. Translation in stress-strain space

The **size** of hysteresis curves at the mean stress value signifies the amount of deformation that does not get reversed over the complete cycle. In case of thin size hysteresis curves, like ply drop configuration, a large amount of deformation is reversed, see Figure 44. In case of more significant size hysteresis curves, like Biax OKD configuration, only some portion of the total deformation gets reversed, and a relatively large amount is accumulated as an inelastic strain over a complete cycle, see Figure 45. Other configurations that are in between these two extremes show the relative change in size and accordingly, the amount of deformation that is reversed.

The size of hysteresis curves does not remain constant throughout the fatigue process, and especially at the fracture stage, the inelastic strain changes drastically. This change in size indicates the effect of damage on the inelastic strain development; in other words: inelasticity-damage coupling. Explanation to change in the size of hysteresis curves can be given by referring to the quasi-static behaviour from section 4.2.1. In the case of Biax OKD, this change of size is due to the ability of a material to undergo significant inelastic deformation before fracture.

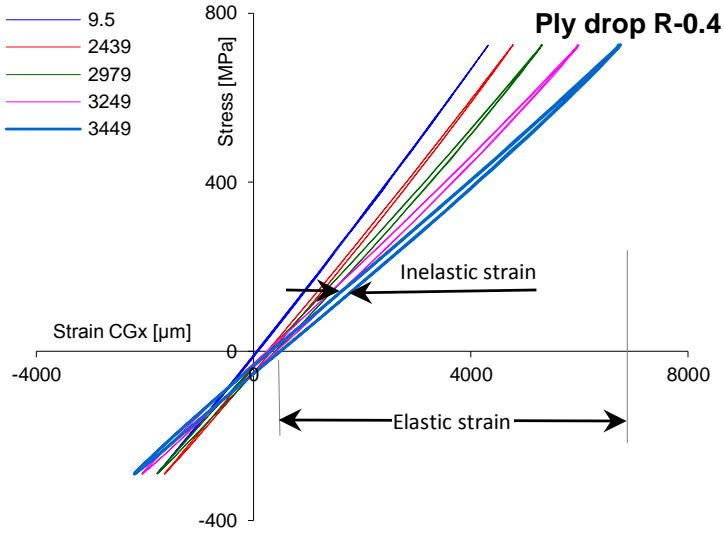


Figure 44 Hysteresis curves from clip gauge sensors for Ply Drop; Load controlled; $R=-0.4$; $\sigma_m=217\text{MPa}$, $\sigma_a=506\text{MPa}$; (legend shows cycle number)

In ply drop, this change of size is due to the distinct damage mechanism. Whereas in the case of Triax and UD material configurations, the material shows minimal inelastic deformation until fracture and due to this, the change in the size of hysteresis curves is also minimal, see Figure 46.

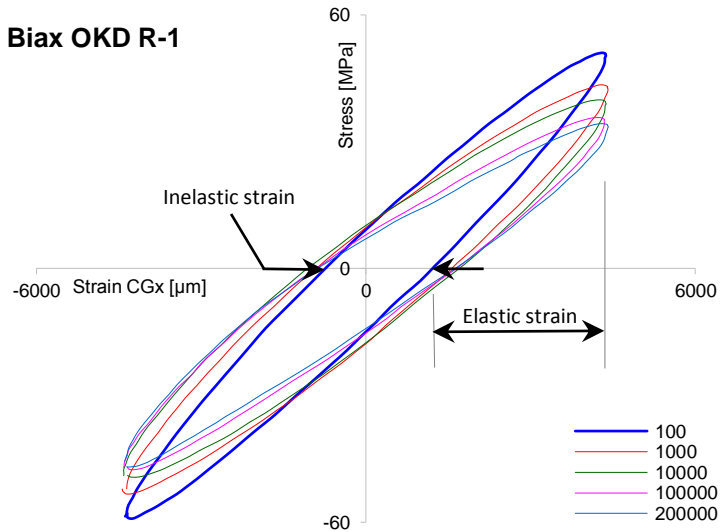


Figure 45 Hysteresis curves from clip gauge sensors for Biax OKD; Strain controlled; $R=-1$; $\epsilon_m=0\mu\epsilon$, $\epsilon_a=4400\mu\epsilon$; (legend shows cycle number)

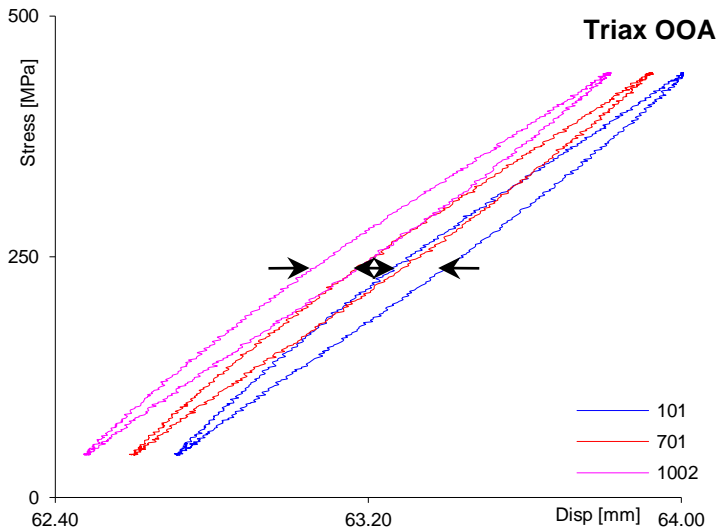


Figure 46 Hysteresis curves from actuator displacement sensors for Triax OOA; Load controlled; $R=0.1$; $\sigma_m=243\text{MPa}$, $\epsilon_a=198\text{MPa}$; (legend shows cycle number); arrow indicates minimal size change in hysteresis curves

The **shape** of hysteresis curves signifies a particular type of deformation mechanism endured and any shape change in subsequent cycles attributes to change in that mechanism due to the presence or occurrence of another mechanism.

In all material configurations except for ply drops under compression dominant fatigue loading, one peculiar observation noticed with the clip-on extensometer is that the shape and size of the hysteresis curves are not symmetrical across the mean stress line [264]. This deviation is mainly towards the end of the fatigue life, whereas at the test start for the same coupon the hysteresis curve is symmetric, refer [Figure 42 \(Middle\)](#) and [Figure 47](#) for Biax OKD [435], [Figure 41 \(Middle\)](#) for UDGH OOA and [Figure 51](#) for UDG OKA configurations. The reason for this observation is the occurrence of a new incidence of deformation and damage modes. In compression dominated fatigue due to the accumulation of inelastic strain and damage, the material is losing its stiffness, and at some point, the critical length to resist buckling is exceeded. Due to this buckling, the clip-on extensometer experiences non-uniform compressive strains that result in shape and size change in the hysteresis curve. Under tension dominated fatigue due to saturation of micro-cracks (in off-axis fibre roving), the material is losing stiffness gradually and hence the slope of hysteresis curve changes at tension side whereas at compression side due to closing of these micro-cracks no further decrease in stiffness occurs, and shape of hysteresis curves remain relatively constant.

The presence of any tension load accelerates the buckling mode under compression due to damage generated from tension loading.

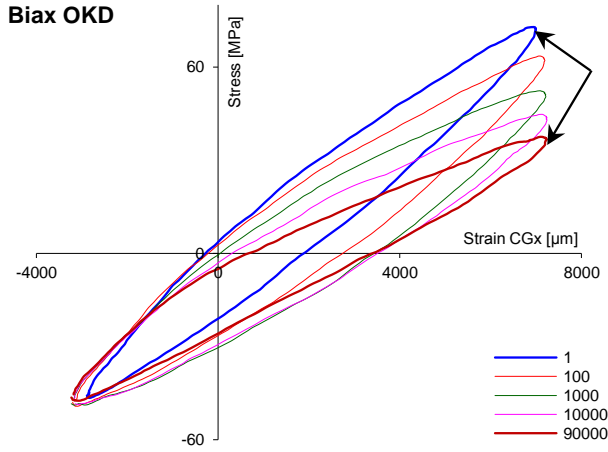


Figure 47 Hysteresis curves from clip gauge sensors for Biax OKD; Strain controlled; $R=-0.44$; $\epsilon_m=2016\mu\epsilon$, $\epsilon_a=5184\mu\epsilon$; (legend shows cycle number); arrow indicates unsymmetrical shape and size deviation in hysteresis curves across the mean stress line

In case of ply drops under both compression and tension dominated fatigue, the change in the shape of hysteresis curves at the last part of the fatigue process is attributed to the generation of complete delamination between dropped and continuous ply towards the clamping area, see Figure 48 and Figure 49.

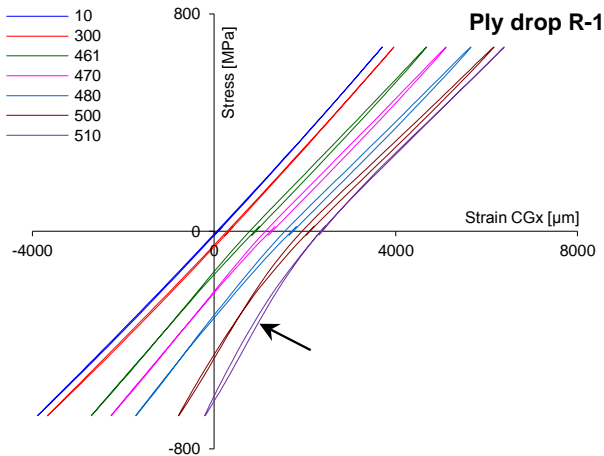


Figure 48 Hysteresis curves from clip gauge sensors for Ply Drop; Load controlled; $R=-1$; $\sigma_m=0\text{MPa}$, $\sigma_a=707\text{MPa}$; (legend shows cycle number); arrow indicates unsymmetrical shape and size deviation in hysteresis curves across the mean stress line

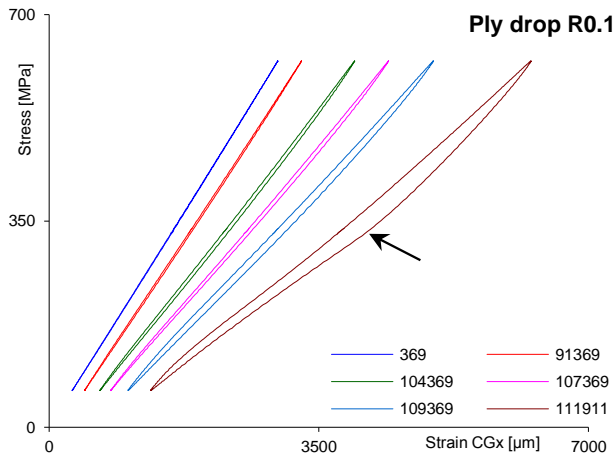


Figure 49 Hysteresis curves from clip gauge sensors for Ply Drop; Load controlled; $R=0.1$; $\sigma_m=340\text{MPa}$, $\sigma_a=278\text{MPa}$; (legend shows cycle number); arrow indicates unsymmetrical shape and size deviation in hysteresis curves across the mean stress line

The shape change in any hysteresis curve due to the occurrence of different deformation and damage mechanisms is captured more clearly by the clip-on extensometer than by the actuator displacement, refer to [Figure 50](#) and [Figure 51](#). Due to buckling mode in coupon gauge length, during loading clip-on extensometer experiences, additional strains whereas actuator experiences uniform compressive displacement. Due to the buckling, the clip-on experiences a reversal of the additional strain resulting in a distorted hysteresis curve, whereas actuator experiences reduced strain resulting in bending backwards of the hysteresis curve [438].

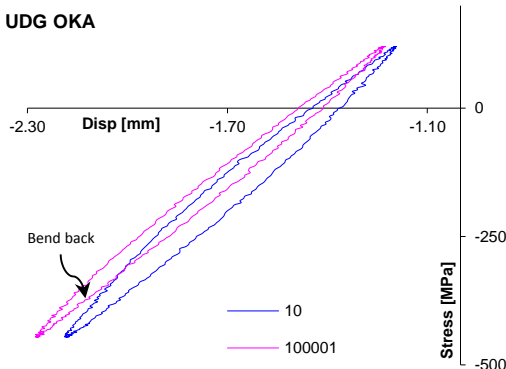


Figure 50 Hysteresis curves from actuator displacement sensors for UDG OKA; Load controlled; $R=-3.7$; $\sigma_m=-162\text{MPa}$, $\sigma_a=283\text{MPa}$; (legend shows cycle number)

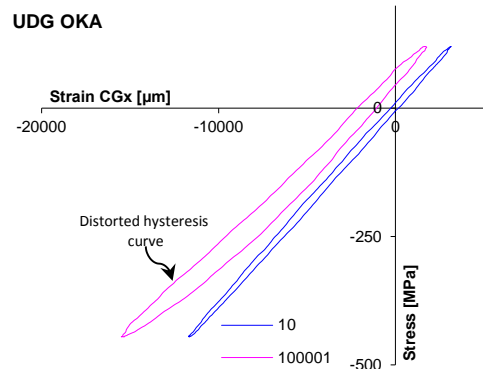


Figure 51 Hysteresis curves from clip gauge sensors for UDG OKA; Load controlled; $R=-3.7$; $\sigma_m=-162\text{MPa}$, $\sigma_a=283\text{MPa}$; (legend shows cycle number)

The third feature of hysteresis curves is its **translation** in stress-strain space. Once the damage gets generated, the material loses some of its stiffness, and the hysteresis curve translates in stress-strain space in either a uniform or a non-uniform manner. In the case of uniform translation, a complete hysteresis curve is translated over the entire stress or strain range to a new space, whereas in non-uniform cases the translation is greater at maximum stress and less at minimum stress. Depending on loading type and intensity, both deformation and damage mechanisms contribute to this translation effect. In all material configurations under any stress ratio, both uniform and non-uniform translation in the hysteresis curves is present.

In case of fully reverse fatigue loading as additional strain and damage are getting generated at both tension and compression side, this results in clockwise rotation of the hysteresis curves, as illustrated in [Figure 52](#) and [Figure 53](#).

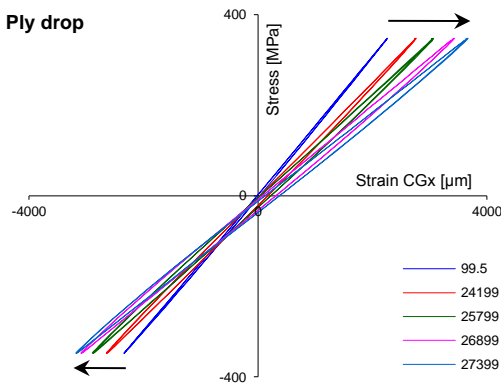


Figure 52 Hysteresis curves from clip gauge sensors for Ply drop; Load controlled; $R=-1$; $\sigma_m=0\text{MPa}$, $\sigma_a=363\text{MPa}$; (legend shows cycle number); arrow indicates clockwise rotation of the hysteresis curves

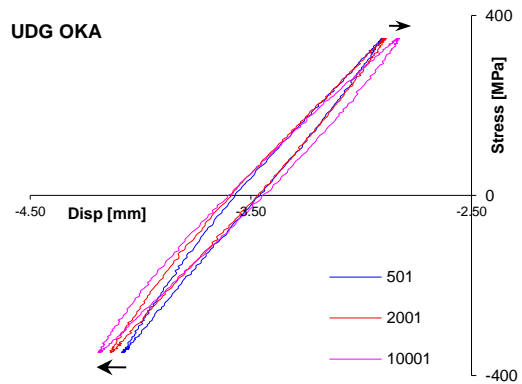


Figure 53 Hysteresis curves from actuator displacement sensors for UDG OKA; Load controlled; $R=10$; $\sigma_m=0\text{MPa}$, $\sigma_a=349\text{MPa}$; (legend shows cycle number); arrow indicates clockwise rotation of the hysteresis curves

In the case of ply drops for all stress ratios, a shakedown-like softening is observed due to delayed initiation of delamination in the ply drop. Until the final part of the fatigue test, the hysteresis curves translate in close proximity and uniformly to new stress-strain space. As the damage mechanism in both tension and compression dominated fatigue is similar, the hysteresis translation is also similar until the damage initiates in the coupon. As the crack develops at the drop ply region, the hysteresis changes the slope due to loss of stiffness. The longer crack length introduces significant rotation in the hysteresis curve, as illustrated in [Figure 54](#) and [Figure 55](#).

Except for ply drop configurations, in the first part of the test, the sudden translation in hysteresis curves due to generation of damage is standard in all configurations.

Also, in the case of tension-tension and compression-compression fatigue loading, a uniform translation is observed, see [Figure 56](#) and [Figure 57](#).

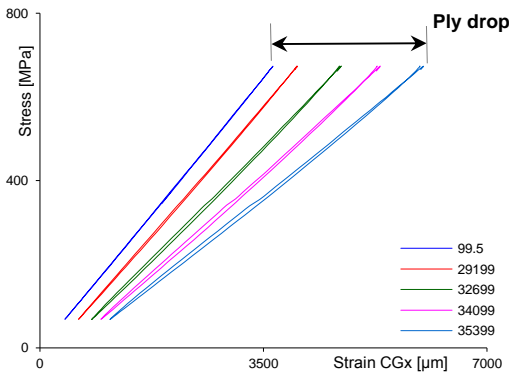


Figure 54 Hysteresis curves from clip gauge sensors for Ply Drop; Load controlled; $R=0.1$; $\sigma_m=368\text{MPa}$, $\sigma_a=301\text{MPa}$; (legend shows cycle number); arrow indicates the change of slope of the hysteresis curves

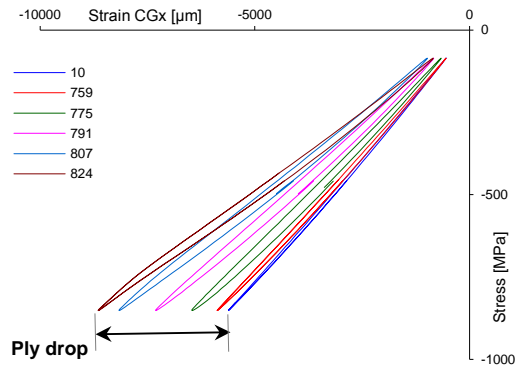


Figure 55 Hysteresis curves from clip gauge sensors for Ply Drop; Load controlled; $R=10$; $\sigma_m=-488\text{MPa}$, $\sigma_a=400\text{MPa}$; (legend shows cycle number); arrow indicates the change of slope of the hysteresis curves

UDGH OOD

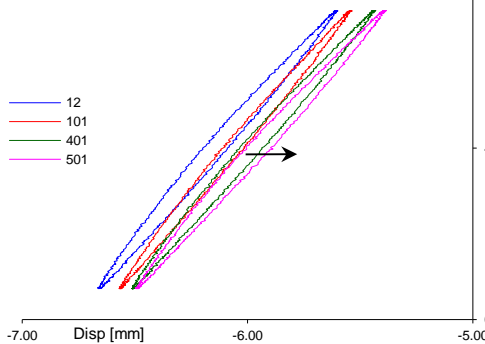
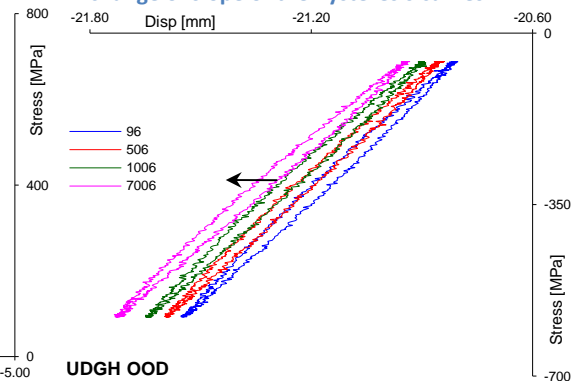


Figure 56 Hysteresis curves from actuator displacement sensors for UDGH OOD; Load controlled; $R=0.1$; $\sigma_m=397\text{MPa}$, $\sigma_a=324\text{MPa}$; (legend shows cycle number)



UDGH OOD

Figure 57 Hysteresis curves from actuator displacement sensors for UDGH OOD; Load controlled; $R=10$; $\sigma_m=-318\text{MPa}$, $\sigma_a=261\text{MPa}$; (legend shows cycle number)

Except for translation in strain space under load-controlled and in stress space under strain-controlled fatigue conditions, other characteristics for hysteresis curve translation are the same for both control modes. All the coupon responses discussed in this section relate to relatively high loads. In the case of low loads, high cycle fatigue, the change in size, shape, and translation of the hysteresis curves is minimum because less damage is generated.

So far, the focus was on obtaining more understanding of the fatigue phenomenon in line with the theory. For practical applications, only understanding is not enough, but an accurate estimation of fatigue life at any damage state based on consistent mathematical formulation is required.

4.3 Validation of mathematical formulation

This section provides the validation of the non-linear damage evolution law and the formulation of constant fatigue life curves derived in section 3.4 for laminate and subcomponent scale material configurations. To validate the mathematical formulation, specific physically tangible parameters are needed, that can quantify the peculiar aspect of these mechanisms in its entirety. Analysis of the hysteresis curves provides identification of the most relevant parameters for validation purposes.

4.3.1 Hysteresis curve analysis

The main distinguishing features of these hysteresis curves are-

- I. Width of the hysteresis curve at mean stress value representing inelastic strain range $\Delta\varepsilon^p$, as recommended in [439]. The recovered elastic strain range is given by

$$\Delta\varepsilon^e = \Delta\varepsilon - \Delta\varepsilon^p \tag{Equation 72}$$

- II. The area enclosed by the curve is the inelastic strain energy W^p . It is resulting in inelastic strain development and heat dissipation in the material. Figure 58 shows the integration scheme used to calculate inelastic strain energy.

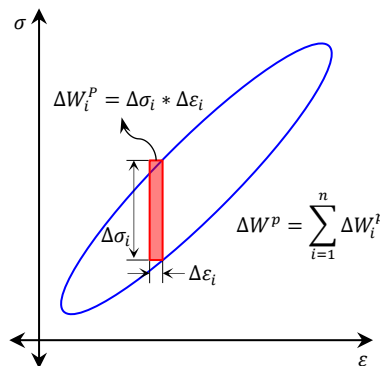


Figure 58 Schematic representation of integration scheme used to compute ΔW^p

The area underneath the hysteresis loop represents elastic strain energy W^e . It is resulting in elastic strain development, as shown in [Figure 59](#). For this area, a similar integration scheme is followed to compute elastic strain energy.

- III. The major axis of the ellipse represents the overall coupon resistance to deformation and is here referred to as hysteresis stiffness \bar{E} . The quadrants formed along the major axis of the ellipse and mean loading axis results in four types of quadrant stiffness: the resistance of material while positively loading, the resistance of material while positively unloading, the resistance of material while negatively loading, the resistance of material while negatively unloading. In case other than fully reverse loading this division is not logical, but due to the shape of an ellipse, geometrically it is plausible to dissect the curve like this. These features are depicted schematically in and [Figure 60](#).

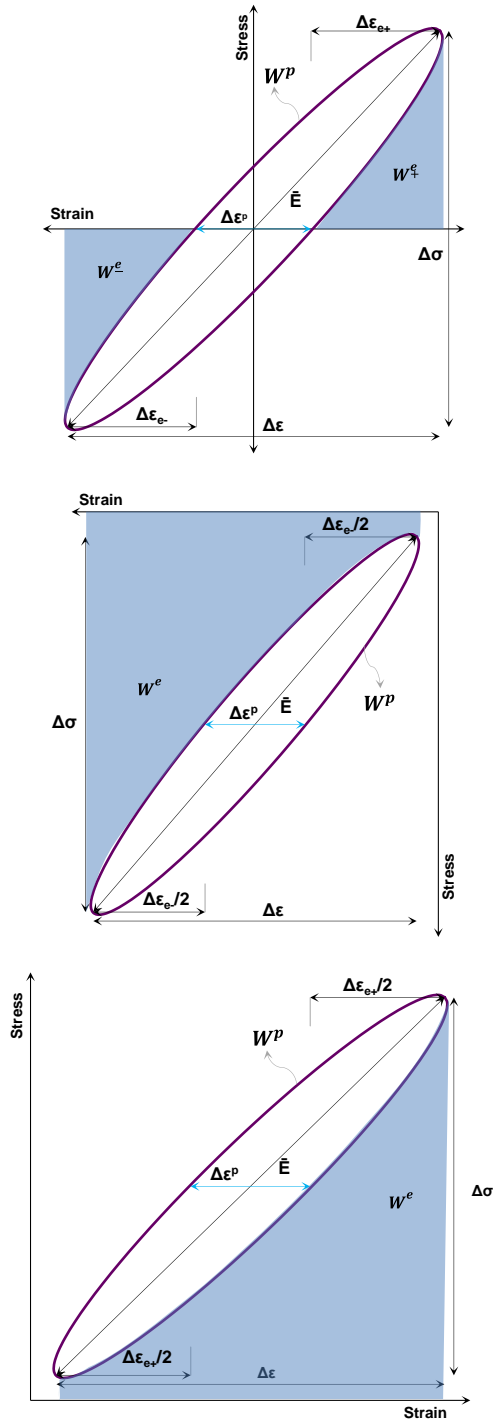


Figure 59 Schematics of hysteresis curves; (top) fully reverse loading, (middle) Tensile mean stress and (bottom) Compressive mean stress

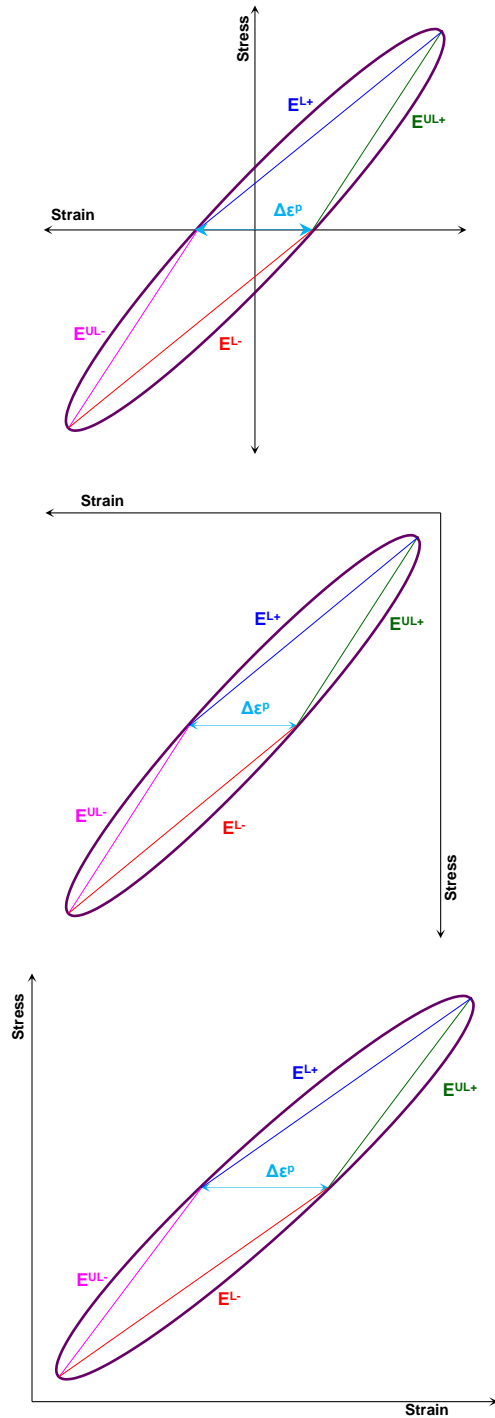


Figure 60 Schematics of four-quadrant of hysteresis curves; (top) fully reverse loading, (middle) Tensile mean stress and (bottom) Compressive mean stress

4.3.2 Damage measurement

The distinguishing features of the hysteresis curve defined in the previous section are referred to as parameters in this section. This section presents and discusses the selection criteria for a parameter to represent the damage. Two selection criteria were formulated as

- The trend of any parameter should show a clear distinction between different load levels
- The trend should show sharp features of all damage development stages

These two criteria provide the validity of the parameter to capture the damage mechanism entirely. The trend of any parameter is not the same for all stress ratios due to the associated different damage mechanisms. [Figure 61](#) illustrate the elastic strain energy development throughout the fatigue life for $R=0.1$ and $R=10$. Here, for $R=0.1$, the stress levels are distant apart from each other and due to this more clear distinction between load levels compared to the $R=10$. The difference in the distinction between load levels for these two stress ratios is because of different damage mechanism associated with each loading. The $R=-1$ consists of both tension and compression loads show a trend somewhat in-between in terms of a clear distinction between load levels and sharp feature for all damage development stages, as shown in [Figure 63](#).

For all material configurations, one general observation is that all three parameters strain, strain energy, and stiffness do not remain constant throughout the fatigue life, see also appendix [A.3.6](#) to [A.3.12](#). A similar trend as that of general damage development stages, as shown in [Figure 25](#), is observed in the trend of these parameters. A sudden change in parameters value during the early stage of the fatigue loading is attributed to damage initiation stage. This change corresponded to $<10\%$ of life and noticed for all material configurations except ply drops. In the case of ply drops, no change in parameters is noticed until the very last part of fatigue life. After the initiation stage, the parameters show a gradual change until the very last part of fatigue life. This stage is referred to as propagation stage and extends up to 70% of the total life. As the readings from all sensors at last part of fatigue (a few tens of cycles) were not recorded, the fracture stage cannot be seen for all coupons.

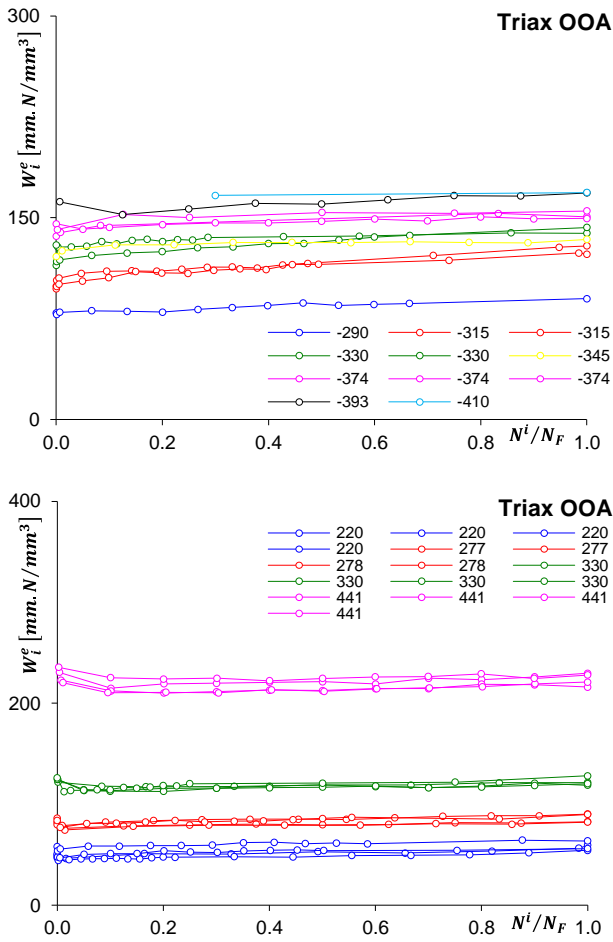


Figure 61 Elastic strain energy for Triax OOA, (top) R=10 and (bottom) R=0.1 (legend shows σ_{max} value in MPa)

The hysteresis curve is the basis for the calculation of the inelastic part of strains and strain energy. Hence, it only captures the inelastic part of deformation as it does not include information about the elastic component. For both strain and strain energy, the absolute value of the inelastic part is minimal compared to the elastic part. For this reason, it exhibits much noise, and a broad scatter band for various load levels resulting in overlapping of curves, see Figure 62 (b) and Figure 63 (b). Due to noise and overlapping of curves, the inelastic part requires extreme precision in the recording of strain as well as in analysis. For the elastic component, the scatter bands for various levels can be distinguished easily due to its higher absolute value, see Figure 62 (a) and Figure 63 (a). Due to the low absolute value of the inelastic component, the total strain range and total strain energy maintain a similar distinguishing feature across different load levels as that of the elastic component.

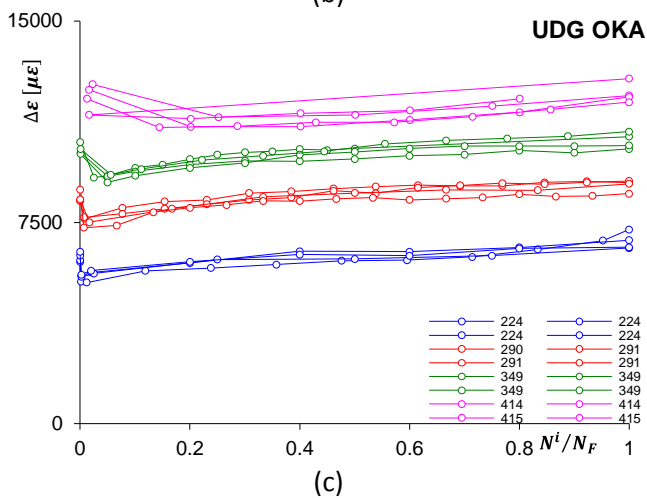
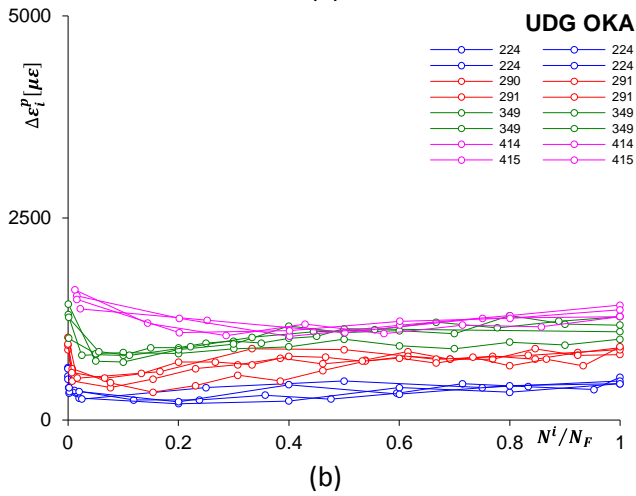
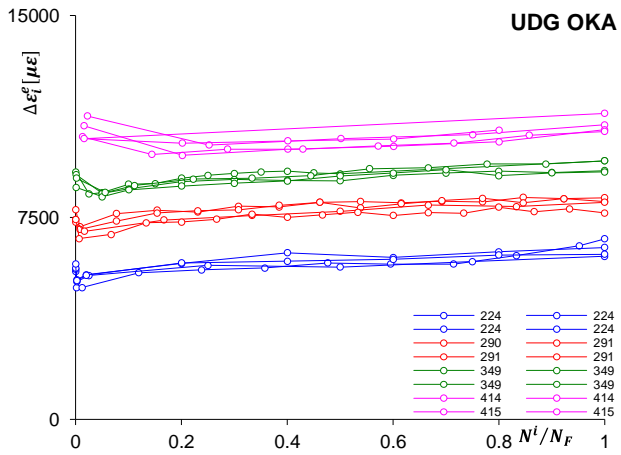
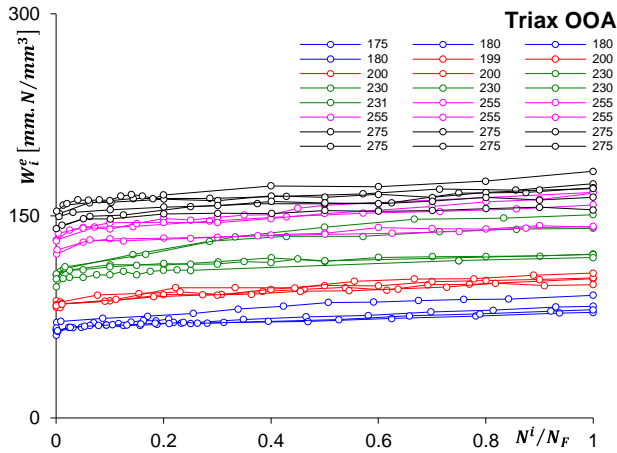
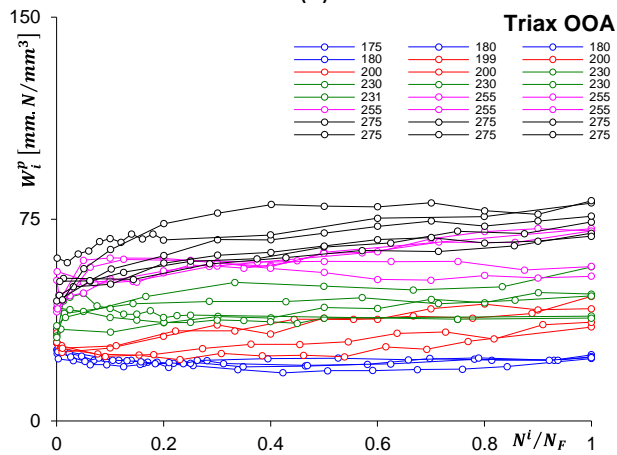


Figure 62 UDG OKA R=-1; (a) Elastic strain range, (b) Inelastic strain range, (c) Total strain range (legend shows σ_{max} value in MPa)

The trend for strain range and strain energy is similar, but the distinction in load levels for strain energies is not as clear as that for strains. Computing the area in stress-strain space is the basis for calculating strain energy, whereas length measurement on the strain axis is the measure of strain range. Hence, the strain energy represents more information about deformation than strain range. As a result of only the change in size and shape of hysteresis curves can be captured for both elastic and inelastic components of strain energy. The case of uniform translation without a change in size or shape cannot be captured adequately by either component.



(a)



(b)

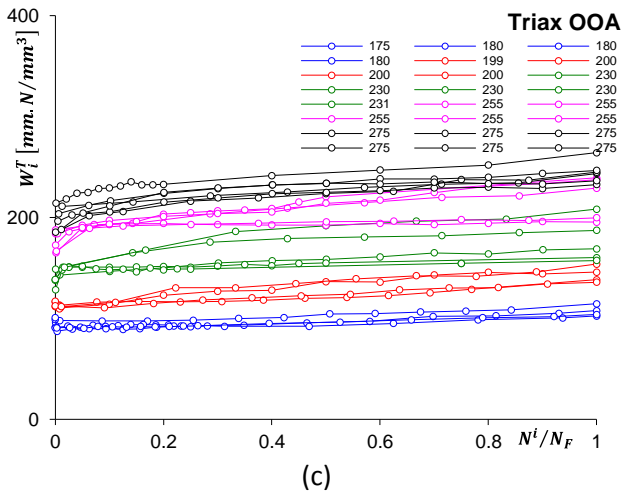


Figure 63 Triax OOA R=-1; (a) Elastic strain energy, (b) Inelastic strain energy, (c) Total strain energy (legend shows σ_{max} value in MPa)

The trend in total strain range or strain energy does not distinguish the change in elastic or plastic components, precisely because of its additive decomposition. Hence if selected as a damage indicator both total strain range or strain energy do not specify whether the damage is created by elastic or inelastic deformation.

Another parameter, quadrant stiffness, is calculated over the entire stress-strain curve in the respective quadrant using both the chord and tangent method. In terms of the absolute value of stiffness, both methods give different values, but the trend is similar. In Figure 64 to Figure 67, the trend in quadrant stiffness computed from the tangent method is shown for Biax OKD configuration. In general, the unloading stiffness is always higher than loading stiffness for all configurations. Depending on the loading or unloading cycle, the quadrant stiffness shows different trends. In case of loading, a transition is observed in stiffness change (see Figure 64 and Figure 65) whereas in the unloading case, a gradual change is observed instead of a transition (see Figure 66 and Figure 67). These changes represent only part of the mechanism, and due to these different trends, quadrant stiffness is not considered a suitable parameter to represent the overall damage [440].

Validation of theory and mathematical formulation

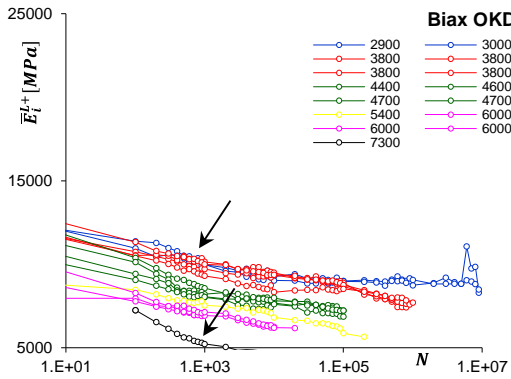


Figure 64 Quadrant stiffness (tension loading) for Biax OKD R=-1 (legend shows ϵ_m value in $\mu\epsilon$); arrow indicates a transition in stiffness change

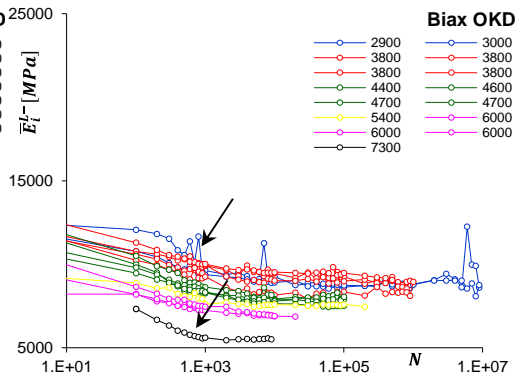


Figure 65 Quadrant stiffness (compression loading) for Biax OKD R=-1 (legend shows ϵ_m value in $\mu\epsilon$); arrow indicates a transition in stiffness change

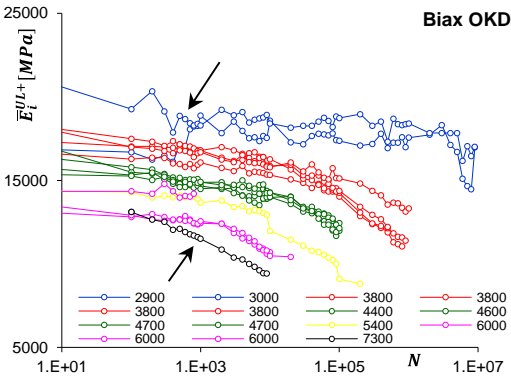


Figure 66 Quadrant stiffness (tension unloading) for Biax OKD R=-1 (legend shows ϵ_m value in $\mu\epsilon$); arrow indicates a gradual stiffness change

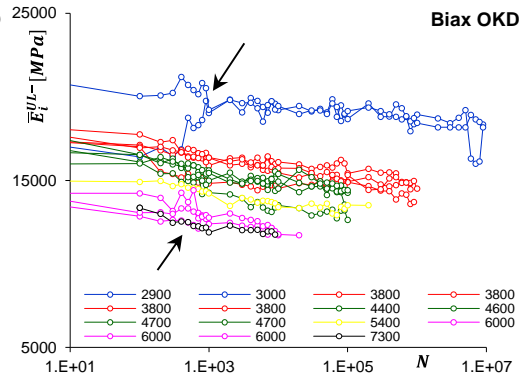


Figure 67 Quadrant stiffness (compression unloading) for Biax OKD R=-1 (legend shows ϵ_m value in $\mu\epsilon$); arrow indicates a gradual stiffness change

The last parameter investigated is hysteresis stiffness, and its value is computed using only the chord method. Appendix A.3.11 gives the trend in hysteresis stiffness for all material configurations. In all load controlled fatigue tests, the hysteresis stiffness does not show distinction in load levels very well, but it shows the trend clearer than strain range and energy trends, see to Figure 68. The trend is sharper in the case of ply drops due to the availability of data from the last few cycles, as seen in Figure 69.

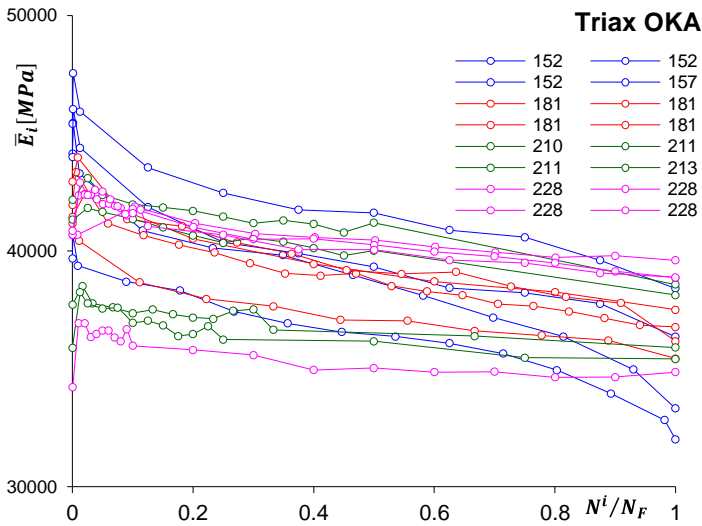


Figure 68 Hysteresis stiffness for Triax OKA R=-1 (legend shows σ_{max} value in MPa)

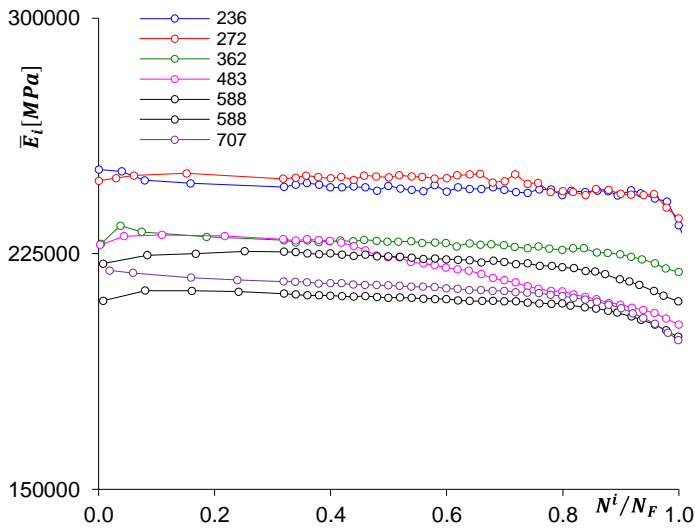


Figure 69 Hysteresis stiffness for ply drop R=-1 (legend shows σ_{max} value in MPa)

As seen in section 4.2.2.3, the hysteresis curves change their size, shape, and location for a growing number of cycles. Computing hysteresis stiffness between the minimum and maximum stress level does not capture the change in size and shape. However, the mechanism that changes the size and shape of hysteresis curves also affects its location, and hysteresis stiffness does capture the location change depending on stress ratio. In the case of the R=-1, both damage and deformation can be

characterized by using hysteresis stiffness, because of the rotation of hysteresis curves. For other stress ratios, only damage can be characterized by hysteresis stiffness as the generation of damage leads to non-uniform translation of the hysteresis curves. For these reasons, the hysteresis stiffness is selected as a parameter to represent damage development.

In the strain-controlled Biax OKD configuration, the stress experienced by the coupon in the respective load level is beyond the static elastic linear region, see [Figure 70](#). Hence, the hysteresis stiffness trend shows a clear distinction in load levels, see [Figure 71](#).

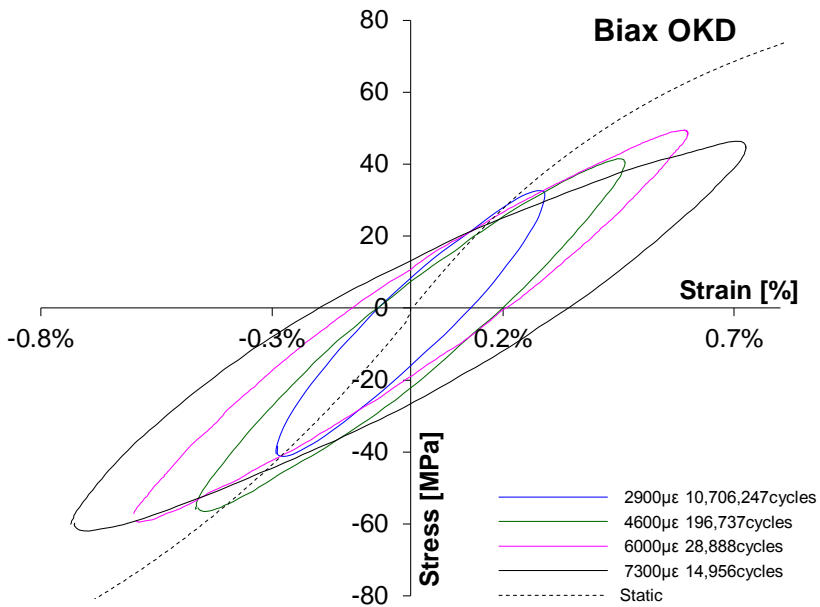


Figure 70 Hysteresis curves for Biax OKD R-1 strain ratio (legend shows mean strain value and associated final fatigue life)

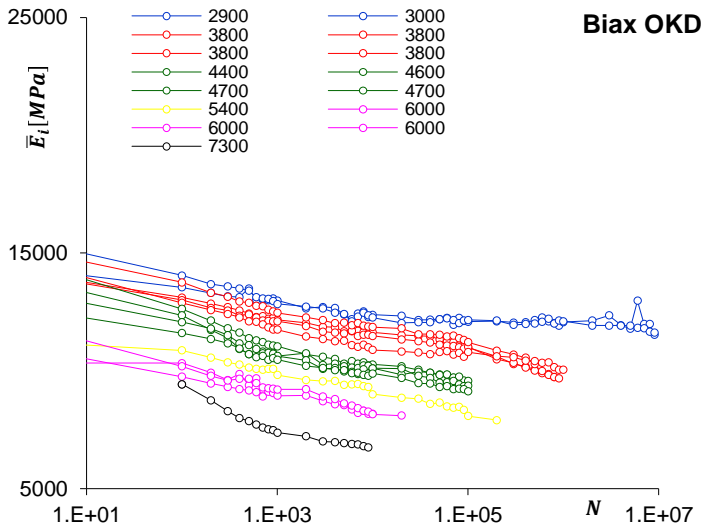


Figure 71 Hysteresis stiffness for Biax OKD R-1 strain ratio (legend shows ε_m value in $\mu\varepsilon$)

Philippidis et al. [441] demonstrated that the cumulative distribution function for any stiffness degradation value could be correlated conservatively to coupons failure survival probability. A similar concept is applied to inelastic strain energy and hysteresis stiffness. Appendix A.3.10 and A.3.12 gives the respective probability distribution function for all material configurations. Although this approach gives more insight into how the damage has developed, it was not explored further because it requires the formulation of a stress level and stress ratio-dependent stiffness degradation rule for each material types. Formulation of such rule is not required in the CDM framework.

Here, some more observations are discussed from the strain range and strain energy trend analysis, that is very similar to observations reported in the literature for analysing metal fatigue. Equation 64 provides a relationship between plastic strain range and stress range for most of the materials. Assuming this empirical relationship is valid for the materials considered in this study, a plasticity coupling with damage is introduced into the mathematical framework in Section 3.4. Figure 72 gives the validity of this cyclic law applicability to all the material configurations used in this study.

Validation of theory and mathematical formulation

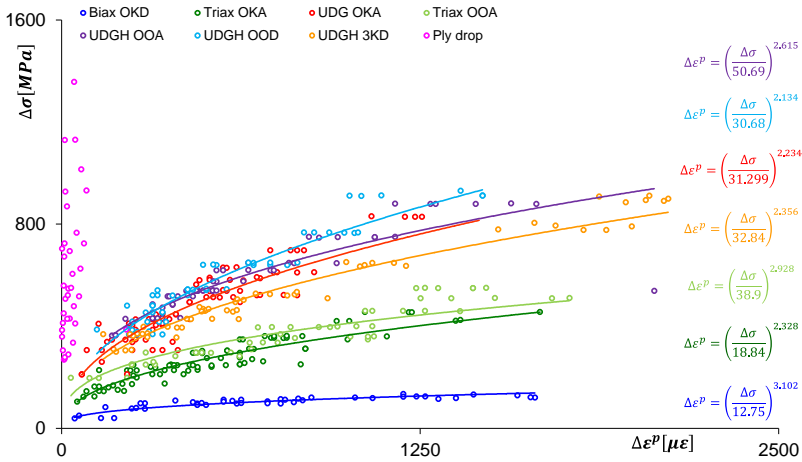


Figure 72 Cyclic law ($\Delta\varepsilon^P$ at early fatigue life vs $\Delta\sigma$)

A similar exercise for finding the dependency of the elastic strain range on the stress range for all material configurations was performed, as shown in Figure 73. Here, the elastic strain range is calculated using Equation 72 and shows a power-law type dependency on stress range. A similar observation was made for A516 Grade 70 carbon steel by Kujawski and Ellyin [440]. The power-law exponents obtained in elastic strain range versus stress range for this steel (1.179) and the composite materials used in this study are of similar magnitude (1.033 to 1.395). Whereas in the case of plastic strain versus stress range, the exponent obtained for this steel (6.211) was almost double than that of composite materials used in this study (2.134 to 3.102).

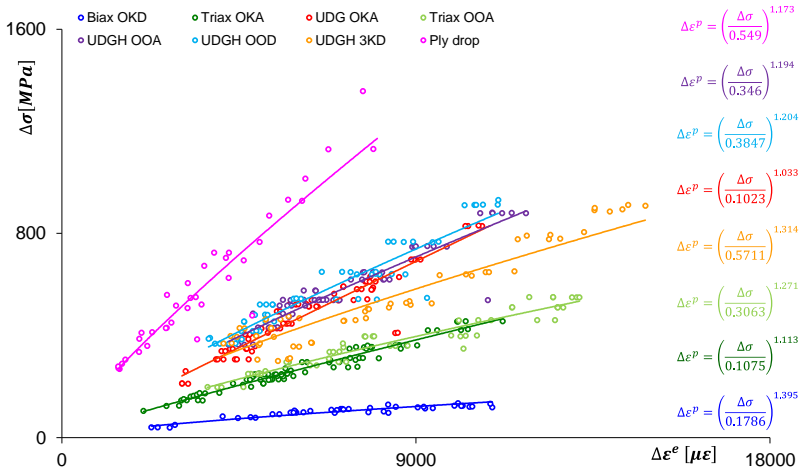


Figure 73 Elastic strain range OOK at early fatigue life (Strain data from clip-on extensometer)

For all material configurations, both the total elastic and inelastic strain energies show a power-law type dependency on final fatigue life, very much similar to metals [336, 442]. The total elastic or inelastic strain energy is a product of the total fatigue life and average elastic or inelastic strain energy incurred over entire fatigue life. On the log-log scale, a linear increase in strain energy density can be observed against the fatigue life in Figure 74 and Figure 75. This observation is in line with the findings from the metal analysis, as discussed in section 2.2.2.1. For inelastic strain energy, Halford [336] generalized the power-law exponent to 1/3 based on a wide variety of metals and alloys under different test conditions. For the composite materials, used in this study, the exponent value (1/1.155 to 1/1.199) is more than double that of the metals. The higher value can be linked directly to the composite material’s capacity to absorb more inelastic strain energy than metals until fracture stage. The inelastic strain energy comprises energy required for deformation as well as damage.

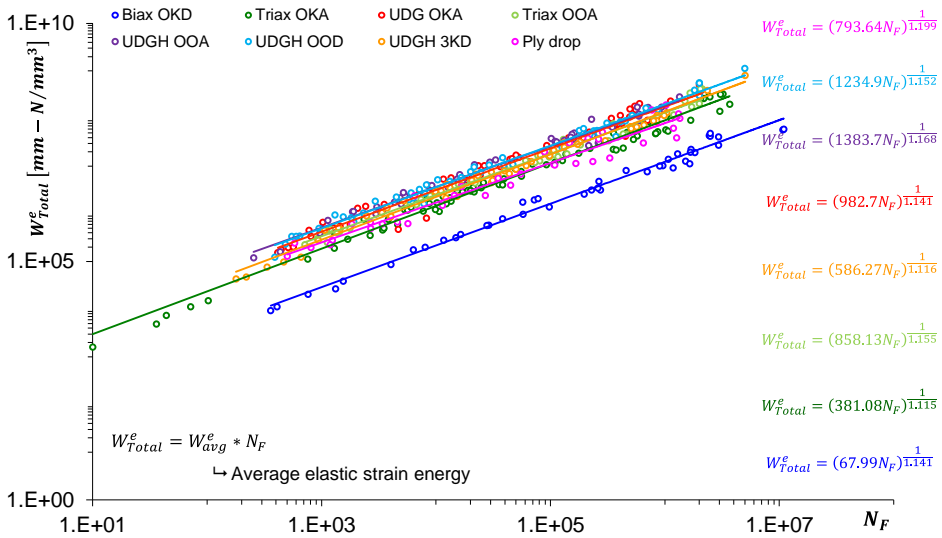


Figure 74 Total elastic strain energy incurred over entire fatigue life for all material configurations

Validation of theory and mathematical formulation

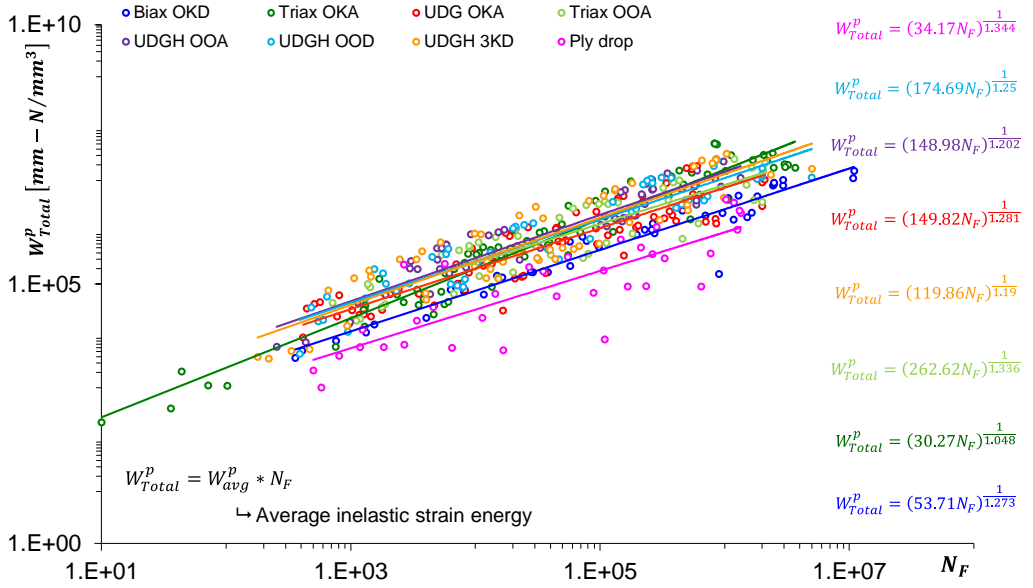


Figure 75 Total inelastic strain energy incurred over entire fatigue life for all material configurations

4.3.3 Softening behaviour

Section 3.4 explains how softening behaviour can be added empirically into the plastic strain development expression. For all the material configurations, this behaviour shows dependency on stress level and the number of cycles. Figure 76 gives the additional strain $\delta\varepsilon_p$ generated at maximum stress for a Triax OKA and UDGH 3KD material configurations under R=-1.

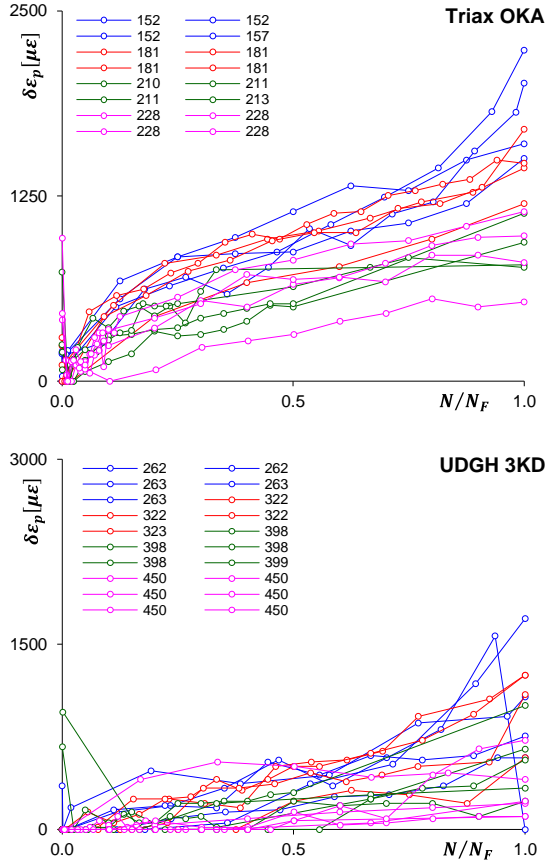


Figure 76 Softening behaviour under R=-1; (top) Triax OKA, (bottom) UDGH 3KD material configurations (legend shows σ_{max} value in MPa)

Like damage development, the additional plastic strain development is stochastic. Because the hysteresis stiffness definition includes this additional plastic strain development, it makes more sense to discuss the variability in the damage development section. Therefore, the cause of this variability is explained in section 4.3.4.2. Hence no further attempt is made here to determine an intricate structure between additional plastic strain development and stress level or fatigue life.

4.3.4 Parameter dependency

Validation consists of demonstrating a limited maximum error between predicted model behaviour and experimental behaviour. Any mathematical model consists of a relationship with variables and parameters. Determining the values for these parameters is the crucial step during validation. The parameters represent a particular characteristic of material under certain conditions. When these conditions change the value of the parameter also changes. In the case of the stress-controlled fatigue test of any given material, the stress ratio, stress level, and temperature determine these conditions. When the stress ratio changes, the parameter's value also changes, and its dependency on stress ratio becomes a key aspect in model validation. Hence in the next subsection, the parameter dependency on stress ratio is addressed first before addressing the comparison between model prediction and experiment results. Within a given stress ratio, the stress level may consist of a low load with purely linear elastic deformation or higher loads with more inelastic deformation. Hence, some parameters may show stress level dependency and need a separate address. The type of dependency of parameters on stress ratio and stress level is identified based on the experimental results.

4.3.4.1 Parameters dependency on stress ratio

The selection of the stress ratios under which the fatigue test get carried out depends on the actual operational conditions of structures or products. Wind turbine blades experience load spectra containing a variety of stress ratios. For example, stress ratios at breaking are primarily of high mean/low amplitudes type. During normal operations, the load cycles have both tension and compression loading with low mean and moderate amplitudes. Only a few stress ratios with constant amplitude get selected for experimental evaluation, mainly due to time and cost constraints. To be able to predict the fatigue performance at non-tested stress ratios accurately, it is crucial to know how the parameters from both the SN curve and the non-linear damage law depend on all the possible stress ratios. Traditionally the stress ratio is defined as

$$R = \frac{\sigma_{min}}{\sigma_{max}} = \frac{\sigma_m - \sigma_a}{\sigma_m + \sigma_a} \quad \text{Equation 73}$$

In the graphical form of CLD, the stress ratio varies from $+1 \rightarrow 0 \rightarrow -1 \rightarrow \infty \rightarrow +1$. This unusual sequence does not reveal any parameter dependency on stress ratio

quickly. Hence another definition of stress ratio was proposed by Westphal [443], which is used here.

$$Q = \frac{\sigma_m}{\sigma_a + |\sigma_m|} \tag{Equation 74}$$

Stress ratio Q varies from $+1 \rightarrow 0 \rightarrow -1$. This sequence is easier to work with and particularly to identify any dependency. Figure 77 shows the schematic of the stress ratio sequence for both definitions.

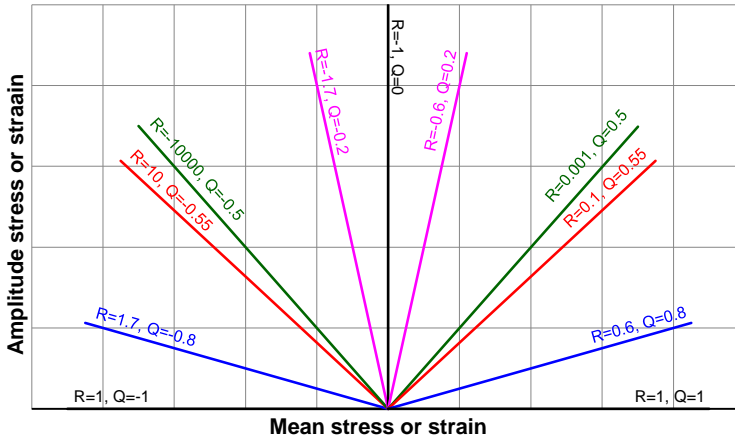


Figure 77 Stress ratio sequence in CLD

The SN curve formulation is represented generally in power-law form, and so far, the most widely adopted representation is the Basquin equation [27]. In terms of stress range, this equation can be written as

$$\Delta\sigma = \sigma'_f (N_F)^{1/n} \tag{Equation 75}$$

Here, the parameter σ'_f is the fatigue coefficient representing stress at cycle 1 for respective stress ratios, which should not be mistaken as ultimate strength and n is fatigue exponent, and its value represent the slope of the curve. A higher value of n means a small change in stress range leads to a significant change in final fatigue life. Both parameters n and σ'_f attain unique values per stress ratio, refer to Table 10.

While constructing Goodman CLD, parameter n is assumed to be constant for all stress ratios. For some metals, this might be true, but for composite materials, experiments have already revealed that the slope of the SN curves varies as per stress

ratio. Over the last one and half-century, many researchers came up with either linear [Piecwise linear [40], Boerstra [43]], or quadratic [Harris and co-worker [39], Kawai [42]] form dependency of SN curve slope on stress ratio.

For all the material configurations used in this study, the parameters from the SN curve (Table 10) shows stress ratio dependency. Here, a quadratic form for the dependency on stress ratio is proposed as

$$Parameter = Parameter_0(1 + C_1Q + CQ^2) \quad \text{Equation 76}$$

$$C = \begin{cases} C_t \text{ for } Q > 0 \\ C_c \text{ for } Q < 0 \end{cases}$$

Where

$Parameter_0$ is the value of the parameter at $Q = 0$, and C and C_1 are fitting parameters

Using this quadratic form both n and σ_f' parameters can be calculated for all stress ratios and all material configurations. The parameters are optimized to get the best fit between Equation 69 and the experimentally obtained fatigue life value. The time required for obtaining the desired fit between actual and predicated depends on the initial value. Hence careful selection of initial value is the key for realistic optimization.

Material	Stress ratio		SN curve formulation
	Q	R	
Triax OKA	0.70	0.4	$\Delta\sigma = 528 * N_F^{-0.109}$
	0.55	0.1	$\Delta\sigma = 876 * N_F^{-0.126}$
	0.40	-0.2	$\Delta\sigma = 1162 * N_F^{-0.127}$
	0	-1	$\Delta\sigma = 910 * N_F^{-0.078}$
	-0.40	-5.0	$\Delta\sigma = 401 * N_F^{-0.028}$
	-0.55	10	$\Delta\sigma = 275 * N_F^{-0.012}$
	-0.70	2.6	$\Delta\sigma = 184 * N_F^{-0.008}$
Triax OOA	0.55	0.1	$\Delta\sigma = 790 * N_F^{-0.100}$
	0	-1	$\Delta\sigma = 911 * N_F^{-0.068}$
	-0.55	10	$\Delta\sigma = 468 * N_F^{-0.035}$
UDG OKA	0.75	0.5	$\Delta\sigma = 869 * N_F^{-0.104}$
	0.55	0.1	$\Delta\sigma = 1243 * N_F^{-0.096}$
	0.35	-0.3	$\Delta\sigma = 1474 * N_F^{-0.097}$
	0	-1	$\Delta\sigma = 1471 * N_F^{-0.084}$
	-0.36	-3.7	$\Delta\sigma = 893 * N_F^{-0.038}$
	-0.55	10	$\Delta\sigma = 693 * N_F^{-0.044}$
	-0.69	2.6	$\Delta\sigma = 485 * N_F^{-0.035}$
UDGH OOD	0.55	0.1	$\Delta\sigma = 1083 * N_F^{-0.079}$
	0	-1	$\Delta\sigma = 1559 * N_F^{-0.075}$
	-0.55	10	$\Delta\sigma = 640 * N_F^{-0.033}$
UDGH OOA	0.55	0.1	$\Delta\sigma = 1314 * N_F^{-0.093}$
	0	-1	$\Delta\sigma = 1706 * N_F^{-0.085}$
	-0.55	10	$\Delta\sigma = 651 * N_F^{-0.022}$
UDGH 3KD	0.55	0.1	$\Delta\sigma = 1457 * N_F^{-0.120}$
	0	-1	$\Delta\sigma = 1646 * N_F^{-0.082}$
	-0.55	10	$\Delta\sigma = 528 * N_F^{-0.026}$
Ply drop	-0.55	10	$\Delta\sigma = 1372 * N_F^{-0.080}$
	0	-1	$\Delta\sigma = 3159 * N_F^{-0.138}$
	0.30	-0.4	$\Delta\sigma = 3296 * N_F^{-0.144}$
	0.55	0.1	$\Delta\sigma = 2407 * N_F^{-0.128}$
	0.75	0.5	$\Delta\sigma = 1483 * N_F^{-0.100}$
	0.90	0.8	$\Delta\sigma = 407 * N_F^{-0.030}$
Biax OKD	0	-1	$\Delta\sigma = 30745 * N_F^{-0.097}$

Table 10 SN curve formulation for all material configurations

4.3.4.2 *Parameters for non-linear damage evolution law*

One difficulty that arises in the identification of parameters in the damage evolution law (Equation 71) is the stochastic nature of the damage, as mentioned in section 2.2. Due to this stochastic nature, no two coupons have exact similarities in performance. The best practice to visualize the data and to identify an intricate structure in it is to draw a scatter plot and perform smoothing of variations. One way to smoothen is by performing locally weighted linear regression (LOWESS) [444]. The drawback of LOWESS is that it requires large datasets, and it does not produce a functional relationship between the dependent and independent variables.

The damage law (Equation 56) proposed in section 3.4 is deterministic, which means there is no uncertainty associated either with the value of damage or the rate of damage growth. The thermodynamic principles do not include any spatial variability while defining either state variables or potentials; hence the damage law also does not include this variability. To understand the damage growth either this deterministic law needs to be extended into the probabilistic domain [445], or the stochastic nature needs to be represented by some average non-random function. Here, it is assumed that there exists such a non-random function, which represents the overall damage evolution and also keeps the physical relevance.

Identification of such function starts with fitting Equation 71 to damage variables calculated by Equation 4 as a function of N/N_f while minimizing the mean squared errors. After applying this fitting process to all the coupons tested within the respective stress levels, a set of fitting parameters per stress level is generated, and the average value of these parameters then be used to represent the average damage state for the individual stress level. This averaging scheme is then applied to all stress levels of each material configurations to compute the average damage evolution.

In the case of ply drops, the averaging scheme is not applicable as only one coupon was tested per stress level, see Figure 78.

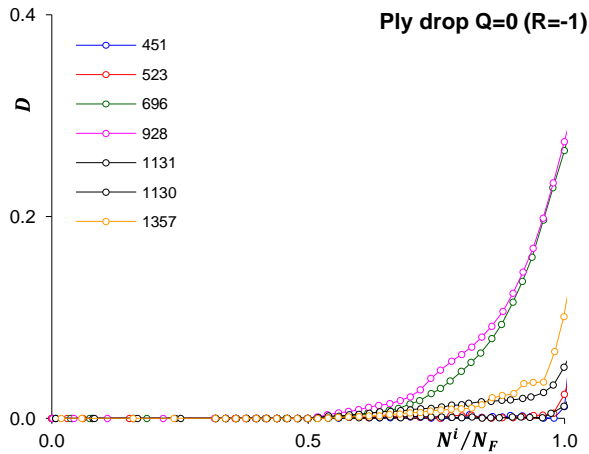


Figure 78 Fatigue damage for Ply drop configuration for Q=0 (legend shows $\Delta\sigma$ value in MPa)

Figure 79 presents the damage evolution for three stress ratios together with the results of the averaging method for the Triax OKA material configuration. The damage evolution trends between different stress levels are different for all three types of stress ratios. Section 4.3.2 already explained the reason for this difference. For Q=0.55, a clear distinction for parameter D trend can be seen, while for Q=-0.55, the trend is diffused between different load levels. The distinction in trend for Q=0 is somewhat in between, and hence for rest of the configurations, trends from only stress Q=0 ratio are discussed.

For all material configurations, the trend between the absolute and average damage value near $N/N_F = 1$ is quite different. The absolute damage value does not reach the value of 1 because of two reasons. First is the unavailability of hysteresis curves data from the last few tens of cycles. Second, the coupon does not separate into the two parts at the fracture stage, and some portion remains intact at $N/N_F = 1$ showing some resistance (Stiffness). Whereas the average damage value does reach to the value of 1 as per Equation 71 giving overestimated damage value near $N/N_F = 1$.

Validation of theory and mathematical formulation

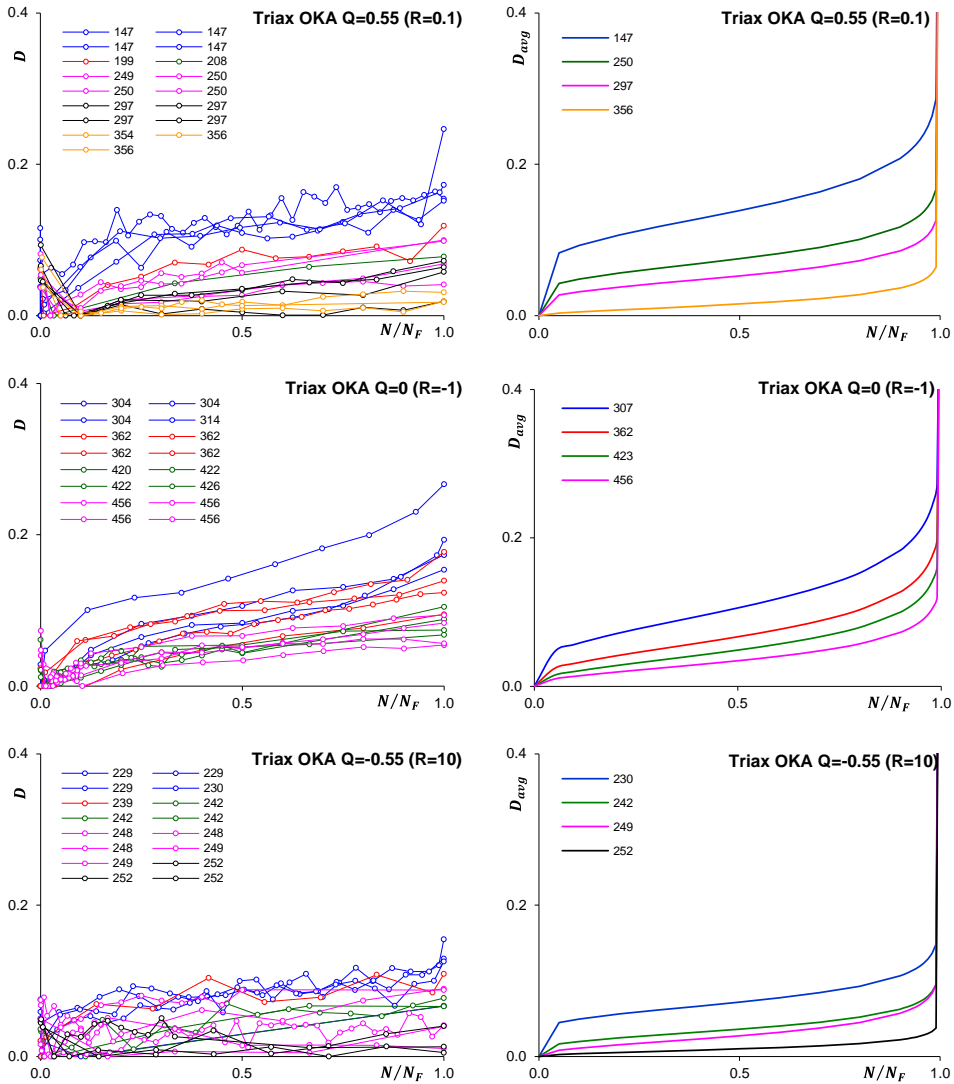


Figure 79 Stochastic nature of fatigue damage for Triax OKA configuration; (top) $Q=0.55$, (middle) $Q=0$, and (bottom) $Q=-0.55$; (left) absolute damage value, (right) average damage value per stress level (legend shows $\Delta\sigma$ value in MPa)

In the case of Biax OKD configuration, the test stopped at 30% loss in initial stiffness hence the average damage value reaches to 1 instead of 0.3 at $N/N_F = 1$, see Figure 80.

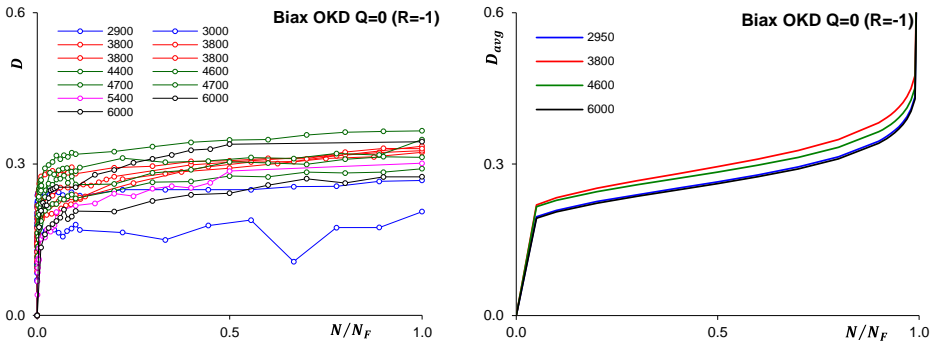


Figure 80 Stochastic nature of fatigue damage for Biax OKD Q=0; (left) absolute damage value, (right) average damage value per stress level (legend shows $\Delta\sigma$ value in MPa)

To identify the parameters in the non-linear damage evolution law, first parameters α and M are optimized to get the best fit between Equation 69 and the average damage value computed using the averaging scheme.

Next, the dependency of the parameter on the stress level must be assessed. Unlike SN curve parameters, the non-linear damage evolution law parameters show stress level dependency. In literature, many forms have been proposed for the dependency of the parameter α on the stress level, and of which Chaboche and Lesne [446] provided a summary. In this work, for most of the material configurations, the parameter α is observed to be decreasing while parameter M as increasing function of applied stress range, as illustrated in Figure 81. Because both dependencies in Figure 81 appear linear, a linear form of parameter dependency on stress levels is proposed.

$$\text{Parameter} = \text{Parameter}_0 \left(\frac{\Delta\sigma}{\sigma_u} \right) + C_2 \quad \text{Equation 77}$$

Where Parameter_0 is the value of the parameter at $Q = 0$, fully reverse loading. Both Parameter_0 and C_2 are stress ratio (as per Equation 76) and material dependent parameter.

Validation of theory and mathematical formulation

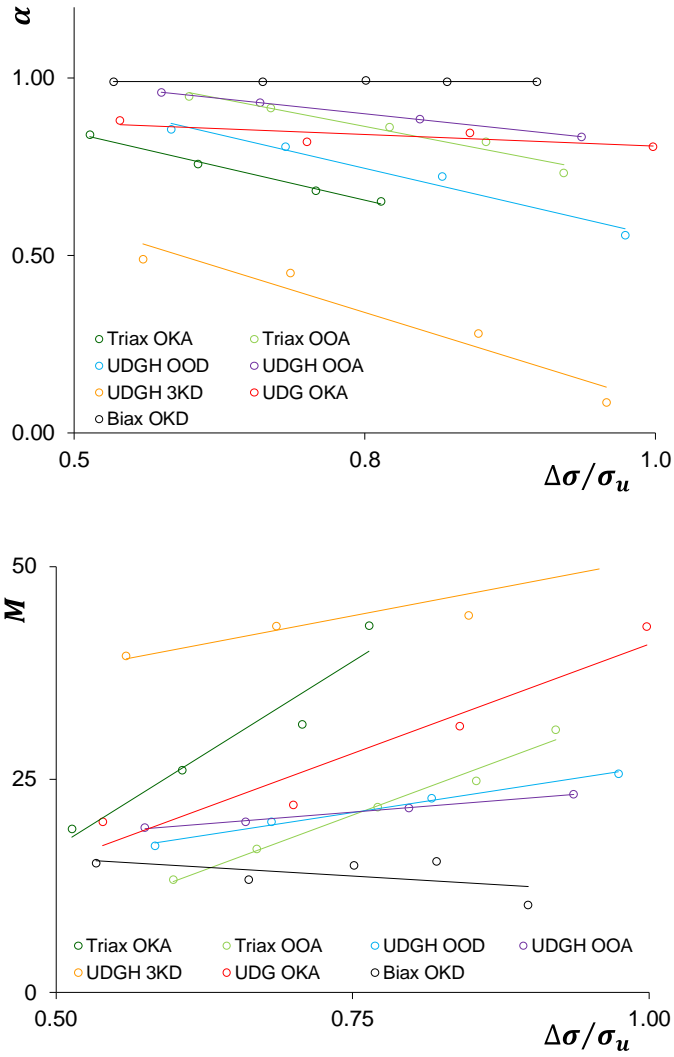


Figure 81 Parameters dependency on stress level for all material configurations under $Q=0$ ($R=-1$)

The parameters in Equation 77 are optimized to get the best fit between Equation 71 and the average damage value using the mean squared errors method.

4.3.4.3 Parameters for constant life diagram

Similar to that of parameter \mathbf{M} , the parameters \mathbf{K} in Equation 69 can be determined by fitting the experimentally obtained final fatigue life value to that of the predicted value. Determining every parameter following this fitting process is time-consuming and increases the complexity of validation. Hence, an alternative simplified methodology is required to estimate a few parameters if not all.

One easy way to identify the parameters K and M is by equating Equation 69 with the Basquin law. To this aim, Equation 69 can be written in the form

$$N_F = \left[\frac{KM(1-\alpha)}{2(M+1)\Delta\sigma^M} \right]^{\frac{1}{1-\alpha}}$$

Which after rearrangement gives

$$\Delta\sigma^M = \frac{KM(1-\alpha)}{2(M+1)N_F^{1-\alpha}}$$

$$\Delta\sigma = \left(\frac{KM(1-\alpha)}{2(M+1)} \right)^{\frac{1}{M}} (N_F)^{-\left(\frac{1-\alpha}{M}\right)} \quad \text{Equation 78}$$

Equating Equation 78 and Equation 75 then yields

$$\sigma_f' = \left(\frac{KM(1-\alpha)}{2(M+1)} \right)^{\frac{1}{M}}$$

which can be restructured to give the unknown parameter K as

$$K = 2 \frac{\sigma_f'^M (M+1)}{M(1-\alpha)} \quad \text{Equation 79}$$

Similarly, the unknown parameter M can be given by

$$M = -\frac{1-\alpha}{n} \quad \text{Equation 80}$$

Equation 79 and Equation 80 give a quick estimation of parameters \mathbf{K} and \mathbf{M} based on known SN curve parameters and are valid only in the domain where SN curves are

expressed by a power function. In the case of non-linear SN curve formulation, this methodology of quick estimation is not valid.

Table 10 shows that for composite materials, the coefficient and exponent from Basquin law are stress ratio-dependent. Hence, to get better accuracy in parameter estimation, using the above equations, testing of more number of stress ratio is required. The testing of more number of stress ratio assures the accurate fitting while interpolating between known stress ratios.

4.3.5 Non-linear damage evolution

With the help of optimized parameters, the damage evolution for all material configurations under any stress ratio and stress level can be computed, because the parameter dependency on stress ratio and stress level is known.

As discussed in section 2.2.1, depending on the load transfer mechanism between various plies, two kinds of damage evolution trends exist. When the damage is caused by interlaminar load transfer, for example, in case of ply drop, the damage evolution over a large part of fatigue life is very low (<2%) with delayed initiation, and it increases rapidly only at the end part of the fatigue life, as illustrated in Figure 82. For homogeneous materials like metals, similar damage evolution trends were observed and generalized [117].

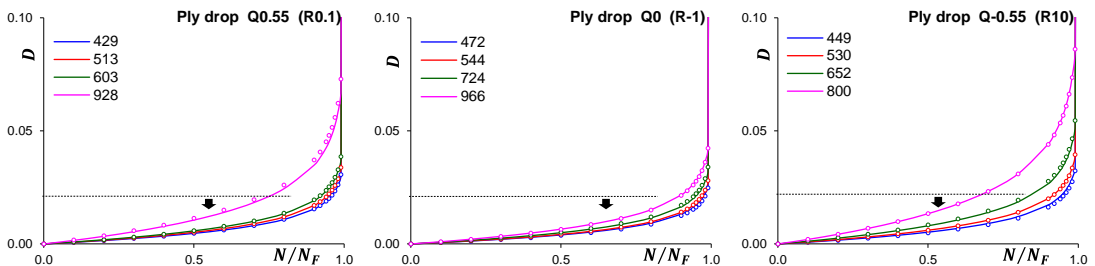


Figure 82 Non-linear damage evolution for ply drop configuration; (left) $Q=0.55$, (middle) $Q=0$, and (right) $Q=-0.55$; (legend shows $\Delta\sigma$ value in MPa)

For all other material configurations, three distinct stages can be observed, because the damage is generated due to in-plane load transfer, see for example Figure 84. The initiation stage corresponds to <15% of total fatigue life, the propagation stage up to 70-80% of total fatigue life, and last fracture stage over remaining fatigue life.

In the case of Biax OKD configuration, the damage evolution is computed only for $Q=0$ ($R=-1$) and is illustrated in Figure 83. In other stress ratios, as only one coupon was tested per stress level, the averaging scheme is not applicable.

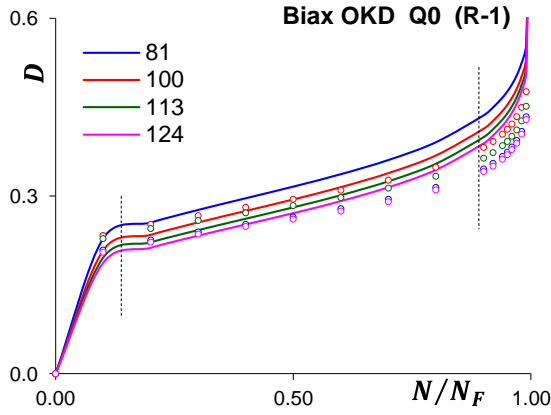
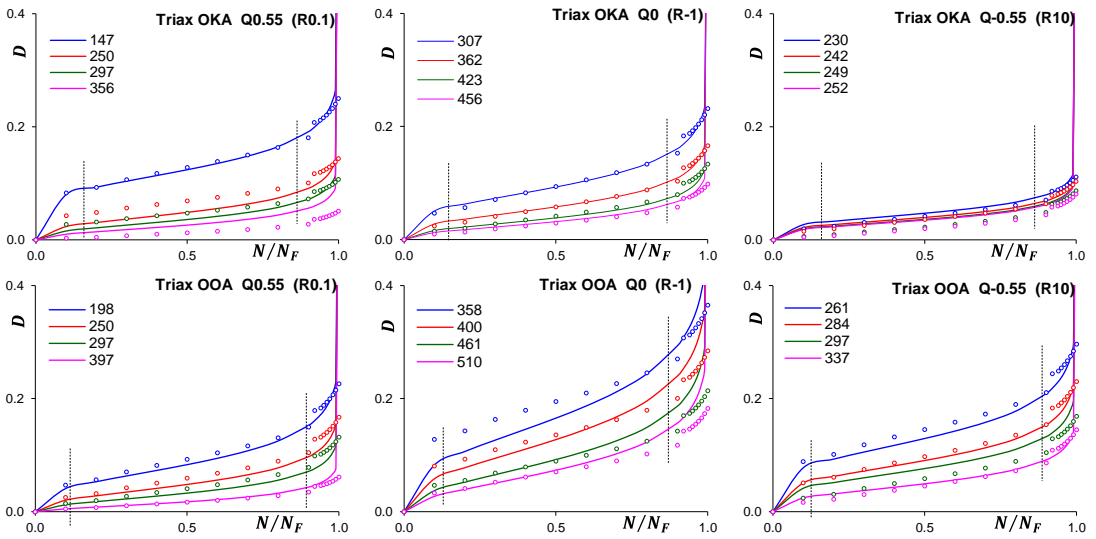


Figure 83 Non-linear damage evolution for Biax OKD configuration $Q=0$;
(legend shows $\Delta\sigma$ value in MPa)



Validation of theory and mathematical formulation

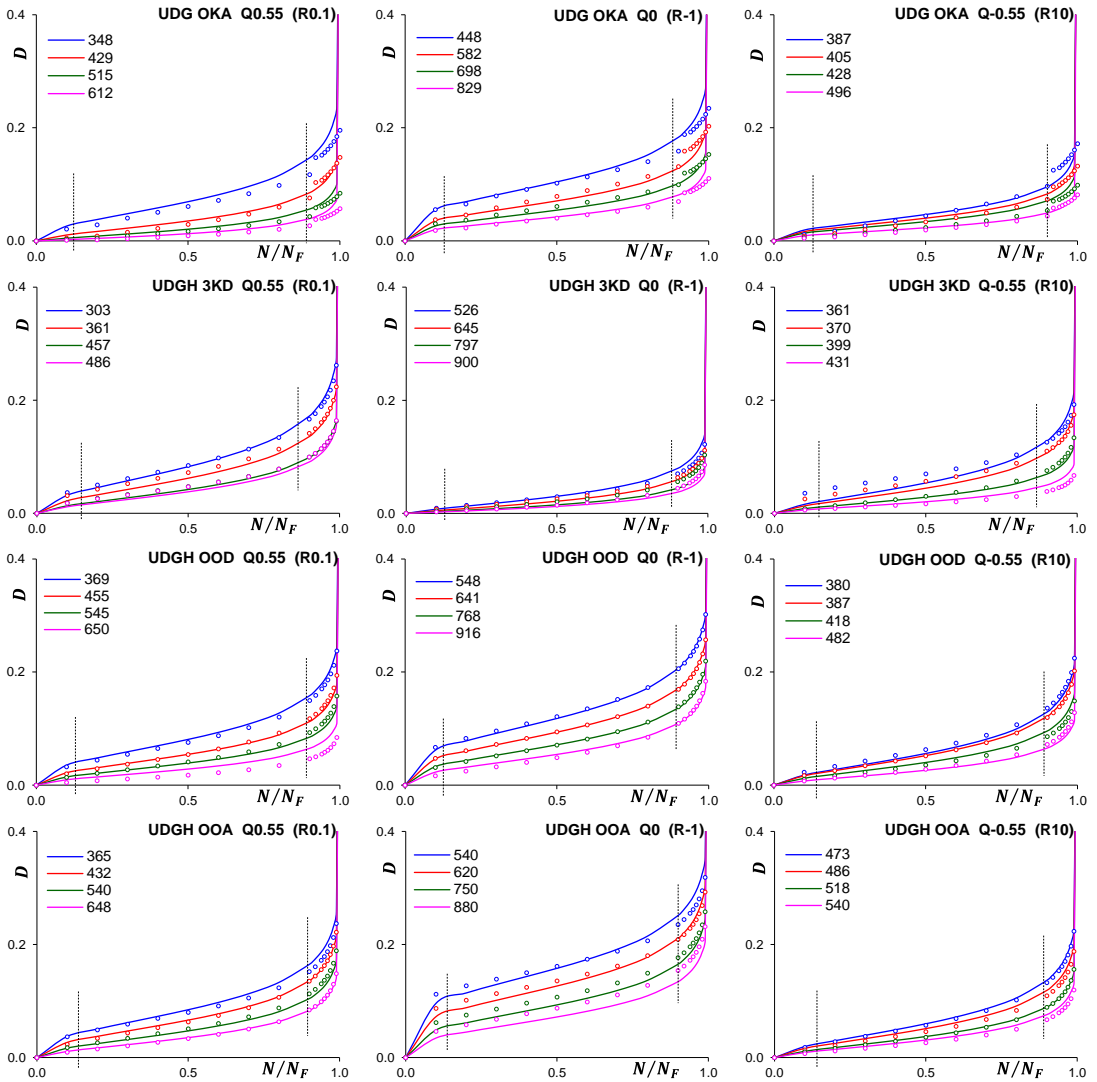


Figure 84 Non-linear damage evolution for rest material configurations (left) $Q=0.55$, (middle) $Q=0$, (right) $Q=-0.55$; (legend shows $\Delta\sigma$ value in MPa)

4.3.6 Construction of constant life diagram

Using the unknown parameters for the SN curves and for the non-linear damage evolution law, constant life diagrams can be constructed using Equation 69 for all material configurations. To verify the CLD constructed using the CDM framework, they are compared with the Multislope CLD model proposed by Boerstra [43]. For comparison, only Boerstra's CLD formulation is selected from the traditional phenomenological framework, because it can accommodate variable slopes for constant life (CL) lines at tension and compression side of the CLD. This multi slope functionality allows applicability of the model to a variety of materials and is therefore used as a baseline for comparison. For comparison between any CLD formulation, the use of error metric based on fatigue life is not enough, because the model formulation consists of many parameters, and hence many possible solutions. To find a solution that is physically most representative, a criterion of accurate prediction of slope parameter also needs to be included for the comparison. The accurate slope parameter intern ensures better accuracy for interpolated values between known stress ratios.

Various error metrics [447, 448] are used in literature to measure and compare the prediction accuracy between different models by providing a quantitative measure of performance. In this work, the sum of squared error (SSE) metric is used for parameter optimization. Minimizing the SSE penalizes more for more substantial errors than smaller ones; hence the optimization is run using this method. The resultant mean absolute percentage error (MAPE) after minimizing SSE is used for the comparison between different models as it is scale-independent, unitless, and easy to interpret.

$$\text{Sum of Squared Error (SSE)} \quad SSE = \sum_{i=1}^n [\ln(A_i) - \ln(M_i)]^2 \quad \text{Equation 81}$$

$$\text{Mean Absolute Percentage Error (MAPE)} \quad MAPE = \frac{100}{n} \sum_{i=1}^n \frac{|A_i - M_i|}{|A_i|} \quad \text{Equation 82}$$

Where M_i is model value and A_i is the actual value

One peculiar observation on the CLD that has been constructed here using the CDM framework is that the constant life lines do not meet at one point on the mean stress axis. Physically this means the effect of mean stress does not vanish at zero amplitude range, which is correct because the material shows creep deformation and damage development at stress levels well below the ultimate static value [449].

Except for ply drop configurations, all the other material configurations shows following peculiarities about both the CLD formulations:

1. The constant life lines in the compression dominant region are closer to each other than in the tension dominant region. Physically this implies that under compression loads, even a small change in stress range leads to a significant change in final fatigue life. This is also evident from the high value of the slope parameter as a result of less steep SN curves for compression dominant loading.
2. At the region close to the zero mean stress axis, the effect of smaller load with opposite sign is different at either side. At the compression dominant side, the effect of smaller tension loads is more, and hence the CL lines change slope rapidly towards zero mean stress axis. Physically this implies that the amount of damage generated by smaller tension loads severely affect the deformation and damage development at compression loads. At tension dominant side, the effect of smaller compression loads are almost negligible, and hence the slope of CL lines does not vary much. In this case, the small compression loads result only in the closure of damage generated by more dominant tension loads and do not generate additional damage. This impact of smaller load can also be seen in hysteresis curves, as discussed in previous section [4.2.2.3](#).
3. In the CLD, the apex point does not occur at a fixed stress ratio, but it moves from the tension to the compression side while going from low to high cycle CL lines. It signifies the diminishing role of smaller loads at low-stress levels.

The peculiarities mentioned above arise due to the difference in damage mechanisms under tension and compression loads. In case of ply drops, as the damage mechanism at macro scale under both these loads is of the same nature, the constant life lines have similar slope changes across different stress levels at either side of CLD, see [Figure 85](#). A substantial error between the actual and predicted value for life is visible for the $Q=0.9$ ($R=0.8$). This error is attributed to the proposed quadratic form ([Equation 76](#)), which does not capture the trend of achieving a high value of the slope of SN curve when the loading reaches towards a fatigue limit. A high value of slope seems reality due to very low amplitude stresses, but the quadratic form does not allow an overall good fit at this region.

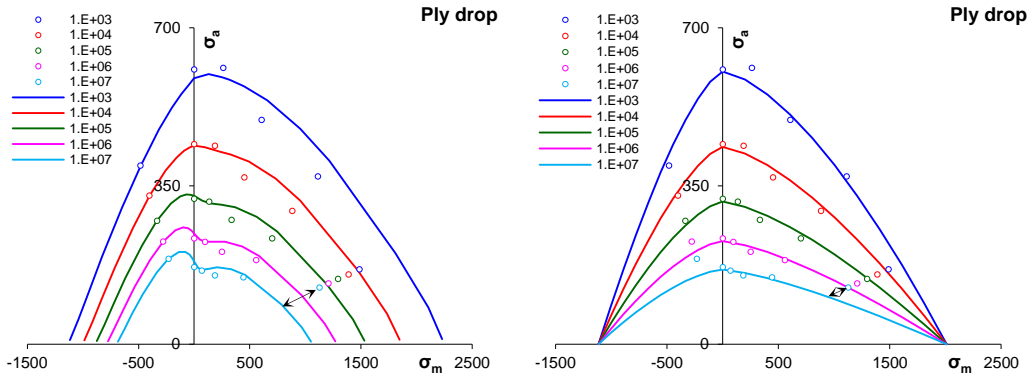


Figure 85 Constant Life Diagram for ply drop configuration; (left) using CDM framework, (right) using Multislope CLD model from the traditional framework

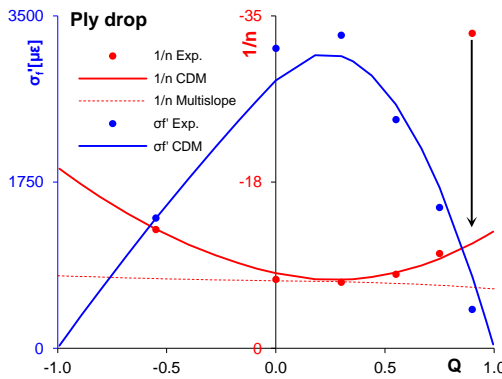


Figure 86 σ'_f and n parameters parameter dependency on stress ratio for ply drop material configurations

In the case of the construction of Multislope CLD for Triax OKA configuration, a lower value for the static ultimate compressive strength is used, see Figure 87 (top). The use of lower strength value is attributed to the different geometries used in static and fatigue testing. In the static test, the gauge length was 12.7mm, and in fatigue, it was 40mm. This extra length results in activation of buckling at low stresses. As the buckling is stress intensity-dependent mechanism, it influences the high-stress level coupon performance by accelerating damage more than at low-stress level. The difference in performance leads to the less steep SN curve with slope approaching unrealistically very high value.

Validation of theory and mathematical formulation

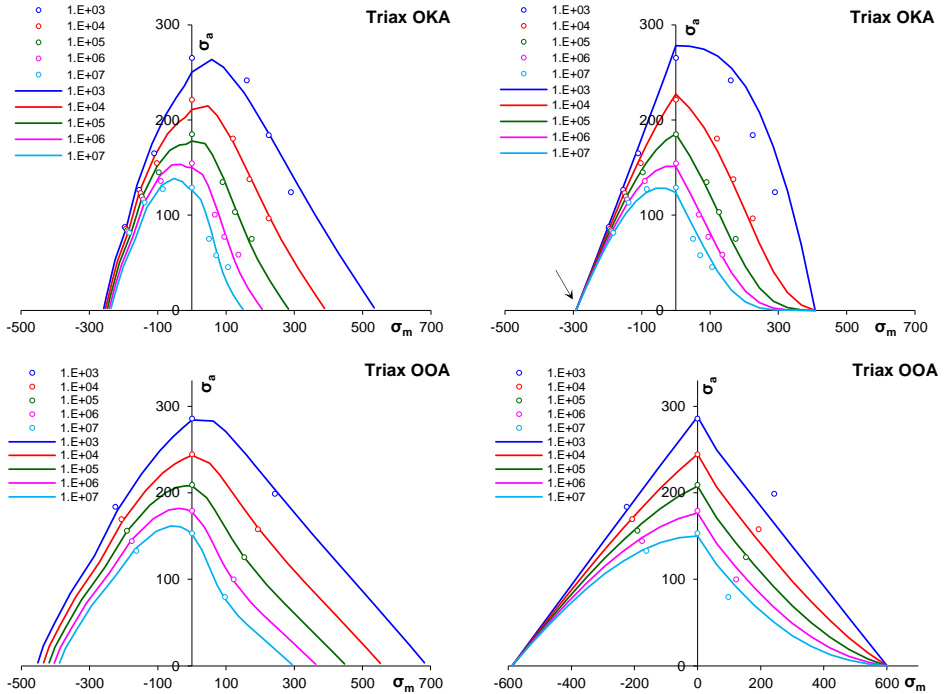


Figure 87 Constant Life Diagram; (top) Triax OKA configuration, (bottom) Triax OOA configuration, (left) using CDM framework, (right) using Multislope CLD model from the traditional framework

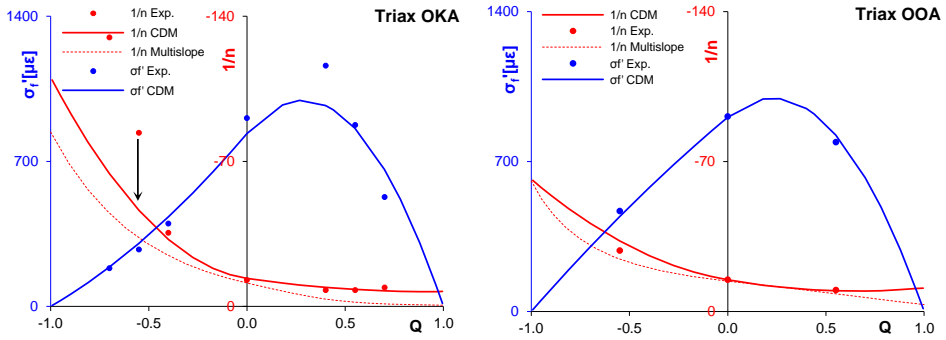
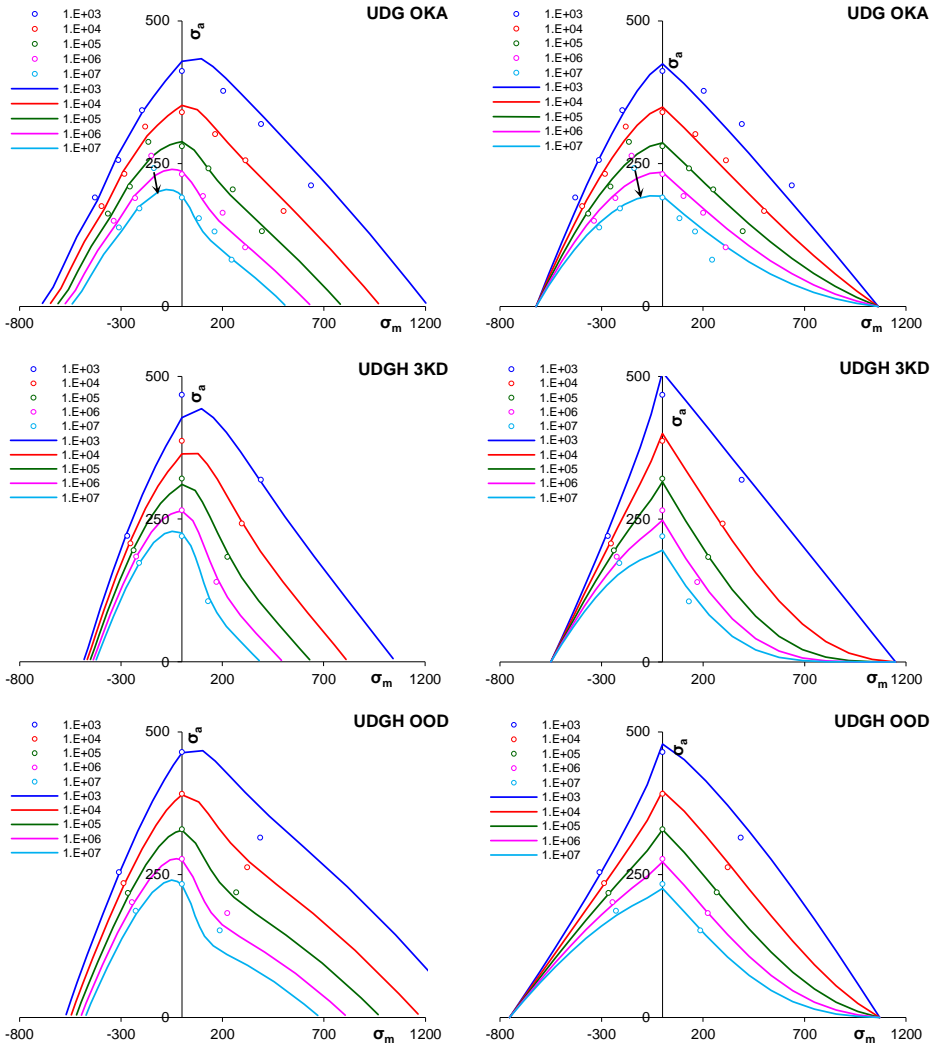


Figure 88 σ'_f and n parameters parameter dependency on stress ratio for (left) Triax OKA, (right) Triax OOA material configurations

Due to the influence of buckling at the compression stress ratios ($Q < 0$), the quadratic form, Equation 76, predicts much smaller slope value than the value obtained experimentally, as shown in Figure 88. In the case Triax OOA configuration as the thickness to gauge length ratio was much better; the predicted slope for SN curves is very close to experimentally obtained slope.

Figure 89 shows the CLD formulations for all UD material configurations. In the case of the UDG OKA material configuration, a significant difference between the actual and predicted value for the fatigue life and the slope of the SN curve can be observed for $Q=-0.36$ ($R=-3.7$). Due to the presence of a significant amount of fibres in the loading direction, the influence of smaller tension load in the alternating fatigue loading is negligible. For the other stress ratios, the quadratic form matches with the experimental values very closely, as illustrated in Figure 90 (a).



Validation of theory and mathematical formulation

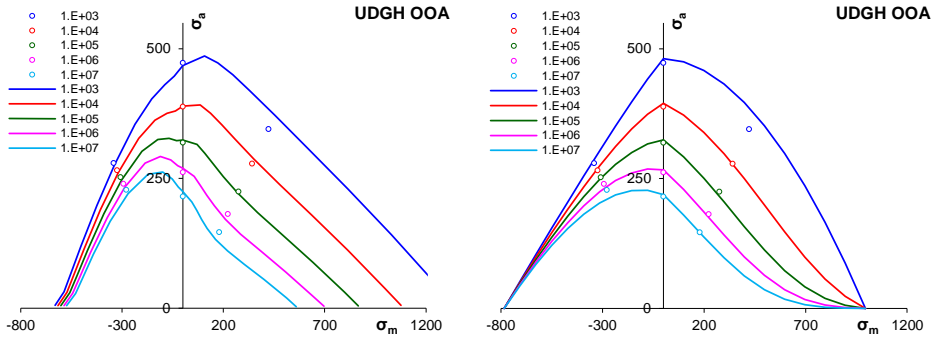


Figure 89 Constant Life Diagram for all UD material configurations; (left) using the CDM framework, (right) using Multislope CLD model from the traditional framework

In the other cases of UDGH configurations, the CDM framework provides a better prediction of fatigue lives and slopes of SN curves compared to the Multislope model, as shown in [Figure 90 \(b to d\)](#).

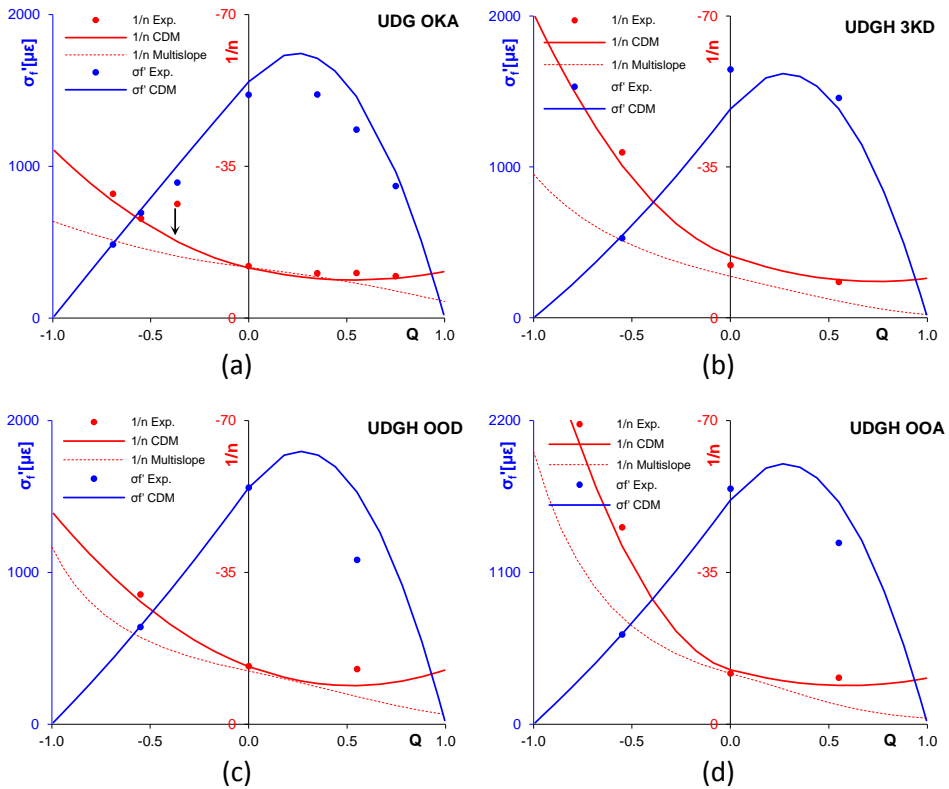


Figure 90 σ_f' and n parameters parameter dependency on stress ratio for (a) UDGH OKA, (b) UDGH 3KD, (c) UDGH OOD, and (d) UDGH OOA configurations

In the case of the Biax OKD configuration, only at $Q=0$ ($R=-1$), more than four stress levels were tested, while for the other stress ratios, only one stress level was tested. With the SN curve parameters available for only one stress ratio, it is not possible to establish the stress ratio dependency. Hence, constructing the CLD for this material was not done.

The analysis of the parameter dependency revealed that the Multislope model predicts the slope value for SN curve more conservative than the CDM framework. The value of the MAPE error metric closer to 100% shows that except for Triax OKA material configuration, the CDM framework predicts the fatigue life more accurate than the Multislope model.

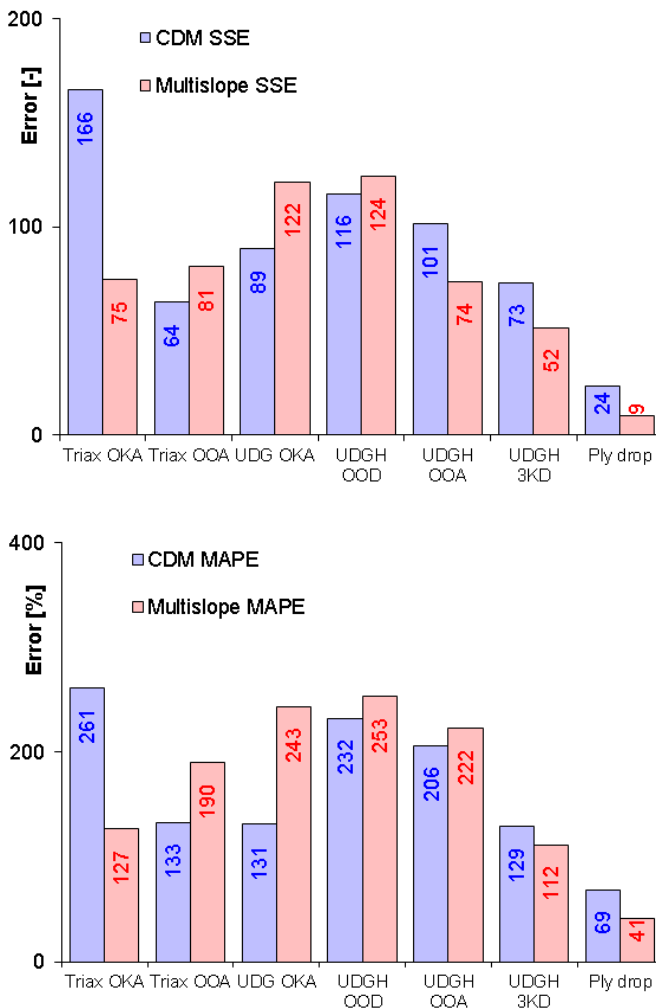


Figure 91 Error metrics; (top) sum of square errors (SSE), (bottom) mean absolute percentage error (MAPE)

Table 11 gives the values for all parameters that shows stress ratio dependency as per Equation 76.

Parameter		Tria x OKA	Tria x OOA	UD G OKA	UDG H OOD	UDG H OOA	UDG H 3KD	Ply dro p	Biax OKD	
σ'_f	Parameter ₀	835	908	1559	1558	1623	1384	2820	4029 5	
	C ₁	1.34	0.85	0.97	1.15	1.19	1.23	0.86	0.25	
	C _t	-2.34	-1.85	-1.97	-2.15	-2.19	-2.23	-1.86	-1.25	
	C _c	0.34	-0.15	-0.03	0.15	0.19	0.23	-0.14	-0.76	
1/n	Parameter ₀	-13.5	-14.8	-11.6	-13.3	-12.5	-14.4	-7.9	-8.0	
	C ₁	-1.02	-1.08	-0.91	-1.26	-0.98	-1.12	-0.65	-0.65	
	C _t	0.56	0.82	0.83	1.21	0.83	0.76	1.21	1.81	
	C _c	6.18	2.11	1.46	1.43	5.76	2.80	0.76	1.12	
α	Parameter ₀	Parameter ₀	-0.8	-0.7	-0.1	-0.3	-0.3	-0.5	-0.03	-0.1
		C ₁	0.20	0.20	0.80	0.38	0.33	0.44	0.50	0.00
		C _t	-0.19	2.08	45.12	3.09	5.05	1.78	2.00	1.00
		C _c	1.58	0.75	2.00	3.36	5.06	-2.52	2.03	1.00
	C ₂	Parameter ₀	1.3	1.2	0.9	1.0	1.1	0.6	0.02	1.0
		C ₁	-0.02	0.15	0.53	0.14	0.05	0.11	0.10	0.00
		C _t	-0.27	-0.64	0.51	-0.48	-0.33	1.09	0.20	0.00
		C _c	0.09	0.37	0.50	-0.43	-0.12	-0.71	0.10	0.00

Table 11 Summary of all parameters used

5

Conclusion

The work done for this thesis is related to understanding the material behaviour using a well-established framework based on the thermodynamics of irreversible processes and continuum damage mechanics. This framework has been applied successfully to many materials like metals, alloys, concrete, elastomers, rocks, composites, and many others (Table 6). This section provides a conclusion about the applicability of this framework to fatigue analysis of wind turbine blade materials. The subsections first provide a retrospective view in comparison with the traditional framework, followed by specific conclusions made about the framework and its validity for the considered materials. A reflective summary for overall fatigue phenomenon is provided in the last.

5.1 A retrospective view on the CDM framework

In contrast to the traditional framework, the thermodynamics of the irreversible process and CDM framework does allow predicting the lifetime of materials by defining each mechanism using a combination of constitutive equations and the evolution equation of the internal variables. The scale at which these equations are derived provides the understanding of the material behaviour accordingly. The macro-scale derivation does not give the understanding of the micro-scale in its exact form. For example, damage defined by macro-scale property like overall stiffness loss does not give information about the exact nature of different micro-damage mechanisms and their interaction. Hence the scale at which the framework gets constructed is its limit of applicability also. One way to overcome this limitation is to construct the framework for multiscale and efforts have been made and also are underway to address this topic, as identified in section 1.1.

The CDM framework can be seen as an extension in solid-state physics theory (thermodynamics of irreversible processes) by adding a phenomenological patch which consists of the definition of internal variables (Figure 29). The internal variable represents the influence of an internal (micro-scale) structure on the macro-scale indirectly. For example, internal variable D , representing damage, that cannot be measured directly but represent the macroscopic description of the damage mechanisms reliably.

One very peculiar aspect of this framework is that it can be generalized for many classes of materials. For example, the elastic potential is any way generalized for all materials along with its coupling with damage. The inelastic and damage potential can also be generalized by using state variables as a state function. The evolution equation

of the state function can be of different form when specific dependency based on material type is present.

The generic framework drafted in section 3.1 provided continuity in the derivation of non-linear damage law. It also allows the derivation of the fatigue life estimation model (Equation 70) based on the actual state of damage at any given time, provided that the load and deformation history is known. Both these are the distinguishing features of this framework compared to the traditional framework where the damage law is linear in nature and fatigue life estimation is based on the final failure and not any intermittent damage state. The fatigue life estimation model has one distinctive feature of capturing the effect of mean stress resulting in crossing constant lifelines on abscissa at the various points instead of one single point of ultimate strength like the traditional framework.

5.2 Specific conclusions

In the case of direct application of this work, specific conclusions are drawn as:

- The CDM framework allows the derivation of a non-linear damage evolution law and a fatigue life estimation consistently with the thermodynamic theory of irreversible processes.
- CDM framework also provides a physical theory-based description of damage and deformation behaviour, including their coupling for material undergoing fatigue process.
- Use of empirical cyclic plasticity law, Equation 64 allows the inclusion of plasticity coupled damage in a quicker way compared to the cyclic inelasticity theory.
- The averaging scheme, proposed in section 4.3.4.2, provides overestimated damage calculation near fracture stage.
- The non-linear damage evolution law, Equation 71 provides an accurate representation of three distinct stages of damage evolution. It also provides computation of the life for any intermittent damage state or vice versa.
- The final fatigue life predicted using CDM framework is more accurate than Multislope CLD model.
- The critical aspect of predicting fatigue life is identifying parameter dependency on stress ratio and stress levels. The proposed form for stress ratio and stress level dependency gives accurate trend except at fatigue limit

region or for very low-stress range. At the fatigue limit region, the slope of the SN curve reaches exceptionally high value resulting in a sigmoidal function type change due to a negligible amount of damage. Whereas the quadratic form dependency gives a continuous change rather a sigmoidal change.

- Regarding strain measurement, recorded data from various sensors need to be checked for its applicability to represent the mechanism under investigation. Actuator displacement is not representative in an absolute manner but relatively can be used to describe damage evolution.
- A parameter to represent the damage is selected based on two criteria; first, the trend of the parameter evolution should show a clear distinction between different load levels and second, the trend should also show sharp features of all damage development stages.
- The hysteresis stiffness is fulfilling both these criteria and hence can be used to represent the damage.
- As the individual components of strains and strain energies (elastic and inelastic) represent only specific mechanisms, they are not suitable for damage representation.
- The total range of strain and strain energy can be used to represent the damage, but it requires separate mathematical formulation to address the hysteresis translation effect.
- The general cyclic laws derived for metals for both elastic and inelastic region are also applicable for composite materials. It also suggests even though composite materials are distinctly different from metals at the microscale, that a common unified framework can describe their behaviour at the continuum scale.

5.3 Contribution to wind turbine blade application

The main contribution from this research to wind turbine blade application is the construction of a CDM framework based on the thermodynamics of irreversible process with internal variables.

- This framework provides a physical theory-based description of behaviour for material undergoing fatigue process.

- It also allows the estimation of more realistic fatigue life at any intermittent damage stage for blade laminate and subcomponent scale.
- By demonstrating the validity at two scales, it also provides a plausible unified way to understand and estimate fatigue phenomenon at full-scale wind turbine blade.

5.4 Reflective summary

Based on the understanding developed throughout this thesis work, a new hypothetical representation of fatigue phenomenon is outlined. The intention here is to devise a unified view of all macro-scale events occurring throughout the fatigue phenomenon. The representation is inspired by astrological charts and shown in [Figure 92](#). It illustrates not only the individual contributions from each underlying mechanism (as the area of each shape) but also the coupling with other mechanisms (location with respect to other shapes). As the representation is hypothetical, a reading guide to this figure is provided in the next paragraphs.

The intersecting [blue](#) lines create four quadrants shown by their number. The tilt in the lines results in different sizes of quadrants. The different mechanisms are represented by different shapes viz. deformation by a circle, damage by a triangle, and thermal effect by an ellipse. The dotted circles (Isotropic and kinematic hardening or softening) is a subset of the inelastic [aqua](#) colour circle.

The [red](#) colour ellipse represents both thermal dissipation and temperature rise where the inner ellipse represents dissipation from various mechanisms and outer ellipse, representing temperature rise due to an increase in internal energy. Placement of inner ellipse on [aqua](#) colour circle indicates that the thermal dissipation is always associated with inelastic deformation. Placement of the [orange](#) triangle of damage and [red](#) colour ellipse of thermal effect on the [blue](#) and [aqua](#) colour circles illustrate that they are the consequence of material deformation response. Whereas, the overlap of thermal effect ellipse with damage triangle suggest the thermal-damage coupling. Such an illustration point towards the importance of consideration of coupling between different mechanisms in the construction of a unified analysis framework.

The different size quadrants represent the difference between loading and unloading portion. The location of damage [orange](#) triangle in the first quadrant indicate damage

gets generated only during the loading cycle. Placement of red colour ellipse at the boundary of first and second quadrant shows the development of thermal effects during both loading and unloading sequence. Such an illustration indicates the importance of the use of either full or partial cycle data for an intended specific analysis. For example, if the intention is only to characterize the damage, use of (loading) half-cycle data can be sufficient. In the case of only deformation characterization, full-cycle data is required during analysis.

At the centre, the overlap between the outer ellipse and the blue circle is shown. Here the only event occurring is the elastic deformation and associated temperature rise, suggesting a potential fatigue limit of the material.

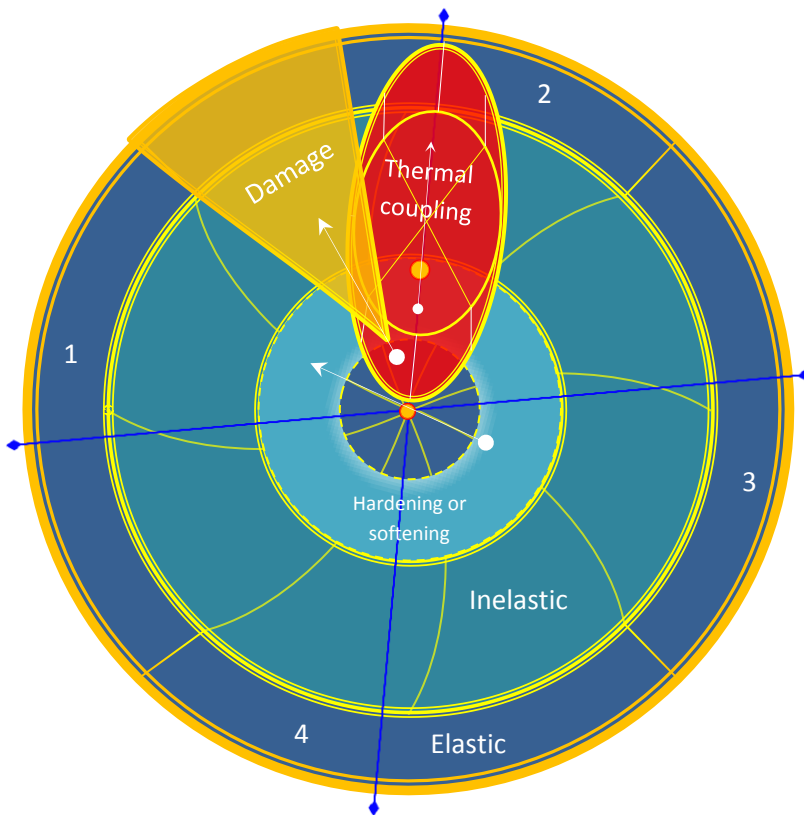


Figure 92 hypothetical representation of fatigue phenomenon and associated mechanisms with their contribution and coupling

6

Future outlook

To achieve the ultimate goal of analysing full-scale wind turbine blade sustaining fatigue throughout its operational life, the application of the CDM framework needs to be extended to other materials (shown in [Figure 16](#)). After validation for other materials, the next step will be to check its applicability to the scale of the blade section and full blade. For this, stepwise inclusion of complexity from other materials and scales needs to be included in the current framework. [Figure 93](#) gives a proposal for such stepwise inclusion of complexity.

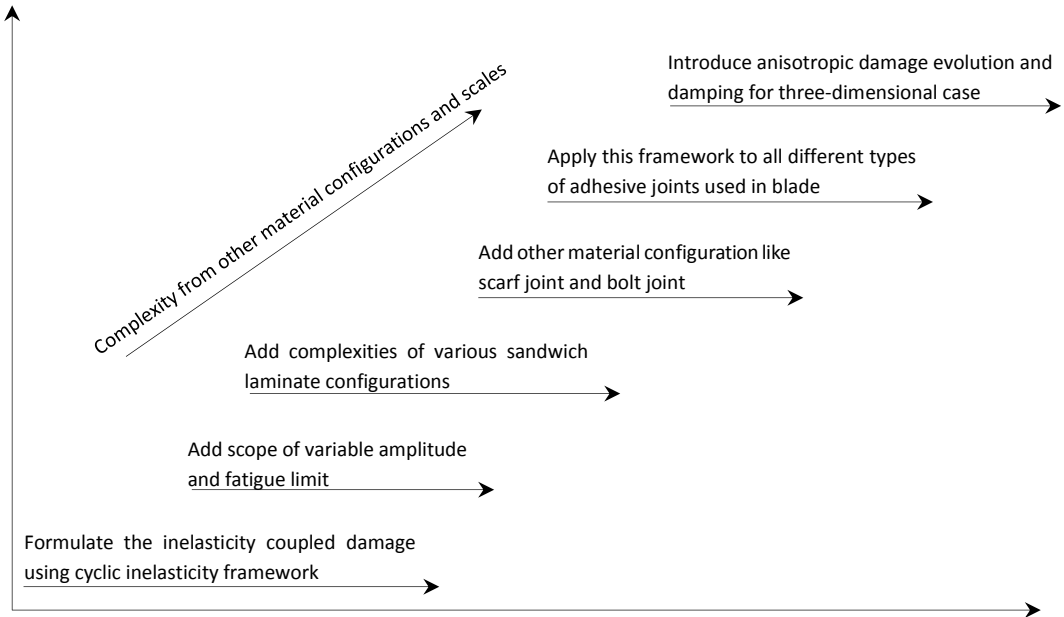


Figure 93 Future outlook – Addition of complexity from other material configurations and scales

In each step, due to the involvement of different scales, a key challenge is to re-evaluate the validity of the underlying assumption used in the generic framework. For example, the framework starts by defining variables as a state function, but at another scale, they might need a definition of path function. The scientific challenge associated with each step is elaborated in the next paragraphs.

In the cyclic inelasticity framework, the challenge is the computation of the plastic strain rate ([Equation 54](#)) simultaneously with the computation of damage rate ([Equation 63](#)) using numerical methods. Here for the computation of the plastic strain rate requires the solution of an exact functional relationship between kinematic X hardening variable and plastic strain (hardening rule given in [Table 5](#)).

The next level of complexity is to add the scope of variable amplitude fatigue. For this step, the integration scheme used to derive Equation 70 needs to be adapted for variable stress range $\Delta\sigma$ and corresponding damage level. The inclusion of a fatigue limit in the analysis framework will require a more accurate form of parameter dependency on stress ratio than the proposed quadratic form (Equation 76).

The challenge in the application of the CDM framework to materials like the sandwich and joint configurations is the validation of the non-linear damage evolution law (Equation 71). This is because the validation stage requires the use of non-standard or specifically designed test geometries and test methods.

At any given time, damage states in the given material configurations will influence each other and determine the ultimate damage state at either blade section or full-scale blade. The influence of various damage states on each other can be captured by defining the damage variable as a tensorial quantity instead of a scalar quantity.

However, all these challenges are still considered as active research fields, and the possible steps itself need iterations to reach the ultimate goal of analysis at full-scale blade level. Here, the feasibility of machine learning technique [450-457] can be explored for some of the tasks to achieve intended results in shorter timelines.

At this point we see this work as a stage-gate, one more stepping stone in the edifice of fatigue analysis, giving a different way for fatigue analysis, raising more questions and allowing to answering only a few.....

References

1. Standard DNVGL-ST-0376. Rotor Blades for Wind Turbines. DNV GL AS; Oslo, Norway: 2015
2. IEC 61400-1 2005-2008 Wind turbines - Part 1: Design requirements, 3rd ed., International Electrotechnical Commission, Geneva
3. Deyuan, L., Zhiquan, Y., Yan, C., & Nengsheng, B. (2003). Load spectrum and fatigue life analysis of the blade of a horizontal axis wind turbine. *Wind Engineering*, 27(6), 495-506. <https://doi.org/10.1260/030952403773617463>
4. Ravikumar, K., Subbiah, R., Ranganathan, N., Bensingh, J., Kader, A., & Nayak, S. K. (2019). A review on fatigue damages in the wind turbines: Challenges in determining and reducing fatigue failures in wind turbine blades. *Wind Engineering*, 44(4), 434-451. <https://doi.org/10.1177/0309524x19849851>
5. Hansen, M. O. (2013). *Aerodynamics of wind turbines*. Earthscan.
6. Brøndsted, P., & Nijssen, R. P. (2013). *Advances in wind turbine blade design and materials*. Elsevier.
7. Burton, T., Sharpe, D., Jenkins, N., & Bossanyi, E. (2001). *Wind energy handbook*. John Wiley & Sons.
8. Noda, M., & Flay, R. (1999). A simulation model for wind turbine blade fatigue loads. *Journal of Wind Engineering and Industrial Aerodynamics*, 83(1-3), 527-540. [https://doi.org/10.1016/s0167-6105\(99\)00099-9](https://doi.org/10.1016/s0167-6105(99)00099-9)
9. Voyiadjis, G., & Yaghoobi, M. (2019). *Size effects in plasticity: From macro to Nano*. Academic Press.
10. Arnold, S. (2019). *2040 Vision Study: an Enlargement of Model-Based Engineering* (20190033452). NASA Glenn Research Center; Cleveland, OH, United States. <https://ntrs.nasa.gov/search.jsp?R=20190033452>
11. Talreja, R. (1998). Recent developments in damage mechanics of composite materials. In K. Reifsnider, D. Dillard, & A. Cardon (Eds.), *Progress in durability analysis of composite systems: Proceedings of the 3rd International Conference DURACOSYS, Blacksburg, Virginia, 14-17 September 1997* (pp. 119-128). CRC Press.
12. Voyiadjis, G. Z. (2014). *Handbook of damage mechanics: Nano to macro-scale for materials and structures*. Springer.
13. Soutis, C., & Beaumont, P. W. (2005). *Multi-scale modelling of composite material systems: The art of predictive damage modelling*. Elsevier.
14. Kwon, Y., Allen, D. H., & Talreja, R. R. (2007). *Multiscale modelling and simulation of composite materials and structures*. Springer Science & Business Media.

15. Diebels, S., & Rjasanow, S. (2019). *Multi-scale simulation of composite materials: Results from the project MuSiKo*. Springer.
16. Fish, J. (2009). *Multiscale methods: Bridging the scales in science and engineering*. Oxford University Press on Demand.
17. Maekawa, K., Ishida, T., & Kishi, T. (2014). *Multi-scale modeling of structural concrete*. CRC Press.
18. Eshelby, J. D. (1997). The determination of the elastic field of an ellipsoidal inclusion and related problems. *Solid Mechanics and its Applications*, 209-229. https://doi.org/10.1007/1-4020-4499-2_18
19. Hill, R. (1965). A self-consistent mechanics of composite materials. *Journal of the Mechanics and Physics of Solids*, 13(4), 213-222. [https://doi.org/10.1016/0022-5096\(65\)90010-4](https://doi.org/10.1016/0022-5096(65)90010-4)
20. Mura, T. (2012). *Micromechanics of defects in solids*. Springer Science & Business Media.
21. Hutchinson, J. W. (1987). *Micro-mechanics of damage in deformation and fracture*, The Technical University of Denmark.
22. Laws, N., Dvorak, G., & Hejazi, M. (1983). Stiffness changes in unidirectional composites caused by crack systems. *Mechanics of Materials*, 2(2), 123-137. [https://doi.org/10.1016/0167-6636\(83\)90032-7](https://doi.org/10.1016/0167-6636(83)90032-7)
23. Hashin, Z. (1985). Analysis of cracked laminates: A variational approach. *Mechanics of Materials*, 4(2), 121-136. [https://doi.org/10.1016/0167-6636\(85\)90011-0](https://doi.org/10.1016/0167-6636(85)90011-0)
24. Aboudi, J. (1987). Stiffness reduction of cracked solids. *Engineering Fracture Mechanics*, 26(5), 637-650. [https://doi.org/10.1016/0013-7944\(87\)90129-9](https://doi.org/10.1016/0013-7944(87)90129-9)
25. Griffith, A. (1921). The phenomena of rupture and flow in solids. *Philosophical Transactions of the Royal Society of London. Series A, Containing Papers of a Mathematical or Physical Character*, 221(582-593), 163-198. <https://doi.org/10.1098/rsta.1921.0006>
26. Paris, P., & Erdogan, F. (1963). A critical analysis of crack propagation laws. *Journal of Basic Engineering*, 85(4), 528-533. <https://doi.org/10.1115/1.3656900>
27. Basquin, O.H. (1910). The exponential law of endurance tests: American Society of Testing Materials, vol 10 pp 625-630.
28. Coffin, L. F. Jr. (1954). A Study of the Effects of Cyclic Thermal Stresses on a Ductile Metal. *Transactions of the ASME*, Vol. 76, 931-950.

29. Manson, S. S. (1954). *The behaviour of materials under conditions of thermal stress* (NACA-TR-1170). National Advisory Committee for Aeronautics. Lewis Flight Propulsion Lab.; Cleveland, OH, United States.
30. Wöhler, A. (1870). *Über die Festigkeitsversuche mit Eisen und Stahl. Zeitschrift für Bauwesen.* **20**: 73–106.
31. Sendekyj, G. (1981). Fitting models to composite materials fatigue data. In Chamis C (Ed). *Test Methods and Design Allowables for Fibrous Composites ASTM STP 734*, 245-260.
32. Kohout, J., & Vechet, S. (2001). A new function for fatigue curves characterization and its various merits. *International Journal of Fatigue*, *23*(2), 175-183. [https://doi.org/10.1016/s0142-1123\(00\)00082-7](https://doi.org/10.1016/s0142-1123(00)00082-7)
33. Zenkert, D., & Burman, M. (2009). Tension, compression and shear fatigue of a closed cell polymer foam. *Composites Science and Technology*, *69*(6), 785-792. <https://doi.org/10.1016/j.compscitech.2008.04.017>
34. Haigh, B.P. (1917). Experiments on the fatigue of brasses, *Journal of the Institute of Metals*, *18*, 55-86.
35. Goodman, J. (1899). *Mechanics applied to engineering*, Longman, Green & Company, London.
36. Gerber, W. Z. (1874) Bestimmung der Zulässigen Spannungen in Eisen Constructionen, *Z. Bayerischen Architekten Ingenieur-Vereins*, *6*, 101–110.
37. Soderberg, C. R., & Sweden, V., (1930), Factor of Safety and Working Stress, *ASME Transaction*, AER-IS, *52*, No. 1.
38. Morrow, J. (1965). Cyclic plastic strain energy and fatigue of metals. In B. Lazan (Ed.), *Internal Friction, Damping, and Cyclic Plasticity*, *STM International*, 45-83.
39. Harris, B. (2003). A parametric constant-life model for prediction of the fatigue lives of fibre-reinforced plastics. In *Fatigue in composites: Science and technology of the fatigue response of fibre-reinforced plastics*. Woodhead Publishing. 546–568. <https://doi.org/10.1533/9781855738577.4.546>
40. Philippidis, T. P. & Vassilopoulos, A. P. (2004). Life prediction methodology for GFRP laminates under spectrum loading. *Composites Part A: Applied Science and Manufacturing*, *35*(6), 657-666. <https://doi.org/10.1016/j.compositesa.2004.02.009>
41. Kassapoglou, C. (2007). Fatigue life prediction of composite structures under constant amplitude loading. *Journal of Composite Materials*, *41*(22), 2737-2754. <https://doi.org/10.1177/0021998307078735>

42. Kawai, M. (2007). A method for identifying asymmetric dissimilar constant fatigue life diagrams for CFRP laminates. *Key Engineering Materials*, 334-335, 61-64. <https://doi.org/10.4028/www.scientific.net/kem.334-335.61>
43. Boerstra, K. (2007). The Multislope model: A new description of the fatigue strength of glass fibre reinforced plastic. *International Journal of Fatigue*, 29(8), 1571-1576. <https://doi.org/10.1016/j.ijfatigue.2006.11.007>
44. Marin, J. (1956). Interpretation of fatigue strength for combined stresses. *Proceedings of International Conference on Fatigue of Metals, London*, 184–192.
45. Degrieck and, J., & Van Paepegem, W. (2001). Fatigue damage modelling of fibre-reinforced composite materials: Review. *Applied Mechanics Reviews*, 54(4), 279-300. <https://doi.org/10.1115/1.1381395>
46. Philippidis, T. P. & Passipoularidis, V. (2003). Residual static strength of fibrous composites after fatigue: A literature survey. OPTIMAT BLADE Deliverable#6 TG5 Technical Report (OB_TG5_R001_UP rev. 000)
47. Ramakrishnan, V., & Jayaraman, N. (1993). Mechanistically based fatigue-damage evolution model for brittle matrix fibre-reinforced composites. *Journal of Materials Science*, 28(20), 5592-5602. <https://doi.org/10.1007/bf00367835>
48. Varvani-Farahani, A., & Shirazi, A. (2007). A fatigue damage model for (0/90) FRP composites based on stiffness degradation of 0° and 90° composite plies. *Journal of Reinforced Plastics and Composites*, 26(13), 1319-1336. <https://doi.org/10.1177/0731684407079771>
49. Varvani-Farahani, A., & Shirazi, A. (2007). Prediction of stiffness degradation and damage of unidirectional GRP composites under fatigue cycles. *Science and Engineering of Composite Materials*, 14(3), 197-204. <https://doi.org/10.1515/secm.2007.14.3.197>
50. ZHANG, Y., VASSILOPOULOS, A., & KELLER, T. (2008). Stiffness degradation and fatigue life prediction of adhesively-bonded joints for fibre-reinforced polymer composites. *International Journal of Fatigue*, 30(10-11), 1813-1820. <https://doi.org/10.1016/j.ijfatigue.2008.02.007>
51. Wu, F., & Yao, W. (2010). A fatigue damage model of composite materials. *International Journal of Fatigue*, 32(1), 134-138. <https://doi.org/10.1016/j.ijfatigue.2009.02.027>
52. Shokrieh, M. M., & Esmkhani, M. (2012). Fatigue life prediction of nanoparticle/fibrous polymeric composites based on the micromechanical and normalized stiffness degradation approaches. *Journal of Materials Science*, 48(3), 1027-1034. <https://doi.org/10.1007/s10853-012-6833-0>

53. Shiri, S., Yazdani, M., & Pourgol-Mohammad, M. (2015). A fatigue damage accumulation model based on stiffness degradation of composite materials. *Materials & Design*, 88, 1290-1295. <https://doi.org/10.1016/j.matdes.2015.09.114>
54. Arrokhhabadi, A., Mohammadi, B., & Hosseini-Toudeshky, H. (2015). A simplified micromechanics model for predicting the stiffness degradation in symmetric composite laminates. *Fatigue & Fracture of Engineering Materials & Structures*, 38(11), 1334-1346. <https://doi.org/10.1111/ffe.12306>
55. Samareh-Mousavi, S. S., & Taheri-Behrooz, F. (2020). A novel creep-fatigue stiffness degradation model for composite materials. *Composite Structures*, 237, 111955. <https://doi.org/10.1016/j.compstruct.2020.111955>
56. Ellyin, F. (2012). *"Fatigue damage, crack growth and life prediction"*. Springer Science & Business Media.
57. Dowling, N. E. (2013). *"Mechanical behaviour of materials: engineering methods for deformation, fracture, and fatigue"*. Prentice-Hall.
58. Stephens, R. I., Fatemi, A., Stephens, R. R., & Fuchs, H. O. (2000). *"Metal fatigue in engineering"*. John Wiley & Sons.
59. Suresh, S. (1998). *"Fatigue of materials"*. Cambridge University Press.
60. Harris, B. (2003). *"Fatigue in composites: Science and technology of the fatigue response of fibre-reinforced plastics"*. Elsevier.
61. Lee, Y., Pan, J., Hathaway, R., & Barkey, M. (2011). *"Fatigue testing and analysis: Theory and practice"*. Elsevier.
62. Manson, S. S., Halford, G. R. (2006). *"Fatigue and durability of structural materials"*. ASM International.
63. Manson, S. S., & Halford, G. R. (2009). *"Fatigue and durability of metals at high temperatures"*. ASM International.
64. Schijve, J. (2008). *"Fatigue of structures and materials"*. Springer Science & Business Media.
65. Vassilopoulos, A. P. (2019). *"Fatigue life prediction of composites and composite structures"*. Woodhead Publishing.
66. Vassilopoulos, A. P., & Keller, T. (2011). *"Fatigue of fibre-reinforced composites"*. Springer Science & Business Media.
67. Alderliesten, R. (2017). *Fatigue and fracture of fibre metal laminates*. Springer.
68. Coffin, L. (1962). Low-Cycle Fatigue A Review. *Applied Material Research*, 1(3), 129-141. <https://doi.org/10.1520/stp33321s>
69. Kaechele, L. (1963). Review of analysis of cumulative fatigue damage theories. *Memorandum RM-3650-PR, Rand corporation, CA*.

70. Manson, S. (1965). *Fatigue-a complex subject. Some simple approximations*. NASA Technical Memorandum TM X-52084.
71. O'Neill, M. (1970). *A review of some cumulative damage theories* (Structure and Materials Report 326). Department of Supply, Australian Defence Scientific Service Aeronautical Research Laboratory.
72. Plumbridge, W. J. (1972). Review: Fatigue-crack propagation in metallic and polymeric materials. *Journal of Materials Science*, 7(8), 939-962. <https://doi.org/10.1007/bf00550441>
73. Schijve, J. (1972). *The accumulation of fatigue damage in aircraft materials and structures* (AGARD-AG-157). NLR, Netherlands.
74. Dew-Hughes, D., & Way, J. (1973). Fatigue of fibre — reinforced plastics: A review. *Composites*, 4(4), 167-173. [https://doi.org/10.1016/0010-4361\(73\)90108-0](https://doi.org/10.1016/0010-4361(73)90108-0)
75. Krempl, E. (1974). The influence of the state of stress on low-cycle fatigue of structural materials. A literature survey and interpretive report. *ASTM STP 549*, ASTM, PA, 1-1-47.
76. Socie, D. F., & Morrow, J. (1980). Review of contemporary approaches to fatigue damage analysis. *Risk and Failure Analysis for Improved Performance and Reliability* 141-194. https://doi.org/10.1007/978-1-4684-7811-2_8
77. Hashin, Z., & Rotom, A. (1978). A cumulative damage theory of fatigue failure. *Materials Science and Engineering*, 34, 147 - 160. <https://doi.org/10.21236/ada041984>
78. Stinchcomb, W., & Reifsnider, K. (1979). Fatigue damage mechanisms in composite materials: A review. *Fatigue Mechanisms*, ASTM STP 675, 762-787. <https://doi.org/10.1520/stp35914s>
79. Garud, Y. (1981). Multiaxial Fatigue A Survey of the State of the Art. *Journal of Testing and Evaluation*, 9(3), 165-178. <https://doi.org/10.1520/JTE11553J>
80. Reifsnider, K. L. (1987). Life prediction analysis: directions and divagations. In F. L. Matthews, N. C. R. Buskell, J. M. Hodgkinson, & J. Morton (Eds.), *Proceedings*, 20-24 July 1987, London, UK: Vol. 4. Sixth international conference on composite materials (ICCM-VI) & second European conference on composite materials (ECCM-II) (pp. 4.1-4.31). Elsevier. <http://iccm-central.org/Proceedings/ICCM6proceedings/index.htm>
81. Konur, O., & Matthews, F. (1989). Effect of the properties of the constituents on the fatigue performance of composites: A review. *Composites*, 20(4), 317-328. [https://doi.org/10.1016/0010-4361\(89\)90657-5](https://doi.org/10.1016/0010-4361(89)90657-5)

82. Bulloch, J. (1991). The influence of mean stress or R-ratio on the fatigue crack threshold characteristics of steels—a review. *Int. J. Pressure vessels piping*, 47(3), 263-292. [https://doi.org/10.1016/0142-1123\(92\)90040-j](https://doi.org/10.1016/0142-1123(92)90040-j)
83. Liu, H. (1991). A review of fatigue cracks growth analyses. *Theoretical and Applied Fracture Mechanics*, 16, 91-108. [https://doi.org/10.1016/0167-8442\(91\)90027-H](https://doi.org/10.1016/0167-8442(91)90027-H)
84. Sendekyj, K. (1991). Life Prediction for Resin-Matrix Composite Materials. In *Reifsnider K (Ed.) Fatigue of composite materials* (pp. 431-483). Elsevier.
85. Kumar, R. (1992). Review on crack closure for constant amplitude loading in fatigue. *Engineering Fracture Mechanics*, 42(2), 389-400. [https://doi.org/10.1016/0013-7944\(92\)90228-7](https://doi.org/10.1016/0013-7944(92)90228-7)
86. Geary, W. (1992). A review of some aspects of fatigue cracks growth under variable amplitude loading. *International Journal of Fatigue*, 14(6), 377-386. [https://doi.org/10.1016/0142-1123\(92\)90225-2](https://doi.org/10.1016/0142-1123(92)90225-2)
87. Bartsch, K., Haenninen, H., & Neiminen, M. (1994). Thermal fatigue: A literature review. *Report Helsinki University of technology, (Julkaisu MTR 3/93)*. [https://doi.org/10.1016/0142-1123\(94\)90568-1](https://doi.org/10.1016/0142-1123(94)90568-1)
88. Andersons, J. (1994). Methods of fatigue prediction for composite laminates. A review. *Mechanics of Composite Materials*, 29(6), 545-554. <https://doi.org/10.1007/bf00616318>
89. Vasudeven, A., Sadananda, K., & Louat, N. (1994). A review of crack closure, fatigue crack threshold and related phenomena. *Materials Science and Engineering: A*, 188(1-2), 1-22. [https://doi.org/10.1016/0921-5093\(94\)90351-4](https://doi.org/10.1016/0921-5093(94)90351-4)
90. Read, P., & Shenoi, R. (1995). A review of fatigue damage modelling in the context of marine FRP laminates. *Marine Structures*, 8(3), 257-278. [https://doi.org/10.1016/0951-8339\(94\)00004-c](https://doi.org/10.1016/0951-8339(94)00004-c)
91. You, B., & Lee, S. (1996). A critical review of multiaxial fatigue assessments of metals. *International Journal of Fatigue*, 18(4), 235-244. [https://doi.org/10.1016/0142-1123\(96\)00002-3](https://doi.org/10.1016/0142-1123(96)00002-3)
92. Schütz, W. (1996). A history of fatigue. *Engineering Fracture Mechanics*, 54(2), 263-300. [https://doi.org/10.1016/0013-7944\(95\)00178-6](https://doi.org/10.1016/0013-7944(95)00178-6)
93. LAWSON, L. (1999). Near-threshold fatigue: A review. *International Journal of Fatigue*, 21, 15-34. [https://doi.org/10.1016/s0142-1123\(99\)00053-5](https://doi.org/10.1016/s0142-1123(99)00053-5)
94. Bogdanovich, A. E., & Sierakowski, R. L. (1999). Composite materials and structures: Science, technology and applications - A compendium of books, review papers, and other sources of information. *Applied Mechanics Reviews*, 52(12), 351-366. <https://doi.org/10.1115/1.3098921>

95. Birman, V., & Byrd, L. W. (2000). Review of fracture and fatigue in ceramic matrix composites. *Applied Mechanics Reviews*, 53(6), 147-174. <https://doi.org/10.1115/1.3097345>
96. Yokobari, T. (2001). A critical review of fatigue crack growth. *Handbook of Materials Behavior Models*, 611-621. <https://doi.org/10.1016/b978-012443341-0/50068-5>
97. Degrieck and, J., & Van Paepegem, W. (2001). Fatigue damage modelling of fibre-reinforced composite materials: Review. *Applied Mechanics Reviews*, 54(4), 279-300. <https://doi.org/10.1115/1.1381395>
98. Lemaitre J. (2001) Petite Histoire de l'Experimentation en Mecanique des Solides. *Meccanica* 36: 13–35. <https://doi.org/10.1023/A:1011977806453>
99. Yu, M. (2002). Advances in strength theories for materials under complex stress state in the 20th century. *Applied Mechanics Reviews*, 55(3), 169-218. <https://doi.org/10.1115/1.1472455>
100. Qatu, M. S. (2002). Recent research advances in the dynamic behaviour of shells: 1989-2000, Part 1: Laminated composite shells. *Applied Mechanics Reviews*, 55(4), 325-350. <https://doi.org/10.1115/1.1483079>
101. Kuang and, K., & Cantwell, W. (2003). Use of conventional optical fibres and fibre Bragg gratings for damage detection in advanced composite structures: A review. *Applied Mechanics Reviews*, 56(5), 493-513. <https://doi.org/10.1115/1.1582883>
102. Harris, B. (2003). A historical review of the fatigue behaviour of fibre-reinforced plastics. *Fatigue in Composites*, 3-35. <https://doi.org/10.1533/9781855738577.1.3>
103. Philippidis, T.P., and Passipoularidis, V. (2002) Residual static strength of fibrous composites after fatigue: a literature survey Optimat Blades Report-TG5-R001_UP rev 000
104. Tay, T. (2003). Characterization and analysis of delamination fracture in composites: An overview of developments from 1990 to 2001. *Applied Mechanics Reviews*, 56(1), 1-32. <https://doi.org/10.1115/1.1504848>
105. Krueger, R. (2004). Virtual crack closure technique: history, approach, and applications. *Applied Mechanics Reviews*, 57(2), 109-143. <https://doi.org/10.1115/1.1595677>
106. Della, C. N., & Shu, D. (2007). The vibration of delaminated composite laminates: A review. *Applied Mechanics Reviews*, 60(1), 1. <https://doi.org/10.1115/1.2375141>

107. Icardi, U., Locatto, S., & Longo, A. (2007). Assessment of recent theories for predicting failure of composite laminates. *Applied Mechanics Reviews*, 60(2), 76. <https://doi.org/10.1115/1.2515639>
108. Post, N., Case, S., & Lesko, J. (2008). Modelling the variable amplitude fatigue of composite materials: A review and evaluation of state of the art for spectrum loading. *International Journal of Fatigue*, 30(12), 2064-2086. <https://doi.org/10.1016/j.ijfatigue.2008.07.002>
109. Passipoularidis, V., & Brøndsted, P. (2010). *Fatigue Evaluation Algorithms: Review*. Danmarks Tekniske Universitet, Risø Nationallaboratoriet for Bæredygtig Energi. Denmark. Forskningscenter Risøe. Risøe-R, No. 1740(EN)
110. Garnich, M. R., & Akula, V. M. (2008). Review of degradation models for progressive failure analysis of fibre-reinforced polymer composites. *Applied Mechanics Reviews*, 62(1). <https://doi.org/10.1115/1.3013822>
111. Wicaksono, S., & Chai, G. B. (2012). A review of advances in fatigue and life prediction of fibre-reinforced composites. *Proceedings of the Institution of Mechanical Engineers, Part L: Journal of Materials: Design and Applications*, 227(3), 179-195. <https://doi.org/10.1177/1464420712458201>
112. Alderliesten, R. (2013). A critical review of the assessment of fatigue and fracture in composite materials and structures. *Engineering Failure Analysis*, 35, 370-379. <https://doi.org/10.1016/j.engfailanal.2013.03.022>
113. Pascoe, J., Alderliesten, R., & Benedictus, R. (2013). Methods for the prediction of fatigue delamination growth in composites and adhesive bonds – A critical review. *Engineering Fracture Mechanics*, 112-113, 72-96. <https://doi.org/10.1016/j.engfracmech.2013.10.003>
114. Wang, P., Takagi, T., Takeno, T., & Miki, H. (2013). Early fatigue damage detecting sensors—A review and prospects. *Sensors and Actuators A: Physical*, 198, 46-60. <https://doi.org/10.1016/j.sna.2013.03.025>
115. Mansor, N., Abdullah, S., Ariffin, A., & Syarif, J. (2014). A review of the fatigue failure mechanism of metallic materials under a corroded environment. *Engineering Failure Analysis*, 42, 353-365. <https://doi.org/10.1016/j.engfailanal.2014.04.016>
116. Bak, B. L., Sarrado, C., Turon, A., & Costa, J. (2014). Delamination under fatigue loads in composite laminates: A review on the observed phenomenology and computational methods. *Applied Mechanics Reviews*, 66(6). <https://doi.org/10.1115/1.4027647>

117. Kaminski, M. Laurin, F. Maire, J.-F. Rakotoarisoa, C. Hémon, E. (2015) Fatigue Damage Modeling of Composite Structures: the ONERA Viewpoint. *Journal AerospaceLab*, 9 AL09-06, <https://doi.org/10.12762/2015.AL09-06>
118. Khan, R., Alderliesten, R., Badshah, S., & Benedictus, R. (2015). Effect of stress ratio or mean stress on fatigue delamination growth in composites: Critical review. *Composite Structures*, 124, 214-227. <https://doi.org/10.1016/j.compstruct.2015.01.016>
119. Mortazavian, S., & Fatemi, A. (2015). Fatigue behaviour and modelling of short fibre reinforced polymer composites: A literature review. *International Journal of Fatigue*, 70, 297-321. <https://doi.org/10.1016/j.ijfatigue.2014.10.005>
120. Sevenois, R. D., & Van Paepegem, W. (2015). Fatigue damage modelling techniques for textile composites: Review and comparison with unidirectional composite modelling techniques. *Applied Mechanics Reviews*, 67(2). <https://doi.org/10.1115/1.4029691>
121. Santecchia, E., Hamouda, A. M., Musharavati, F., Zalnezhad, E., Cabibbo, M., El Mehtedi, M., & Spigarelli, S. (2016). A review of fatigue life prediction methods for metals. *Advances in Materials Science and Engineering*, 2016, 1-26. <https://doi.org/10.1155/2016/9573524>
122. Vacchieri, E. (2016). Review: Creep-fatigue interaction testing and damage assessment for high-temperature materials. Reference Module in Materials Science and Materials Engineering. <https://doi.org/10.1016/b978-0-12-803581-8.04046-7>
123. Zerbst, U., Vormwald, M., Pippan, R., Gänser, H., Sarrazin-Baudoux, C., & Madia, M. (2016). About the fatigue crack propagation threshold of metals as a design criterion – A review. *Engineering Fracture Mechanics*, 153, 190-243. <https://doi.org/10.1016/j.engfracmech.2015.12.002>
124. Chowdhury, P., & Sehitoglu, H. (2016). Mechanisms of fatigue crack growth - a critical digest of theoretical developments. *Fatigue & Fracture of Engineering Materials & Structures*, 39(6), 652-674. <https://doi.org/10.1111/ffe.12392>
125. Adedipe, O., Brennan, F., & Kolios, A. (2016). Review of corrosion fatigue in offshore structures: Present status and challenges in the offshore wind sector. *Renewable and Sustainable Energy Reviews*, 61, 141-154. <https://doi.org/10.1016/j.rser.2016.02.017>
126. Antolovich, S. D., Saxena, A., & Gerberich, W. W. (2018). Fracture mechanics – An interpretive technical history *Mechanics Research Communications*, 91, 46-86 <https://doi.org/10.1016/j.mechrescom.2018.03.003>

127. Tabiei, A., & Zhang, W. (2018). Composite laminate delamination simulation and experiment: A review of recent development. *Applied Mechanics Reviews*, 70(3). <https://doi.org/10.1115/1.4040448>
128. Maierhofer, J., Kolitsch, S., Pippan, R., Gänser, H., Madia, M., & Zerbst, U. (2018). The cyclic R-curve – Determination, problems, limitations and application. *Engineering Fracture Mechanics*, 198, 45-64. <https://doi.org/10.1016/j.engfracmech.2017.09.032>
129. Alam, P., Mamalis, D., Robert, C., Floreani, C., & Ó Brádaigh, C. M. (2019). The fatigue of carbon fibre reinforced plastics - A review. *Composites Part B: Engineering*, 166, 555-579 <https://doi.org/10.1016/j.compositesb.2019.02.016>
130. Ravikumar, K., Subbiah, R., Ranganathan, N., Bensingh, J., Kader, A., & Nayak, S. K. (2019). A review on fatigue damages in the wind turbines: Challenges in determining and reducing fatigue failures in wind turbine blades. *Wind Engineering*, 0309524X1984985. <https://doi.org/10.1177/0309524x19849851>
131. Jimenez-Martinez, M. (2020). Fatigue of offshore structures: A review of statistical fatigue damage assessment for stochastic loadings. *International Journal of Fatigue*, 132, 105327. <https://doi.org/10.1016/j.ijfatigue.2019.105327>
132. Vassilopoulos, A. P. (2020). The history of fibre-reinforced polymer composite laminate fatigue. *International Journal of Fatigue*, 134, 105512. <https://doi.org/10.1016/j.ijfatigue.2020.105512>
133. Perzyna P. (1968) On Thermodynamic Foundations of Viscoplasticity. In: Lindholm U.S. (eds) *Mechanical Behavior of Materials under Dynamic Loads*. Springer, Berlin, Heidelberg
134. Eckart, C. (1948). The thermodynamics of irreversible processes. IV. The theory of elasticity and Anelasticity. *Physical Review*, 73(4), 373-382. <https://doi.org/10.1103/physrev.73.373>
135. Meixner, J. (1954). Thermodynamische Theorie Der elastischen relaxation. *Zeitschrift für Naturforschung A*, 9(7-8), 654-663. <https://doi.org/10.1515/zna-1954-7-812>
136. Biot, M. A. (1954). Theory of stress-strain relations in anisotropic viscoelasticity and relaxation phenomena. *Journal of Applied Physics*, 25(11), 1385-1391. <https://doi.org/10.1063/1.1721573>
137. Green, A. E., & Rivlin, R. S. (1957). The mechanics of non-linear materials with memory. *Archive for Rational Mechanics and Analysis*, 1(1), 1-21. <https://doi.org/10.1007/bf00297992>

138. Ziegler, H. (1957). Thermodynamik und rheologische Probleme. *Ingenieur-Archiv*, 25(1), 58-70. <https://doi.org/10.1007/bf00536645>
139. Vakulenko, A., & Kachanov, M. (1971). A continuum model of medium with cracks (in Russian). *Mekhanika Tverdogo Tela*, 4, 159-166.
140. Noll, W. (1974). *The foundations of mechanics and thermodynamics: Selected papers*. Springer Science & Business Media.
141. Truesdell, C., & Noll, W. (1965). *The non-linear field theories of mechanics*. Springer Science & Business Media.
142. Green, A. E., & Adkins, J. E. (1960). *Large elastic deformations and non-linear continuum mechanics*. Oxford.
143. Kluitenberg, G. (1962). Thermodynamical theory of elasticity and plasticity. *Physica*, 28(3), 217-232. [https://doi.org/10.1016/0031-8914\(62\)90041-1](https://doi.org/10.1016/0031-8914(62)90041-1)
144. Coleman, B. D. (1964). Thermodynamics of materials with memory. *Archive for Rational Mechanics and Analysis*, 17(1), 1-46. <https://doi.org/10.1007/bf00283864>
145. Lebon, G., & Perzyna, P. (1980). *Recent developments in Thermomechanics of solids*. Springer.
146. DRUCKER, D. C. (1964) On the Postulate of Stability of Material in the Mechanics of Continua. *Journal de Mécanique*, 3, 235–249.
147. Gurtin, M. E. (1965). Thermodynamics and the possibility of spatial interaction in elastic materials. *Archive for Rational Mechanics and Analysis*, 19(5), 339-352. <https://doi.org/10.1007/bf00253483>
148. Pipkin, A. C., & Rivlin, R. S. (1965). Mechanics of rate-independent materials. *Zeitschrift für angewandte Mathematik und Physik ZAMP*, 16(3), 313-327. <https://doi.org/10.1007/bf01591911>
149. Casey, J., & Crochet, M. J. (2012). *Theoretical, experimental, and numerical contributions to the mechanics of fluids and solids: A collection of papers in honour of Paul M. Naghdi*. Birkhäuser.
150. Barenblatt, G. I., & Joseph, D. D. (2013). *Collected papers of R.S. Rivlin: Volume I and II*. Springer Science & Business Media.
151. VALANIS, K. C. (1968). The Viscoelastic potential and its thermodynamic foundations. *Journal of Mathematics and Physics*, 47(1-4), 262-275. <https://doi.org/10.1002/sapm1968471262>
152. Kestin, J., & Rice, J. R. (1970). Paradoxes in the application of thermodynamics to strained solids. In *Stuart, E. Gal-Or, B. Brainard, A. (eds.) A Critical Review of Thermodynamics* (pp. 275-298).

153. Kestin, J. (1979). *A course in thermodynamics*. CRC Press.
154. Dillon, O. (1963). Coupled thermoplasticity. *Journal of the Mechanics and Physics of Solids*, 11(1), 21-33. [https://doi.org/10.1016/0022-5096\(63\)90004-8](https://doi.org/10.1016/0022-5096(63)90004-8)
155. Germain, P. (1962). *Mécanique des milieux continus*. Masson, Paris
156. Maugin, G. A. (2016). *Non-classical continuum mechanics: A dictionary*. Springer.
157. Maugin, Gerard. (2015). The saga of internal variables of state in continuum thermo-mechanics (1893-2013). *Mechanics Research Communications*. 69:79-86. <https://doi.org/10.1016/j.mechrescom.2015.06.009>
158. Kachanov, L. (1958) Time of the Rupture Process under Creep Conditions. *Izvestiia Akademii Nauk SSSR, Otdelenie Teckhnicheskikh Nauk*, 8, 26-31. (in Russian)
159. Rabotnov, Y. N. (1968). Creep rupture. *Applied Mechanics*, 342-349. https://doi.org/10.1007/978-3-642-85640-2_26
160. Lemaitre, J. & Chaboche, J. (1978) Aspect phenomenologie de la rupture par endommagement, *J. Mecanique Appl.* 2 317-365.
161. Hayhurst, D. (1972). Creep rupture under multi-axial states of stress. *Journal of the Mechanics and Physics of Solids*, 20(6), 381-382. [https://doi.org/10.1016/0022-5096\(72\)90015-4](https://doi.org/10.1016/0022-5096(72)90015-4)
162. Leckie F. (1974) Creep rupture of structures. *Proceedings of the Royal Society of London. A. Mathematical and Physical Sciences*, 340(1622), 323-347. <https://doi.org/10.1098/rspa.1974.0155>
163. Sidoroff, F.,(1975) On the formulation of plasticity and viscoplasticity with internal variables, *Archives of Mechanics* 27, 5/6, 807-819.
164. Dafalias, Y. F. & Popov, E. P. (1976). Plastic internal variables formalism of cyclic plasticity. *Journal of Applied Mechanics*, 43(4), 645-651. <https://doi.org/10.1115/1.3423948>
165. Chaboche, J. L., (1977), Sur l'utilisation des variables d'état interne pour la description du comportement viscoplastique et de la rupture par endommagement, *Problemes non linéaires de mécanique, Symp. Franco-Polonais de Rhéologie et Mécanique*, Cracovie, 137-159
166. Savalle S. et Culie J.P. ´ (1978). Méthodes de calcul associées aux lois de comportement cyclique et d'endommagement. *La Recherche Aérospatiale*, vol. 5, pp 263–278.
167. Chrzanowski, M., & Hult, J. (1987). Ductile creep rupture of fibre bundles. *Engineering Fracture Mechanics*, 28(5-6), 681-688. [https://doi.org/10.1016/0013-7944\(87\)90061-0](https://doi.org/10.1016/0013-7944(87)90061-0)

168. Murakami, S., & Ohno, N. (1981). A continuum theory of creep and creep damage. *Creep in Structures*, 422-444. https://doi.org/10.1007/978-3-642-81598-0_28
169. Cordebois, J. P., & Sidoroff, F. (1982). Damage Induced Elastic Anisotropy. *Mechanical Behavior of Anisotropic Solids / Comportment Mécanique Des Solides Anisotropies*, 761–774. https://doi.org/10.1007/978-94-009-6827-1_44
170. Krajcinovic, D., & Fonseka, G. U. (1981). The Continuous Damage Theory of Brittle Materials, Part 1: General Theory. *Journal of Applied Mechanics*, 48(4), 809–815. <https://doi.org/10.1115/1.3157739>
171. Mazars, J. (1982). Mechanical damage and fracture of concrete structures. In *François, D., Métallurgie. S. (Eds) Advances in fracture research (Fracture 81): Proceedings of the 5th International Conference on fracture (ICF5), Cannes, France, 29 March - 3 April 1981*.
172. Ladevèze, P. (1982). On an anisotropic damage theory. In *International CNRS Colloquium 351: Failure criteria of structured media. Fibre Science and Technology*, 355–363. [https://doi.org/10.1016/0015-0568\(82\)90025-2](https://doi.org/10.1016/0015-0568(82)90025-2).
173. Ortiz, M. (1985). A constitutive theory for the inelastic behaviour of concrete. *Mechanics of Materials*, 4(1), 67-93. [https://doi.org/10.1016/0167-6636\(85\)90007-9](https://doi.org/10.1016/0167-6636(85)90007-9)
174. Simo, J., & Ju, J. (1987). Strain- and stress-based continuum damage models—I. Formulation. *International Journal of Solids and Structures*, 23(7), 821-840. [https://doi.org/10.1016/0020-7683\(87\)90083-7](https://doi.org/10.1016/0020-7683(87)90083-7)
175. Chow, C. L., & Wang, J. (1987). An anisotropic theory of elasticity for continuum damage mechanics. *International Journal of Fracture*, 33(1), 3-16. <https://doi.org/10.1007/bf00034895>
176. Chrysochoos, A., Maisonneuve, O., Martin, G., Caumon, H., & Chezeaux, J. (1989). Plastic and dissipated work and stored energy. *Nuclear Engineering and Design*, 114(3), 323-333. [https://doi.org/10.1016/0029-5493\(89\)90110-6](https://doi.org/10.1016/0029-5493(89)90110-6)
177. LESNE, P. M. et SAVALLE, S. (1987). A differential damage rule with micro-initiation and micropropagation, *La recherche Aérospatiale*, 2. 33-47 [In French]
178. Benallal, A. (1989). *Thermoviscoplasticité et endommagement des structures* [Doctoral dissertation]. Université de Paris 6.
179. Talreja, R. (1990). Internal variable damage mechanics of composite materials. In *Boehler. J. (Ed) Yielding, damage, and failure of anisotropic solids (EGF publication 5)*, 509-533. Wiley.
180. Voyiadjis, G. Z., & Kattan, P. I. (1993). Damage of fibre-reinforced composite materials with micromechanical characterization. *International Journal of Solids*

- and *Structures*, 30(20), 2757-2778. [https://doi.org/10.1016/0020-7683\(93\)90153-x](https://doi.org/10.1016/0020-7683(93)90153-x)
181. Saanouni, K., Forster, C., & Hatira, F. B. (1994). On the Anelastic flow with damage. *International Journal of Damage Mechanics*, 3(2), 140-169. <https://doi.org/10.1177/105678959400300203>
 182. Lemaitre, J., & Desmorat, R. (2006). "Engineering damage mechanics: Ductile, creep, fatigue and brittle failures". Springer Science & Business Media.
 183. Miner, M. (1945). Cumulative damage in fatigue. *Journal of applied mechanics*, 12, A159-A164.
 184. Manson, S. S., Freche, J. C., & Ensign, C. R. (1967). *Application of a double linear damage rule to cumulative fatigue* (TN D-3839). NASA.
 185. Kachanov, L.M. (1958). Time of the rupture process under creep conditions. *Izv. Akad. Nauk. SSR, Otd Tekh. Nauk*, 8, 26–31. (In Russian)
 186. Chaboche, J.L. (1974). Une loi différentielle d'endommagement de fatigue avec cumulation non linéaire, *Revue Française de Mécanique*, 50-51, 71-82 (In French)
 187. Lemaitre, J., & Plumtree, A. (1979). Application of damage concepts to predict creep-fatigue failures. *Journal of Engineering Materials and Technology*, 101(3), 284-292. <https://doi.org/10.1115/1.3443689>
 188. Lemaitre, J. (1984). How to use damage mechanics. *Nuclear Engineering and Design*, 80(2), 233-245. [https://doi.org/10.1016/0029-5493\(84\)90169-9](https://doi.org/10.1016/0029-5493(84)90169-9)
 189. Lemaitre, J. (1987). Formulation and identification of damage kinetic constitutive equations. *Continuum Damage Mechanics Theory and Application*, 37-89. https://doi.org/10.1007/978-3-7091-2806-0_2
 190. Dufailly, J., & Lemaitre, J. (1995). Modelling very low cycle fatigue. *International Journal of Damage Mechanics*, 4(2), 153-170. <https://doi.org/10.1177/105678959500400204>
 191. Cordebois, J. P., & Sidoroff, F. (1982). Damage induced elastic anisotropy. *Mechanical Behavior of Anisotropic Solids / Comportment Mécanique des Solides Anisotropes*, 761-774. https://doi.org/10.1007/978-94-009-6827-1_44
 192. Wang, T., & Lou, Z. (1990). A continuum damage model for the weld heat-affected zone under low cycle fatigue loading. *Engineering Fracture Mechanics*, 37(4), 825-829. [https://doi.org/10.1016/0013-7944\(90\)90081-q](https://doi.org/10.1016/0013-7944(90)90081-q)
 193. Jessen, S., & Plumtree, A. (1991). Continuum damage mechanics applied to cyclic behaviour of a glass fibre composite pultrusion. *Composites*, 22(3), 181-190. [https://doi.org/10.1016/0010-4361\(91\)90317-a](https://doi.org/10.1016/0010-4361(91)90317-a)

194. Chow, C., & Wei, Y. (1991). A damage mechanics model of fatigue cracks initiation in notched plates. *Theoretical and Applied Fracture Mechanics*, 16(2), 123-133. [https://doi.org/10.1016/0167-8442\(91\)90029-j](https://doi.org/10.1016/0167-8442(91)90029-j)
195. Arnold, S., & Kruch, S. (1991). Differential continuum damage mechanics models for creep and fatigue of unidirectional metal matrix composites, NASA TM-105213 54 pp. *International Journal of Fatigue*, 15(3), 249-249. [https://doi.org/10.1016/0142-1123\(93\)90186-t](https://doi.org/10.1016/0142-1123(93)90186-t)
196. Paas, M., Schreurs, P., & Brekelmans, W. (1993). A continuum approach to brittle and fatigue damage: Theory and numerical procedures. *International Journal of Solids and Structures*, 30(4), 579-599. [https://doi.org/10.1016/0020-7683\(93\)90189-e](https://doi.org/10.1016/0020-7683(93)90189-e)
197. Guang-Xu Cheng, Jian-Zheng Zuo, Zhi-Wen Lou, & Zhen-Bang Kuang. (1996). Continuum damage model of low-cycle fatigue and fatigue damage analysis of welded joint. *Engineering Fracture Mechanics*, 55(1), 155-161. [https://doi.org/10.1016/0013-7944\(95\)00261-8](https://doi.org/10.1016/0013-7944(95)00261-8)
198. Voyiadjis, G. Z., & Echle, R. (1998). High cycle fatigue damage evolution in unidirectional metal matrix composites using a micro-mechanical approach. *Mechanics of Materials*, 30(2), 91-110. [https://doi.org/10.1016/s0167-6636\(98\)00040-4](https://doi.org/10.1016/s0167-6636(98)00040-4)
199. Peerlings, R. H., Brekelmans, W. A., De Borst, R., & Geers, M. G. (2000). Gradient-enhanced damage modelling of high-cycle fatigue. *International Journal for Numerical Methods in Engineering*, 49(12), 1547-1569. [https://doi.org/10.1002/1097-0207\(20001230\)49:12<1547::aid-nme16>3.0.co;2-d](https://doi.org/10.1002/1097-0207(20001230)49:12<1547::aid-nme16>3.0.co;2-d)
200. Wahab, M. M., Ashcroft, I. A., Crocombe, A. D., & Shaw, S. J. (2001). Prediction of fatigue thresholds in adhesively bonded joints using damage mechanics and fracture mechanics. *Journal of Adhesion Science and Technology*, 15(7), 763-781. <https://doi.org/10.1163/15685610152540830>
201. Naderi, M., Amiri, M., & Khonsari, M. M. (2009). On the thermodynamic entropy of fatigue fracture. *Proceedings of the Royal Society A: Mathematical, Physical and Engineering Sciences*, 466(2114), 423-438. <https://doi.org/10.1098/rspa.2009.0348>
202. Pandey, V., Singh, I., Mishra, B., Ahmad, S., Venugopal Rao, A., & Kumar, V. (2019). A new framework based on continuum damage mechanics and XFEM for high cycle fatigue crack growth simulations. *Engineering Fracture Mechanics*, 206, 172-200. <https://doi.org/10.1016/j.engfracmech.2018.11.021>

203. Dunne, F., & Petrinic, N. (2005). *Introduction to computational plasticity*. OUP Oxford.
204. Flügge, S. (1958). *Encyclopedia of physics - Elasticity and Plasticity*. Springer, Berlin, Heidelberg. <https://doi.org/10.1007/978-3-662-43081-1>
205. Chaboche, J. (1989). Constitutive equations for cyclic plasticity and cyclic viscoplasticity. *International Journal of Plasticity*, 5(3), 247-302. [https://doi.org/10.1016/0749-6419\(89\)90015-6](https://doi.org/10.1016/0749-6419(89)90015-6)
206. Guedes, R. M. (2019). *"Creep and fatigue in polymer matrix composites"*. Woodhead Publishing.
207. Lee, Y., Barkey, M. E., & Kang, H. (2011). *"Metal fatigue analysis handbook: Practical problem-solving techniques for computer-aided engineering"*. Elsevier.
208. Masing, G. (1923). Eigenspannungen und verfestigung beim messing (Self stretching and hardening for brass), in: Proceedings of the Second International Congress for Applied Mechanics, Zurich, Switzerland, 1926, pp. 332–335 (in German).
209. Prager, W. (1956) A New Method of Analyzing Stresses and Strains in Work-Hardening Plastic Solids. *Journal of Applied Mechanics*, 23, 493-496.
210. Ziegler, H. (1959). A modification of Prager's hardening rule. *Quarterly of Applied Mathematics*, 17(1), 55-65. <https://doi.org/10.1090/qam/104405>
211. Armstrong, P.J. and Frederick, C.O. (1966) A Mathematical Representation of the Multi-Axial Bauschinger Effect. CEGB Report RD/B/N 731, Central Electricity Generating Board. The Report Is Reproduced as a Paper: 2007. *Materials at High Temperatures*, 24(1), 1-26. <https://doi.org/10.3184/096034007x207589>
212. Mróz, Z. (1967). On the description of anisotropic work hardening. *Journal of the Mechanics and Physics of Solids*, 15(3), 163-175. [https://doi.org/10.1016/0022-5096\(67\)90030-0](https://doi.org/10.1016/0022-5096(67)90030-0)
213. Dafalias, Y. F. & Popov, E. P. (1975). A model of nonlinearly hardening materials for complex loading. *Acta Mechanica*, 21(3), 173-192. <https://doi.org/10.1007/bf01181053>
214. Chaboche, J.L., Dang Van, K., & Cordier, G. Boley, B.A. (Ed.). (1979). Modelization of the strain memory effect on the cyclic hardening of 316 stainless steel. L - Materials Modeling and Inelastic Analysis of Metal Structures L11 – Damage SMiRT 5 – Berlin, Germany. <http://www.lib.ncsu.edu/resolver/1840.20/26854>
215. Chaboche, J. (1991). On some modifications of kinematic hardening to improve the description of ratchetting effects. *International Journal of Plasticity*, 7(7), 661-678. [https://doi.org/10.1016/0749-6419\(91\)90050-9](https://doi.org/10.1016/0749-6419(91)90050-9)

216. Tanaka, E. (1994). A non-proportionality parameter and a cyclic viscoplastic constitutive model taking into account amplitude dependences and memory effects of isotropic hardening *European Journal of Mechanics A/Solids*, 13, 155-173
217. Burlet, H., & Cailletaud, G. (1986). Numerical techniques for cyclic plasticity at variable temperature. *Engineering Computations*, 3(2), 143-153. <https://doi.org/10.1108/eb023652>
218. Benallal, A., & Marquis, D. (1987). Constitutive equations for Nonproportional cyclic elasto-viscoplasticity. *Journal of Engineering Materials and Technology*, 109(4), 326-336. <https://doi.org/10.1115/1.3225985>
219. Bower, A. (1989). Cyclic hardening properties of hard-drawn copper and rail steel. *Journal of the Mechanics and Physics of Solids*, 37(4), 455-470. [https://doi.org/10.1016/0022-5096\(89\)90024-0](https://doi.org/10.1016/0022-5096(89)90024-0)
220. Guionnet, C. (1992). Modelling of Ratchetting in biaxial experiments. *Journal of Engineering Materials and Technology*, 114(1), 56-62. <https://doi.org/10.1115/1.2904141>
221. Ohno, N., & Wang, J. (1993). Kinematic hardening rules with critical state of dynamic recovery, part I and Part II. *International Journal of Plasticity*, 9(3), 375-403. [https://doi.org/10.1016/0749-6419\(93\)90042-o](https://doi.org/10.1016/0749-6419(93)90042-o)
222. McDowell, D. (1995). Stress state dependence of cyclic ratchetting behaviour of two rail steels, *International Journal of Plasticity*, 11(4), 397-421. [https://doi.org/10.1016/s0749-6419\(95\)00005-4](https://doi.org/10.1016/s0749-6419(95)00005-4)
223. Calloch, S., & Marquis, D. (1996). Triaxial tension-compression loadings in cyclic elastoplasticity: experimental and numerical aspects. In *Abe, T. Tsuruta, T. (eds) Advances in engineering plasticity and its applications (AEPA '96)* (pp. 135-140). Elsevier.
224. Jiang, Y., & Sehitoglu, H. (1996). Modelling of cyclic Ratchetting plasticity, part I: Development of constitutive relations. *Journal of Applied Mechanics*, 63(3), 720-733. <https://doi.org/10.1115/1.2823355>
225. Voyiadjis, G. Z., & Basuroychowdhury, I. N. (1998). A plasticity model for multiaxial cyclic loading and ratchetting. *Acta Mechanica*, 126(1-4), 19-35. <https://doi.org/10.1007/bf01172796>
226. Abdel-Karim, M., & Ohno, N. (2000). Kinematic hardening model suitable for ratchetting with steady-state. *International Journal of Plasticity*, 16(3-4), 225-240. [https://doi.org/10.1016/s0749-6419\(99\)00052-2](https://doi.org/10.1016/s0749-6419(99)00052-2)
227. Yoshida, F., & Uemori, T. (2002). A model of large-strain cyclic plasticity describing the Bauschinger effect and work hardening stagnation. *International*

- Journal of Plasticity*, 18(5-6), 661-686. [https://doi.org/10.1016/s0749-6419\(01\)00050-x](https://doi.org/10.1016/s0749-6419(01)00050-x)
228. Bari, S., & Hassan, T. (2002). An advancement in cyclic plasticity modelling for multiaxial ratcheting simulation. *International Journal of Plasticity*, 18(7), 873-894. [https://doi.org/10.1016/s0749-6419\(01\)00012-2](https://doi.org/10.1016/s0749-6419(01)00012-2)
229. Döring, R., Hoffmeyer, J., Seeger, T., & Vormwald, M. (2003). A plasticity model for calculating stress-strain sequences under multiaxial nonproportional cyclic loading. *Computational Materials Science*, 28(3-4), 587-596. <https://doi.org/10.1016/j.commatsci.2003.08.015>
230. Kang, G., Gao, Q., & Yang, X. (2002). A Viscoplastic constitutive model incorporated with cyclic hardening for uniaxial/multiaxial ratcheting of SS304 stainless steel at room temperature. *Mechanics of Materials*, 34(9), 521-531. [https://doi.org/10.1016/s0167-6636\(02\)00153-9](https://doi.org/10.1016/s0167-6636(02)00153-9)
231. Gao, Q., Kang, G., & Yang, X. (2003). Uniaxial ratcheting of SS304 stainless steel at high temperatures: Visco-plastic constitutive model. *Theoretical and Applied Fracture Mechanics*, 40(1), 105-111. [https://doi.org/10.1016/s0167-8442\(03\)00038-7](https://doi.org/10.1016/s0167-8442(03)00038-7)
232. Kang, G., Li, Y., & Gao, Q. (2005). Non-proportionally multiaxial ratcheting of cyclic hardening materials at elevated temperatures: Experiments and simulations. *Mechanics of Materials*, 37(11), 1101-1118. <https://doi.org/10.1016/j.mechmat.2005.01.006>
233. KANG, G. Z., Li, Y., GAO, Q., KAN, Q. H., & ZHANG, J. (2006). Uniaxial ratchetting in steels with different cyclic softening/hardening behaviours. *Fatigue and Fracture of Engineering Materials and Structures*, 29(2), 93-103. <https://doi.org/10.1111/j.1460-2695.2006.00964.x>
234. Kang, G., Liu, Y., Ding, J., & Gao, Q. (2009). Uniaxial ratcheting and fatigue failure of tempered 42CrMo steel: Damage evolution and damage-coupled Viscoplastic constitutive model. *International Journal of Plasticity*, 25(5), 838-860. <https://doi.org/10.1016/j.ijplas.2008.06.004>
235. Chen, X. (2005). On the Ohno and Wang kinematic hardening rules for multiaxial ratcheting modelling of medium carbon steel. *International Journal of Plasticity*, 21(1), 161-184. <https://doi.org/10.1016/j.ijplas.2004.05.005>
236. Halama, Radim. (2006). Ratcheting simulations with modified AbdelKarim–Ohno cyclic plasticity model. *Trans VŠB – Tech Univ Ostrava, Mech Ser.* 52. 155-162.
237. Halama, R. (2008). A modification of AbdelKarim–Ohno model for ratcheting simulations. *Tehnički vjesnik*, 15 (3), 3-9. Retrieved from <https://hrcak.srce.hr/28536>

238. Halama, R., Fumfera, J., Gál, P., Kumar, T., & Markopoulos, A. (2019). Modelling the strain range dependent cyclic hardening of SS304 and 08Ch18N10T stainless steel with a memory surface. *Metals*, 9(8), 832. <https://doi.org/10.3390/met9080832>
239. Ahmadzadeh, G. R., & Varvani-Farahani, A. (2013). Ratcheting assessment of GFRP composites in low-cycle fatigue domain. *Applied Composite Materials*, 21(3), 417-428. <https://doi.org/10.1007/s10443-013-9341-8>
240. König, J. A., & Maier, G. (1981). Shakedown analysis of elastoplastic structures: A review of recent developments. *Nuclear Engineering and Design*, 66(1), 81-95. [https://doi.org/10.1016/0029-5493\(81\)90183-7](https://doi.org/10.1016/0029-5493(81)90183-7)
241. Chaboche, J. (1986). Time-independent constitutive theories for cyclic plasticity. *International Journal of Plasticity*, 2(2), 149-188. [https://doi.org/10.1016/0749-6419\(86\)90010-0](https://doi.org/10.1016/0749-6419(86)90010-0)
242. Murakami, S. (1987). Progress of continuum damage mechanics. *JSME international journal*, 30(263), 701-710. <https://doi.org/10.1299/jsme1987.30.701>
243. Chaboche, J. (1987). Continuum damage mechanics: Present state and future trends. *Nuclear Engineering and Design*, 105(1), 19-33. [https://doi.org/10.1016/0029-5493\(87\)90225-1](https://doi.org/10.1016/0029-5493(87)90225-1)
244. Skrzypek, J., & Ganczarski, A. (1998). Application of the orthotropic damage growth rule to principal variable directions. *International Journal of Damage Mechanics*, 7(2), 180-206. <https://doi.org/10.1177/105678959800700206>
245. Pandey, K., & Chand, S. (2003). Deformation based temperature rise: A review. *International Journal of Pressure Vessels and Piping*, 80(10), 673-687. <https://doi.org/10.1016/j.ijpvp.2003.07.001>
246. Desmorat, R. (2006). Damage and fatigue. *Revue Européenne de Génie Civil*, 10(6-7), 849-877. <https://doi.org/10.1080/17747120.2006.9692859>
247. Ambroziak, A. Klosowski, P. (2006). Survey of modern trends in the analysis of continuum damage mechanics. *TASK Q Sci Bull Acad Comput Centre Gdansk*, 10 (No 4), pp. 437-454
248. Chaboche, J. (2008). A review of some plasticity and viscoplasticity constitutive theories. *International Journal of Plasticity*, 24(10), 1642-1693. <https://doi.org/10.1016/j.ijplas.2008.03.009>
249. Kang, G. (2008). Ratchetting: Recent progress in phenomenon observation, constitutive modelling and application. *International Journal of Fatigue*, 30(8), 1448-1472. <https://doi.org/10.1016/j.ijfatigue.2007.10.002>

250. Horstemeyer, M. F., & Bammann, D. J. (2010). Historical review of internal state variable theory for inelasticity. *International Journal of Plasticity*, 26(9), 1310-1334. <https://doi.org/10.1016/j.ijplas.2010.06.005>
251. Amiri, M., & Khonsari, M. M. (2010). On the thermodynamics of friction and Wear—A review. *Entropy*, 12(5), 1021-1049. <https://doi.org/10.3390/e12051021>
252. Ohno, N. (2015). Material models of cyclic plasticity with extended isotropic hardening: A review. *Mechanical Engineering Reviews*, 2(1), 14-00425-14-00425. <https://doi.org/10.1299/mer.14-00425>
253. Hashiguchi, K. (2017). *Foundations of Elastoplasticity: Subloading surface model*. Springer, 235-256.
254. Varvani-Farahani, A., & Nayebi, A. (2018). Ratcheting in pressurized pipes and equipment: A review on affecting parameters, modelling, safety codes, and challenges. *Fatigue & Fracture of Engineering Materials & Structures*, 41(3), 503-538. <https://doi.org/10.1111/ffe.12775>
255. Paul, S. K. (2019). A critical review of experimental aspects in ratcheting fatigue: Microstructure to a specimen to component, *Journal of Materials Research and Technology*, 8(5), 4894-4914 <https://doi.org/10.1016/j.jmrt.2019.06.014>
256. Lopes, C. S., González, C., Falcó, O., Naya, F., Llorca, J., & Tijs, B. (2016). Multiscale virtual testing: The roadmap to efficient design of composites for damage resistance and tolerance. *CEAS Aeronautical Journal*, 7(4), 607-619. <https://doi.org/10.1007/s13272-016-0210-7>
257. Haigh, B. P. (1928). Hysteresis in relation to cohesion and fatigue. *Transactions of the Faraday Society*, 24, 125. <https://doi.org/10.1039/tf9282400125>
258. Chrysochoos, A. (2012). Thermomechanical analysis of the cyclic behaviour of materials. *Procedia IUTAM*, 4, 15-26.
259. Kotil, T., Holmes, J. W., & Comninou, M. (1990). Origin of hysteresis observed during fatigue of ceramic-matrix composites. *Journal of the American Ceramic Society*, 73(7), 1879-1883. <https://doi.org/10.1111/j.1151-2916.1990.tb05239.x>
260. Vagaggini, E., Domergue, J., & Evans, A. G. (1995). Relationships between hysteresis measurements and the constituent properties of ceramic matrix composites: I and II. *Journal of the American Ceramic Society*, 78(10), 2709-2731. <https://doi.org/10.1111/j.1151-2916.1995.tb08046.x>
261. Morelle, X. P., Chevalier, J., Bailly, C., Pardoën, T., & Lani, F. (2017). Mechanical characterization and modelling of the deformation and failure of the highly crosslinked RTM6 epoxy resin. *Mechanics of Time-Dependent Materials*, 21(3), 419-454. <https://doi.org/10.1007/s11043-016-9336-6>

262. Chaboche, J. (1991). On some modifications of kinematic hardening to improve the description of ratchetting effects. *International Journal of Plasticity*, 7(7), 661-678. [https://doi.org/10.1016/0749-6419\(91\)90050-9](https://doi.org/10.1016/0749-6419(91)90050-9)
263. Lemaitre, J., & Chaboche, J. (1990). *Mechanics of solid materials*. Cambridge University Press.
264. Beardmore, P., & Rabinowitz, S. (1975). Fatigue Deformation of Polymers. In R. Arsenault (Ed.), *Treatise on Materials Science and Technology, Vol. 6: Plastic Deformation of Materials*, Academic Press, New York, (p. 267–331).
265. Krempl, E. (1971). Cyclic plasticity: Some properties of the hysteresis curve of structural metals at room temperature. *Journal of Basic Engineering*, 93(2), 317-323. <https://doi.org/10.1115/1.3425236>
266. Dvorak, G. J., & Rao, M. (1976). Axisymmetric plasticity theory of fibrous composites. *International Journal of Engineering Science*, 14(4), 361-373. [https://doi.org/10.1016/0020-7225\(76\)90009-4](https://doi.org/10.1016/0020-7225(76)90009-4)
267. Hart-Smith, L. J. (2001). What the Textbooks Won't Teach You About Interactive Composite Failure Criteria. In Grant, P. Rousseau, C. (eds) *Composite structures: Theory and practice ASTM STP 1383* (pp. 413-436). ASTM International.
268. Reifsnider, K. (2012). *"Fatigue of composite materials"*. Elsevier, New York.
269. Carvelli, V., & Lomov, S. V. (2015). *"Fatigue of textile composites"*. Elsevier.
270. Talreja, R., & Varna, J. (2015). *"Modeling damage, fatigue and failure of composite materials"*. Elsevier.
271. Hashin, Z., & Herakovich, C. T. (2013). *"Mechanics of composite materials: Recent advances"*. Elsevier.
272. Gamstedt, E., & Sjögren, B. (1999). Micromechanisms in tension-compression fatigue of composite laminates containing transverse plies. *Composites Science and Technology*, 59(2), 167-178. [https://doi.org/10.1016/s0266-3538\(98\)00061-x](https://doi.org/10.1016/s0266-3538(98)00061-x)
273. Reifsnider, K., Schulte, K., & Duke, J. (1983). Long-term fatigue behaviour of composite materials. In ed T. O'Brien *Long-Term Behavior of Composites*, 136-159, West Conshohocken, PA: ASTM International.
274. Highsmith, A., & Reifsnider, K. (1982). Stiffness-reduction mechanisms in composite laminates. In *Damage in Composite Materials ASTM STP 775*, K. Reifsnider, Ed., American Society for Testing and Materials, 103-117.
275. Dougill, J. W. (1976). On stable progressively fracturing solids. *Zeitschrift für angewandte Mathematik und Physik ZAMP*, 27(4), 423-437.
276. Petersen, H. N., Thomason, J. L., Minty, R., Brøndsted, P., Kusano, Y., & Almdal, K. (2015). The testing temperature on interfacial shear strength measurements

- of epoxy resins at different mixing ratios. In *Proceedings of the 20th International Conference on Composite Materials*. ICCM20 Secretariat.
277. Chamis, C. C. (1972). *Mechanics of load transfer at the fibre/matrix interface* (NASA TN D-6588). NASA.
278. Hashin, Z. (2002). Thin interphase/imperfect interface in elasticity with application to coated fibre composites. *Journal of the Mechanics and Physics of Solids*, 50(12), 2509-2537. [https://doi.org/10.1016/s0022-5096\(02\)00050-9](https://doi.org/10.1016/s0022-5096(02)00050-9)
279. Longbiao, L. (2014). Assessment of the interfacial properties from fatigue hysteresis loss energy in ceramic-matrix composites with different fibre preforms at room and elevated temperatures. *Materials Science and Engineering: A*, 613, 17-36. <https://doi.org/10.1016/j.msea.2014.06.092>
280. Petersen, H. (2017). *Investigation of sizing - from glass fibre surface to composite interface* [Doctoral dissertation]. Department of Micro- and Nanotechnology, Technical University of Denmark.
281. Otto, A. (1956). Relationship between the diameter and tensile strength of glass fibres. *Glass and Ceramics*, 13(4), 199-199. <https://doi.org/10.1007/bf00673410>
282. Makishima, A., & Mackenzie, J. (1973). Direct calculation of young's modulus of glass. *Journal of Non-Crystalline Solids*, 12(1), 35-45. [https://doi.org/10.1016/0022-3093\(73\)90053-7](https://doi.org/10.1016/0022-3093(73)90053-7)
283. Yamini, S., & Young, R. J. (1980). The mechanical properties of epoxy resins Part 1 and 2. *Journal of Materials Science*, 15(7), 1814-1831. <https://doi.org/10.1007/bf00550602>
284. Mayr, A. E., Cook, W. D., & Edward, G. H. (1998). Yielding behaviour in model epoxy thermosets I & II. *Polymer*, 39(16), 3719-3733. [https://doi.org/10.1016/s0032-3861\(97\)10334-2](https://doi.org/10.1016/s0032-3861(97)10334-2)
285. Li, C., Jaramillo, E., & Strachan, A. (2013). Molecular dynamics simulations on cyclic deformation of an epoxy thermoset. *Polymer*, 54(2), 881-890. <https://doi.org/10.1016/j.polymer.2012.12.007>
286. Park, H., Kim, B., Choi, J., & Cho, M. (2018). Influences of the molecular structures of curing agents on the inelastic-deformation mechanisms in highly-crosslinked epoxy polymers. *Polymer*, 136, 128-142. <https://doi.org/10.1016/j.polymer.2017.12.055>
287. Truong, T. C., Vettori, M., Lomov, S., & Verpoest, I. (2005). Carbon composites based on multi-axial multi-ply stitched preforms. Part 4. Mechanical properties of composites and damage observation. *Composites Part A: Applied Science and Manufacturing*, 36(9), 1207-1221. <https://doi.org/10.1016/j.compositesa.2005.02.004>

288. Mattsson, D., Joffe, R., & Varna, J. (2007). Methodology for characterization of internal structure parameters governing performance in NCF composites. *Composites Part B: Engineering*, 38(1), 44-57 <https://doi.org/10.1016/j.compositesb.2006.04.004>
289. Wei, Y., & Zhang, J. (2008). Characterization of microstructure in stitched unidirectional composite laminates. *Composites Part A: Applied Science and Manufacturing*, 39(5), 815-824. <https://doi.org/10.1016/j.compositesa.2008.01.012>
290. Yavari, V., & Kadivar, M. (2011). Fibre volume fraction around the stitch in NCF composites. *Procedia Engineering*, 14, 3191-3198 <https://doi.org/10.1016/j.proeng.2011.07.403>
291. Hansen, J. Z., Brøndsted, P., & Østergaard, R. (2013). The effects of fibre architecture on the fatigue lifetime of composite materials. [Doctoral dissertation] DTU Wind Energy. (PhD; No. 0018(EN)). [LINK](#)
292. Lomov, S. V. (2011). *Non-crimp fabric composites: Manufacturing, properties and applications*. Elsevier.
293. Emerson, M. J., Dahl, V. A., Conradsen, K., Mikkelsen, L. P., & Dahl, A. B. (2018). A multimodal data-set of a unidirectional glass fibre reinforced polymer composite. *Data in Brief*, 18, 1388-1393. <https://doi.org/10.1016/j.dib.2018.04.039>
294. Jespersen, K. M., Glud, J. A., Zangenberg, J., Hosoi, A., Kawada, H., & Mikkelsen, L. P. (2018). Ex-situ X-ray computed tomography, tension clamp and in-situ transilluminated white light imaging data of non-crimp fabric based fibre composite under fatigue loading. *Data in Brief*, 21, 228-233. <https://doi.org/10.1016/j.dib.2018.09.109>
295. Jespersen, K. M., Glud, J. A., Zangenberg, J., Hosoi, A., Kawada, H., & Mikkelsen, L. P. (2018). Uncovering the fatigue damage initiation and progression in uni-directional non-crimp fabric reinforced polyester composite. *Composites Part A: Applied Science and Manufacturing*, 109, 481-497. <https://doi.org/10.1016/j.compositesa.2018.03.002>
296. Jespersen, K. M., & Mikkelsen, L. P. (2017). Ex-situ X-ray computed tomography data for a non-crimp fabric based glass fibre composite under fatigue loading. *Data in Brief*, 15, 1003-1005. <https://doi.org/10.1016/j.dib.2017.10.074>
297. Emerson, M. J., Jespersen, K. M., Dahl, A. B., Conradsen, K., & Mikkelsen, L. P. (2017). Individual fibre segmentation from 3D X-ray computed tomography for characterising the fibre orientation in unidirectional composite

- materials. *Composites Part A: Applied Science and Manufacturing*, 97, 83-92. <https://doi.org/10.1016/j.compositesa.2016.12.028>
298. Jespersen, K. M., Zangenberg, J., Lowe, T., Withers, P. J., & Mikkelsen, L. P. (2016). Fatigue damage assessment of unidirectional non-crimp fabric reinforced polyester composite using X-ray computed tomography. *Composites Science and Technology*, 136, 94-103. <https://doi.org/10.1016/j.compscitech.2016.10.006>
299. Ullah Nasir, S., & Shahzad, A. (2019). Effects of stabilization patterns on the static and fatigue behaviour of glass fibre non-crimp fabric composites. *Journal of Composite Materials*, 53(25), 3589-3598. <https://doi.org/10.1177/0021998319843994>
300. Cui, W., Wisnom, M. R., & Jones, M. (1994). Effect of step spacing on delamination of tapered laminates. *Composites Science and Technology*, 52(1), 39-46. [https://doi.org/10.1016/0266-3538\(94\)90006-x](https://doi.org/10.1016/0266-3538(94)90006-x)
301. Botting, A. D., Vizzini, A. J., & Lee, S. W. (1996). Effect of ply-drop configuration on delamination strength of tapered composite structures. *AIAA Journal*, 34(8), 1650-1656. <https://doi.org/10.2514/3.13285>
302. Cairns, D., Mandell, J., Scott, M., Maccagnano, J., Cairns, D., Mandell, J., Scott, M., & Maccagnano, J. (1997). Design considerations for ply drops in composite wind turbine blades. *35th Aerospace Sciences Meeting and Exhibit*. <https://doi.org/10.2514/6.1997-953>
303. Scott, M. (1997). *Effects of ply drops on the fatigue resistance of composite materials and structures* [Master's thesis]. Chemical Engineering, Montana State University.
304. He, K., Hoa, S., & Ganesan, R. (2000). The study of tapered laminated composite structures: A review. *Composites Science and Technology*, 60(14), 2643-2657. [https://doi.org/10.1016/s0266-3538\(00\)00138-x](https://doi.org/10.1016/s0266-3538(00)00138-x)
305. Shim, D. (2002). *Role of delamination and interlaminar fatigue in the failure of laminates with ply dropoffs* [Doctoral dissertation]. Massachusetts Institute of Technology, Dept. of Aeronautics and Astronautics, <http://dspace.mit.edu/handle/1721.1/7582>.
306. Samborsky, D. D., Wilson, T. J., Agastra, P., & Mandell, J. F. (2008). Delamination at thick ply drops in carbon and glass fibre laminates under fatigue loading. *Journal of Solar Energy Engineering*, 130(3). <https://doi.org/10.1115/1.2931496>
307. Weiss, A., Trabelsi, W., Michel, L., Barrau, J., & Mahdi, S. (2010). Influence of ply-drop location on the fatigue behaviour of tapered composites

- laminates. *Procedia Engineering*, 2(1), 1105-1114. <https://doi.org/10.1016/j.proeng.2010.03.119>
308. Dhurvey, P., & Mittal, N. (2013). Review on various studies of composite laminates with ply drop-off. *ARNP Journal of Engineering and Applied Sciences*, 8, 595-605. http://www.arnpjournals.com/jeas/volume_08_2013.htm
309. Mollenhauer, David & Fredrickson, B. & Schoeppner, G. & larve, E.V. & Palazotto, Anthony. (2007). Analysis and measurement of scarf-lap and step-lap joint repair in composite laminates. ICCM International Conferences on Composite Materials.
310. L.J. Hart-Smith (1973) Adhesive bonded single lap joints, NASA (Report CR-112236)
311. Wang, C., & Gunnion, A. (2006). *Design Methodology for Scarf Repairs to Composite Structures* (DSTO-RR-0317). Air Vehicles Division, Defence Science and Technology Organisation.
312. L.J. Hart-Smith (1973) Adhesive bonded scarf and stepped lap joints, NASA (Report CR-112237)
313. Sims, G., & Gladman, D. (1978). *Effect of Test Conditions on the Fatigue Strength of Glass Fabric Laminate Part A Frequency*. *Plastics and Rubber: Materials and Applications*, 1, 41–48.
314. Sims, G., & Gladman, D. (1980). Effect of test conditions on the Fatigue Strength of Glass Fabric Laminate Part B Specimen condition. *Plastics and Rubber: Materials and Applications*, 3, 122–128.
315. Xu, F., Arthur Jones, I., & Li, S. (2019). A continuum damage model for transverse cracking in UD composites of linear viscoelastic behaviour. *Composite Structures*, 225, 110812. <https://doi.org/10.1016/j.compstruct.2019.03.084>
316. Kazmi, S., Govignon, Q., & Bickerton, S. (2018). Control of laminate quality for parts manufactured using the resin infusion process. *Journal of Composite Materials*, 53(3), 327-343. <https://doi.org/10.1177/0021998318783308>
317. Ma, L., Athreya, S. R., Mehta, R., Barpanda, D., & Shafi, A. (2017). Numerical modelling and experimental validation of nonisothermal resin infusion and cure processes in large composites. *Journal of Reinforced Plastics and Composites*, 36(10), 780-794. <https://doi.org/10.1177/0731684417691673>
318. Sirtautas, J. (2017). Coupled fabric deformation and infusion process simulation [Doctoral dissertation]. Institute of Aircraft Design, University of Stuttgart.
319. Li, L., Zhao, Y., Yang, J., Zhang, J., & Duan, Y. (2015). An experimental investigation of the compaction behaviour of carbon non-crimp fabrics for liquid

- composite moulding. *Journal of Materials Science*, 50(7), 2960-2972. <https://doi.org/10.1007/s10853-015-8860-0>
320. Chung Hae Park, & Saouab, A. (2009). Analytical modelling of composite moulding by resin infusion with flexible tooling: VARI and RFI processes. *Journal of Composite Materials*, 43(18), 1877-1900. <https://doi.org/10.1177/0021998309341848>
321. Klunker, F., Aranda, S., Ziegmann, G., Fideu, P., Baisch, P., & Herrmann, A. (2008, July). *Permeability and Compaction Models for Non-Crimped Fabrics to perform a 3D-filling simulation of Vacuum Assisted Resin Infusion* [Paper presentation]. The 9th International Conference on Flow Processes in Composite Materials, Montréal (Québec), Canada.
322. Ladeveze, P. (2002). An Anisotropic Damage Theory with Unilateral Effects: Applications to Laminates and Three and Four-Dimensional Composites. In Allix, O., & Hild, F. (eds.) *“Continuum damage mechanics of materials and structures”* 205-233. Elsevier.
323. Stinchcomb, W., Reifsnider, K., Yeung, P., & Masters, J. (1981). Effect of ply constraint on fatigue damage development in composite material laminates. In *Fatigue of Fibrous Composite Materials*, ASTM STP 723, American Society for Testing and Materials, 64-84.
324. Talreja, R. (1989). Damage development in composites: Mechanisms and modelling. *The Journal of Strain Analysis for Engineering Design*, 24(4), 215-222. <https://doi.org/10.1243/03093247v244215>
325. Van Paepegem, W. (2010). Fatigue damage modelling of composite materials with the phenomenological residual stiffness approach. *Fatigue Life Prediction of Composites and Composite Structures*, 102-138. <https://doi.org/10.1533/9781845699796.1.102>
326. Vassilopoulos, A. (2013). Fatigue life prediction of wind turbine blade composite materials. In Brøndsted, P. & Nijssen, R. (eds.) *Advances in Wind Turbine Blade Design and Materials*, 251-297, Elsevier.
327. Ladeveze, P. (1995). A computational damage approach for composites: Basic aspects and micromechanical relations. *Computational Mechanics*, 17(1-2), 142-150 <https://doi.org/10.1007/s004660050099>
328. Lemaitre, J., & Dufailly, J. (1987). Damage measurements. *Engineering Fracture Mechanics*, 28(5-6), 643-661. [https://doi.org/10.1016/0013-7944\(87\)90059-2](https://doi.org/10.1016/0013-7944(87)90059-2)
329. Ewing, J. (1889). On Hysteresis in the relation of Strain to Stress. In the 59th meeting of the British Association for the advancement of science (pp. 502-504). John Murray, London.

330. Bairstow, L. (1911). II. The elastic limits of iron and steel under cyclical variations of stress. *Philosophical Transactions of the Royal Society of London. Series A, Containing Papers of a Mathematical and Physical Character*, 210(459-470), 35-55. <http://doi.org/10.1098/rsta.1911.0002>
331. Hopkinson, B. (1912). The elastic hysteresis of steel. *Proceedings of the Royal Society of London. Series A, Containing Papers of a Mathematical and Physical Character*, 87(598), 502-511. <https://doi.org/10.1098/rspa.1912.0104>
332. Haigh, B. P. (1928). Hysteresis in relation to cohesion and fatigue. *Transactions of the Faraday Society*, 24, 125. <https://doi.org/10.1039/tf9282400125>
333. Lazan, B., & Demer, L. (1953). *Damping Elasticity and Fatigue Properties of Unnotched and Notched N-155 at Room and Elevated Temperatures* (WADC technical report 53-70). The University of Minnesota.
334. Lazan, B. (1954). *Fatigue Failure Under Resonant Vibration Conditions* (WADC technical report 54-20). The University of Minnesota.
335. Morrow, J. (1965). Cyclic plastic strain energy and fatigue of metals. *Internal Friction, Damping, and Cyclic Plasticity*, 45-45-43. <https://doi.org/10.1520/stp43764s>
336. Halford, G.R. (1966) The energy required for fatigue. *Journal of Materials*, 1(1), pp. 3-18
337. Ellyin, F., & Kujawski, D. (1984). Plastic strain energy in fatigue failure. *Journal of Pressure Vessel Technology*, 106(4), 342-347. <https://doi.org/10.1115/1.3264362>
338. Jhansale, H., & Topper, T. (1973). Engineering analysis of the inelastic stress response of a structural metal under variable cyclic strains. *Cyclic Stress-Strain Behavior—Analysis, Experimentation, and Failure Prediction*, 246-246-25. <https://doi.org/10.1520/stp38034s>
339. Quesnel, D., & Meshii, M. (1977). The response of high-strength low alloy steel to cyclic plastic deformation. *Materials Science and Engineering*, 30(3), 223-241. [https://doi.org/10.1016/0025-5416\(77\)90133-1](https://doi.org/10.1016/0025-5416(77)90133-1)
340. Ellyin, F. (1989). Cyclic strain energy density as criteria for multiaxial fatigue failure. In M. W. Brown & K. J. Miller (Eds.), *Biaxial and Multiaxial fatigue (EGF 3)* (pp. 571-583). Wiley-Blackwell.
341. Lefebvre, D., & Ellyin, F. (1984). Cyclic response and inelastic strain energy in low cycle fatigue. *International Journal of Fatigue*, 6(1), 9-15. [https://doi.org/10.1016/0142-1123\(84\)90003-3](https://doi.org/10.1016/0142-1123(84)90003-3)

342. Golos, K., & Ellyin, F. (1987). Generalization of cumulative damage criterion to multilevel cyclic loading. *Theoretical and Applied Fracture Mechanics*, 7(3), 169-176. [https://doi.org/10.1016/0167-8442\(87\)90032-2](https://doi.org/10.1016/0167-8442(87)90032-2)
343. Kujawski, D., & Ellyin, F. (1995). A unified approach to mean stress effect on fatigue threshold conditions. *International Journal of Fatigue*, 17(2), 101-106. [https://doi.org/10.1016/0142-1123\(95\)95888-n](https://doi.org/10.1016/0142-1123(95)95888-n)
344. Kliman, V., & Bílý, M. (1984). Hysteresis energy of cyclic loading. *Materials Science and Engineering*, 68(1), 11-18. [https://doi.org/10.1016/0025-5416\(84\)90239-8](https://doi.org/10.1016/0025-5416(84)90239-8)
345. Ince, A. (2017). A generalized mean stress correction model based on distortional strain energy. *International Journal of Fatigue*, 104, 273-282. <https://doi.org/10.1016/j.ijfatigue.2017.07.023>
346. Lazan, B., & Morrow, J. (1965). *Internal friction, damping, and cyclic plasticity STP 378, A symposium presented at the sixty-seventh annual meeting, American society for testing and materials, Chicago, ill., June 22, 1964.*
347. Dharan, C. K., & Tan, T. F. (2007). A hysteresis-based damage parameter for notched composite laminates subjected to cyclic loading. *Journal of Materials Science*, 42(6), 2204-2207. <https://doi.org/10.1007/s10853-007-1498-9>
348. Tan, T., & Dharan, C. (2010). Cyclic hysteresis evolution as a damage parameter for notched composite laminates. *Journal of Composite Materials*, 44(16), 1977-1990. <https://doi.org/10.1177/0021998309360942>
349. Mehdi, N. A. (2011). *Thermodynamic Approach to Fatigue Failure Analysis in Metals and Composite Materials* [Doctoral dissertation]. The Department of Mechanical Engineering, Louisiana State University, LA 70803, United States.
350. Ince, A., & Glinka, G. (2014). A generalized fatigue damage parameter for multiaxial fatigue life prediction under proportional and non-proportional loadings. *International Journal of Fatigue*, 62, 34-41. <https://doi.org/10.1016/j.ijfatigue.2013.10.007>
351. Golos, K., & Ellyin, F. (1989). Total strain energy density as a fatigue damage parameter. *Advances in Fatigue Science and Technology*, 849-858. https://doi.org/10.1007/978-94-009-2277-8_42
352. Kujawski, D. (1989). Fatigue failure criteria based on strain energy density. *Mechanika Teoretyczna i Stosowana*, 1(27), 15-22. <http://www.ptmts.org.pl/jtam/index.php/jtam/article/view/v27n1p15>
353. Zhu, S., Lei, Q., Huang, H., Yang, Y., & Peng, W. (2016). Mean stress effect correction in strain energy-based fatigue life prediction of metals. *International*

- Journal of Damage Mechanics*, 26(8), 1219-1241. <https://doi.org/10.1177/1056789516651920>
354. Tan, T., & Dharan, C. (2010). Cyclic hysteresis evolution as a damage parameter for notched composite laminates. *Journal of Composite Materials*, 44(16), 1977-1990. <https://doi.org/10.1177/0021998309360942>
355. Hojo, M., Sawada, Y., & Miyairi, H. (1994). Influence of clamping method on tensile properties of unidirectional CFRP in 0° and 90° directions — round Robin activity for international standardization in Japan. *Composites*, 25(8), 786-796. [https://doi.org/10.1016/0010-4361\(94\)90139-2](https://doi.org/10.1016/0010-4361(94)90139-2)
356. Millette, J. (1995). *Static and Fatigue Behaviour of Unidirectional Composites in Compression* [Master's thesis]. Mechanical Engineering Department McGill University Montréal, Québec, Canada.
357. Sims, G., & Niklewicz, J. (2002). *Size effects in composite materials* (Report MATC (A) 74). NPL Materials Centre National Physical Laboratory.
358. De Baere, I., Van Paepegem, W., & Degrieck, J. (2009). On the design of end tabs for quasi-static and fatigue testing of fibre-reinforced composites. *Polymer Composites*, 30(4), 381-390. <https://doi.org/10.1002/pc.20564>
359. Mikkelsen, L. P., & Bech, J. I. (2013). Secondary stress effects during load introduction into unidirectional composite test coupons. In O. T. Thomsen, B. F. Sørensen, & C. Berggreen (Eds.), *6th International Conference on Composites Testing and Model Identification*.
360. Bailey, P. B., & Lafferty, A. D. (2015). Specimen gripping effects in composites fatigue testing – concerns from the initial investigation. *Express Polymer Letters*, 9(5), 480-488. <https://doi.org/10.3144/expresspolymlett.2015.45>
361. Tost, A., Heinrich, F., & Ridzewski, J. (2016). *Novel test method for characterization of unidirectional composite fatigue properties*. Paper presented at *ECCM17: 17th European conference on composite materials, Munich, Germany, 26 - 30th June 2016*.
362. Luthada, P. (2016). *Tension-Tension Fatigue Testing of Pultruded Carbon Fibre Composite Profiles* [Master's thesis]. School of Engineering, Department of Mechanical Engineering, Aalto University, Espoo, Finland.
363. Fraisse, A., & Brøndsted, P. (2017). Compression fatigue of Wind Turbine Blade composites materials and damage mechanisms. Paper presented at *21st International Conference on Composite Materials (ICCM-21), Xi'an, China*
364. Afshar, A., Alkhader, M., Korach, C. S., & Chiang, F. (2015). Synergistic effects of fatigue and marine environments on carbon fibre vinyl-ester

- composites. *Journal of Engineering Materials and Technology*, 137(4).
<https://doi.org/10.1115/1.4030481>
365. Germain P, Nguyen QS, Suquet P. (1983) Continuum thermodynamics. *Journal of Applied Mechanics*;50:1010-1020. <https://doi.org/10.1115/1.3167184>
366. Boulanger, T. (2004). Calorimetric analysis of dissipative and thermoelastic effects associated with the fatigue behaviour of steels. *International Journal of Fatigue*, 26(3), 221-229. [https://doi.org/10.1016/s0142-1123\(03\)00171-3](https://doi.org/10.1016/s0142-1123(03)00171-3)
367. Bledzki, A. K., Gassan, J., & Kurek, K. (1997). The accumulated dissipated energy of composites under cyclic-dynamic stress. *Experimental Mechanics*, 37(3), 324-327. <https://doi.org/10.1007/bf02317425>
368. Reifsnider, K. L., & Williams, R. S. (1974). Determination of fatigue-related heat emission in composite materials. *Experimental Mechanics*, 14(12), 479-485. <https://doi.org/10.1007/bf02323148>
369. Aglan, H. A., Gan, Y. X., Chu, F., & Zhong, W. H. (2003). Fatigue fracture resistance analysis of polymer composites based on the energy expended on damage formation. *Journal of Reinforced Plastics and Composites*, 22(4), 339-360. <https://doi.org/10.1177/0731684403022004842>
370. Meneghetti G. Quaresimin M. (2011) Fatigue strength of a short fibre composite based on the specific heat dissipation. *Composites Part B*, 42:217–25. <https://doi.org/10.1016/j.compositesb.2010.12.002>
371. Naderi, M., Kahirdeh, A., & Khonsari, M. (2012). Dissipated thermal energy and damage evolution of glass/Epoxy using infrared thermography and acoustic emission. *Composites Part B: Engineering*, 43(3), 1613-1620 <https://doi.org/10.1016/j.compositesb.2011.08.002>
372. Dafalias, Y. F. (1977). Elasto-plastic coupling within a thermodynamic strain space formulation of plasticity. *International Journal of Non-Linear Mechanics*, 12(5), 327-337. [https://doi.org/10.1016/0020-7462\(77\)90009-9](https://doi.org/10.1016/0020-7462(77)90009-9)
373. Dafalias, Y. F. & Popov, E. P. (1977). Cyclic loading for materials with a vanishing elastic region. *Nuclear Engineering and Design*, 41(2), 293-302. [https://doi.org/10.1016/0029-5493\(77\)90117-0](https://doi.org/10.1016/0029-5493(77)90117-0)
374. Lemaitre, J. (2001). *Handbook of materials behaviour models, three-volume set: Nonlinear models and properties*. Elsevier.
375. Skelton, R. (1994). The determination of hysteresis loops in thermo-mechanical fatigue using isothermal stress-strain data. *Fatigue & Fracture of Engineering Materials & Structures*, 17(4), 479-496, <https://doi.org/10.1111/j.1460-2695.1994.tb00247.x>

376. Biot, M. A. (1956). Thermoelasticity and irreversible thermodynamics. *Journal of Applied Physics*, 27(3), 240-253. <https://doi.org/10.1063/1.1722351>
377. Perzyna, P. (1993) Constitutive Equations for Thermoelasticity and Instability Phenomena in Thermodynamic Flow Processes. In Stein, E. (Ed.) "*Progress in computational analysis of inelastic structures*" (pp. 1-73). Springer.
378. Olszak, W., Perzyna, P. (1969) On thermal effects in viscoplasticity. *Journal of Applied Mathematics and Physics (ZAMP)* 20, 676–680. <https://doi.org/10.1007/bf01590623>
379. Perzyna, P., & Sawczuk, A. (1973). Problems of thermoplasticity. *Nuclear Engineering and Design*, 24(1), 1-55. [https://doi.org/10.1016/0029-5493\(73\)90017-4](https://doi.org/10.1016/0029-5493(73)90017-4)
380. Kestin, J. (1966). *A course in thermodynamics*. CRC Press.
381. De Groot, S. R., & Mazur, P. (1984). *Non-equilibrium thermodynamics*. Courier Corporation.
382. Noll, W. (1974). *The foundations of mechanics and thermodynamics: Selected papers*. Springer Science & Business Media.
383. Boehler, J. P. (1987). (Ed.), *I.U.T.A.M./I.C.M. Symposium, Yielding, damage, and failure of anisotropic solids (EGF Publication 5)*. Wiley, Grenoble.
384. Drouot, R., & Sidoroff, F. (2002). *Continuum Thermomechanics: The art and science of modelling material behaviour*. Springer Science & Business Media.
385. DeHoff, R. (2006). *Thermodynamics in materials science* (2nd ed.). CRC Press.
386. Khonsari, M. M., & Amiri, M. (2013). *Introduction to thermodynamics of mechanical fatigue*. CRC Press.
387. Kachanov, L. (1986). *Introduction to continuum damage mechanics*. Springer Science & Business Media.
388. Krajcinovic, D. (1989). *Damage mechanics*. Elsevier.
389. Talreja, R. (1994). *Damage mechanics of composite materials*. Elsevier Science.
390. Ju, J. W., Chaboche, J., & Voyiadjis, G. Z. (1998). *Damage mechanics in engineering materials*. Elsevier.
391. Voyiadjis, G. Z. (1999). *Advances in damage mechanics: Metals and metal matrix composites*. Elsevier.
392. Skrzypek, J. J., & Ganczarski, A. (1999). *Modelling of material damage and failure of structures: Theory and applications*. Springer Science & Business Media.
393. Allix, O., & Hild, F. (2002). *Continuum damage mechanics of materials and structures*. Elsevier.

394. Saanouni, K. (2003). *Numerical modelling in damage mechanics*. Elsevier Science & Technology.
395. Skrzypek, J. J., & Ganczarski, A. W. (2003). *Anisotropic behaviour of damaged materials*. Springer Science & Business Media.
396. Sadowski, T. (2005). *IUTAM Symposium on Multiscale modelling of damage and fracture processes in composite materials: Proceedings of the IUTAM Symposium held in Kazimierz Dolny, Poland, 23-27 May 2005*. Springer Science & Business Media.
397. Lemaitre, J., & Desmorat, R. (2005). *Engineering damage mechanics: Ductile, creep, fatigue and brittle failures*. Springer Science & Business Media.
398. Voyiadjis, G. Z. (2011). *Damage mechanics and Micromechanics of localized fracture phenomena in inelastic solids*. Springer Science & Business Media.
399. Zhang, W., & Cai, Y. (2011). *Continuum damage mechanics and numerical applications*. Springer Science & Business Media.
400. Murakami, S. (2012). *Continuum damage mechanics: A continuum mechanics approach to the analysis of damage and fracture*. Springer Science & Business Media.
401. Voyiadjis, G. Z. (2015). *Handbook of damage mechanics: Nano to macro-scale for materials and structures*. Springer.
402. Li, L. (2018). *Damage, fracture, and fatigue of ceramic-matrix composites*. Springer.
403. Marquis, D., & Lemaitre, J. (1988). Constitutive equations for the coupling between elasto-plasticity damage and aging. *Revue de Physique Appliquée*, 23(4), 615-624.
<https://doi.org/10.1051/rphysap:01988002304061500>
404. Chaboche, J. (1993). Cyclic Viscoplastic constitutive equations, part I and Part II. *Journal of Applied Mechanics*, 60(4), 813-828.
<https://doi.org/10.1115/1.2900988>
405. Lemaitre, J., Sermage, J., & Desmorat, R. (1999). A two-scale damage concept applied to fatigue. *International Journal of Fracture*, 97, 67-81.
<https://doi.org/10.1023/a:1018641414428>
406. Desmorat, R., Ragueneau, F., & Pham, H. (2007). Continuum damage mechanics for hysteresis and fatigue of quasi-brittle materials and structures. *International Journal for Numerical and Analytical Methods in Geomechanics*, 31(2), 307-329.
<https://doi.org/10.1002/nag.532>

407. Chrysochoos, A., Maisonneuve, O., Martin, G., Caumon, H., & Chezeaux, J. (1989). Plastic and dissipated work and stored energy. *Nuclear Engineering and Design*, 114(3), 323-333. [https://doi.org/10.1016/0029-5493\(89\)90110-6](https://doi.org/10.1016/0029-5493(89)90110-6)
408. Chrysochoos, A. (2012). Thermomechanical analysis of the cyclic behaviour of materials. *Procedia IUTAM*, 4, 15-26. <https://doi.org/10.1016/j.piutam.2012.05.003>
409. Benaarbia, A., Chrysochoos, A., & Robert, G. (2016). Thermomechanical analysis of the onset of strain concentration zones in wet polyamide 6.6 subjected to cyclic loading. *Mechanics of Materials*, 99, 9-25. <https://doi.org/10.1016/j.mechmat.2016.04.011>
410. Rice, J. (1971). Inelastic constitutive relations for solids: An internal-variable theory and its application to metal plasticity. *Journal of the Mechanics and Physics of Solids*, 19(6), 433-455. [https://doi.org/10.1016/0022-5096\(71\)90010-x](https://doi.org/10.1016/0022-5096(71)90010-x)
411. Lunn., A. C. (1920). A principle of duality in thermodynamics. *Physical Review*, 15(4), 269-276. <https://doi.org/10.1103/physrev.15.269>
412. Rockafellar, R. T. (2015). *Convex analysis: (PMS-28)*. Princeton University Press.
413. Lemaitre, J., & Marquis, D. (1992). Modelling complex behaviour of metals by the "state-kinetic coupling theory". *Journal of Engineering Materials and Technology*, 114(3), 250-254. <https://doi.org/10.1115/1.2904169>
414. Prager, W. (1955). The theory of plasticity: A survey of recent achievements. *Proceedings of the Institution of Mechanical Engineers*, 169(1), 41-57. https://doi.org/10.1243/PIME_PROC_1955_169_015_02
415. Lemaitre, J. (1985). Coupled elastoplasticity and damage constitutive equations, *Computer Methods in Applied Mechanics and Engineering*, 51(1-3), 31-49 [https://doi.org/10.1016/0045-7825\(85\)90026-x](https://doi.org/10.1016/0045-7825(85)90026-x)
416. Krajcinovic, D., & Lemaitre, J. (1987). *Continuum damage mechanics theory and application*. Springer.
417. Lemaitre, J. (1996). *A course on damage mechanics*. Springer Science & Business Media.
418. Altenbach, H., & Skrzypek, J. J. (1999). *Creep and damage in materials and structures*. Springer.
419. Chaboche, J. (1981). Continuous damage mechanics — A tool to describe phenomena before crack initiation. *Nuclear Engineering and Design*, 64(2), 233-247. [https://doi.org/10.1016/0029-5493\(81\)90007-8](https://doi.org/10.1016/0029-5493(81)90007-8)
420. Lemaitre, J. (1984). How to use damage mechanics. *Nuclear Engineering and Design*, 80(2), 233-245. [https://doi.org/10.1016/0029-5493\(84\)90169-9](https://doi.org/10.1016/0029-5493(84)90169-9)

421. Manson, S. S. (1960) Cyclic Life of Ductile Materials, Part 19', *Thermal Stresses in Design*, pp. 139–144.
422. Ramberg, W., & Osgood, W. R. (1943). *Description of stress-strain curves by three parameters* (NACA-TN-902). NASA Scientific and Technical Information Facility.
423. Li, S., Xu, J., Tao, Y., Tang, X., & Yang, H. (2009). Low cycle fatigue damage model and damage variable expression of rock (in Chinese). *Rock and Soil Mechanics*, 30(6), 1611–1619.
424. Liu, Q., Huang, S., Kang, Y., & Liu, X. (2015). A prediction model for uniaxial compressive strength of deteriorated rocks due to freeze-thaw, *Cold Regions Science and Technology*, 120, 96-107. <https://doi.org/10.1016/j.coldregions.2015.09.013>
425. Nijssen, R. P., Van Delft, D. R., & Van Wingerde, A. M. (2002). Alternative fatigue lifetime prediction formulations for variable-amplitude loading. *Journal of Solar Energy Engineering*, 124(4), 396-403. <https://doi.org/10.1115/1.1510524>
426. Vassilopoulos, A. P., Manshadi, B. D., & Keller, T. (2010). Influence of the constant life diagram formulation on the fatigue life prediction of composite materials. *International Journal of Fatigue*, 32(4), 659-669. <https://doi.org/10.1016/j.ijfatigue.2009.09.008>
427. Marco, S., & Starkey, W. (1954). A concept of fatigue damage. *Transactions ASME*, 76, 627-632.
428. ISO 13003:2003(en) Fibre-reinforced plastics — Determination of fatigue properties under cyclic loading conditions
429. ASTM D3479 / D3479M-19, Standard Test Method for Tension-Tension Fatigue of Polymer Matrix Composite Materials, ASTM International, West Conshohocken, PA, 2019
430. Van Delft, Vincent & Janssen, L. & Philippidis, P. & Brøndsted, Povl & Dutton, Andrew & Jacobsen, T. & Nijssen, R. & Kensche, C. & Lekou, Denja & Hemelrijck, Danny. (2006). OPTIMAT BLADES: Results and perspectives. Scientific Proceedings of the European Wind Energy Conference and Exhibition, Athens.
431. Talreja, R. (2016). Physical modelling of failure in composites. *Philosophical Transactions of the Royal Society A: Mathematical, Physical and Engineering Sciences*, 374(2071), 20150280. <https://doi.org/10.1098/rsta.2015.0280>
432. Aroush, D. R., Maire, E., Gauthier, C., Youssef, S., Cloetens, P., & Wagner, H. (2006). A study of fracture of unidirectional composites using in situ high-resolution synchrotron X-ray microtomography. *Composites Science and*

- Technology*, 66(10), 1348-1353. <https://doi.org/10.1016/j.compscitech.2005.09.010>
433. Sandor, B. I. (1972). *Fundamentals of cyclic stress and strain*.
434. Kliman, V., & Bílý, M. (1984). Hysteresis energy of cyclic loading. *Materials Science and Engineering*, 68(1), 11-18. [https://doi.org/10.1016/0025-5416\(84\)90239-8](https://doi.org/10.1016/0025-5416(84)90239-8)
435. Momenkhani, K., Sarkani, S., & Jones, D. L. (2005). Development and application of a model using the centre of gravity of hysteresis loops to predict fatigue damage accumulation in fibre-reinforced plastic laminates. *Journal of Composite Materials*, 39(6), 557-575. <https://doi.org/10.1177/0021998305047101>
436. Longbiao, Li., & Yingdong Song. (2010). Influence of fibre failure on fatigue hysteresis loops of ceramic matrix composites. *Journal of Reinforced Plastics and Composites*, 30(1), 12-25. <https://doi.org/10.1177/0731684410386273>
437. Longbiao, L. (2020). *The durability of ceramic-matrix composites*. Woodhead Publishing.
438. Brunbauer, J., & Pinter, G. (2015). Effects of mean stress and fibre volume content on the fatigue-induced damage mechanisms in CFRP. *International Journal of Fatigue*, 75, 28-38. <https://doi.org/10.1016/j.ijfatigue.2015.01.014>
439. Kandil, F. (1999). Potential ambiguity in the determination of the plastic strain range component in LCF testing. *International Journal of Fatigue*, 21(10), 1013-1018. [https://doi.org/10.1016/s0142-1123\(99\)00103-6](https://doi.org/10.1016/s0142-1123(99)00103-6)
440. Kujawski, D., & Ellyin, F. (1987). The effect of cyclic loading on the slope of the stress-strain immediately upon load reversal. *Res Mechanica*, 22(4), 295-299.
441. Philippidis, T., & Vassilopoulos, A. (2000). Fatigue design allowable for GRP laminates based on stiffness degradation measurements. *Composites Science and Technology*, 60(15), 2819-2828. [https://doi.org/10.1016/s0266-3538\(00\)00150-0](https://doi.org/10.1016/s0266-3538(00)00150-0)
442. Ellyin, F. (1985). Effect of tensile-mean-Strain on plastic strain energy and cyclic response. *Journal of Engineering Materials and Technology*, 107(2), 119-125. <https://doi.org/10.1115/1.3225786>
443. Westphal, T. (2013). *Integral Material Models for Composites* (Project: ECN-P02 / TUD-P07). ADEM. https://www.adem-innovationlab.nl/wp-content/uploads/2018/12/Annual_Report_2013_LR.pdf
444. Cleveland, W. S. (1979). Robust locally weighted regression and smoothing Scatterplots. *Journal of the American Statistical Association*, 74(368), 829-836. <https://doi.org/10.1080/01621459.1979.10481038>

445. Paas, M. (1990). *Continuum damage mechanics with an application to fatigue* [Doctoral dissertation]. <https://doi.org/10.6100/IR339927>
446. Chaboche, J. L., & Lesne, P. M. (1988). A non-linear continuous fatigue damage model. *Fatigue & Fracture of Engineering Materials and Structures*, 11(1), 1-17. <https://doi.org/10.1111/j.1460-2695.1988.tb01216.x>
447. Botchkarev, A. (2019). A new typology design of performance metrics to measure errors in machine learning regression algorithms. *Interdisciplinary Journal of Information, Knowledge, and Management*, 14, 045-076. <https://doi.org/10.28945/4184>
448. Tofallis, C. (2015). A better measure of relative prediction accuracy for model selection and model estimation. *Journal of the Operational Research Society*, 66(8), 1352-1362. <https://doi.org/10.1057/jors.2014.103>
449. Guedes, R. M. (2019). *Creep and fatigue in polymer matrix composites*. Woodhead Publishing.
450. Zhang, Z., & Friedrich, K. (2003). Artificial neural networks applied to polymer composites: A review. *Composites Science and Technology*, 63(14), 2029-2044. [https://doi.org/10.1016/s0266-3538\(03\)00106-4](https://doi.org/10.1016/s0266-3538(03)00106-4)
451. Gu, G. X., Chen, C., & Buehler, M. J. (2018). De Novo composite design based on machine learning algorithm. *Extreme Mechanics Letters*, 18, 19-28. <https://doi.org/10.1016/j.eml.2017.10.001>
452. Bock, F. E., Aydin, R. C., Cyron, C. J., Huber, N., Kalidindi, S. R., & Klusemann, B. (2019). A review of the application of machine learning and data mining approaches in continuum materials mechanics. *Frontiers in Materials*, 6. <https://doi.org/10.3389/fmats.2019.00110>
453. Le Hien Nguyen, D., Thi Thanh Do, D., Lee, J., Rabczuk, T., & Nguyen-Xuan, H. (2019). Forecasting damage mechanics by deep learning. *Computers, Materials & Continua*, 61(3), 951-977. <https://doi.org/10.32604/cmc.2019.08001>
454. Chen, C., & Gu, G. X. (2019). Machine learning for composite materials. *MRS Communications*, 9(02), 556-566. <https://doi.org/10.1557/mrc.2019.32>
455. Chen, C., & Gu, G. X. (2019). Composite materials: Effect of constituent materials on composite performance: Exploring design strategies via machine learning (Adv. Theory simul. 6/2019). *Advanced Theory and Simulations*, 2(6), 1970018. <https://doi.org/10.1002/adts.201970018>
456. Haghghat, E., Raissi, M., Moure, A., Gomez, H., & Juanes, R. (2020). A deep learning framework for solution and discovery in solid mechanics. <https://arxiv.org/abs/2003.02751v2>

457. Liu, X., Athanasiou, C. E., Padture, N. P., Sheldon, B. W., & Gao, H. (2020). A machine learning approach to fracture mechanics problems. *Acta Materialia*, 190, 105-112. <https://doi.org/10.1016/j.actamat.2020.03.016>

A

Appendix

A.1 Traditional literature reviews and surveys

Table 12 provides an extended timestamp overview of reviews done in the area of fatigue. This list act as a guide in terms of the specific topic reviewed in the past.

Researchers	Year	Area of focus
Coffin L. F.	1962	Low cycle fatigue
Kaechele L.	1963	Review of analysis of cumulative fatigue damage theories
Manson S.S.	1965	Simple approximations in fatigue
O'Neill M. J.	1970	Metallurgical and empirical-based cumulative damage theories
Plumbridge W. Ryder D.A.	1972	Fatigue-crack propagation mechanism study based on the metallographic study
Schijve J.	1972	The accumulation of fatigue damage in aircraft materials and structures
Dew-Hughes D., Way J. L.	1973	A short review on the fatigue of glass-reinforced resins
Krempf E.	1974	Low cycle fatigue of structural materials
Socie D. F., Marrow J.	1976	Methods used in fatigue damage analysis and their computer base synthesis
Hashin Z., Rotem A.	1978	Cumulative damage theory of fatigue failure
Reifsnider K.L., Stinchomb W.	1979	Fatigue damage mechanisms in notched and un-notched composite materials
Garud Y. S.	1981	Methods used in the evaluation of fatigue strength under multiaxial loading until 1980
Reifsnider K.L.	1987	Life prediction methodology for composite materials
Konur O., Matthews F.L.	1989	Effect of constituents properties on the fatigue performance of composites
Bulloch J. H.	1991	Influence of mean stress or R-ratio on the fatigue crack threshold stress intensity range of number of steels
Liu H. W.	1991	Theories associated with stress intensity factor range and fatigue crack growth rate analyses
Sendeckyj G. P.	1991	Empirical, residual strength degradation, stiffness degradation, and actual damage state-based theories for predicting the fatigue life of composite materials
Kumar R.	1992	Crack closure influence for constant amplitude loading in fatigue
Geary W.	1992	Influence of variable amplitude loading on fatigue crack growth
Bartsch et al	1993	Theories and testing methods in thermal fatigue
Andersons J.	1994	Methods used for predicting the fatigue characteristics of composite materials
Vasudeven et al	1994	Concepts of crack closure and fatigue crack threshold
Read P.C.J.L., Shenoi R. A.	1995	Theories of fatigue damage modelling and damage accumulation in marine FRP laminates
Schutz W.	1996	History of fatigue from 1838 to 1996
Lee S., You B.	1996	Multiaxial fatigue analysis of metals from 1980 to 1996
Lawson et al	1999	The methodology used in near-threshold fatigue crack growth analysis
Bogdanovich A., Sierakowski R.	1999	Compendium of books, review papers, and other sources of information
Birman, V., Byrd L.	2000	Damage and fatigue of ceramic matrix composites
Lemaitre J.	2001	A short history of mechanical experimentation of solids
Yokobori T.	2001	Fatigue crack growth
Degrieck J, Van Pappaegem W	2001	Fatigue life prediction methodologies for composite materials
Mao-hong Yu	2002	Strength theories for materials under complex stress state in the 20th Century

Appendix

Qatu M.	2002	The research from 1989-2000 on the dynamic behaviour of composite shells
Philippidis T. P., Passipoularidis V. A.	2003	Residual strength-based fatigue life predictive models
Harris B.	2003	Fatigue behaviour of fibre-reinforced plastics
Kuang K., Cantwell W.	2003	Use of optical fibres and fibre Bragg gratings for damage detection in composite structures
Tay T.	2003	Developments in characterization and analysis of delamination fracture in composite from 1990 to 2001
Krueger R.	2004	Virtual crack closure technique
Della C., Shu D.	2007	Vibration analysis of composite laminates with delamination
Icardi et al	2007	Failure theories of composite laminates
Post et al	2008	Modelling damage accumulation and residual strength under variable amplitude fatigue of composite materials
Passipoularidis V. A., Brøndsted P.	2009	Fatigue evaluation methodologies used in composite materials
Garnich M. Akula V.	2009	Failure criteria and degradation models for unidirectional polymer matrix composites
Wicaksono S., Chai G. B.	2012	Fatigue damage and life prediction of fibre-reinforced composites
Pascoe et al	2013	Methods used for the prediction of fatigue delamination growth in composites and adhesive bonds
Alderliesten R. C.	2013	Generic fatigue evaluation methodology and their scope
Wang et al	2013	Early fatigue damage detecting sensors
Abdullah et al	2014	Review of the fatigue failure mechanism of pipeline steels under a corroded environment
Bak et al	2014	Experimental observations, phenomenological models and computational simulation methods for delamination under fatigue
Khan et al	2015	Effect of stress ratio or mean stress on fatigue delamination growth in composites
Kaminski et al	2015	ONERA viewpoint on fatigue damage modelling of composite structures
Mortazavian S. Fatemi A.	2015	Detailed fatigue analysis and influencing parameters study for short fibre reinforced polymer composite
Sevenois R., Paepegem W.	2015	Fatigue damage modelling techniques for textile composites
Zerbst et al	2016	Determination and application of fatigue crack propagation threshold
Chowdhury P., Sehitoglu H.	2016	Mechanistic and analytical theories on the fatigue crack growth mechanisms
Adedipe et al	2016	Corrosion fatigue in structures related to the offshore wind sector
Santecchia et al	2016	Fatigue life prediction techniques for metallic materials
Vacchieri E.	2016	Creep-fatigue Interaction and damage assessment for high-temperature materials
Antolovich et al	2018	Selective development in Fracture Mechanics
Tabiei, A., Zhang W.	2018	Fatigue delamination onset and propagation criteria in composite materials
Maierhofer et al	2018	Cyclic R-curve determination, problems, limitations, and application
Alam et al	2019	Fatigue of carbon fibre reinforced plastics
Rajkumar et al	2019	Fatigue damages in the wind turbines
Jimenez-Martinez M.	2020	Statistical fatigue damage assessment for stochastic loadings of offshore structures
Vassilopoulos A.	2020	History of fibre-reinforced polymer composite laminate fatigue

Table 12 Extended timestamp overview of reviews done in the area of fatigue

A.2 Test results

This section lists the experimental results obtained for all eight material configurations in tabular format.

A.2.1 Biax OKD

Laminate fibre volume fraction 53.4% and the glass transition temperature is 86.8°C.

ID	Width	Thickn ess	Gauge length	Total length	ϵ_{min}	ϵ_{max}	Frequ ency	R	N_f^{14}
	[mm]	[mm]	[mm]	[mm]	[$\mu\epsilon$]	[$\mu\epsilon$]	[Hz]	[-]	[-]
A13F104	25	3.4	40	149	-4400	4400	5	-1	273,187
A13F110	25	3.4	40	149	-6000	6000	1	-1	1,324
A13F111	25	3.4	40	149	-3800	3800	3	-1	961,656
A13F112	25	3.4	40	149	-6000	6000	1	-1	28,888
A13F116	25	3.4	40	149	-3000	3000	10	-1	13,782,548
A13F201	25	3.3	40	147	-6000	6000	1	-1	27,892
A13F207	25	3.3	40	147	-4700	4700	3	-1	228,943
A13F208	25	3.3	40	147	-3800	3800	3	-1	1,825,534
A13F209	25	3.3	40	147	-4700	4700	3	-1	260,262
A13F215	25	3.4	40	147	-3000	3000	10	-1	10,943,246
A13F301	25	3.2	40	148	-5400	5400	2	-1	457,462
A13F302	25	3.2	40	148	-7300	7300	2	-1	14,956
A13F303	25	3.2	40	149	-4600	4600	3	-1	196,737
A13F307	25	3.2	40	149	-3800	3800	3	-1	699,469
A13F312	25	3.3	40	148	-2900	2900	10	-1	10,706,247
A13F315	25	3.3	40	148	-3800	3800	5	-1	2,944,900
A13F102	25	3.3	40	149	3500	6500	5	0.5	900,219
A13F106	25	3.4	40	149	-500	10500	1	0.1	38,257
A13F108	25	3.4	40	149	3500	6500	5	0.5	1,690,001
A13F203	25	3.3	40	147	400	9600	1	0	57,604
A13F204	25	3.3	40	147	-500	10500	1	0.1	4,048
A13F205	25	3.3	40	147	3500	6500	5	0.5	1,675,620
A13F309	25	3.2	40	148	-2000	12000	1	0.2	16,443
A13F103	25	3.4	40	149	-5300	9300	1	-0.6	8,066
A13F105	25	3.4	40	149	-1150	5150	5	-0.2	1,521,670
A13F202	25	3.3	40	147	-1150	5150	5	-0.2	1,177,496
A13F206	25	3.3	40	147	-5300	9300	1	-0.6	359
A13F305	25	3.2	40	148	-1150	5150	5	-0.2	1,643,975
A13F306	25	3.2	40	149	-5300	9300	1	-0.6	1,546
A13F308	25	3.2	40	148	-3200	7200	2	-0.4	97,904
A13F109	25	3.4	40	149	-500	-11500	1	23	11,704
A13F115	25	3.4	40	149	-1600	-10400	5	6.5	2,493,352
A13F211	25	3.3	40	147	800	-12800	1	16	78,022
A13F213	25	3.4	40	147	2000	-14000	1	-7	72,003
A13F214	25	3.4	40	147	-2000	-10000	5	5	2,442,912
A13F313	26	3.3	40	148	2000	-14000	1	-7	57,207
A13F314	26	3.3	40	148	-2000	-10000	5	5	2,484,689
A13F113	25	3.4	40	149	5300	-11300	1	-2.1	764
A13F114	25	3.4	40	149	1600	-7600	5	-4.8	1,294,617
A13F210	25	3.3	40	150	5300	-11300	1	-2.1	6,323

¹⁴ specimens taken out of test frame after approx. 30% stiffness degradation.

A13F212	25	3.4	40	147	1300	-7300	5	-5.6	2,940,058
A13F304	25	3.2	41	148	2000	-8000	2	-4	264,646
A13F310	25	3.3	40	148	5300	-11300	1	-2.1	409
A13F311	25	3.3	40	148	1600	-7600	5	-4.8	1,073,973

Table 13 Biax OKD test results

A.2.2 Triax OKA

Laminate fibre volume fraction 53.9% and the glass transition temperature is 80.3°C.

ID	Width	Thickness	Gauge length	Total length	σ_{min}	σ_{max}	Frequency	R	N_F
	[mm]	[mm]	[mm]	[mm]	[$\mu\epsilon$]	[$\mu\epsilon$]	[Hz]	[-]	[-]
P753TOF301	24.8	3.38	40	140	-181	181	2	-1	92,289
P753TOF302	24.9	3.28	40	140	-228	228	2	-1	1,694
P753TOF303	24.9	3.25	40	140	-152	152	6	-1	865,529
P753TOF304	24.9	3.24	40	140	-211	211	2	-1	32,773
P753TOF305	24.9	3.24	40	140	-181	181	3	-1	176,894
P753TOF306	24.9	3.23	40	140	-228	228	1	-1	11,554
P753TOF307	24.9	3.23	40	140	-152	152	6	-1	829,122
P753TOF308	24.9	3.24	40	140	-211	211	2	-1	20,100
P753TOF309	24.9	3.27	40	140	-181	181	3	-1	55,681
P753TOF310	24.9	3.27	39	140	-228	228	1	-1	15,290
P753TOF312	24.8	3.30	39	140	-210	210	2	-1	20,195
P753TOF313	24.7	3.27	39	140	-181	181	3	-1	110,058
P753TOF314	24.7	3.25	39	140	-228	228	1	-1	8,722
P753TOF315	24.8	3.23	40	140	-213	213	2	-1	49,543
P753TOF316	24.8	3.22	40	140	-157	157	6	-1	1,129,990
P753TOF317	24.8	3.24	40	140	-152	152	6	-1	835,574
P753TOF402	24.9	3.33	40	140	33	329	2	0.1	5,718
P753TOF403	24.8	3.31	40	140	40	395	1	0.1	1,294
P753TOF404	24.8	3.29	40	140	28	277	3	0.1	19,024
P753TOF405	24.9	3.29	40	140	22	221	6	0.1	126,884
P753TOF406	24.8	3.28	40	140	40	396	1	0.1	2,344
P753TOF407	24.9	3.27	40	140	33	329	2	0.1	8,211
P753TOF408	24.9	3.27	38	140	28	277	3	0.1	25,934
P753TOF410	24.6	3.32	40	140	33	329	2	0.1	6,776
P753TOF411	24.8	3.30	40	140	40	395	1	0.1	1,266
P753TOF412	24.8	3.28	40	140	28	276	3	0.1	20,529
P753TOF413	24.8	3.26	40	140	39	393	1	0.1	1,307
P753TOF414	24.9	3.26	40	140	33	329	2	0.1	5,314
P753TOF415 ¹⁵	24.8	3.25	40	140	16	163	6	0.1	3,682,929
P753TOF416	24.8	3.26	40	140	28	277	3	0.1	21,160
P753TOF417	24.9	3.25	40	140	23	231	6	0.1	75,345
P753TOF418	24.8	3.23	40	140	16	163	6	0.1	1,684,151
P753TOF419	24.7	3.36	40	140	23	231	6	0.1	35,515
P753TOF420	24.9	3.27	40	140	16	163	6	0.1	1,014,890
P753TOF428	24.5	3.26	40	140	16	163	6	0.1	1,063,762
P753TOF502	24.8	3.35	39	140	-28	-276	3	10	3,418
P753TOF503	24.8	3.37	39	140	-25	-254	3	10	2,430,068
P753TOF504	24.8	3.39	39	140	-28	-275	2	10	3,485

¹⁵ Runout.

P753TOF505	24.8	3.37	39	140	-27	-265	3	10	9,858
P753TOF506	24.9	3.38	39	140	-30	-302	1	10	10
P753TOF507	24.9	3.37	39	140	-28	-275	2	10	69,257
P753TOF509	24.9	3.33	39	140	-27	-268	3	10	39,083
P753TOF510	24.8	3.31	39	140	-26	-255	6	10	728,791
P753TOF617	24.8	3.33	40	140	-28	-275	2	10	55,516
P753TOF620	24.7	3.35	40	140	-29	-290	1	10	72
P753TOF621	24.7	3.36	39	140	-27	-268	3	10	136,786
P753TOF622	24.8	3.35	39	140	-28	-275	2	10	24,876
P753TOF623	24.7	3.38	39	140	-25	-254	6	10	2,182,707
P753TOF624	24.8	3.35	39	140	-25	-254	6	10	2,054,425
P753TOF625	24.9	3.33	38	140	-28	-276	2	10	7,720
P753TOF626	24.7	3.31	40	140	-28	-279	1	10	3,505
P753TOF628	24.2	3.27	40	140	-28	-279	1	10	755
P753TOF629	24.6	3.31	40	140	-27	-268	3	10	357,242
P753TOF630	24.7	3.34	39	140	-28	-283	1	10	102
P753TOF632	24.7	3.34	39	140	-28	-279	1	10	1,289
P753TOF421	24.8	3.27	39	140	141	354	2	0.4	3,830
P753TOF422	24.9	3.26	40	140	101	253	6	0.4	38,101
P753TOF423	24.8	3.26	40	140	141	353	2	0.4	5,655
P753TOF424 ¹⁶	24.8	3.24	40	140	70	175	6	0.4	3,012,495
P753TOF425	24.9	3.25	39	140	142	354	2	0.4	6,063
P753TOF426	24.9	3.25	40	140	84	209	6	0.4	573,764
P753TOF427	24.7	3.23	40	140	84	210	6	0.4	529,567
P753TOF429	24.8	3.25	40	140	-58	290	2	-0.2	17,128
P753TOF430	24.7	3.25	40	140	-38	188	6	-0.2	354,661
P753TOF431	24.7	3.24	40	140	-58	291	2	-0.2	10,172
P753TOF432	24.8	3.27	40	140	-38	189	6	-0.2	430,909
P753TOF433	24.7	3.28	40	140	-58	291	2	-0.2	13,289
P753TOF434	24.8	3.29	40	140	-38	189	6	-0.2	376,301
P753TOF602 ¹⁷	24.8	3.28	40	140	-101	-261	6	2.6	92,001
P753TOF603	24.8	3.31	40	140	-106	-275	2	2.6	630,690
P753TOF604	24.7	3.34	40	140	-101	-261	6	2.6	3,231,381
P753TOF605	24.6	3.34	40	140	-110	-285	2	2.6	13,527
P753TOF606	24.7	3.32	40	140	-102	-266	6	2.6	2,477,038
P753TOF607	24.7	3.31	40	140	-110	-286	2	2.6	36
P753TOF608	24.8	3.28	39	140	-102	-266	6	2.6	3,062,374
P753TOF610	24.5	3.33	39	140	-109	-283	2	2.6	4,635
P753TOF611	24.7	3.37	40	140	-260	52	2	-5	2,655
P753TOF612	24.7	3.38	40	140	-231	46	5	-5	467,054
P753TOF613	24.9	3.39	40	140	-260	52	2	-5	21,523
P753TOF614	24.8	3.38	38	140	-231	46	5	-5	543,884
P753TOF615	24.8	3.37	40	140	-301	60	2	-5	44
P753TOF616	24.8	3.36	40	140	-260	52	2	-5	12,318
P753TOF633	24.7	3.34	39	140	-232	46	5	-5	220,717

Table 14 Triax OKA test results

A.2.3 Triax 00A

Laminate fibre volume fraction 51.2% and the glass transition temperature is 81.2°C.

¹⁶ Runout.

¹⁷ Air cooling fan was not pointed at the specimen.

Appendix

ID	Width	Thickness	Gauge length	Total length	σ_{min}	σ_{max}	Frequency	R	N_F
	[mm]	[mm]	[mm]	[mm]	[$\mu\epsilon$]	[$\mu\epsilon$]	[Hz]	[-]	[-]
WS2TXAF201	24.9	5.12	40	150	-275	275	1	-1	714
WS2TXAF202	25.0	5.14	40	150	-255	255	1	-1	8,244
WS2TXAF203	25.0	5.16	40	150	-200	200	1.5	-1	109,807
WS2TXAF204 ¹⁸	25.0	5.17	40	150	-230	230	2	-1	1,118
WS2TXAF205	25.0	5.18	40	150	-275	275	1	-1	8,909
WS2TXAF206	25.0	5.16	40	150	-255	255	1	-1	7,383
WS2TXAF207	25.0	5.14	40	150	-200	200	1.5	-1	116,116
WS2TXAF208	24.9	5.11	40	150	-230	230	1	-1	77,545
WS2TXAF209	24.9	5.09	40	150	-275	275	1	-1	1,392
WS2TXAF210	24.9	5.08	40	150	-255	255	1	-1	21,288
WS2TXAF211	24.9	5.09	40	150	-200	200	1.5	-1	97,828
WS2TXAF212	25.0	5.05	40	150	-231	231	1	-1	60,755
WS2TXAF213	24.9	5.05	40	150	-275	275	1	-1	1,435
WS2TXAF214	25.0	5.04	40	150	-255	255	1	-1	10,635
WS2TXAF215	25.0	5.02	40	150	-199	199	2	-1	139,552
WS2TXAF216	25.0	5.01	40	150	-230	230	1	-1	21,985
WS2TXAF217	25.0	4.98	40	150	-275	275	1	-1	5,348
WS2TXAF301	24.9	4.97	40	150	-175	175	2.5	-1	1,192,951
WS2TXAF302	24.9	5.00	40	150	-255	255	1	-1	14,556
WS2TXAF303	24.9	5.00	40	150	-180	180	2.5	-1	431,455
WS2TXAF304	24.9	4.98	40	150	-230	230	1	-1	47,115
WS2TXAF305	24.9	4.99	40	150	-180	180	2.5	-1	321,970
WS2TXAF306	24.8	4.99	40	150	-275	275	1	-1	1,373
WS2TXAF307	24.8	5.01	40	150	-180	180	2.5	-1	387,658
WS2TXAF308	24.8	5.03	40	150	-255	255	1	-1	8,973
WS2TXAF101	24.9	3.13	40	150	33	330	2	0.1	6,702
WS2TXAF102	25.0	3.18	40	150	44	441	1	0.1	1,017
WS2TXAF103	25.0	3.20	40	150	28	277	3	0.1	80,521
WS2TXAF104	24.9	3.22	40	150	22	220	6	0.1	617,504
WS2TXAF105	25.0	3.23	40	150	33	330	2	0.1	15,176
WS2TXAF106	24.9	3.11	40	150	44	441	1	0.1	1,187
WS2TXAF107	24.9	3.17	40	150	28	277	3	0.1	73,163
WS2TXAF108	25.0	3.19	40	150	22	220	6	0.1	458,185
WS2TXAF109	24.9	3.21	40	150	33	330	2	0.1	20,012
WS2TXAF110	25.0	3.21	40	150	44	441	1	0.1	1,108
WS2TXAF111	24.8	3.01	40	150	28	278	3	0.1	112,879
WS2TXAF112 ¹⁹	24.9	3.05	40	150	22	220	6	0.1	2,000,001
WS2TXAF113	25.0	3.09	40	150	33	330	2	0.1	40,093
WS2TXAF114	24.9	3.09	40	150	44	441	1	0.1	1,885
WS2TXAF115	24.9	3.09	40	150	28	278	3	0.1	182,248
WS2TXAF401	24.9	3.25	40	150	22	220	6	0.1	1,717,000
WS2TXAF309 ²⁰	24.8	5.06	40	150	-29	-290	5	10	1,500,001
WS2TXAF310 ²¹	24.8	5.07	40	150	-37	-374	3	10	129,412
WS2TXAF311	24.8	5.07	40	150	-41	-410	1	10	920
WS2TXAF312	24.9	5.09	40	150	-39	-393	1	10	2,641
WS2TXAF313	24.8	5.10	40	150	-34	-344	2.5	10	155,899

¹⁸ Temperature of coupon was too high.

¹⁹ Runout.

²⁰ Runout, Frequency increased to 2 Hz, after 19 kcycles, Frequency increased to 3 Hz, after 141 kcycles, Frequency increased to 4 Hz, after 416 kcycles.

²¹ Frequency increased to 2 Hz, after 62 kcycles.

WS2TXAF314	24.9	5.13	40	150	-37	-374	2	10	28,390
WS2TXAF315	24.8	5.13	40	150	-41	-410	1	10	3,224
WS2TXAF316	24.7	5.13	40	150	-39	-393	1	10	1,774
WS2TXAF317	25.3	5.14	40	150	-34	-343	2.5	10	54,487
WS2TXAF501	24.9	5.47	40	150	-41	-410	1	10	1,369
WS2TXAF502	25.0	5.51	40	150	-35	-345	2	10	12,966
WS2TXAF503	25.0	5.49	40	150	-41	-410	1	10	767
WS2TXAF504	24.9	5.50	40	150	-35	-345	2	10	94,156
WS2TXAF505	24.9	5.46	40	150	-37	-374	1.5	10	15,680
WS2TXAF507	24.9	5.49	40	150	-37	-374	1.5	10	10,767
WS2TXAF508 ²²	25.0	5.47	40	150	-32	-315	2.5	10	2,114,971
WS2TXAF509 ²³	25.0	5.44	40	150	-32	-315	2.5	10	2,034,691
WS2TXAF510	25.0	5.51	40	150	-33	-330	2.5	10	354,043
WS2TXAF511	25.0	5.52	40	150	-33	-330	2.5	10	1,658,211

Table 15 Triax OKD test results

A.2.4 UDG OKA

Laminate fibre volume fraction 55.2% and the glass transition temperature is 80.0°C.

ID	Width	Thickn ess	Gauge length	Total length	σ_{min}	σ_{max}	Frequ ency	R	N_F
	[mm]	[mm]	[mm]	[mm]	[$\mu\epsilon$]	[$\mu\epsilon$]	[Hz]	[-]	[-]
P753U0F302 ²⁴	19.9	3.4	20	129	-224	224	6	-1	840,516
P753U0F303	19.9	3.5	20	130	-349	349	2	-1	26,485
P753U0F304	19.9	3.5	20	130	-291	291	3	-1	136,035
P753U0F305	20.0	3.5	20	130	-415	415	1	-1	808
P753U0F306	19.9	3.5	20	130	-224	224	6	-1	571,350
P753U0F307	19.9	3.6	20	130	-349	349	2	-1	18,850
P753U0F308	20.0	3.6	20	129	-290	290	3	-1	139,013
P753U0F309	19.9	3.6	20	130	-414	414	1	-1	443
P753U0F311	19.9	3.6	20	130	-349	349	2	-1	17,505
P753U0F312	19.9	3.6	20	130	-291	291	3	-1	64,110
P753U0F313	19.9	3.6	20	130	-414	414	1	-1	510
P753U0F314	19.9	3.6	20	130	-224	224	6	-1	453,647
P753U0F315	20.0	3.6	20	130	-349	349	2	-1	9,389
P753U0F316	19.9	3.6	20	129	-291	291	3	-1	154,200
P753U0F317	19.9	3.6	20	129	-415	415	1	-1	566
P753U0F318	20.0	3.6	20	130	-224	224	6	-1	588,043
P753U0F319	19.9	3.6	20	130	57	571	2	0.1	11,589
P753U0F320	20.0	3.6	20	129	68	680	1	0.1	1,026
P753U0F321	20.0	3.6	20	129	48	476	3	0.1	46,368
P753U0F322	20.0	3.6	20	130	39	387	6	0.1	361,667
P753U0F323	19.0	3.6	20	130	57	571	2	0.1	8,860
P753U0F324	18.9	3.5	20	130	68	680	1	0.1	776
P753U0F501	19.9	3.5	20	130	48	475	3	0.1	53,148
P753U0F502	20.0	3.5	20	130	39	386	6	0.1	379,028
P753U0F503	20.0	3.5	20	130	57	572	2	0.1	13,567
P753U0F504	20.0	3.5	20	130	68	680	1	0.1	2,063

²² Runout.

²³ Runout.

²⁴ After 253k cycles the frequency was increased from 3 to 6 Hz.

Appendix

P753U0F505	20.0	3.5	20	130	48	476	3	0.1	92,601
P753U0F506	19.9	3.6	20	130	39	387	6	0.1	490,824
P753U0F507	19.9	3.6	20	130	57	571	2	0.1	23,471
P753U0F508	19.9	3.6	19	130	68	680	1	0.1	2,421
P753U0F509	19.9	3.6	20	130	48	476	3	0.1	49,894
P753U0F510	19.9	3.6	20	130	39	386	6	0.1	692,459
P753U0F512	19.9	3.6	20	130	-58	-581	1	10	1,273
P753U0F513 ²⁵	19.9	3.6	20	130	-40	-398	3	10	2,089,787
P753U0F514	19.9	3.6	20	130	-48	-476	3	10	202,485
P753U0F515	20.0	3.6	20	130	-55	-550	2	10	7,202
P753U0F516	19.9	3.6	20	130	-58	-580	1	10	1,174
P753U0F517	19.9	3.6	20	130	-45	-450	6	10	194,017
P753U0F518	19.9	3.5	20	130	-48	-475	3	10	115,661
P753U0F519	19.9	3.5	20	130	-55	-550	2	10	1,784
P753U0F520	20.0	3.4	20	130	-58	-581	1	10	414
P753U0F701	19.9	3.4	20	130	-45	-450	5	10	94,488
P753U0F703	19.9	3.5	20	130	-55	-551	2	10	1,452
P753U0F704	19.9	3.5	20	130	-58	-580	1	10	3,520
P753U0F705	19.9	3.5	20	130	-45	-449	5	10	327,907
P753U0F706	19.9	3.5	20	130	-48	-475	3	10	143,488
P753U0F707	19.8	3.5	20	130	-43	-430	6	10	420,323
P753U0F708	19.8	3.6	20	130	-43	-430	6	10	269,545
P753U0F709	19.8	3.6	19	130	307	614	2	0.5	20,690
P753U0F710	19.8	3.6	20	130	212	424	6	0.5	843,774
P753U0F711	19.9	3.6	20	130	307	614	2	0.5	23,566
P753U0F712	19.9	3.6	20	130	212	424	6	0.5	853,953
P753U0F713	19.9	3.6	20	130	307	613	2	0.5	24,293
P753U0F714	19.9	3.6	20	130	212	424	6	0.5	704,205
P753U0F715	19.9	3.6	20	130	-146	486	2	-0.3	4,677
P753U0F716	19.9	3.6	20	130	-95	316	6	-0.3	556,562
P753U0F717	19.9	3.6	20	130	-146	485	2	-0.3	8,224
P753U0F718	19.9	3.6	20	130	-95	315	6	-0.3	495,151
P753U0F719	19.9	3.5	20	130	-146	485	2	-0.3	7,025
P753U0F720	19.9	3.5	20	130	-95	316	6	-0.3	554,207
P753U0F721 ²⁶	19.8	3.4	20	130	-163	-424	2	2.6	2,000,001
P753U0F722	19.9	3.4	20	130	-192	-498	6	2.6	1,122,561
P753U0F723	19.9	3.5	20	130	-212	-551	2	2.6	16,683
P753U0F724	19.9	3.5	20	130	-192	-499	6	2.6	155,068
P753U0F725	19.9	3.5	20	130	-212	-551	2	2.6	36,497
P753U0F726 ²⁷	19.9	3.6	20	130	-192	-498	6	2.6	2,000,001
P753U0F736	19.9	3.6	20	130	-212	-550	2	2.6	407,535
P753U0F727 ²⁸	19.9	3.6	20	130	120	-445	2	-3.7	219,149
P753U0F728	19.8	3.6	20	130	126	-467	2	-3.7	93,474
P753U0F729 ²⁹	19.8	3.6	20	130	115	-424	4	-3.7	14,219
P753U0F730	19.8	3.6	20	130	126	-465	2	-3.7	44,710
P753U0F731	19.9	3.6	20	130	115	-424	2	-3.7	341,668
P753U0F732	19.9	3.6	20	130	125	-463	2	-3.7	44,380
P753U0F733	19.8	3.6	20	130	115	-427	3	-3.7	598,714
P753U0F734	19.8	3.6	20	130	115	-424	3	-3.7	545,487

²⁵ Runout.

²⁶ Runout.

²⁷ Runout.

²⁸ after 219k cycles the frequency was increased from 2 to 5 Hz, temperature increased rapidly and the specimen failed shortly after

²⁹ Too high frequency.

Table 16 UDG OKA test results

A.2.5 UDGH 3KD

Laminate fibre volume fraction 56.3% and the glass transition temperature is 82.8°C.

ID	Width	Thickness	Gauge length	Total length	σ_{min}	σ_{max}	Frequency	R	N_F
	[mm]	[mm]	[mm]	[mm]	[$\mu\epsilon$]	[$\mu\epsilon$]	[Hz]	[-]	[-]
WRS115F201	20.4	3.35	20.1	129	-398	398	2	-1	1,450
WRS115F202	20.3	3.40	20.1	129	-323	323	2	-1	81,394
WRS115F203 ³⁰	20.3	3.44	20.1	129	-263	263	6	-1	852,376
WRS115F204	20.4	3.47	20.0	129	-450	450	1	-1	662
WRS115F205	20.4	3.49	20.0	129	-450	450	1	-1	5,243
WRS115F206	20.4	3.50	19.9	129	-263	263	6	-1	1,035,107
WRS115F207	20.3	3.50	19.8	129	-322	322	3	-1	131,695
WRS115F208	20.4	3.35	20.5	129	-399	399	1	-1	9,851
WRS115F209	20.4	3.38	20.5	129	-450	450	1	-1	3,732
WRS115F210	20.4	3.41	20.5	129	-262	262	6	-1	567,315
WRS115F211	20.4	3.42	20.5	129	-322	322	3	-1	181,369
WRS115F212	20.4	3.42	20.5	129	-398	398	1	-1	30,394
WRS115F213	20.3	3.42	20.5	130	-450	450	1	-1	2,471
WRS115F214 ³¹	20.4	3.36	20.1	130	-262	262	6	-1	656,987
WRS115F215	20.3	3.39	20.2	130	-322	322	3	-1	106,711
WRS115F216	20.4	3.43	20.2	130	-398	398	1	-1	22,569
WRS115F217	20.3	3.45	20.2	130	-450	450	1	-1	1,403
WRS115F218	20.3	3.47	20.3	130	-263	263	6	-1	795,097
WRS115F219 ³²	20.3	3.47	20.3	130	-322	322	3	-1	132,479
WRS115F220	20.3	3.37	20.2	129	-398	398	2	-1	11,064
WRS115F221	20.3	3.43	20.1	129	-450	450	1	-1	1,065
WRS115F222	20.3	3.46	20.1	129	-262	262	6	-1	855,615
WRS115F223 ³³	20.3	3.48	20.0	129	-322	322	3	-1	35,000
WRS115F224	20.3	3.49	19.9	128	-398	398	2	-1	3,375
WRS115F401	20.6	3.32	21.0	133	41	406	3	0.1	31,269
WRS115F402	20.5	3.44	21.0	133	51	506	6	0.1	22,378
WRS115F403	20.6	3.43	20.5	133	34	337	3	0.1	988,498
WRS115F404	20.6	3.40	20.9	133	53	530	1	0.1	13,185
WRS115F405	20.6	3.37	20.9	133	51	514	2	0.1	20,538
WRS115F406	20.6	3.39	20.9	133	34	335	6	0.1	300,727
WRS115F407	20.5	3.35	20.8	133	41	405	3	0.1	32,200
WRS115F408	20.6	3.52	20.3	134	53	531	1	0.1	23,311
WRS115F409	20.5	3.52	20.4	134	51	505	2	0.1	30,520
WRS115F410	20.5	3.49	20.7	134	34	335	6	0.1	500,415
WRS115F411	20.6	3.51	20.3	134	40	402	3	0.1	172,586
WRS115F412	20.6	3.46	21.1	134	55	550	1	0.1	9,855
WRS115F413	20.6	3.45	21.2	134	51	505	2	0.1	16,639
WRS115F414	20.6	3.51	20.9	133	34	336	6	0.1	509,002
WRS115F415	20.6	3.51	20.8	133	40	400	3	0.1	61,525

³⁰ Extensometers fell off during testing (at ~156400 cycles).

³¹ Extensometers fell off during testing (at ~69600 cycles).

³² Test stopped at 9436 cycles due to shut-down of hydraulic pumps.

³³ Extensometers fell off during testing (at ~30200 cycles).

Appendix

WRS115F416	20.6	3.48	20.8	133	55	549	1	0.1	12,410
WRS115F503	20.1	3.47	20.0	130	-48	-478	2	10	3,992
WRS115F504	20.1	3.50	19.7	130	-40	-401	6	10	2,354,340
WRS115F505	20.0	3.46	19.7	130	-44	-443	3	10	50,047
WRS115F506	20.3	3.48	19.8	130	-52	-517	1	10	938
WRS115F507	20.3	3.44	19.8	130	-48	-478	2	10	4,045
WRS115F508	20.0	3.44	20.4	130	-41	-411	6	10	43,797
WRS115F509	20.1	3.45	20.2	130	-44	-442	3	10	12,255
WRS115F510	20.2	3.45	20.8	130	-52	-515	1	10	179
WRS115F511	20.2	3.48	20.0	130	-48	-478	2	10	39,653
WRS115F512 ³⁴	20.2	3.48	19.8	130	-41	-410	6	10	5,027,390
WRS115F513	20.3	3.43	20.3	130	-44	-443	3	10	68,020
WRS115F514	20.3	3.39	20.0	130	-52	-516	1	10	220
WRS115F515	20.0	3.42	20.0	130	-48	-477	2	10	467
WRS115F516	20.0	3.42	19.9	130	-41	-411	6	10	98,647
WRS115F519	20.0	3.40	20.1	130	-44	-442	3	10	15,339
WRS115F520	20.2	3.41	20.1	130	-52	-515	1	10	334

Table 17 UDGH 3KD test results

A.2.6 UDGH OOD

Laminate fibre volume fraction 57.2% and the glass transition temperature is 84.4°C.

ID	Width	Thickn ess	Gauge length	Total length	σ_{min}	σ_{max}	Frequ ency	R	N_F
	[mm]	[mm]	[mm]	[mm]	[$\mu\epsilon$]	[$\mu\epsilon$]	[Hz]	[-]	[-]
WS2UDHF101	19.8	3.38	20	130	-320	320	3	-1	221,460
WS2UDHF102	20.0	3.36	20	130	-384	384	2	-1	24,650
WS2UDHF103	20.0	3.34	20	130	-456	456	1	-1	482
WS2UDHF104	20.1	3.31	20	130	-274	274	6	-1	815,090
WS2UDHF105	20.1	3.32	20	130	-320	320	3	-1	254,193
WS2UDHF106	20.0	3.33	20	130	-384	384	2	-1	1,914
WS2UDHF107	20.0	3.33	20	130	-321	321	3	-1	310,852
WS2UDHF108	20.0	3.35	20	130	-455	455	1	-1	6,060
WS2UDHF109	20.0	3.35	20	130	-320	320	3	-1	239,191
WS2UDHF110	20.0	3.36	20	130	-274	274	6	-1	14,354
WS2UDHF111	20.0	3.37	20	130	-383	383	2	-1	29,186
WS2UDHF112	20.0	3.39	20	130	-456	456	1	-1	4,502
WS2UDHF113	20.0	3.39	20	130	-320	320	3	-1	126,396
WS2UDHF115	20.0	3.39	20	130	-384	384	2	-1	20,919
WS2UDHF116	20.0	3.36	20	130	-456	456	1	-1	645
WS2UDHF117	20.0	3.36	20	130	-320	320	3	-1	263,253
WS2UDHF118	20.0	3.36	20	130	-274	274	6	-1	515,691
WS2UDHF119	20.1	3.39	20	130	-384	384	2	-1	19,995
WS2UDHF120	20.0	3.42	20	130	-456	456	1	-1	1,818
WS2UDHF121	20.0	3.43	20	130	-274	274	6	-1	868,925
WS2UDHF122	20.0	3.42	20	130	-274	274	6	-1	372,094
WS2UDHF203	19.9	3.34	20	127	-465	465	1	-1	1,546
WS2UDHF204	20.0	3.35	20	127	-383	383	2	-1	5,841
WS2UDHF205	20.0	3.36	20	127	-275	275	6	-1	611,534
WS2UDHF206	20.0	3.38	20	127	-273	273	6	-1	539,499

³⁴ Runout.

WS2UDHF207	20.0	3.38	20	127	60	604	2	0	13,194
WS2UDHF208	20.0	3.38	20	127	72	721	1	0	2,946
WS2UDHF209	19.9	3.38	20	127	51	505	3	0	195,088
WS2UDHF210	19.9	3.39	20	127	41	410	6	0	728,011
WS2UDHF211	19.9	3.40	20	127	61	605	2	0	10,344
WS2UDHF212	19.9	3.40	20	127	41	409	6	0	453,419
WS2UDHF213	19.9	3.40	20	127	72	722	1	0	1,309
WS2UDHF214	19.9	3.40	20	127	50	504	3	0	16,654
WS2UDHF215	20.0	3.40	20	127	51	506	3	0	6,317
WS2UDHF216	19.9	3.40	20	127	72	722	1	0	602
WS2UDHF217	19.8	3.41	20	127	41	410	6	0	682,381
WS2UDHF218	20.0	3.43	20	127	50	504	3	0	178,463
WS2UDHF219	20.0	3.44	20	127	61	606	2	0	2,318
WS2UDHF220	20.0	3.43	20	127	72	721	1	0	550
WS2UDHF221	20.0	3.43	20	127	41	410	6	0	517,288
WS2UDHF222	19.9	3.41	20	127	61	605	2	0	21,470
WS2UDHF303	20.0	3.39	22	130	-464	-46	2	10	406,720
WS2UDHF304	20.0	3.43	22	130	-580	-58	1	10	38,173
WS2UDHF305	20.0	3.43	22	130	-419	-42	3	10	1,814,453
WS2UDHF307	20.0	3.44	21	130	-464	-46	2	10	7,828
WS2UDHF308	20.0	3.44	21	130	-535	-54	2	10	7,981
WS2UDHF309 ³⁵	19.9	3.45	21	130	-422	-42	6	10	2,000,002
WS2UDHF310	20.0	3.45	21	130	-535	-54	2	10	389
WS2UDHF311 ³⁶	19.9	3.46	21	130	-430	-43	6	10	2,006,124
WS2UDHF312	19.9	3.44	21	130	-579	-58	1	10	7,165
WS2UDHF316	20.0	3.45	21	130	-465	-47	3	10	83,288
WS2UDHF317	19.9	3.45	21	130	-578	-58	1	10	8,272
WS2UDHF318	20.0	3.44	21	130	-535	-54	2	10	39,199
WS2UDHF319 ³⁷	20.0	3.42	21	130	-463	-46	3	10	2,000,001
WS2UDHF320 ³⁸	20.0	3.38	21	130	-429	-43	6	10	46,800
WS2UDHF321	20.0	3.34	21	130	-580	-58	1	10	947
WS2UDHF322	19.9	3.31	21	130	-430	-43	6	10	4,995,933

Table 18 UDGH OOD test results

A.2.7 UDGH OOA

Laminate fibre volume fraction 54.2% and the glass transition temperature is 84.1°C.

ID	Width	Thickness	Gauge length	Total length	σ_{min}	σ_{max}	Frequency	R	N_F
	[mm]	[mm]	[mm]	[mm]	[$\mu\epsilon$]	[$\mu\epsilon$]	[Hz]	[-]	[-]
WS3UHAF101	19.9	3.74	20	130	-376	376	2	-1	2,990
WS3UHAF102	20.0	3.74	20	130	-375	375	2	-1	3,446
WS3UHAF103	20.0	3.67	20	130	-439	439	1	-1	5,775
WS3UHAF104	20.0	3.67	20	130	-440	440	1	-1	3,044
WS3UHAF105	19.9	3.66	20	130	-375	375	2	-1	17,076
WS3UHAF106	19.9	3.66	20	130	-374	374	2	-1	12,795
WS3UHAF107	20.0	3.69	20	130	-440	440	1	-1	4,944

³⁵ Runout, Frequency was increased at 461 kcycles to 6 Hz.

³⁶ Runout.

³⁷ Runout, Frequency was increased at 1.5 million cycles to 5 Hz.

³⁸ Specimen taken out of the test frame after a power failure.

Appendix

WS3UHAF108	20.0	3.69	20	130	-310	310	3	-1	262,405
WS3UHAF109	20.0	3.70	20	130	-310	310	3	-1	111,469
WS3UHAF110	19.9	3.54	20	130	-310	310	3	-1	347,512
WS3UHAF111	20.0	3.56	20	130	-310	310	3	-1	157,992
WS3UHAF112	20.0	3.55	20	130	-310	310	3	-1	146,912
WS3UHAF113	20.0	3.53	20	130	-310	310	3	-1	234,705
WS3UHAF114	19.9	3.52	20	130	-440	440	1	-1	5,855
WS3UHAF115	19.9	3.53	20	130	-374	374	2	-1	15,348
WS3UHAF116	20.0	3.54	20	130	-440	440	1	-1	9,194
WS3UHAF117	20.0	3.55	20	130	-270	270	6	-1	601,306
WS3UHAF118	20.0	3.55	20	130	-270	270	6	-1	712,299
WS3UHAF202	20.2	3.50	20	130	-374	374	2	-1	4,971
WS3UHAF203	20.0	3.50	20	130	-269	269	6	-1	5,624
WS3UHAF204	20.0	3.50	20	130	-270	270	6	-1	977,018
WS3UHAF205	20.0	3.51	20	130	-270	270	6	-1	261,641
WS3UHAF206	20.0	3.51	20	130	-270	270	5	-1	215,048
WS3UHAF207	20.1	3.53	20	130	-440	440	1	-1	5,364
WS3UHAF208	20.1	3.55	20	130	-270	270	5	-1	266,823
WS3UHAF209	20.1	3.55	20	130	48	480	3	0.1	192,726
WS3UHAF210	20.0	3.56	20	130	60	599	2	0.1	21,621
WS3UHAF211	20.1	3.56	20	130	48	480	3	0.1	113,556
WS3UHAF212	20.0	3.57	20	130	41	405	6	0.1	594,380
WS3UHAF213	20.1	3.68	20	130	48	480	3	0.1	150,029
WS3UHAF214	20.0	3.68	20	130	60	600	2	0.1	16,080
WS3UHAF215	20.1	3.70	20	130	48	480	3	0.1	132,375
WS3UHAF216	20.0	3.67	20	130	72	719	1	0.1	1,860
WS3UHAF217	20.1	3.66	20	130	41	405	6	0.1	938,963
WS3UHAF218	20.1	3.66	20	130	60	600	2	0.1	29,544
WS3UHAF219	20.0	3.66	19	130	48	480	3	0.1	187,169
WS3UHAF220	20.2	3.67	20	130	72	720	1	0.1	1,138
WS3UHAF221	20.1	3.63	20	130	41	405	6	0.1	592,511
WS3UHAF222	20.1	3.59	19	130	60	599	2	0.1	6,171
WS3UHAF223	20.1	3.56	19	130	72	720	1	0.1	5,198
WS3UHAF224	20.1	3.54	19	130	41	405	6	0.1	1,346,336
WS3UHAF225	20.0	3.62	20	130	72	720	1	0.1	1,905
WS3UHAF226	20.0	3.57	20	130	-641	-64	1	10	987
WS3UHAF227	20.1	3.59	20	130	-540	-54	3	10	573,149
WS3UHAF228	20.0	3.57	20	130	-599	-60	2	10	33,123
WS3UHAF229	20.1	3.60	20	130	-600	-60	2	10	228,198
WS3UHAF230	20.1	3.59	20	130	-575	-58	3	10	101,739
WS3UHAF231	20.1	3.65	20	130	-540	-54	4	10	154,773
WS3UHAF232	20.1	3.62	20	130	-600	-60	2	10	44,870
WS3UHAF233	20.1	3.63	20	130	-576	-58	3	10	110,014
WS3UHAF234	20.0	3.65	20	130	-525	-53	42462	10	1,242,966
WS3UHAF235	19.9	3.47	20	130	-540	-54	4	10	22,605
WS3UHAF236	20.1	3.47	20	130	-601	-60	2	10	4,322
WS3UHAF237	20.1	3.54	20	130	-575	-58	3	10	435
WS3UHAF238	20.1	3.55	20	130	-641	-64	1	10	17
WS3UHAF239	20.0	3.56	20	130	-640	-64	1	10	255
WS3UHAF240	20.1	3.58	20	130	-575	-58	3	10	967
WS3UHAF241	20.0	3.59	20	130	-640	-64	1	10	8,394
WS3UHAF242	20.0	3.59	20	130	-525	-53	4	10	161,339
WS3UHAF243	20.1	3.58	20	130	-525	-53	3	10	10,438

Table 19 UDGH OOA test results

A.2.8 Ply drop

Laminate fibre volume fraction 62% and the glass transition temperature is °C.

ID	Width	Thickn ess	Gauge length	Total length	σ_{min}	σ_{max}	Frequ ency	R	N_F
	[mm]	[mm]	[mm]	[mm]	[$\mu\epsilon$]	[$\mu\epsilon$]	[Hz]	[-]	[-]
ST1-B-5	24.0	13.4		260	-707	707	2	-1	618
ST1-B-1	24.1	13.2		260	-588	588	2	-1	1,240
ST1-B-4	24.0	13.3		260	-483	483	2	-1	4,590
ST1-A-5	24.0	13.5		260	-272	272	2	-1	330,000
ST1-A-3	24.0	13.5		260	-362	362	2	-1	26,900
ST1-C-5	23.9	13.7		260	-236	236	3	-1	1,263,645
ST1-A-4	24.0	13.5		260	-588	588	3	-1	1,190
STI E-03	24.0	6.7	100	280	103	1033	3	0.1	1,840
STI A-03	24.1	6.6	100	280	67	670	3	0.1	34,800
STI F-03	24.0	6.7	100	280	57	569	3	0.1	167,000
STI C-03	24.0	6.6	100	280	48	476	3.6	0.1	647,907
STI-B-03	24.0	6.7	100	280	45	454	3.8	0.1	1,191,222
STI-F-02	24.0	6.8	100	280	83	826	2.1	0.1	5,694
STI-D-03	24.1	6.6	100	280	62	619	2.8	0.1	109,369
STI A-04	24.1	6.6	100	280	103	1031	1	0.1	2,681
ST1-C-6	24.1	13.7		260	-81	-812	2	10	2,690
ST1-B-2	24.0	13.2		260	-72	-724	2.2	10	14,489
ST1-C-2	24.0	13.5		260	-63	-633	2.5	10	55,000
ST1-B3	24.0	13.2		260	-50	-498	3.2	10	1,350,186
ST1-C-4	24.0	13.6		260	-59	-588	3	10	107,000
ST1-A-6	24.0	13.5		260	-89	-888	2	10	807
ST1-A5	24.1	6.6	100	280	669	1338	2.5	0.5	6,500
ST1-E5	24.0	6.7	100	280	387	775	4.3	0.5	774,000
ST1-A6	24.0	6.5	100	280	413	826	4	0.5	263,329
ST1-C-5	24.1	6.6	100	280	516	1031	3.2	0.5	88,800
ST1-E4 ³⁹	24.0	6.6	100	280	335	671	4.9	0.5	1,317,671
ST1-B-5	24.1	6.6	100	280	722	1443	2.3	0.5	580
ST1-B-4	24.0	6.5	100	280	-289	723	1.6	-0.4	3,390
ST1-C-4	24.0	6.6	100	280	-207	516	2.3	-0.4	44,700
ST1-C-6	24.1	6.4	100	280	-247	619	1.9	-0.4	11,400
ST1-F-4	24.0	6.7	100	280	-157	393	3	-0.4	234,000
ST1-E6	23.8	6.8	100	280	1088	1360	5	0.8	1,023,556
ST1-F5	24.0	6.5	100	280	1117	1396	5	0.8	213,000
ST1-E-2	24.0	6.8	100	280	1155	1444	5	0.8	146,766
ST1-F-6	24.0	6.7	100	280	1091	1364	5	0.8	284,941
ST1-D-5	24.1	6.6	100	280	1219	1524	5	0.8	16,800

Table 20 Ply drop test results

³⁹ Runout.

A.3 Test result analysis

A.3.1 Failure images for all configurations

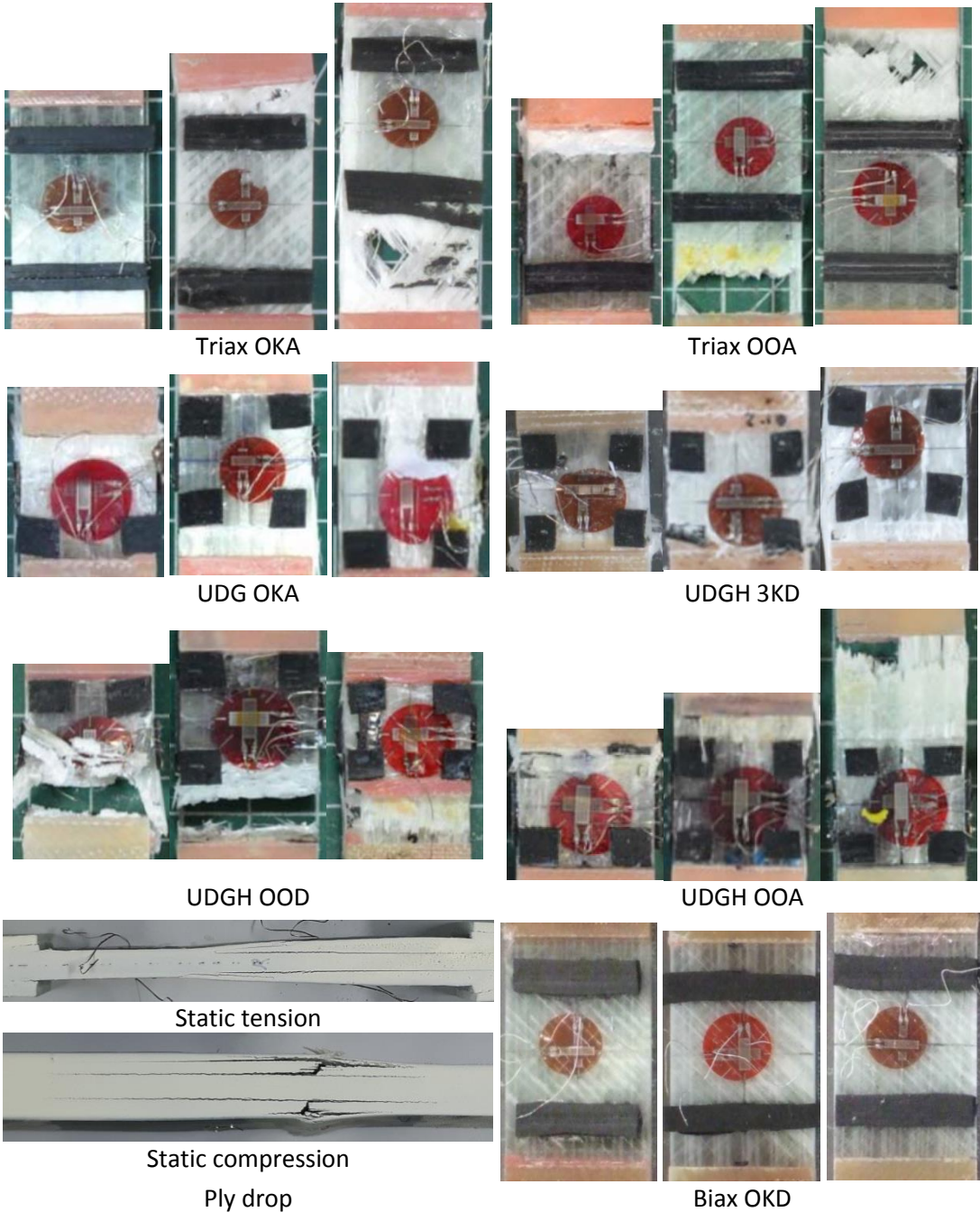
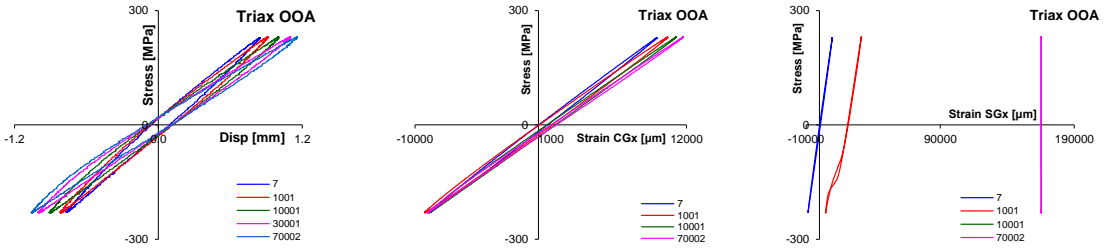


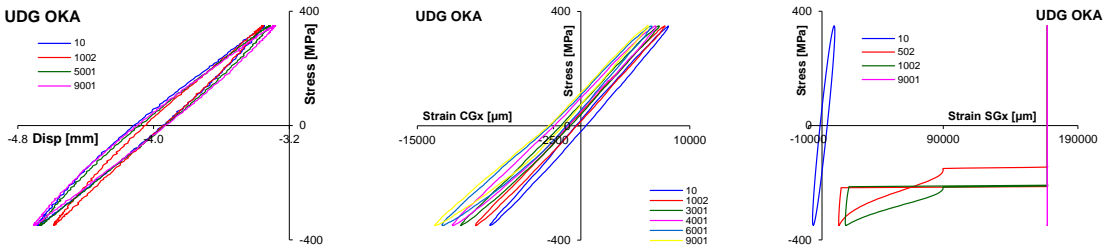
Figure 94 Final damage images for all configurations; Left (R10), middle (R-1) and right (R0.1)

A.3.2 Hysteresis curves from various strain sensors



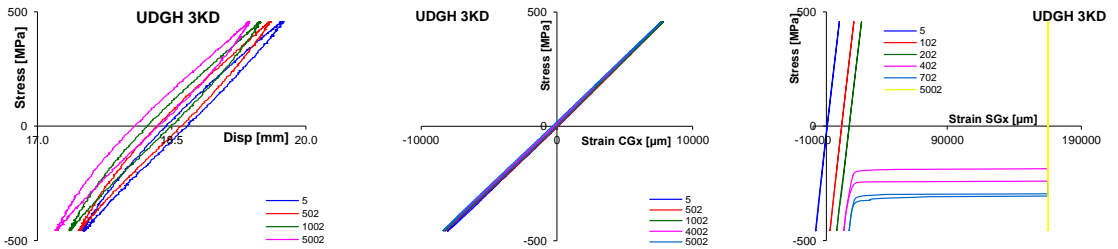
(a) Triax OOA; Load controlled; $\sigma_m=0\text{MPa}$, $\sigma_a=230\text{MPa}$

Actuator displacement and clip-on extensometer show some similarities. Strain gauge detached from coupon surface after 1000cycles



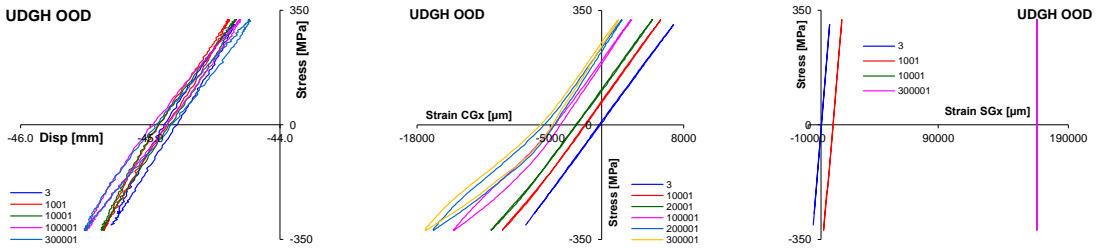
(b) UDG OKA; Load controlled; $\sigma_m=0\text{MPa}$, $\sigma_a=349\text{MPa}$

Actuator displacement and clip-on extensometer show consistent trends. Strain gauge detached from coupon surface at 500cycles



(c) UDGH 3KD; Load controlled; $\sigma_m=0\text{MPa}$, $\sigma_a=450\text{MPa}$

Actuator displacement and clip-on extensometer show consistent trends. Strain gauge detached from coupon surface after 300cycles



(d) UDGH OOD; Load controlled; $\sigma_m=0\text{MPa}$, $\sigma_a=321\text{MPa}$

Actuator displacement and clip-on extensometer show some similarities. Strain gauge detached from coupon surface after 1000cycles

Figure 95 Hysteresis curves from various strain sensors; (Left) Actuator displacement, (Middle) Clip-on extensometer, and (Right) Strain gauge

A.3.3 Hysteresis curves for R-1 stress ratio

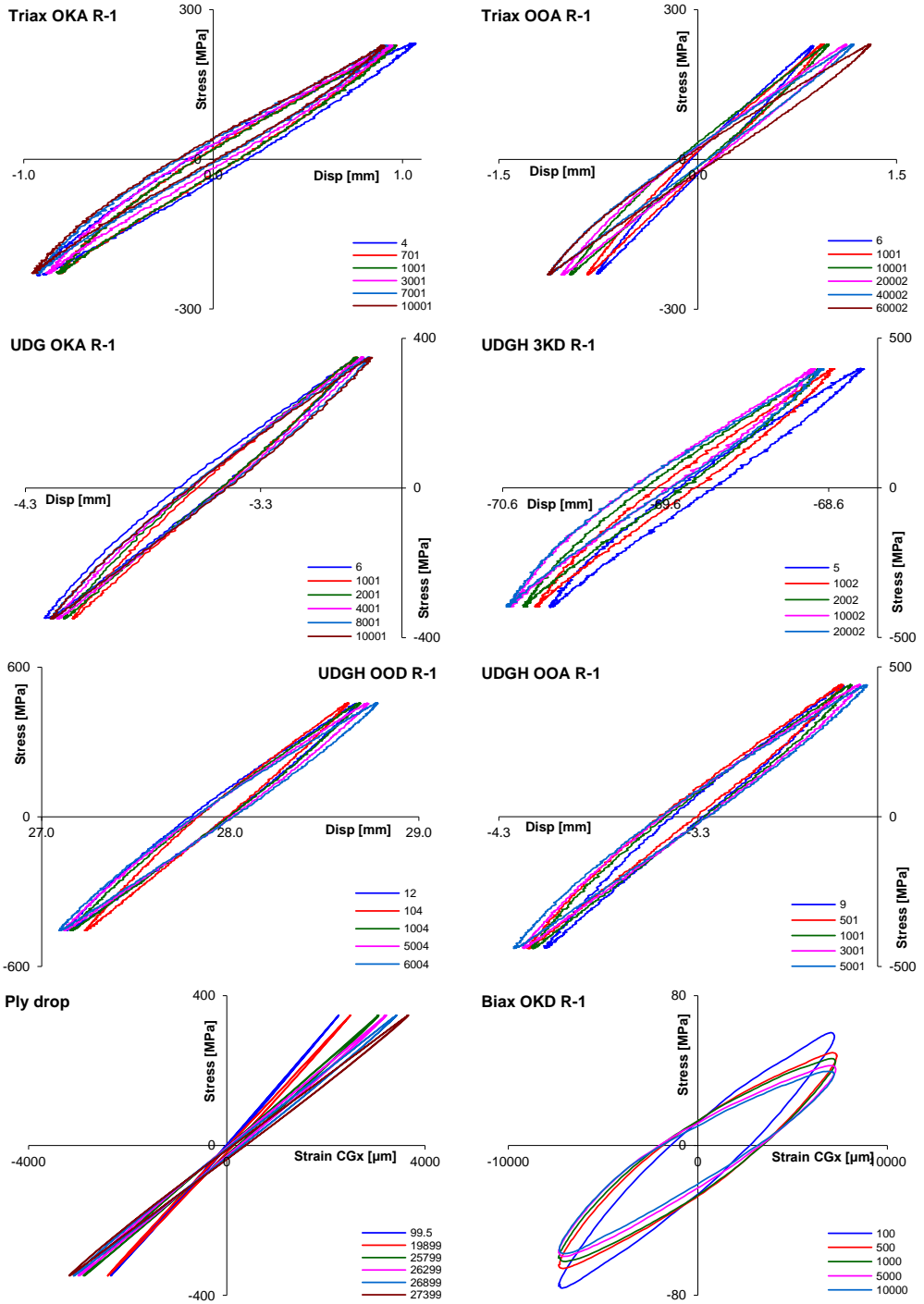


Figure 96 Hysteresis curves for all eight configurations under R-1 stress ratio

A.3.4 Hysteresis curves for R0.1 stress ratio

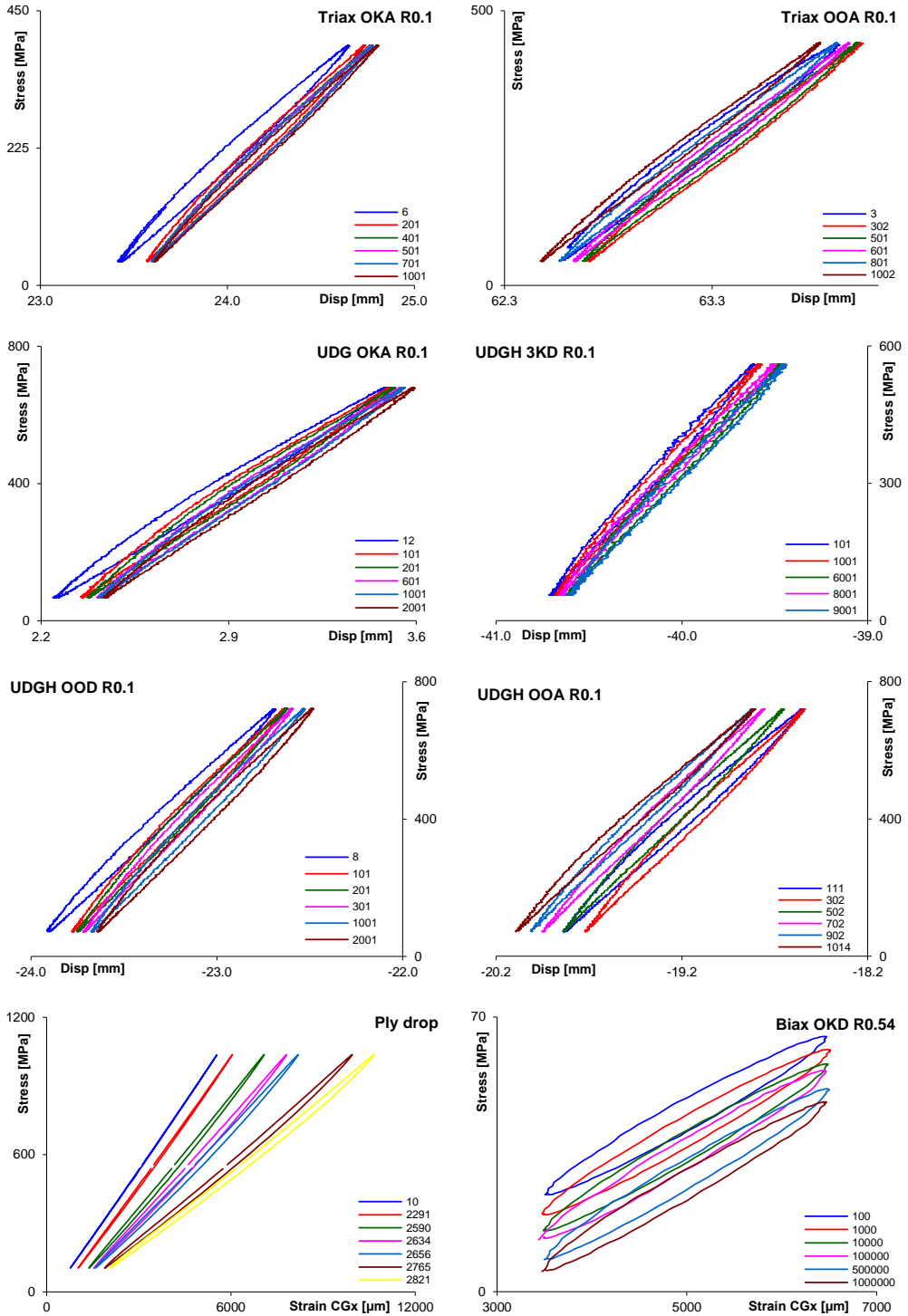


Figure 97 Hysteresis curves for all eight configurations under tensile stress ratio

A.3.5 Hysteresis curves for R10 stress ratio

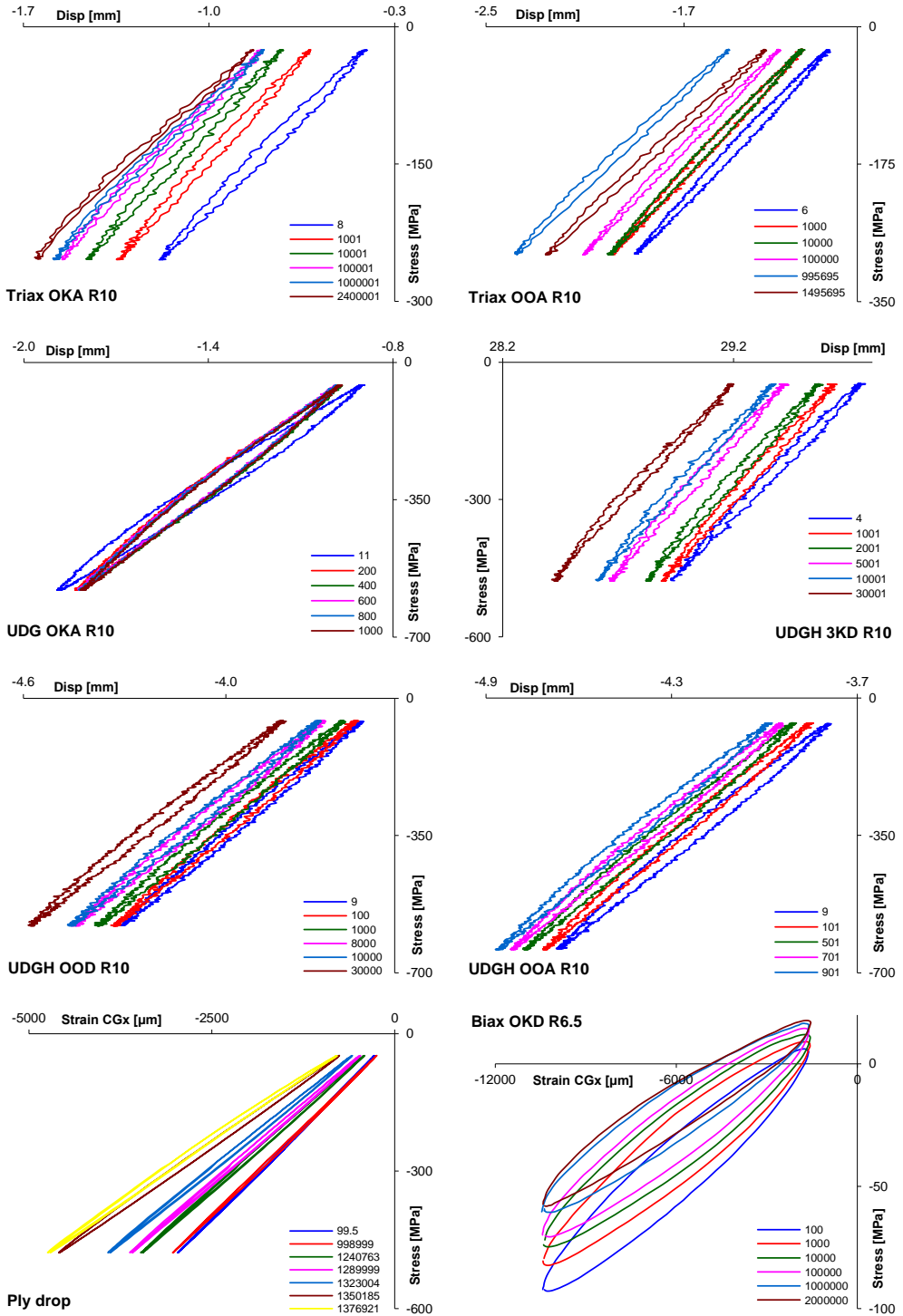


Figure 98 Hysteresis curves for all eight configurations under compressive stress ratio

A.3.6 Elastic strain development for all material configurations

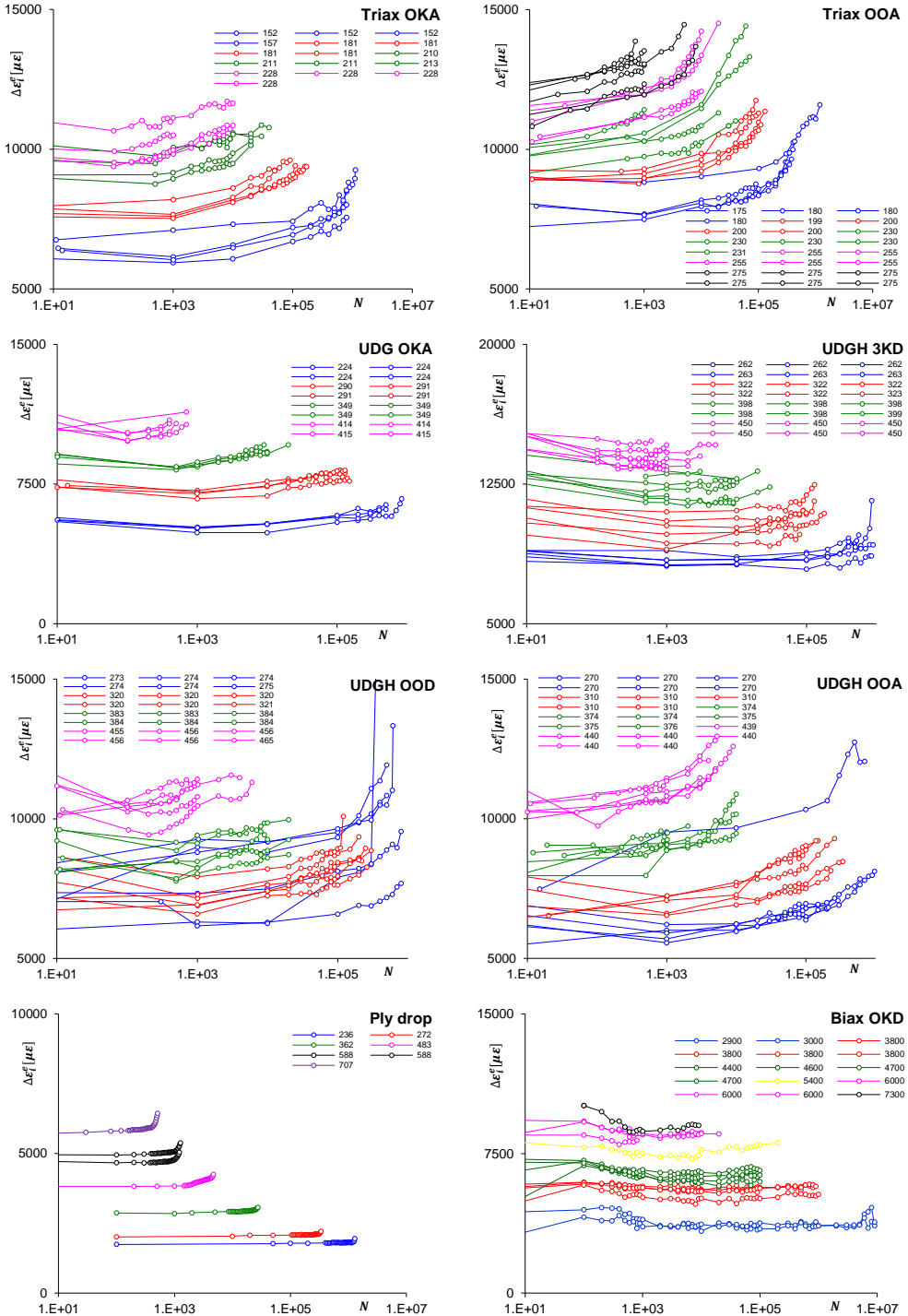


Figure 99 Elastic strain development under R-1 stress ratio for all material configurations

A.3.7 Inelastic strain development for all material configurations

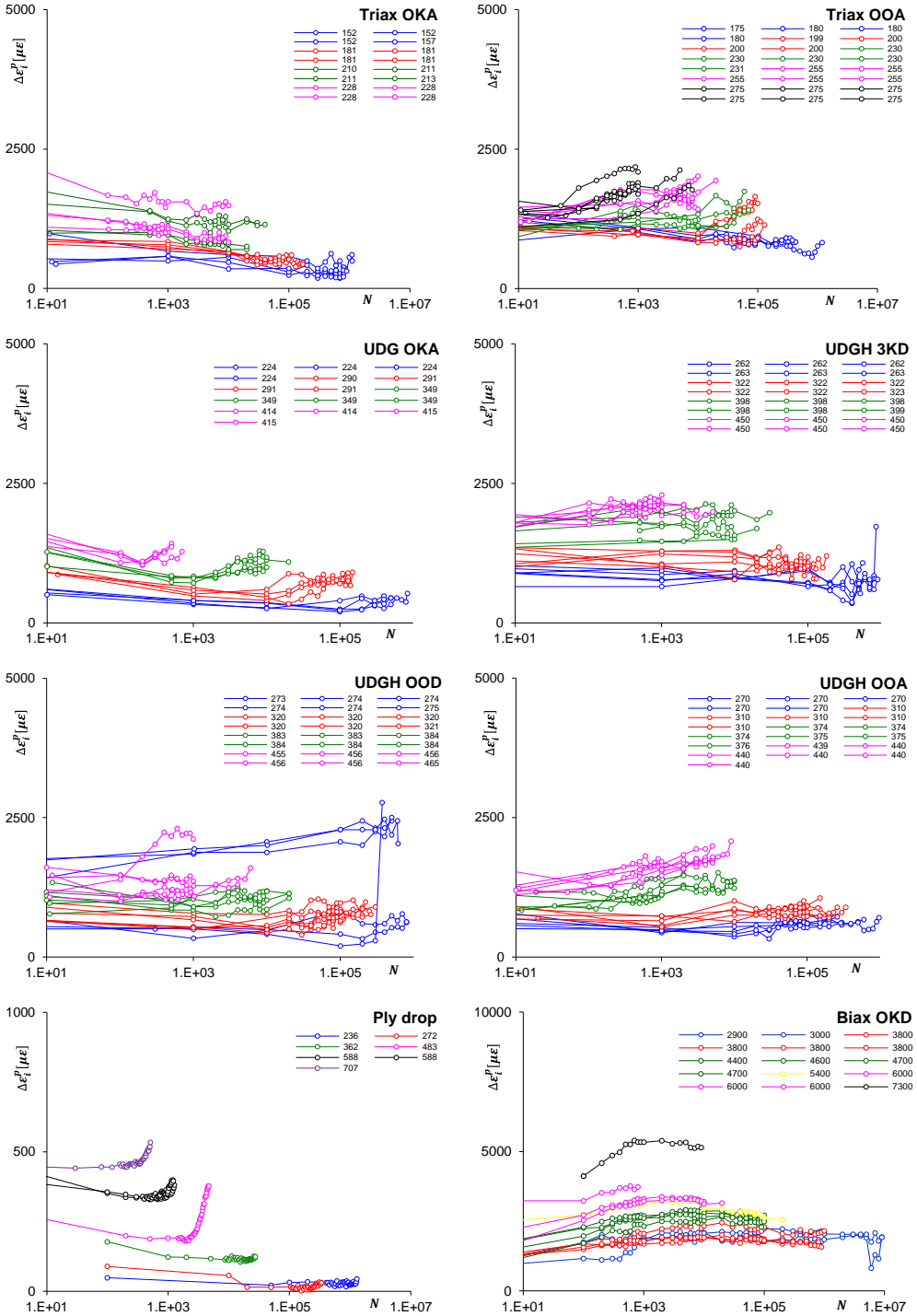


Figure 100 Plastic strain development under R-1 stress ratio for all material configurations

A.3.8 Elastic strain energy development for all material configurations

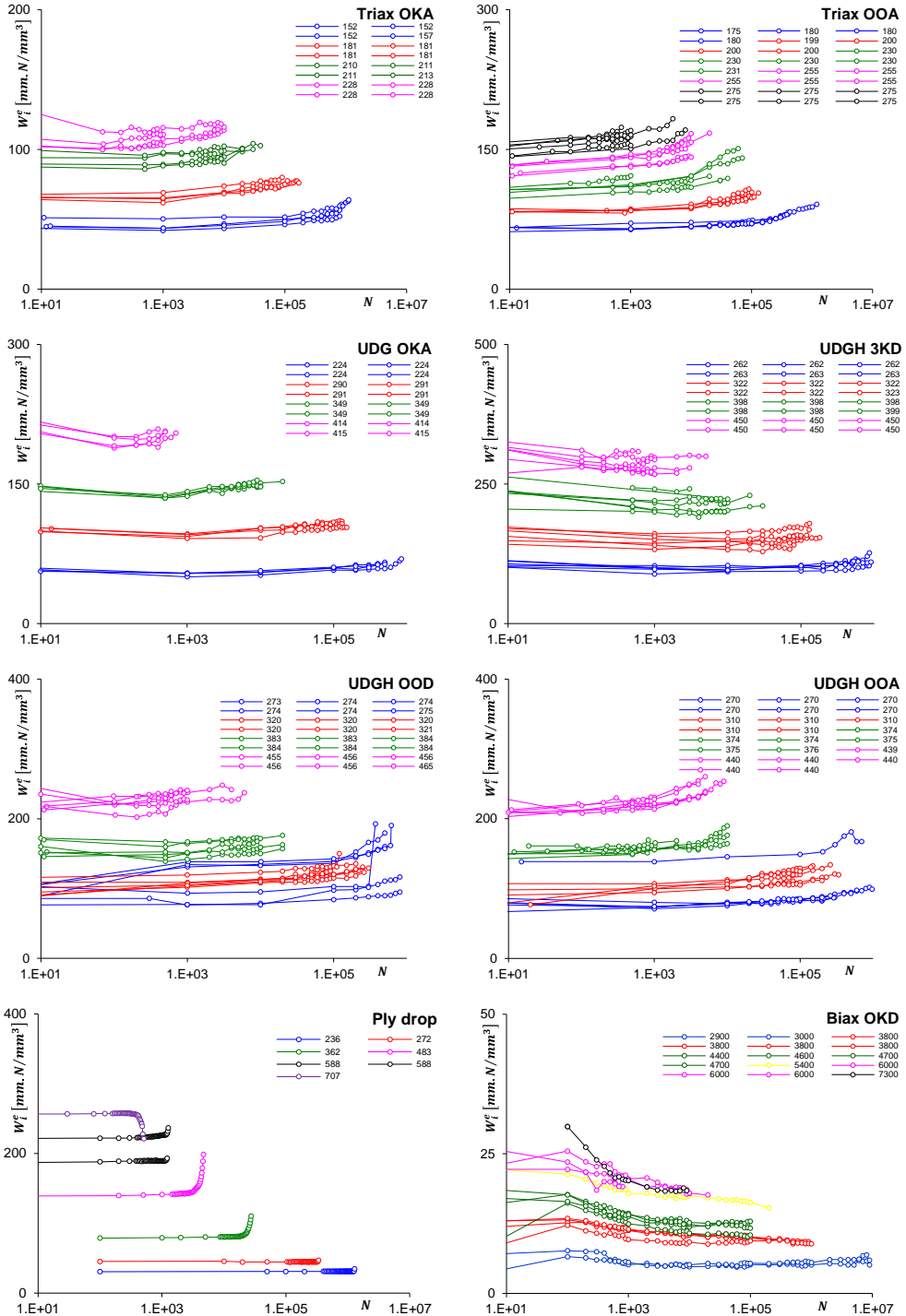


Figure 101 Elastic strain energy development under R-1 stress ratio for all material configurations

A.3.9 Inelastic strain energy development for all material configurations

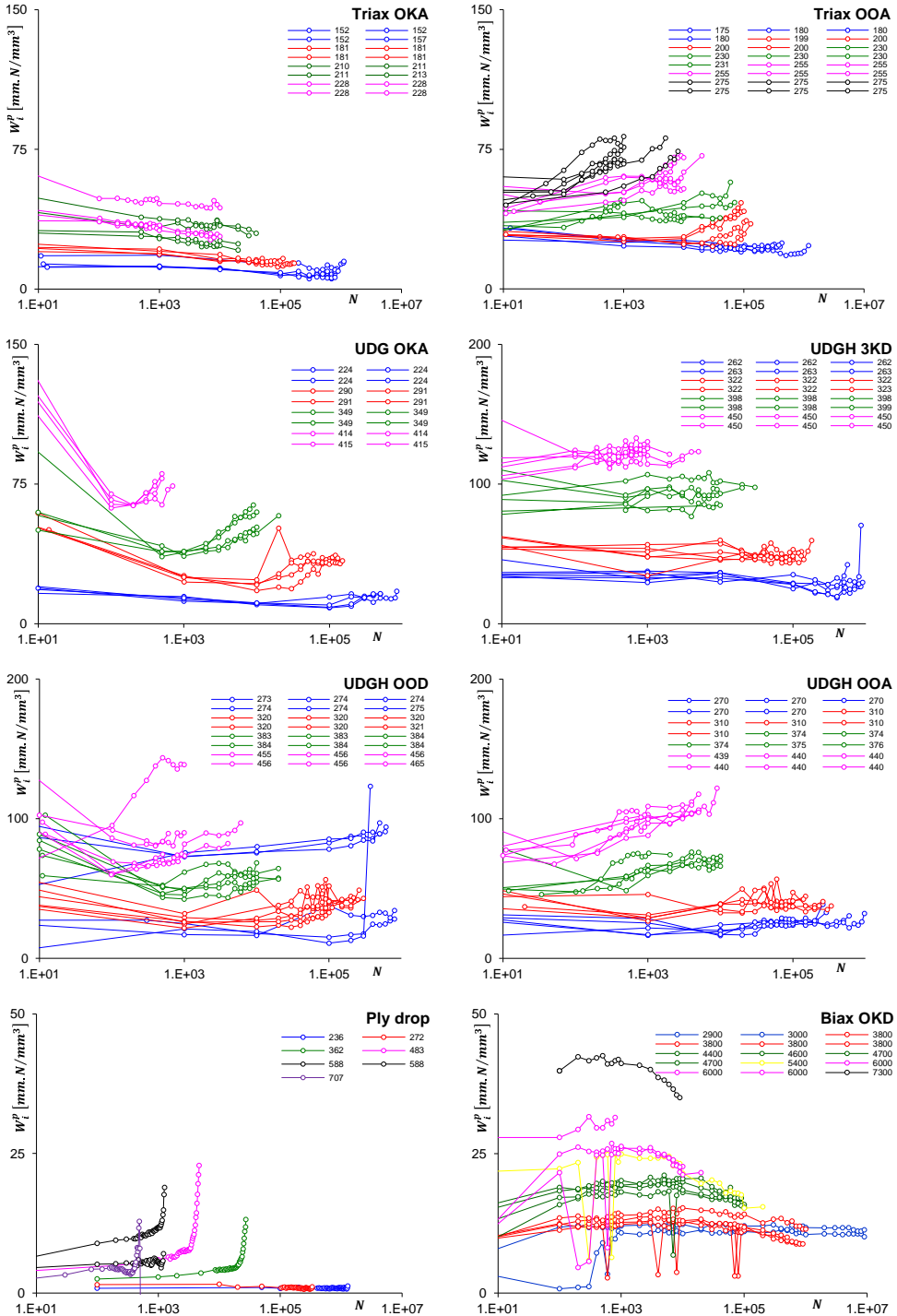


Figure 102 Plastic strain energy development under R-1 stress ratio for all material configurations

A.3.10 The probability distribution function of inelastic strain energy for all material configurations

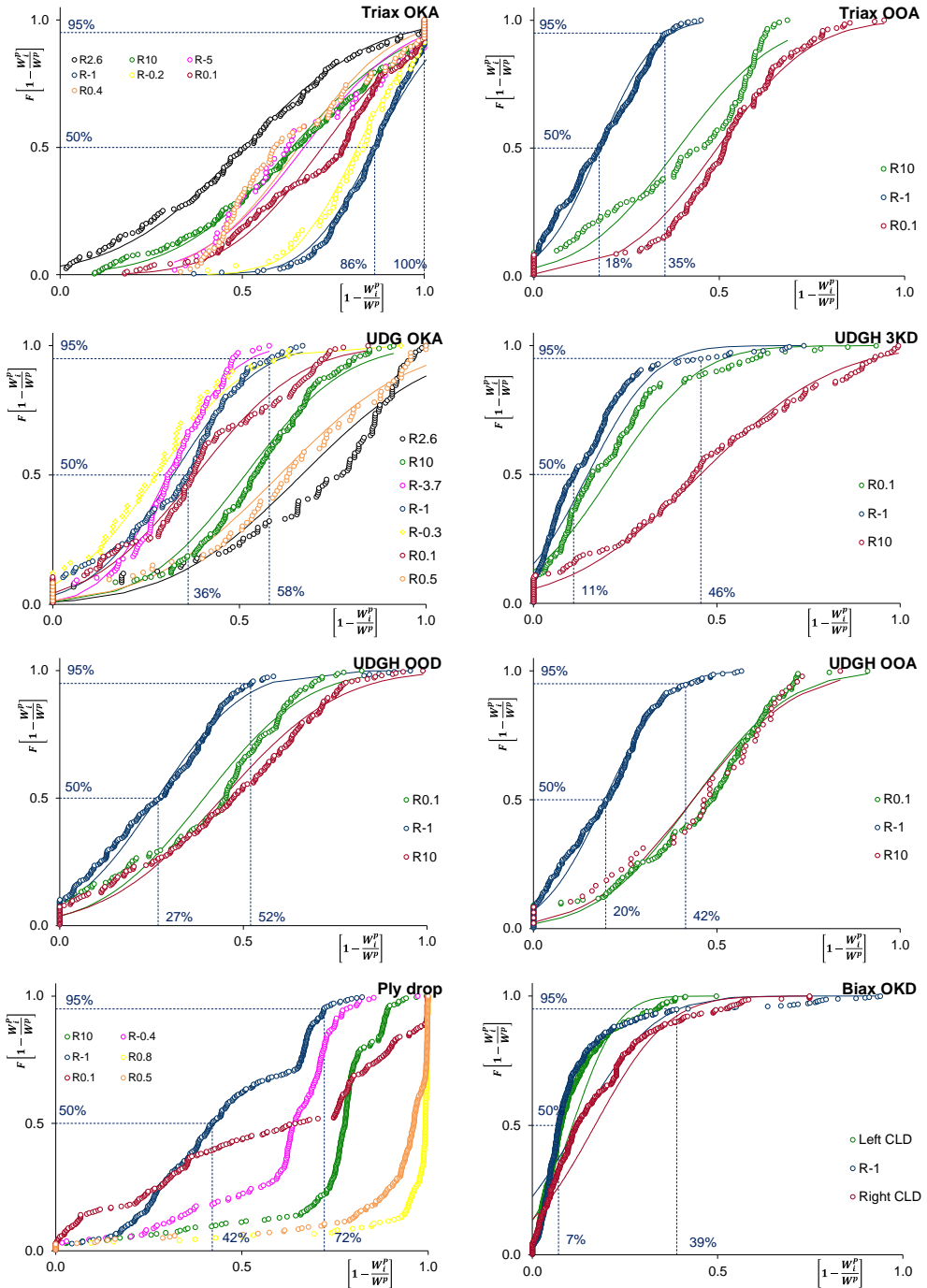


Figure 103 Probability distribution function of plastic strain energy for all material configurations

A.3.11 Stiffness degradation for all material configurations

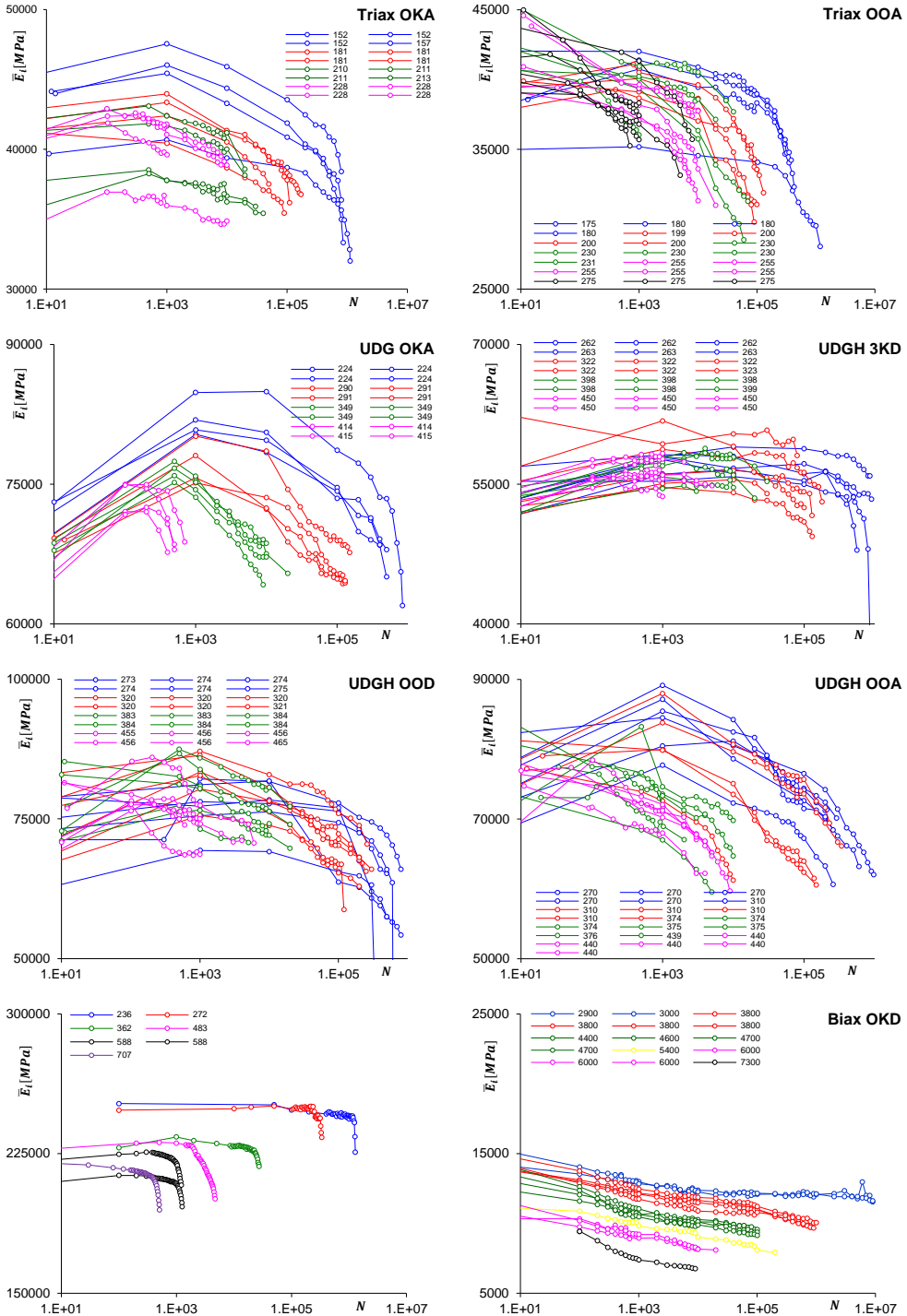


Figure 104 Stiffness degradation under R-1 stress ratio for all material configurations

A.3.12 The probability distribution function of hysteresis stiffness for all material configurations

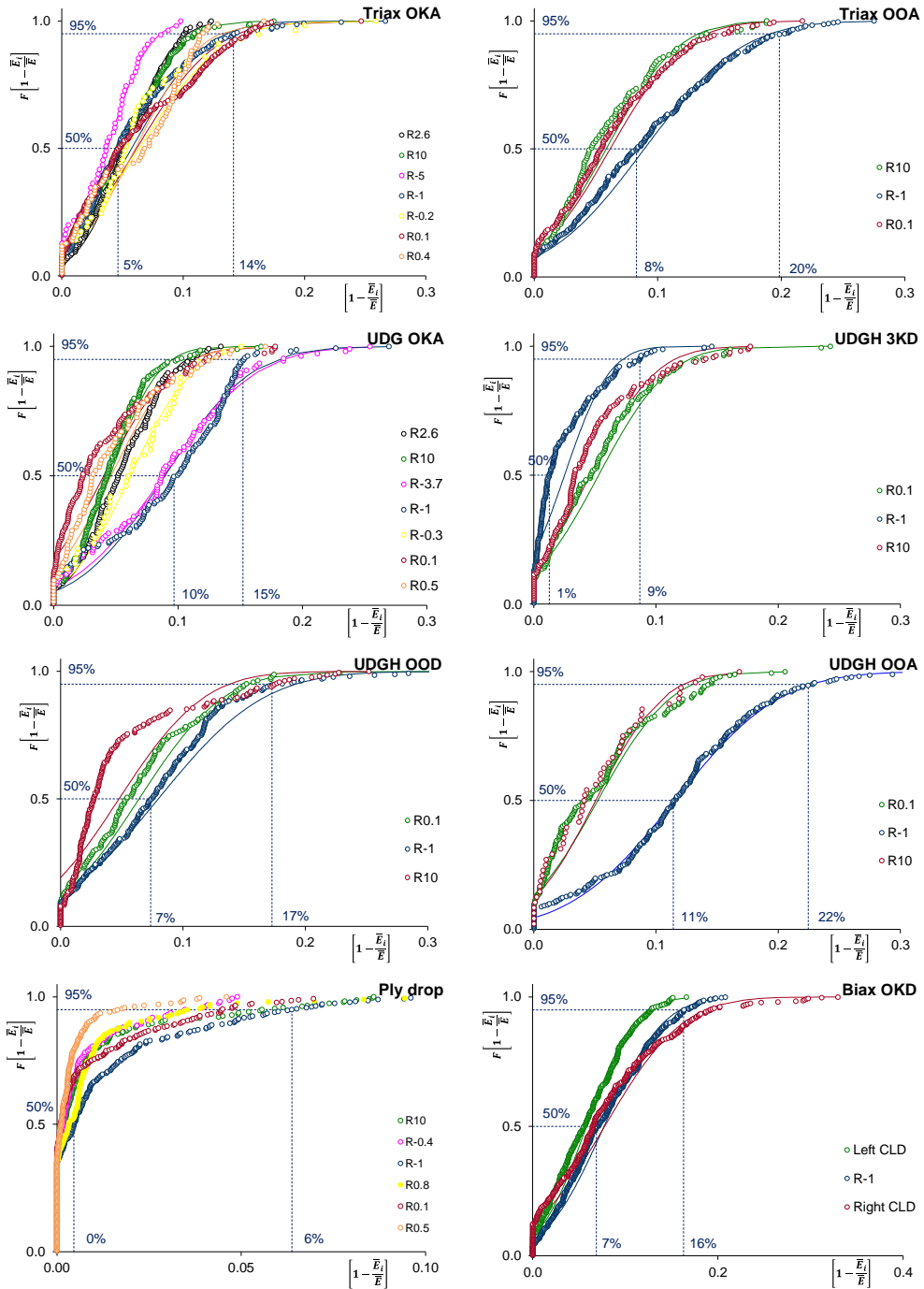
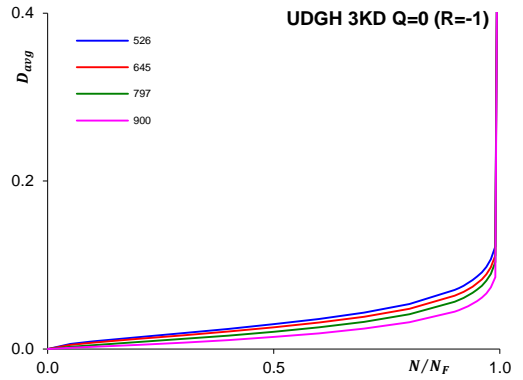
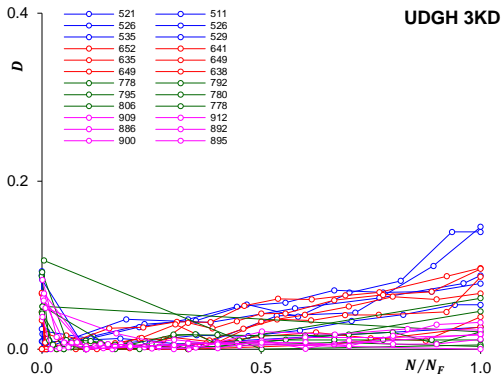
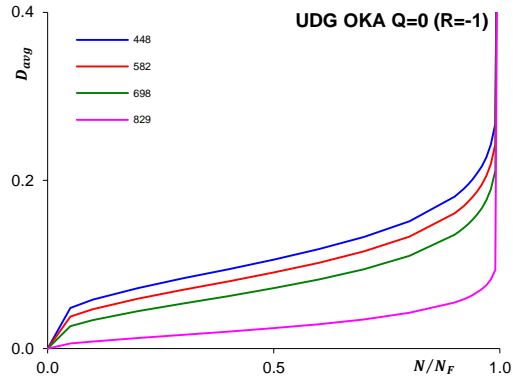
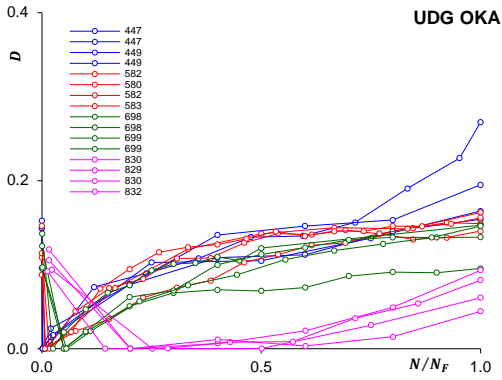
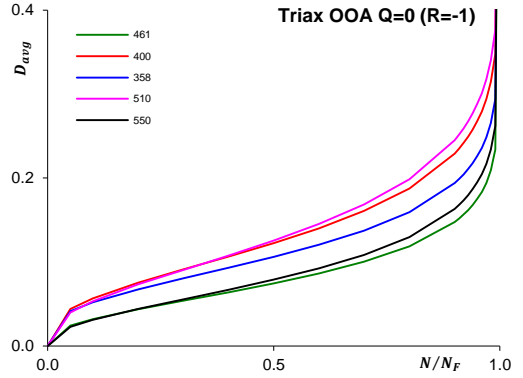
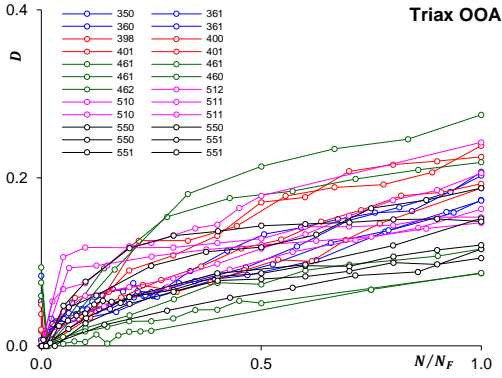


Figure 105 Probability distribution function of hysteresis stiffness for all material configurations

A.3.13 Averaging scheme to identify damage evolution trend



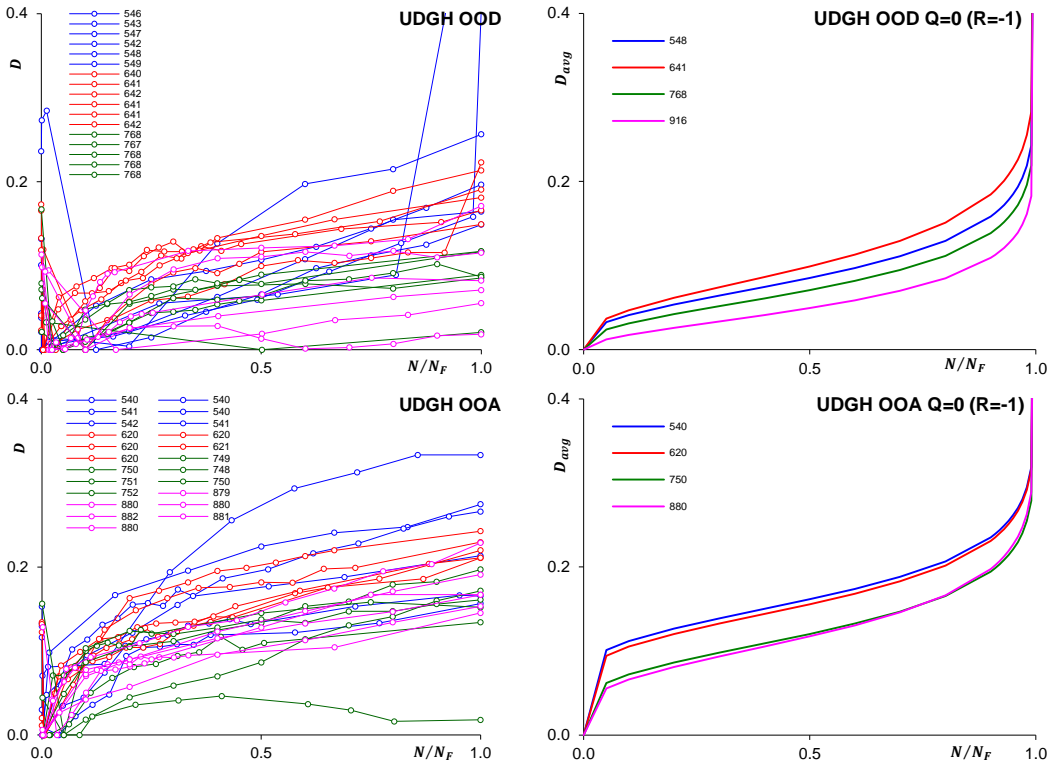


Figure 106 Averaging scheme applied to stochastic nature of fatigue damage for stress ratio $Q=0$; (Left side) absolute damage value, (Right side) average damage value per stress level (Graph legend shows $\Delta\sigma$ value in MPa)

Acknowledgements

When flower blossoms, it gives beauty and fragrance. Flower attain this beauty and fragrance, not by itself but is a result of many contributors playing their role even long before the flower existence. The thesis in its final form is also a result of a specific role played by many magnanimous contributors, to name a few. I would like to mention a few of them and show my gratitude for their contribution.

First and foremost, my sincere gratitude to my promotor Dr.ir. Rene Alderliesten for his trust and confidence in me. He inspired me to look at fatigue phenomenon through physics lens and ignited the longing for its understanding. His support and guidance throughout the research stages and physics-based views become vital ingredients in achieving the final results. Special thanks to Prof.dr.ir. Rinze Benedictus and Dr.ir. Harald Bersee for giving me this opportunity and their trust and support.

To all the members of the Suzlon Energy Ltd. research group and Structural Integrity and Composites group from Aerospace Structures and Materials department, I express my gratitude for having participated jointly or from afar in this work with Special thanks to Klass Boerstra, for countless discussion on fatigue and Klaas de Haas, for the initiating the idea for this research.

I would also like to thanks my friends and family members, especially my father whose final words were “Jay life’s ultimate goal is seeking knowledge”, my mother for her confidence in me and last but not the least, my wife Bhavana for her patience, support and taking care of my family responsibilities during the research period.

Curriculum Vitae

- 2016 – 2021 **Doctor of Philosophy (PhD)**
Faculty of Aerospace Engineering,
Department: Aerospace Structures and Materials,
Section: Structural Integrity and Composites
Delft University of Technology, Delft, The Netherlands
Promotors: Prof.dr.ir. R. Benedictus, Dr.ir. R.C. Alderliesten
- 2011 – Present **Material Expert**
Suzlon Energy Ltd., Netherlands
- 2009 – 2011 **Material Expert**
Suzlon Energy Ltd., Pune India
- 2009 – 2011 **Master of Engineering - Polymer Engineering** *Drop out in 2nd year*
Maharashtra Institute of Technology
Pune University, India
- 2005 – 2009 **Quality Assurance Engineer**
Suzlon Energy Ltd., Daman India
- 2000 – 2005 **Bachelor of Engineering - Polymer Engineering** *with Distinction*
Maharashtra Institute of Technology
Pune University, India
- 1992 – 2000 **Secondary and Higher secondary school**
Shri Chhatrapati Shivaji Vidyalyaya, Kolpewadi
Maharashtra, India
- 16-04-1983 Born in Maharashtra, India

List of publications

1. **Bhangale J.A.**, Alderliesten R.C., Benedictus R., Bersee H.E.N. (2021) How literature reviews influence the selection of fatigue analysis framework, Manuscript in preparation
2. **Bhangale J.A.**, Alderliesten R.C., Benedictus R., Bersee H.E.N. (2021) Fatigue analysis of wind turbine blade materials using the framework of continuum damage mechanics Part 1: Theory and mathematical formulation, Manuscript submitted to International Journal of Fatigue
3. **Bhangale J.A.**, Alderliesten R.C., Benedictus R., Bersee H.E.N. (2021) Fatigue analysis of wind turbine blade materials using the framework of continuum damage mechanics Part 2: validation, Manuscript submitted to International Journal of Fatigue

